DISSERTATION

IMPROVING TELESCOPE MECHANICAL ERROR ESTIMATES USING POINTING DATA

Submitted by

Robert L. Meeks

Department of Mechanical Engineering

In partial fulfillment of the requirements

for the Degree of Doctor of Philosophy

Colorado State University

Fort Collins, Colorado

Spring 2003

UMI Number: 3092685

UMI

UMI Microform 3092685

ProQuest Information and Learning Company
300 North Zeeb Road
P.O. Box 1346
Ann Arbor, MI 48106-1346

COLORADO STATE UNIVERSITY

November 8, 2002

WE HEREBY RECOMMEND THAT THE DISSERTATION PREPARED UNDER OUR SUPERVISION BY ROBERT L. MEEKS, ENTITLED "IMPROVING TELESCOPE MECHANICAL ERROR ESTIMATES USING POINTING DATA" BE ACCEPTED AS FULFILLING IN PART REQUIREMENTS FOR THE DEGREE OF DOCTOR OF PHILOSOPHY.

Committee on Graduate Work

____

C. Byron Winn

Thomas J Boardman

____

Adviser

Allan Kirkpatrick

Department Head

ABSTRACT OF DISSERTATION

IMPROVING TELESCOPE MECHANICAL ERROR ESTIMATES USING POINTING DATA

A procedure was developed to make precise estimates of mechanical errors in telescopes using observed pointing error data. A kinematic model was used to relate pointing errors to mechanical errors and the parameters of the kinematic model were estimated with a statistical model fit using data from four large astronomical telescopes as well as simulated data containing known errors. Modified ordinary least squares regression provided a baseline solution that was found to yield mechanical error estimates with relatively large standard errors due to correlation among the terms. The baseline results were comparable to those typically obtained on large research telescopes.

Bootstrapping, ridge regression, and Bayesian regression were each investigated as methods to improve the estimated parameter precision. Bootstrapping estimates of parameters associated with uncorrelated errors were more precise than the baseline model but the parameter estimates related to the correlated errors were not improved. Bootstrapping, however, allowed the form of the distribution of each mechanical error estimate to be studied in addition to allowing its parameters to be quantified.

Ridge regression yielded more precise parameter estimates than the baseline model and the proper selection of the ridge parameter was found to have only a week dependence on the specific data. This is a useful property because it eliminates much of the judgement associated with employing ridge regression for telescope mount modeling.

Bayesian regression produced the greatest improvement in precision over the baseline results. The Bayesian regression error estimates were precise enough to be of practical use in designing, operating and maintaining large telescopes and related equipment. The method provides a way to estimate geometric errors with greater precision than they can be measured using current approaches.

The improvement in precision of the model parameters also lead to better telescope pointing. Predictions from the model showed that the Bayesian regression results will produce pointing errors on large telescopes that are approximately 15% less than typical errors using current techniques.

Robert L. Meeks
Department of Mechanical Engineering
Colorado State University
Fort Collins, Colorado
Spring 2003

ACKNOWLEDGEMENTS

The ideas developed in this work came about through working with a long list of individuals through the years, primarily at Steward Observatory at the University of Arizona, EOS Technologies, Inc., and Electro Optic Systems Pty Ltd. A complete list would include the staff of these organizations as well as numerous customers, consultants, partners, and collaborators. One individual who was especially helpful is Patrick Wallace who was one of the pioneers of telescope mount modeling and developed the software program TPOINT that is now used at many large astronomical observatories. Pat shared some of the technical details of TPOINT and made several useful suggestions for this work.

The telescope data used for this study were collected from four telescopes: the ARC 3.5-meter telescope, the SDSS 2.5-meter telescope, and the twin W. M. Keck 10-meter telescopes. Without the data provided by these observatories and the assistance of some staff members, this work would not have been possible.

The SDSS and ARC telescopes are both operated by the Astronomical Research Consortium (ARC) on behalf of 13 Participating Institutions including The University of Chicago, Fermilab, the Institute for Advanced Study, the Japan Participation Group, The Johns Hopkins University, Los Alamos National Laboratory, the Max-Planck-Institute for Astronomy (MPIA), the Max-Planck-Institute for Astrophysics (MPA), New Mexico State University, University of Pittsburgh, Princeton University, the United States Naval Observatory, and the University of Washington. Two individuals associated with the ARC who were especially helpful are Russell Owen and Walter Siegmund. Russell provided data and TPOINT solutions for the ARC and SDSS telescopes and described some of the details of how mount modeling is carried out there. Walt supplied extensive measured data on telescope components collected during the manufacture of the SDSS and ARC telescopes.

The W.M. Keck Observatory is operated as a scientific partnership among the California Institute of Technology, the University of California and the National Aeronautics and Space Administration and was made possible by the generous financial support of the W.M. Keck Foundation. Hilton Lewis, Kyle Kinoshita, Wayne Dahl and several other members of the technical staff supplied data from those telescopes, provided an early opportunity to discuss the results, and made several helpful recommendations.

Finally, this work would not have been possible without the support of my wife Dr. Denise Meeks. Besides providing emotional support through the entire process, she also spent countless hours editing drafts and offering helpful criticism and suggestions.

TABLE OF CONTENTS

ABSTRACT iii

ACKNOWLEDGEMENTS v

LIST OF TABLES xi

LIST OF FIGURES xiii

NOMENCLATURE xv

1 INTRODUCTION 1
- 1.1 Background 1
- 1.2 Statement of the Problem and Research Questions 4
- 1.3 Application and Usefulness of Results 5
- 1.4 Approach to the problem 8

2 OVERVIEW OF TELESCOPE MOUNT MODELING PRACTICE 9
- 2.1 Introduction 9
- 2.2 Telescope Functions and Architecture 10
  - 2.2.1 Overview 10
  - 2.2.2 Optical System 10
  - 2.2.3 Gimbal 15
  - 2.2.4 Bearings 19
  - 2.2.5 Drives and Control System 21
- 2.3 Current Approaches 22
- 2.4 Telescope Error Sources 25
  - 2.4.1 Manufacturing Errors 27
    - 2.4.1.1 Axis Nonperpendicularity 28
    - 2.4.1.2 Optical Axis Misalignment 29
    - 2.4.1.3 Bearings 30
    - 2.4.1.4 Encoders 33
    - 2.4.1.5 Other Manufacturing Errors 35
  - 2.4.2 Installation Errors 35
    - 2.4.2.1 Leveling and Compass Orientation 35
    - 2.4.2.2 Initialization 39
  - 2.4.3 Operating Errors 39
    - 2.4.3.1 Flexure 40
    - 2.4.3.2 Thermal Expansion 42
    - 2.4.3.3 Optical Alignment 44
    - 2.4.3.4 Servo Error 45
    - 2.4.3.5 Geophysical Factors 46
    - 2.4.3.6 Observatory Operations Factors 47
  - 2.4.4 Measurement Errors 49
    - 2.4.4.1 Atmosphere 49

2.4.4.2 Detector Errors ... 50
2.4.5 Summary of Errors ... 51
2.5 Typical Results ... 52
2.5.1 Approaches and Errors Modeled ... 53
2.5.2 Results for Working Telescopes ... 54
2.5.3 Modeling Problems ... 56

3 REVIEW OF RELATED LITERATURE ... 59
3.1 Introduction ... 59
3.2 Modeling and Calibration of Machines and Robots ... 59
3.2.1 Overview ... 59
3.2.2 The Robot Calibration Process ... 61
3.2.3 Kinematic Representation ... 62
3.2.3.1 Overview ... 62
3.2.3.2 The Finite Element Method Approach ... 63
3.2.3.3 The Denavit-Hartenberg Approach ... 64
3.2.3.4 The Screw Representation ... 64
3.2.3.5 Optical System Modeling Representations ... 65
3.2.4 Research Topics in Robot Calibration ... 66
3.3 Solution Techniques ... 69
3.3.1 Overview ... 69
3.3.2 Selecting the Objective Function ... 70
3.3.3 Model Classification and Estimation Methods ... 71
3.3.3.1 Regression ... 72
3.3.3.2 Maximum Likelihood Estimation ... 74
3.3.3.3 Other Methods ... 75
3.3.4 Data Considerations ... 76

4 RESEARCH METHODOLOGY ... 78
4.1 Overview ... 78
4.2 Kinematic Model ... 79
4.2.1 Representation ... 79
4.2.2 Telescope References ... 81
4.2.3 Ideal Axis Settings ... 83
4.2.4 Geometric Error Effects ... 86
4.2.5 Pointing Error ... 90
4.3 Data Sources and Collection ... 91
4.3.1 Sources of Data ... 91
4.3.1.1 Data from Telescopes ... 91
4.3.1.2 Simulated Data Sets ... 93
4.3.2 Selecting Calibration Stars ... 95
4.3.3 Determination of True Coordinates ... 96
4.3.3.1 Star Catalog Coordinates ... 97
4.3.3.2 Reduction of Coordinates ... 97
4.3.3.3 Coordinate Transformations ... 98
4.3.4 Making Observations ... 101

4.3.5 Resulting Data 102
4.4 Statistical Model 103
4.4.1 Overview 103
4.4.2 Regression Model 103
4.5 Parameter Identification 104
4.5.1 Modified Ordinary Least Squares Regression 104
4.5.1.1 Parameter Estimates 104
4.5.1.2 Parameter Precision 107
4.5.2 Bootstrapping 112
4.5.2.1 Parameter Estimates and Precision 112
4.5.2.2 Determining the Required Number of Resamples 113
4.5.3 Ridge Regression 114
4.5.3.1 Estimated Parameters 114
4.5.3.2 Selecting the Biasing Parameter 115
4.5.4 Bayesian Regression 116
4.5.4.1 Parameter Estimates 116
4.5.4.2 Prior Distribution Information 119
4.6 Assessing Pointing Accuracy 126
4.6.1 Observed Performance 126
4.6.2 Predicted Performance 127
4.6.3 Positions for Assessing Pointing 129
4.7 Position Determination 130

5 RESULTS 132
5.1 Overview 132
5.2 Model Validation 134
5.3 Baseline Solution 138
5.3.1 Summary 138
5.3.2 Sloan Digital Sky Survey Telescope Data 138
5.3.3 Astronomical Research Consortium Telescope Data 139
5.3.4 W. M. Keck Observatory Data 139
5.3.5 Simulated Data 141
5.3.6 Comparison with a Reduced Model 143
5.4 Bootstrapping 145
5.4.1 Selecting the Number of Resamples 145
5.4.2 Sloan Digital Sky Survey Telescope Data 146
5.4.3 Astronomical Research Consortium Telescope Data 147
5.4.4 W. M. Keck Observatory Data 148
5.4.5 Simulated Data 150
5.4.6 Coefficient Distributions 152
5.5 Ridge Regression 159
5.5.1 Sloan Digital Sky Survey Telescope Data 160
5.5.2 Astronomical Research Consortium Telescope Data 162
5.5.3 W. M. Keck Observatory Data 164
5.5.4 Simulated Data 168
5.6 Bayesian Regression 176

5.6.1 Sloan Digital Sky Survey Telescope 177
5.6.2 Astronomical Research Consortium Telescope Data 177
5.6.3 W. M. Keck Observatory Data 178
5.6.4 Simulated Data 180
5.7 Pointing and Position Determination Accuracy 182
5.8 Summary of Results 183

6 DISCUSSION 185
6.1 Conclusions 185
6.1.1 Baseline Results 185
6.1.2 Other Techniques 186
6.1.2.1 Bootstrapping 186
6.1.2.2 Ridge Regression 187
6.1.2.3 Bayesian Regression 187
6.1.3 Pointing and Positioning 188
6.2 Applications 188
6.2.1 Telescope Operations and Maintenance 188
6.2.2 Telescope Design and Manufacturing 190
6.2.3 Observatory Systems Engineering 192
6.2.4 Robot Calibration 192
6.3 Recommendations for Future Research 192
6.3.1 Model Improvements 192
6.3.2 Extensions 193

REFERENCES 195

APPENDIX A: DATA LISTINGS 203

APPENDIX B: DERIVATIONS OF ERROR EFFECT TERMS 217
B.1 Introduction 217
B.2 Optical Axis Misalignment 220
B.3 Axis Nonperpendicularity 223
B.4 Tilt Toward North 225
B.5 Tilt Toward East 228
B.6 Bearing Errors 228
B.7 Flexure 230

GLOSSARY 231

LIST OF TABLES

Table 2.1	Summary of geometric errors	51
Table 2.2	Summary of random error sources in calibration data	52
Table 2.3	TPOINT nomenclature for common telescope geometric errors	53
Table 2.4	Mount model results for the SDSS telescope	54
Table 2.5	Mount model results for the ARC telescope	55
Table 2.6	Mount model results for the TNG	55
Table 2.7	Mount model results for the Keck I telescope	56
Table 4.1	Summary of all axis rotations and geometric error effects	87
Table 4.2	Algebraic representation of telescope geometric errors	89
Table 4.3	Geometric errors introduced into simulated data sets	94
Table 4.4	Random errors introduced into simulated data sets	94
Table 4.5	Prior distribution information for the working telescopes	124
Table 4.6	Prior distribution information for the simulated data sets	125
Table 5.1	Comparison of solutions for the SDSS telescope	136
Table 5.2	Comparison of solutions for the ARC telescope	137
Table 5.3	MOLS results for the SDSS telescope	138
Table 5.4	MOLS results for the ARC telescope	139
Table 5.5	MOLS results for the Keck I telescope	140
Table 5.6	MOLS results for the Keck II telescope	141
Table 5.7a	MOLS results for the simulated data	142
Table 5.7b	MOLS results for the simulated data (cont.)	143
Table 5.8	Comparison of full and reduced models for simulated data set 3	144
Table 5.9	Bootstrapping parameter estimates for the SDSS telescope	147
Table 5.10	Bootstrapping parameter estimates for the ARC telescope	148
Table 5.11	Bootstrapping parameter estimates for the Keck I telescope	149
Table 5.12	Bootstrapping parameter estimates for the Keck II telescope	147
Table 5.13a	Bootstrapping parameter estimates for the simulated data	151
Table 5.13b	Bootstrapping parameter estimates for the simulated data (cont.)	152
Table 5.14	Ridge estimates of parameters for the SDSS telescope	162
Table 5.15	Ridge estimates of parameters for the ARC telescope	164
Table 5.16	Ridge estimates of parameters for the Keck I telescope	167

Table 5.17	Ridge estimates of parameters for the Keck II telescope	168
Table 5.18a	Ridge estimates of parameters for the simulated data	175
Table 5.18b	Ridge estimates of parameters for the simulated data (cont.)	176
Table 5.19	Bayesian estimates of parameters for the SDSS telescope	177
Table 5.20	Bayesian estimates of parameters for the ARC telescope	178
Table 5.21	Bayesian estimates of parameters for the Keck I telescope	179
Table 5.22	Bayesian estimates of parameters for the Keck II telescope	180
Table 5.23a	Bayesian estimates of parameters for the simulated data	181
Table 5.23b	Bayesian estimates of parameters for the simulated data (cont.)	182
Table 5.24	Predicted pointing and position determination accuracy	183

LIST OF FIGURES

Figure 2.1 A 1.8-meter telescope at the manufacturer's facility 11
Figure 2.2 Typical telescope optical arrangement 12
Figure 2.3 Collimation misalignment (tilt and decenter) 14
Figure 2.4 Focus misalignment (despace) 15
Figure 2.5 General arrangement of an equatorial telescope mount 16
Figure 2.6 General arrangement of an altazimuth telescope mount 18
Figure 2.7 A telescope with nonperpendicular axes 29
Figure 2.8 A telescope with misaligned optical axis 31
Figure 2.9 A telescope tilted toward the north 36
Figure 2.10 A telescope tilted toward the east 37
Figure 2.11 The effect of flexure on telescope pointing 41
Figure 4.1 Telescope references 82
Figure 4.2 Principal axis rotations 84
Figure 4.3 Partial data file containing reference star observations 102
Figure 4.4 Location of reference positions for assessing pointing accuracy 130
Figure 5.1 Effect of number of resamples on coefficient precision 146
Figure 5.2 Bootstrap estimate histogram for azimuth encoder offset 153
Figure 5.3 Bootstrap estimate histogram for elevation encoder offset 153
Figure 5.4 Bootstrap estimate histogram for azimuth encoder scale 154
Figure 5.5 Bootstrap estimate histogram for elevation encoder scale 154
Figure 5.6 Bootstrap estimate histogram for axis nonperpendicularity 155
Figure 5.7 Bootstrap estimate histogram for optical axis misalignment 155
Figure 5.8 Bootstrap estimate histogram for north-south tilt 156
Figure 5.9 Bootstrap estimate histogram for east-west tilt 156
Figure 5.10 Bootstrap estimate histogram for tube flexure 157
Figure 5.11 Bootstrap estimate histogram for north-south bearing wobble 157
Figure 5.12 Bootstrap estimate histogram for east-west bearing wobble 158
Figure 5.13 Bootstrap estimate histogram for elevation bearing wobble (cos E) 158
Figure 5.14 Bootstrap estimate histogram for elevation bearing wobble (sin E) 159
Figure 5.15 Effect of bias on estimated coefficients for the SDSS telescope 160
Figure 5.16 Effect of bias on estimated error for the SDSS telescope 161

Figure 5.17 Effect of bias on estimated coefficients for the ARC telescope..........163
Figure 5.18 Effect of bias on estimated error for the ARC telescope....................163
Figure 5.19 Effect of bias on estimated coefficients for the Keck I telescope.......165
Figure 5.20 Effect of bias on estimated coefficients for the Keck II telescope......165
Figure 5.21 Effect of bias on estimated error for the Keck I telescope 166
Figure 5.22 Effect of bias on estimated error for the Keck II telescope................166
Figure 5.23 Effect of bias on estimated coefficients for simulated data set 0 169
Figure 5.24 Effect of bias on estimated coefficients for simulated data set 1 169
Figure 5.25 Effect of bias on estimated coefficients for simulated data set 2 170
Figure 5.26 Effect of bias on estimated coefficients for simulated data set 3 170
Figure 5.27 Effect of bias on estimated coefficients for simulated data set 4 171
Figure 5.28 Effect of bias on estimated coefficients for simulated data set 5 171
Figure 5.29 Effect of bias on estimated error for simulated data set 1 172
Figure 5.30 Effect of bias on estimated error for simulated data set 2 172
Figure 5.31 Effect of bias on estimated error for simulated data set 3 173
Figure 5.32 Effect of bias on estimated error for simulated data set 4 173
Figure 5.33 Effect of bias on estimated error for simulated data set 5 174

NOMENCLATURE

English Letters

A	Azimuth angle (rad)
AA	Azimuth axis
AE	AZ-EL line
B,C	Constants in atmospheric refraction formula (rad)
E	Elevation angle (rad)
EA	Elevation axis
EW	East-west line
$\mathbf{F}(\cdot)$	Function of
GST	Greenwich sidereal time (rad)
H	Hour angle (rad)
$\mathbf{I}$	Identity matrix (dimensionless)
$\mathbf{J}$	Matrix of 1s (dimensionless)
$\mathbf{K}$	Bias matrix for ridge regression (dimensionless)
k	Ridge parameter for ridge regression (dimensionless)
LST	Local sidereal time (rad)
LOS	Line-of-sight
MSE	Mean square error (rad)
m	Number of new positions for determining pointing accuracy
NS	North-south line
n	Number of stars observed for calibration
p	Number of terms (parameters) in the kinematic model
$\mathbf{P}$	Pointing vector (rad or m)
q	Quantile indicated by subscript (varies)
Q	Total squared pointing error (rad^2)
R^2	Coefficient of multiple determination (dimensionless)
$\mathbf{R}$	Rotation matrix (dimensionless)
s	Sample standard deviation or standard error (varies)

$\mathbf{s}[\cdot]$	Standard error matrix (varies)
$SSTO$	Total sum of squares (rad^2)
SSR	Regression sum of squares (rad^2)
SSE	Error sum of squares (rad^2)
t	t-statistic (dimensionless)
x, y, z	Coordinate or rotation angle (m or rad)
z	Zenith angle (rad)
$\mathbf{T}$	Transformation matrix (mixed)
$\mathbf{V}$	Normalized variance-covariance matrix (dimensionless)
$\mathbf{X}$	Matrix of error effects (dimensionless)

Greek Letters

α	Confidence level (dimensionless)
α	Right ascension (rad)
$\boldsymbol{\beta}$	Vector of regression coefficients (rad)
γ	Optical axis misalignment angle (rad)
Δ	Change, error, or deviation in a quantity (varies)
δ	Declination (rad)
δ_T	Maximum pointing error due to tube flexure (rad)
$\boldsymbol{\varepsilon}$	Random component of a pointing error vector (rad)
η	Axis nonperpendicularity angle (rad)
θ	Rotation angle (rad)
λ	East longitude (rad)
ξ	Bearing wobble angle (rad)
σ	Population standard deviation (varies)
$\boldsymbol{\sigma}^2[\cdot]$	Variance-covariance matrix (varies)
ϕ	Latitude (rad)
ψ	Mislevel angle (rad)

Subscripts

A	Associated with azimuth angle
Ah	Azimuth angle of new position
Aobs	Observed azimuth angle
a	Apparent, with reference to refraction
B1,B2,B3,B4	Associated with the indicated bearing effect
E	Associated with elevation angle
Eh	Elevation angle of new position
Eobs	Observed elevation angle
e	As read by encoders
F	Associated with tube flexure
i	Observation number
j	Parameter number
k	Associated with using the value k for the ridge parameter
M	Associated with optical axis misalignment
N	Associated with axis nonperpendicularity
r	Refracted
rms	Root-mean-square value
S	Setting, associated with azimuth and elevation only
T	Total, associated with applying all effects
X	Associated with north-south mislevel
Y	Associated with east-west mislevel
1,2,3	Vector components
0	Prior estimate or initial value

Superscripts

x^*	Bayesian estimate of x
$\hat{x}$	Estimated value of x
$\bar{x}$	Mean value of x
T	Matrix or vector transpose

1 INTRODUCTION

1.1 Background

Telescopes and similar gimbaled optical systems are used for a wide variety of scientific, military, and commercial applications. They are used scientifically for astronomy, atmospheric research, and to make precise geophysical measurements across large distances. The military uses telescopes to track satellites, as part of missile detection systems, and to support development of advanced optical weapon systems. Commercial applications for telescopes are currently limited but they are employed for satellite tracking and remote sensing. Private satellite and orbital debris tracking is growing in response to proliferation of commercial communications satellites and government privatization worldwide.

Telescope performance is generally measured by two factors: optical quality and positioning accuracy. Optical quality may be measured in any of several ways depending on the telescope application and concerns how well the telescope's mirrors or lenses transfer light through the system. Optical quality is affected by the optical design, the quality of the optical components, how well the telescope is aligned and the rigidity of the mechanical structure. Optical quality usually does not significantly affect pointing accuracy.

Positioning accuracy relates to the precision of the motion of the mechanical system and is influenced by mechanical, electronic, and software factors. Previously, the positioning capabilities of telescopes were limited by the quality of electronic components available. More recently, mechanical errors arising from misalignments, manufacturing errors in components, and similar sources have become significant.

Scientific and technological advances have produced requirements for larger and more precise telescopes. Building larger telescopes complicates the mechanical design substantially because many errors that are insignificant on small telescopes begin to limit the performance of larger instruments. Overcoming small residual errors on large telescopes is a very active research area in astronomy and optical engineering. Much of that research involves correcting random errors introduced by the atmosphere, one of the largest contributors of random error in a modern telescope. These errors are dynamic and correction requires fast, active compensation systems.

Mechanical errors originating from misalignment within the telescope, bearing defects, and structural changes are primarily static and can be reduced by compensating with a computer *mount model*, which is now a standard feature on most large and medium-sized telescopes. Errors are systematically identified during a calibration process and then corrected during operation by adjusting the signals used to move the telescope.

Calibration involves measuring the pointing error at known positions in the sky and identifying the parameters of a model that are most consistent with the observed data. The pointing error in an observation is the difference between the location in the sky that the telescope is directed to be pointed to and the actual location it points to. Stars provide good absolute position references for calibration observations, even on telescopes not used for astronomy. Calibration data consist of desired pointing coordinates (the calculated location of each calibration star) and observed errors in two orthogonal directions.

The telescope model typically assumes certain mechanical errors are present and uses regression to identify the parameters of a mathematical model that will compensate for those errors. The terms of the mathematical model are usually trigonometric functions of the angular positions of the axes. Because the terms are not mathematically orthogonal over the set of calibration positions, the estimates of the parameters are correlated and are imprecise. In effect, some of the physical errors compensate for each other in complex ways and it becomes difficult to identify the true source of a problem.

But, the goal of telescope mount modeling is usually to predict the pointing error at a particular location and use it to determine appropriate corrections to apply to eliminate the error in the future. In contrast, the goal of this work was to predict the magnitude of the individual effects in order to identify the mechanical errors in the telescope.

This research extended the mount modeling process to the problem of estimating the physical errors. The mathematical techniques for addressing this problem were similar to those used for the mount modeling problem but with the objective of estimating the model parameters instead of the response. Characteristics of the data also complicated the problem by causing the terms to be highly correlated. This was addressed by applying alternative solution techniques described in the statistical literature.

1.2 Statement of the Problem and Research Questions

A mount model is a critical component of a modern large telescope. Procedures for developing a mount model have evolved to a point where static telescope pointing errors can be corrected very well. The focus, however, has always been on making corrections, not on identifying and quantifying the sources of errors. Current techniques do not provide a means for studying the underlying mechanical errors in telescopes in any statistically meaningful way. This work addressed an extension of the analysis of telescope pointing error data to this problem.

Information gathered for telescope mount models was used for making precise and statistically significant estimates of the physical errors present in the telescope and for assessing the uncertainty in the actual position of an observed object. The goals of this work were to:

- describe a technique for making precise, statistically significant estimates of the physical errors in a telescope using data collected for mount modeling;
- develop a process for predicting the accuracy of a telescope given the presence of imprecisely known physical errors; and
- improve the understanding of the relationship between telescope performance and physical errors.

Three specific research questions were answered:

- *What is the precision of the estimates of the geometric errors in a telescope and how can it be improved?*

- *What is the expected pointing error of a telescope when a mount model is used to compensate for imprecisely known physical errors?*
- *What is the uncertainty associated with an estimate of the actual coordinates of an object observed through the telescope using the telescope's encoders as a reference?*

The importance and application of the knowledge obtained from answering each of these questions is discussed in the next section.

Several related questions were also addressed. For example, determining the quantity and distribution of reference stars used for a mount model is not always obvious. Current practice is to select a set of reference stars distributed over as wide a range of elevation and azimuth angles as possible, subject to limits imposed by telescope range of motion, enclosure range of motion, or line-of-sight obstructions at the site. Quantifying how many stars should be used and over what coordinate range would be useful.

1.3 Application and Usefulness of Results

A better understanding of errors in the telescope mount modeling process is useful for several reasons. Mount model results are already informally used for many of these applications but, since it is well known that the parameter estimates are imprecise and correlated, application beyond correcting telescope performance is limited. By improving the precision of the results, the techniques developed in this work will contribute in several key areas.

Better design and manufacturing of new telescopes. The current approach to telescope design involves building a telescope to be "as good as is practical" and then using a mount model to make fine corrections. A clear understanding of how component and assembly errors influence the performance of a telescope and how well each can be compensated could improve the process. Areas where cost savings are possible without significant degradation of performance could be identified and the fidelity of performance predictions could be enhanced.

New methods for testing telescopes. The mount modeling process also provides a straightforward way to measure certain assembly errors. Estimates of mechanical errors could be useful for demonstrating compliance with specifications during acceptance testing of a telescope. Without the ability to assess the precision of these measurements, however, they are of little use. The ability to show statistical significance of measurements and assign confidence limits adds substantially to their value.

Improved pointing of existing telescopes. Since the process developed in this work produces models that are predicted to produce better pointing than current techniques, pointing on existing telescopes could be improved. The Bayesian regression approach described in this work produced predicted pointing errors that were about 15% less than those produced with current techniques. This is a substantial improvement.

Observatory maintenance and operations. Understanding the magnitude and precision of the physical errors and tracking changes over time is of interest to engineering personnel because it may signal the need for corrective maintenance, for example, replacing a bearing that has exhibited increasing wobble. Everett (1993) made a similar suggestion regarding machine tools. A precise estimate of an error that previously could not be measured precisely, axis nonperpendicularity, for example, may also facilitate repairing the misalignment on an existing telescope to improve pointing results.

Better tracking system performance. Finally, when a telescope is used to measure an object's position, as would be the case in missile tracking, satellite orbit determination systems, and geodetic research programs, the error in the position determined by the telescope is an important factor in overall system performance. When an object appears centered in the telescope field-of-view, the readings of the telescope encoders provide an uncertain estimate of the actual position of the object. Understanding this uncertainty is of practical importance in designing and operating tracking systems. For example, a satellite tracking network often functions by observing a satellite from a succession of ground stations located around the globe. To initiate tracking, each station must find the satellite, calculate its relative track, and then follow it for a period of time while data is transferred. A satellite in low earth orbit may only be visible to a particular ground station for 60 to 90 seconds during each orbit. Reducing the time required to find the satellite by only a few seconds can significantly increase the time available to do productive work and improve system performance. Position information forwarded from a previous station is used to facilitate finding the satellite and more precise information allows a smaller search area to be considered, shortening the search time.

The extension of the mount modeling process to new applications and its treatment as a general machine calibration problem make this work potentially applicable to a wide variety of other problems. Current applications of telescope mount modeling are restricted to correcting pointing. Development of new uses for the data may lead to better tools for telescope engineers and generalizing the problem will allow future developments in machine modeling to be applied to telescopes.

1.4 Approach to the problem

The problem of developing a model to estimate and correct positioning errors is not unique to telescopes. Calibrating an industrial robot is very similar to constructing a telescope mount model and that problem is widely discussed in the literature. The basic techniques are similar to those used for telescope mount modeling. As with telescopes, the goal of calibration is usually to improve performance, not necessarily to estimate the mechanical errors.

To exploit the large body of literature on robot calibration a similar modeling approach was used. The main steps in the project were:

- developing a model of the telescope behavior to predict the positioning error at each location in the sky;
- fitting the model using data from working telescopes as well as simulated data;
- estimating the physical errors using the parameters of the fitted model; and
- relating the uncertainty in the physical errors to telescope performance.

Chapter 2 discusses previous findings related to telescope modeling and Chapter 3 describes related research in robot calibration and solution techniques. Chapter 4 outlines the methodology utilized to solve the problem and Chapter 5 presents results for several data sets. Finally, Chapter 6 discusses some of the implications of this research and suggests some applications and avenues for future studies.

2 OVERVIEW OF TELESCOPE MOUNT MODELING PRACTICE

2.1 Introduction

Computer mount models were developed in the 1970s to compensate for static pointing errors in telescopes. The models operate by modifying the position commands that control the telescope axes to compensate for repeatable pointing errors. One approach uses an empirical mathematical model to explain observed differences between the expected position and the observed position of a telescope when pointed at objects in the sky. A single function can be used for corrections across the entire sky or the sky can be broken down into regions and a different function used for each. The parameters of this type of model are not easily attributable to a physical source (Wallace, 1993).

Another approach involves identifying the physical relationships responsible for pointing errors and developing a model based on those relationships. Using this approach, the terms in the mount model correspond to physical errors within the telescope. This approach has several advantages. It allows physical tolerances allocated during design to be used to predict the performance of the finished telescope; enables the mount model to be used as a diagnostic tool for identifying physical errors in the telescope; and is more likely to produce good results when used to extrapolate outside the range of sky over which the model was originally fit (Wallace, 1993). The second approach was used for this work.

This chapter summarizes the function and architecture of modern telescopes, outlines the current approach to mount modeling, describes the mechanical errors usually encountered, and presents some results from large research telescopes.

2.2 Telescope Functions and Architecture

2.2.1 Overview

A telescope performs two basic functions: pointing to an object of interest and redirecting light from a source into an instrument or detector. A wide variety of telescope designs are in use but most share this commonality of function and it is reflected in a uniform architecture seen in most modern telescopes.

The components of a modern telescope can be divided into functional subsystems that are useful in understanding the errors that affect pointing. The gimbal and bearings provide the physical support and allow for motion of the axes. The drive and control systems produce and coordinate the motion, and the optical system collects and relays light into an instrument. The role and common arrangement for each of these is illustrated in Fig 2.1 and discussed below to familiarize the reader.

2.2.2 Optical System

The optical system of a telescope consists of the mirrors and lenses used to collect and focus the light. The most common optical configuration for a large telescope uses two curved mirrors to concentrate light at a focus as illustrated in Fig. 2.2. Designs using three or more mirrors are also used and additional lenses or mirrors are frequently required to relay the light into an instrument or to make small optical corrections

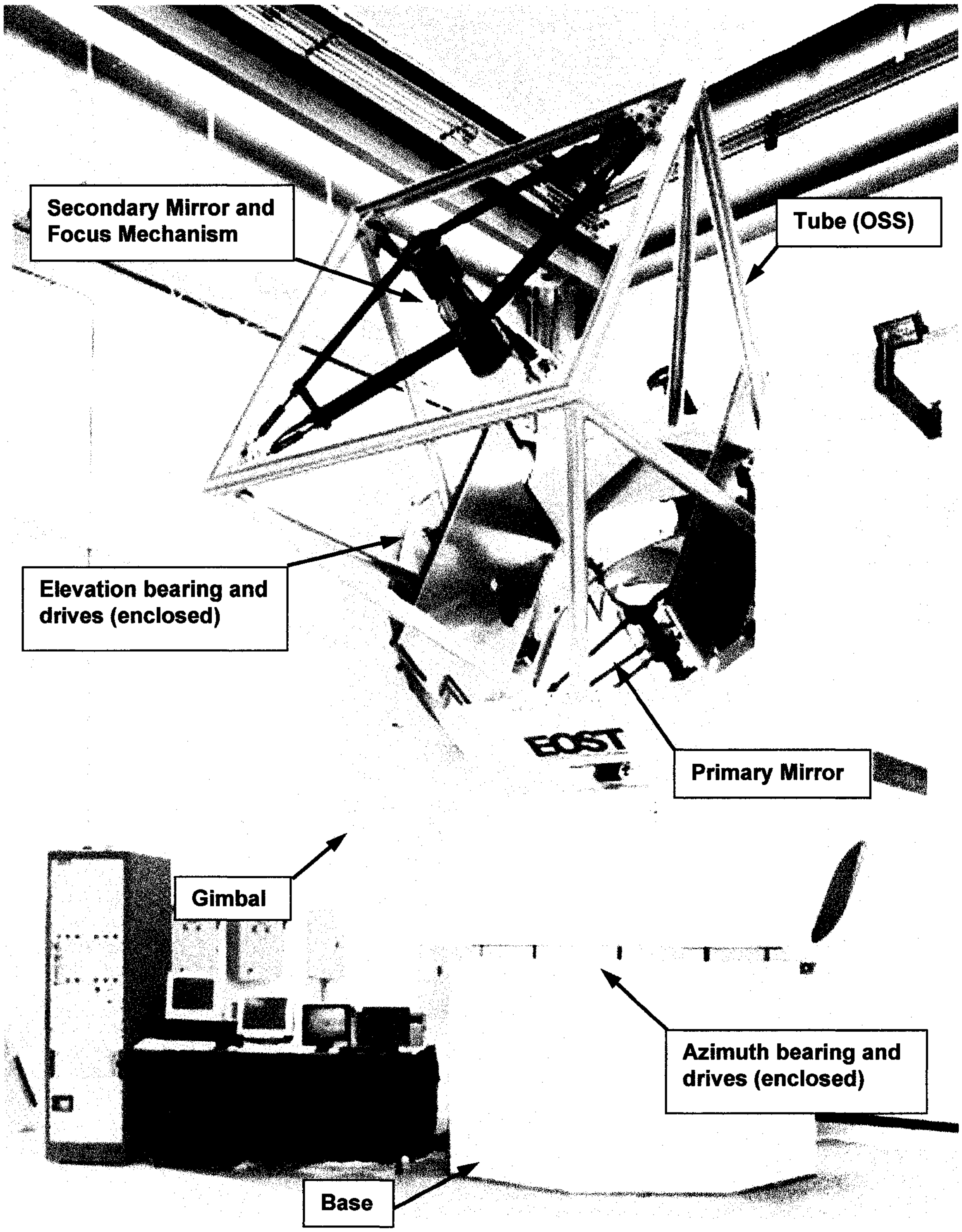

Fig 2.1 A 1.8-meter telescope at the manufacturer's facility (Photo by Edward G. Winrow, courtesy of EOS Technologies, Inc.)

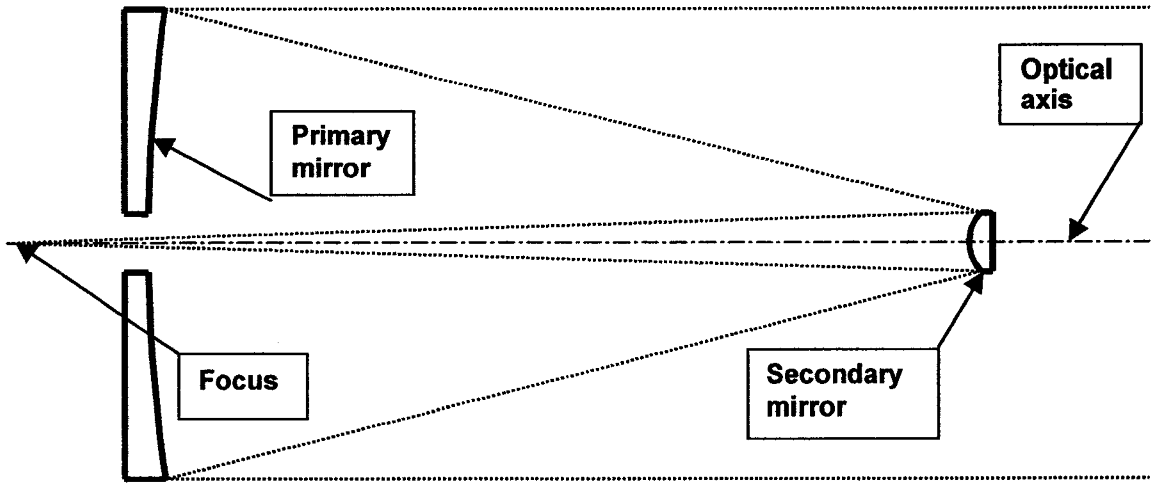

Figure 2.2 Typical telescope optical arrangement (light rays also shown).

The diameter of the largest mirror, the *primary mirror* or *M1*, is generally used as the "size" or aperture of a telescope (e. g. a one-meter telescope has a primary mirror that is nominally one meter in diameter). The primary mirror usually has a roughly parabolic shape with the exact shape, measured by the *conic constant* and *radius-of-curvature (ROC)* determined by specific optical requirements of the telescope. The *secondary mirror* or *M2* is normally smaller and is mounted near the focus of the primary mirror. It may be concave or convex and its exact shape is also defined by its radius-of-curvature and conic constant. The distance between the mirror vertices is called the *separation.* Telescope designs with a large mirror separation are longer and deform more under their own weight. However, designs with a short separation (fast optical systems) are typically more sensitive to misalignments such as those caused by self-weight deflection (Schroeder, 1987).

The optical performance requirements of a telescope generally represent a compromise among several goals. Large telescopes are seldom built for a single purpose and the requirements reflect competing uses as well as flexibility for future upgrades. The optical design of a telescope consists of the specification of the exact shape and arrangement of each mirror to achieve specific overall optical characteristics relevant to the requirements of the telescope. Several classical telescope optical designs have been developed to optimize specific optical performance characteristics. One of these or a variant is generally used on any modern telescope although advances in optical fabrication and testing techniques have produced new options. The *classical Cassegrain* optical design was assumed here. It uses a paraboloidal primary mirror and a convex hyperboloidal secondary mirror (Schroeder, 1987).

Rodkevich and Robachevskaya (1977) described the key requirements of the material and construction of a large precision mirror. Stability, rigidity, and the capability of being formed into a precise shape are critical. Glass satisfies these criteria so most telescope mirrors are made from glass. Low expansion glass (or zero expansion glass-ceramic) is often used to minimize the effects of thermal expansion on the polished figure. A solid blank is usually cast, ground to within a few microns of the correct shape and then polished to within a few nanometers of the desired figure. Lightweight designs are often used to decrease the weight and heat capacity of the mirror. After polishing, each mirror is coated with a reflective metal coating. Various coatings may be used to maximize reflectivity over a particular wavelength of light or improve durability. The effects of the mirror material and coatings on pointing are negligible and were ignored.

The optics are supported and held in position by a support system that distributes the weight of each mirror to control the deformation of the surface. The design and performance of mirror supports were discussed extensively by Yoder (1993). If a mirror is not supported properly, significant optical errors are produced that limit performance of a telescope. In some cases, active force actuators are used to apply corrective forces to bend the primary mirror slightly to the correct the shape to improve the quality of the images formed (Martin et al., 1994; Sawyer et al., 2000). It was assumed here that no errors were produced by improper mirror supports because such errors would be unusual and their effect on pointing would depend strongly on the nature of the support problem. The support for the secondary mirror usually includes a mechanism for moving the mirror to focus the telescope and compensate for thermal expansion of the truss supporting it.

The two mirrors must be positioned correctly with respect to each other to perform properly. The positioning and orientation of the optical elements relative to each other transverse to the optical axis is referred to as *collimation* and a collimation misalignment is illustrated in Fig 2.3. The positioning along the optical axis is called *focus* and a focus misalignment is shown in Fig 2.4.

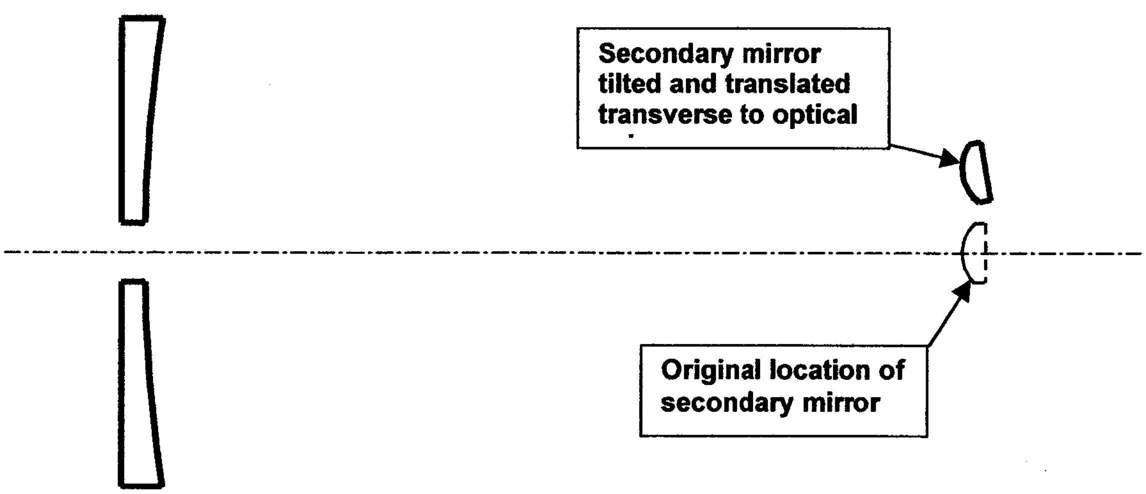

Figure 2.3 Collimation misalignment (tilt and decenter)

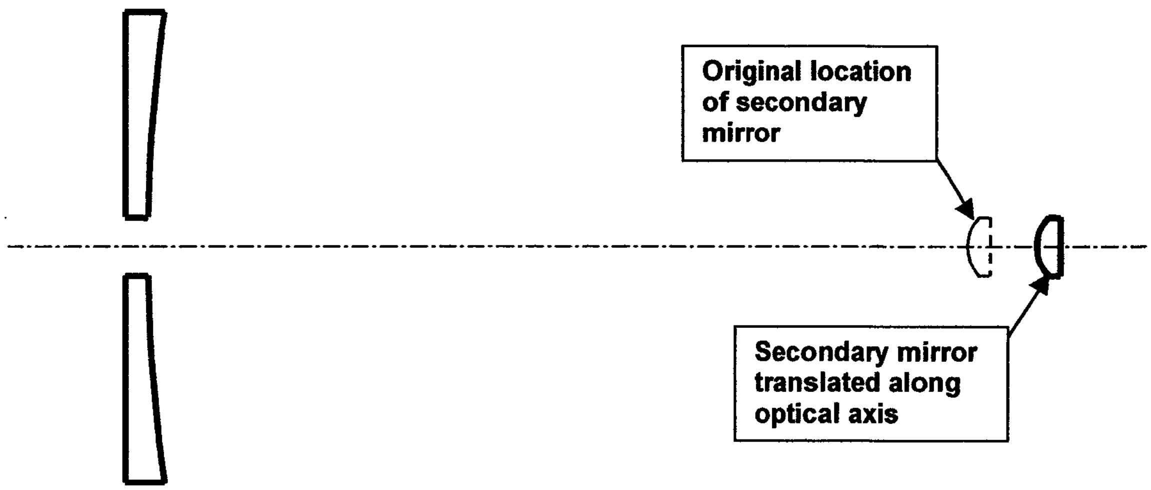

Figure 2.4 Focus misalignment (despace)

Many types of optical errors can be neglected in a pointing analysis because they only blur an image, they do not change its position. Optical errors were considered here only where they affected the star position measurements made during the calibration process or contributed to the variability in the model.

2.2.3 Gimbal

A gimbal consisting of a *base*, a *fork*, and a *tube* supports and positions the optics. The base, also called a *pedestal*, is a structure used to support the telescope and attach it to the foundation. The base and fork are usually large plate or beam structures and are generally constructed of structural steel or cast iron although other materials have been used. The gimbal structure must be stiff, lightweight, and have a low thermal mass.

The traditional gimbal arrangement for astronomy was the *equatorial mount* (see Fig. 2.5). In this configuration, one axis of the telescope, the *polar axis*, is tilted so that it points toward the *North Celestial Pole* (NCP), the point in the sky that all stars appear to rotate about on a daily basis, (the NCP is currently close to the North Star, Polaris). This is accomplished by setting the angle between the horizon and the polar axis to the latitude where the telescope is located. The other axis, the *declination axis*, is perpendicular to the polar axis. In principle, this arrangement allows stars to be tracked by moving only the polar axis at a constant rate (Meinel, 1965). Historically, this made it possible to use modified clock movements to drive telescopes (McMath and Mohler, 1960). Motion on the declination axis was only required for setting the telescope position and could be done manually. In a modern equatorial telescope both axes are usually motorized to allow the declination axis to correct errors caused by inaccuracies in the polar axis. While the equatorial arrangement evolved because it was easy to control, it still offers advantages and continues to be used today for astronomy.

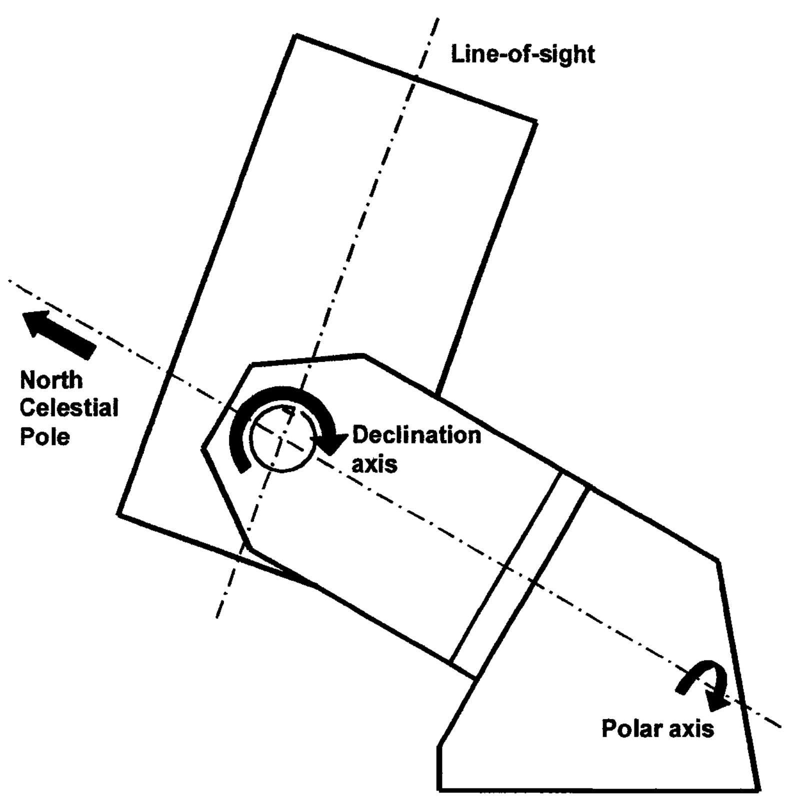

Figure 2.5 General arrangement of an equatorial telescope mount

More recently, telescopes have been built with altitude over azimuth, *altazimuth*, configurations as shown in Fig 2.6. An altazimuth telescope has a horizontal elevation axis mounted over a vertical azimuth axis. Positioning an altazimuth telescope involves coordinating the motion of two separate rotation axes. Before the advent of computer control systems, this was difficult to do accurately. From a design and manufacturing standpoint, altazimuth telescopes have several advantages: the design does not have to be customized for different latitudes making a standard design possible and gravitational loads are relatively constant simplifying the structural design. Disadvantages include the requirement to coordinate the motion of the axes and the fact that, near the zenith, tracking requires extreme velocity and acceleration. This makes it difficult to track objects directly overhead, a serious drawback for some applications.

Telescopes have also been built using other arrangements and sometimes with three or more axes. Usually these were for satellite tracking and were designed to simplify the telescope motion by allowing one axis to be aligned with the pole of the satellite's orbit or to reposition the motion singularity (Hodge et al., 1992). This effectively creates an equatorial telescope with a variable polar angle. Few multiple-axis telescopes have been built since the early 1970s. The kinematic analysis of a multiple axis telescope is more complex than that of a two-axis telescope because there are additional dependencies that must be considered. Any position in the sky is completely defined by two coordinates. When three axes are available, the setting of one is always dependent on the other two. Hodge et al. (1992) compared three alternative mount configurations for a large laser telescope and concluded the altazimuth configuration was best overall.

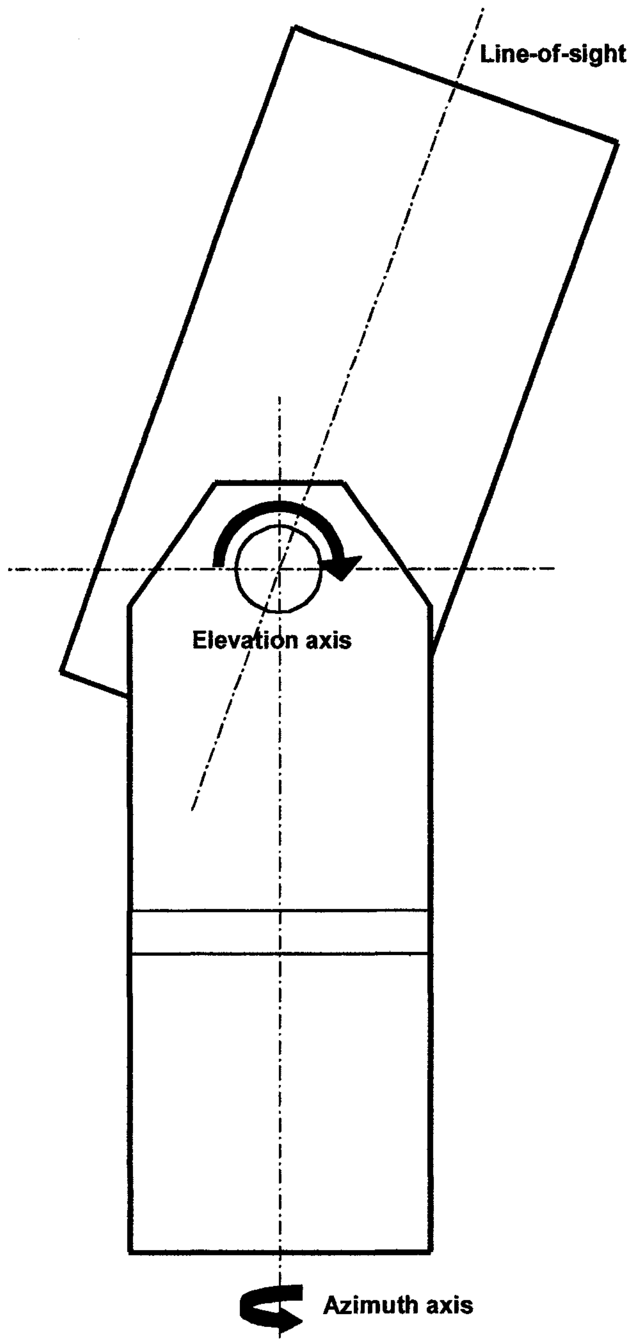

Figure 2.6 General arrangement of an altazimuth telescope mount

The optical system is mounted in a *tube* or *optics support structure (OSS)*. The tube usually consists of a *center-section* and a *truss*. The center-section is a structure that connects the truss to the fork through the elevation bearings. The tube supports the optics and maintains their alignment and separation as the telescope is pointed to different parts of the sky. For a small telescope, a rigid metal tube is frequently used, providing a structure rigid enough to make flexure negligible. In a larger telescope, a solid tube is no longer structurally efficient and leads to optical errors associated with thermal anisotropy of the air within the tube. An open truss is used instead (Meinel, 1965).

In a large telescope, flexure within the tube can produce deformation that is well outside the tolerances of the optical design. Instead of trying to eliminate deformation, the truss is often designed to minimize the effect of deformations on performance. For the common optical designs, distortions are minimized if the primary and secondary mirrors maintain their relative position and orientation (Schroeder, 1987). This requires equal and parallel flexure of both ends of the truss.

An early solution to the problem of designing a structure that behaved this way was developed by Serrurier (1938) and has come to be called a *Serrurier truss*. It uses a rigid central box structure with a simple triangular truss connected to each side to support the optics mounts. Proper sizing of the members ensures that the optics deflect equally and in a parallel fashion regardless of where the telescope is pointed. Many telescopes use the Serrurier truss or a variation but there is a size above which a single bay truss is no longer sufficient. Meinel and Meinel (1986) discussed a variety of truss topologies for large telescopes and considered the performance of each when subjected to gravity and wind forces.

2.2.4 Bearings

In an altazimuth telescope, an azimuth bearing between the base and fork allows the telescope to turn in azimuth and a pair of elevation bearings between the tube and fork provides for elevation motion. A similar arrangement is used on an equatorial telescope.

Bearings serve two functions in a telescope: supporting loads and defining the axes of rotation. The bearing systems used must provide high stiffness to resist disturbances while having low frictional drag. The relative importance of each depends on the application and specific telescope design. On the W. M. Keck Telescope, stiffness was sacrificed to reduce friction (Sirota and Thompson, 1988).

Both rolling element and hydrostatic bearings are used on modern telescopes (Siegmund et al., 1995; Sirota and Thompson, 1994). Rolling element bearings are relatively inexpensive and are commercially available in diameters up to about 3.6 meters (Chivens and Chivens, 1999). However, high friction at low speed with rolling element bearings presents a major challenge for a control system (Haessig and Friedland, 1991).

Hydrostatic bearings allow the axes to turn with very little friction but are relatively expensive, produce more heat than rolling element bearings, and require more frequent maintenance. Chivens and Chivens (1999) discussed the important influence hydrostatic bearings have had on the design and performance of large optical telescopes.

Meinel (1965) stated that hydrostatic bearings are necessary for telescopes larger than 2.1 meters because rolling element bearings produce too much friction. After reviewing several alternative bearing choices for a new 4.2-meter telescope, Hermann et al. (2000) concluded that ball bearings were most suitable, partly because friction, though high, does not vary greatly. This apparent disagreement reflects control system improvements made possible over the last few decades.

2.2.5 Drives and Control System

Pointing the telescope involves adjusting and maintaining the angular position of two or more rotational axes with a precision on the order of 1 μrad. Angular motion of this precision is difficult to achieve and requires that a number of subtle effects be considered in the control system design. Progress in precision control is occurring rapidly and is partially responsible for renewed interest in reducing other system errors that affect telescope pointing.

A typical telescope control system consists of one or more motors on each axis, a position sensing system, control electronics and a computer system. The motors may be mounted directly on the motion axis or may turn the axis through a reducing mechanism. Historically, high reduction worm drives were used to produce a "stiff" axis that did not respond to external disturbances. Gear drives are subject to backlash and wear that limit their performance. On telescopes built more recently, metal-on-metal friction-coupled reducers are frequently used. Large torque motors mounted directly on the motion axes are also utilized.

The angular position sensing system measures the angular position of each axis and the computer and electronics control the motion of the motors. Two basic types of position sensors are used: inductive resolvers and optical encoders. Both function in a similar manner and the generic term "encoder" is used to refer to any angular position sensor. Encoders can be mounted directly on the motion axis or may be friction-coupled. Packaged units are sometimes used but many large telescopes built recently use tape encoders consisting of a metal tape with precisely etched marks and electronic detectors (read heads) to sense the passage of the marks.

The control electronics include the signal generators, power supplies, and amplifiers needed to drive the motors and read the encoders. A wide variety of computer types are used as well as a broad range of control and user interface software. The mount model itself generally resides in the control computer.

The control system causes the telescope to point in the desired direction by sensing the difference between current position measured by the encoders and the desired position determined by the control computer. This difference is known as the *following error*. The control servo produces a drive signal related to the following error and that signal is amplified to cause the motors to move the telescope to decrease the difference. The rate at which the difference is recalculated and the drive signal revised is called the servo *update rate*.

For an astronomical telescope, the desired position of the telescope is usually known in advance and predictive control techniques are possible. Tracking a missile or other object for which the future track is not known in advance requires a different approach. Specific control algorithms are usually not important in mount modeling and were not addressed here. Similarly, servo errors were ignored except as sources of error in calibration measurements because they are dynamic and not generally compensated for in a mount model.

2.3 Current Approaches

In current practice, telescope mount models are used almost exclusively for one purpose: to correct positioning errors during observations. Positioning errors are important for several reasons, the most obvious being the ability to find and observe a particular object. Modern observing techniques in astronomy often require long exposures during which the telescope must accurately track an object's motion across the sky. Pointing errors may also affect operational efficiency in a tracking system (Keitzer et al., 1991), system accuracy for laser ranging (Rue and Fisk, 1968), or throughput in a communication system (Ulich, 1981).

Keitzer et al. (1991) listed the steps involved in formulating a telescope mount model:

- implementation of a mathematical model of the errors to be corrected;
- measurement of pointing error as a function of commanded data;
- computation of the parameters to be used in the error model equations; and
- execution of the equations in real time to generate corrected pointing angles.

Keitzer et al. were describing a general approach but went on to discuss an application on a 1.5-meter laser ranging telescope using a proprietary software package called STARCAL. A common software package used for astronomical telescopes, TPOINT, is used in a similar fashion (Wallace, 1993).

Both STARCAL and TPOINT use a physical error approach (Keitzer et al., 1991; Wallace, 1993). In addition to terms for physical errors, the TPOINT program also provides for the inclusion of arbitrary polynomial and harmonic terms to model errors. The extra terms could be used to compensate for residual errors remaining after constructing a model based on geometric terms or could be used for a pointing model based solely on empirical terms (Wallace, 1993).

Using either STARCAL or TPOINT, calibration measurements are made by pointing the telescope at stars with well-known positions and recording the difference between the observed positions reported by the telescope encoders and the actual star locations. Error measurements are usually made using an electronic camera and 30 to 80 stars (Keitzer et al., 1991). Wallace (1993) suggested using 50 to 100 stars for a medium fidelity TPOINT model.

Lewis et al. (1994) described the mount modeling process used for the W. M. Keck telescopes, currently the largest in the world. Five physical errors and three empirical harmonic corrections are used. The process described did not include encoder errors and it was noted that some of the model coefficients may have been accounting for the omitted effects. Between 40 and 100 stars are observed with a CCD camera to obtain the data for mount modeling and the model is fit using TPOINT.

On the tracking telescopes at the Air Force Maui Optical Station (AMOS), the mount model is updated frequently, usually before each satellite pass. A customized model for the pass is created using stars near the predicted path. Ten stars are typically used but more may be required if significant changes to the mount have been made. A model may be incrementally improved "on the fly" using a single star (Air Force Research Lab, 1999).

Ulich (1981) described the pointing calibration process for millimeter wave radio telescope antennas. The error terms in the model are similar to those described above and it was suggested that about 50 stars evenly distributed over the sky be used. Ulich noted that the mount for the Multiple Mirror Telescope (MMT) is similar to those used for large radio telescopes and presented results from a pointing model fitted for the MMT using observations made through a small auxiliary (guide) telescope.

2.4 Telescope Error Sources

Errors that affect pointing arise during the manufacturing, assembly, installation, and operation of a telescope. Machining errors in the bearings and other components can allow the axes to wobble while turning and introduce cyclical and random errors. Misalignments during assembly can produce geometrical variations in the kinematic relationships between axis position and pointing direction. Similarly, if the telescope is not installed properly, additional geometrical variations are introduced. The purpose of the mount model is to compensate for these effects. Several important sources of error considered in a mount model are described below.

In general, errors from a particular source have two components: a deterministic part and a random part. The relative magnitudes of the two components will vary depending on the ultimate source of the error. For example, if the telescope is not level, a pointing error will be produced but this error would be entirely deterministic since it arises from a constant geometrical error. Errors originating from a bearing, on the other hand, might be expected to have more randomness resulting from the components moving with respect to each other.

Constructing a mount model for correcting pointing errors requires identifying all error sources. Thoroughness is important because, if the model is incomplete, effects from unmodeled sources may be attributed to effects in the model and the parameters will no longer relate to the physical errors, even when the fit is good. When the goal is simply to make corrections, however, knowledge of the cause of each error is not required. The same situation arises in robot calibration and was described by Chen and Chao (1986).

When estimating the individual parameters, an understanding of the cause of each physical error may be helpful. Knowledge of the relative magnitudes of each error, the expected distribution of each parameter, and the mathematical relationships among the terms can be used to improve the parameter estimates. In this section, previous findings regarding the physical errors in telescopes is reviewed to quantify the expected magnitude of each error, make predictions regarding the distribution, and identify the relationships and interdependencies that might be present in the data. The expected magnitude for each error was also used to construct realistic simulated data sets to complement the real telescope data used to develop the model described in Chapter 4.

The physical errors in a telescope arise from four main sources: manufacturing errors in the components, assembly errors in the system, installation errors, and disturbances that occur during operation. Keitzer et al. (1991) divided the errors into three classes. Component errors and system assembly errors were grouped together and referred to as *intrinsic errors*. They are integral to the telescope and are difficult to change. *Installation errors* occur when the telescope is set up in the field and relate to the orientation of the telescope with respect to the earth. Errors resulting from wind, temperature, vibration, and gravity acting on the telescope were called *environmental errors*. In addition to errors in the telescope, observations may also be effected by measurement errors, mainly from the atmosphere and the detector.

Fisk and Rue (1966) listed six sources of error relating the orientation of a gimbaled sensor to a fixed reference. Modifying their terminology to correspond to that used here, their list included inaccuracy of the encoders, mislevel of the gimbal, runout of the gimbal bearings, nonperpendicularity of the gimbal axes, misalignment of the optical axis, and servo error. They did not consider elastic deformation within the system but otherwise their list is essentially the same as that produced by Keitzer et al. (1991).

Lewis et al. (1994) presented a typical "pointing flow" to describe how various factors affect the observed position of a star. In addition to the effects from the telescope, they included astronomical motions that determine where a star appears in the sky. The telescope effects considered included azimuth axis tilt, axes nonperpendicularity, pointing origin, position of rotator center, secondary mirror position, tube elastic deformation, empirical corrections, guider corrections, and telescope servos. Prestage et al. (1998) presented a similar diagram for a radio telescope and included several empirical terms.

2.4.1 Manufacturing Errors

Manufacturing errors occur in individual components and in the system assembly. System assembly errors generally relate to misalignments in the geometry introduced during assembly at a manufacturing facility or in the field. For large telescopes it is often impractical or impossible to manufacture components to the accuracy that would be required to eliminate assembly errors. A practical solution is to machine components to commercial specifications and compensate during assembly by carefully measuring and adjusting until the required precision is achieved. Similarly, shipping limitations often require that a large telescope be partially assembled on-site where conditions limit the accuracy that can be achieved.

Two critical tasks accomplished during the mechanical assembly of the system are positioning the gimbal axes relative to each other and aligning the optics. The gimbal axes must be made perpendicular and, ideally, to intersect. Optical alignment consists of installing the mirrors so that their axes are aligned to the mechanical axes of the telescope and to each other. Each of these alignments is fixed when the telescope is assembled and does not change considerably unless the telescope is disassembled, as might be the case during major maintenance. In addition, ordinarily there is no mechanism by which any of the mechanical alignments would be affected by the angular position of the telescope except for the flexure discussed below. Some variation in these alignments might result from vibration or thermal anisotropy but true random errors would be unusual.

The component errors relate primarily to bearings and encoders. These are generally commercial off-the-shelf components and a great deal of information regarding their errors was derived from manufacturers' data, a consideration of their construction, or from measurements made by others. Errors generally originate with machining of bearing races, drive surfaces, or similar large circular pieces.

2.4.1.1 Axis Nonperpendicularity

Ideally, the rotation axes of a telescope intersect and are exactly perpendicular. In practice, the angle deviates slightly from 90° as illustrated in Fig. 2.7. Setting and measuring the axis perpendicularity during assembly can only be done with a precision of about 25 μrad (Wallace, 1996). Nonperpendicularity causes the motions of the axes to influence each other and, if the error is extreme, the telescope cannot be pointed to certain locations of the sky. If the axes fail to intersect, no pointing error is introduced but performance for some applications is degraded. Intersection errors were not considered in this work.

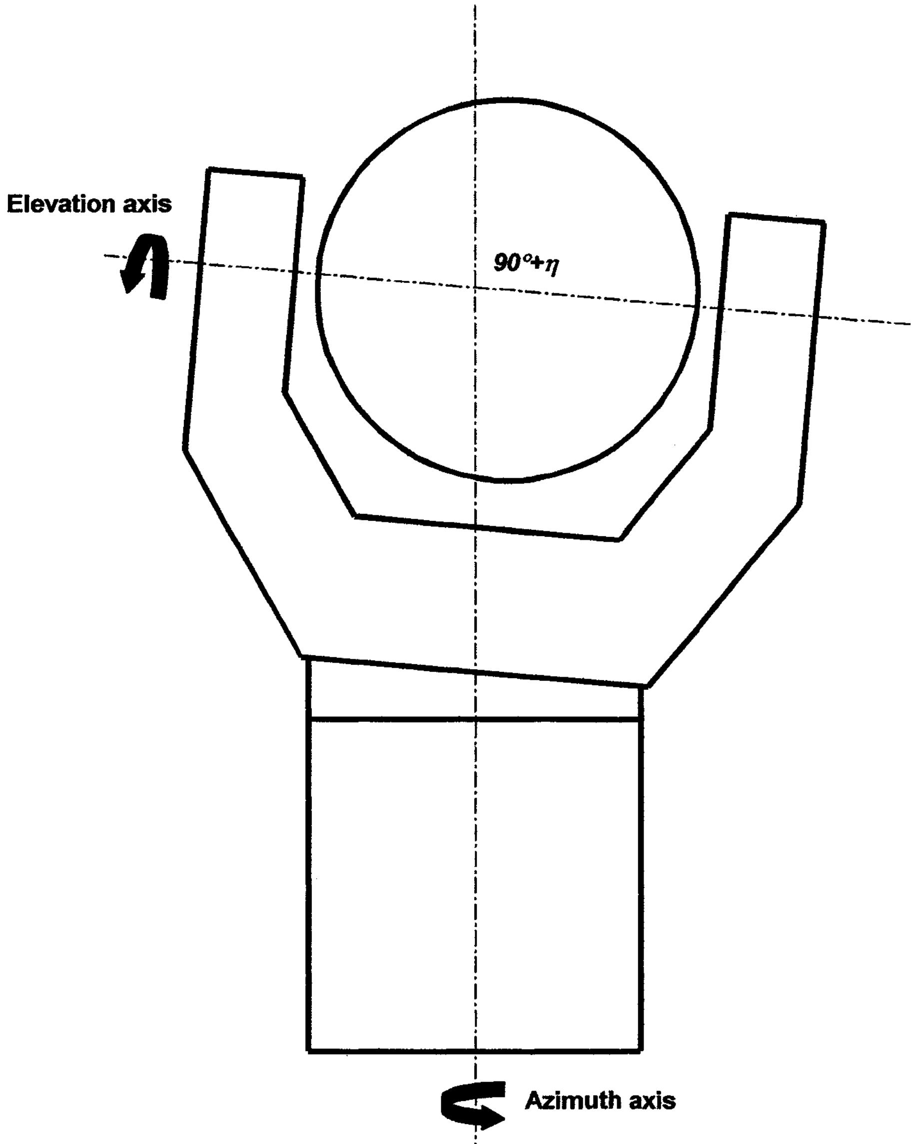

Fig 2.7 A telescope with nonperpendicular axes (from south, looking north)

2.4.1.2 Optical Axis Misalignment

The optical axis of a telescope should be perpendicular to the elevation axis and parallel to the azimuth axis when the telescope is pointed at the zenith. If this is not the case, the angle between the optical axis and elevation axis can be decomposed into a rotation about a line perpendicular to both the elevation and azimuth axes (the AZ-EL line) and a rotation about the elevation axis. The rotation about the elevation axis is indistinguishable from an offset in the elevation encoder. The rotation about the AZ-EL line is illustrated in Fig. 2.8. Wallace (1996) suggested this misalignment is typically "a few tens of arcseconds." A figure of 125 μrad was used which is consistent with that estimate.

2.4.1.3 Bearings

Bearings define the axis of rotation and allow the telescope axes to turn freely. Wobble and runout in a bearing cause the instantaneous axis of rotation to change and directly result in pointing error. These errors can be separated into repeatable and random components. In a telescope, the mount model will compensate for much of the repeatable error in the bearings while the random component contributes to the overall pointing variability. The errors contributed by rolling element (ball) bearings and hydrostatic bearings are similar in form but have different magnitudes.

A large ball bearing consists of three main components: inner and outer races (rings), balls, and separators. The geometric errors originate primarily from imperfections in the balls or races (Kimbrell et al., 1991). The separator can have a significant influence on torque variation, but, with proper selection, its effect can be neglected. The races of a large bearing are usually machined steel rings. Steel balls are placed between the races so that the balls roll on both and allow one to move with respect to the other. Imperfections in either race will cause relative translation between them and produce runout in the bearing that has a low frequency cyclic form. A ball that is misshapen will have the same effect but the frequency will be higher and continuous reorientation of the balls caused by rolling will effectively randomize the effect.

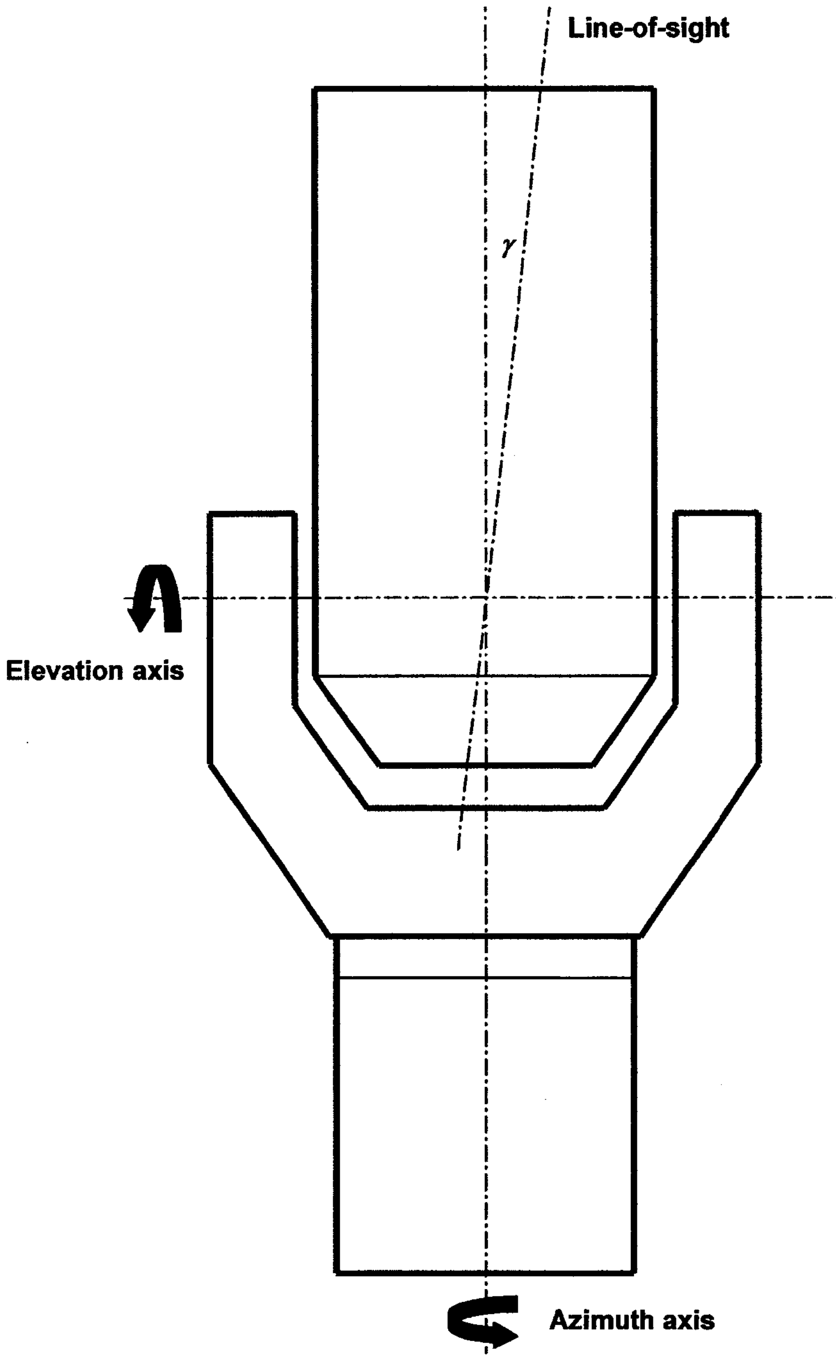

Fig 2.8 A telescope with misaligned optical axis (from south, looking north)

Manufacturers' data was used to estimate the error in bearings. Rotek Incorporated (1995), one of only a few manufacturers of large bearings stated its commercial precision capability for a 60-inch diameter bearing as 0.0006 inches total indicated runout (TIR), an error of approximately 1 part in 100,000. Other manufacturers quoted similar capabilities but most can provide better precision for the custom bearings used on telescopes (Kaydon Corporation, 1991). A TIR of 1 part in 100,000 produces a tilt error of 10 μrad. Siegmund et al. (1995) made extensive measurements of telescope bearings and components (drive rings) similar in shape and material to those used for large bearing rings. Those measurements and subsequent analysis showed that the errors typically were slightly less than the 1 part per 100,000 estimate, were harmonic and that approximately 75% of the error was repeatable and could be removed with low frequency harmonic correction terms.

Robinson and Spracklin (1966) discussed the design, manufacturing, and analysis of hydrostatic bearings for deep space communication antennas with requirements similar to those of large telescopes. A hydrostatic bearing supports a load through pressure in a thin film of fluid between two hard surfaces. The axis of motion is defined either by the accuracy of the hard surfaces or by a smaller, rolling element bearing incorporated for this purpose. Errors may be introduced by both the defining surfaces and by pressure fluctuations in the fluid supplied to the bearing. The defining surfaces are similar to large ball bearing rings and similar errors can be expected. Chivens and Chivens (1999) measured a 39 μrad repeatable error in a telescope hydrostatic bearing. Random errors are highly influenced by the design of the hydraulic system and are difficult to predict.

Any bearing may also have *point defects* which cause local errors centered around a particular rotational position. Modeling a point defect with a harmonic series requires very high frequency terms and is difficult in the context of telescope calibration. No provision for point defects was made in this work.

Kimbrell et al. (1991) considered the dynamic effect of random errors in bearings on telescope control systems and concluded that the effect is negligible compared to about 4 μrad of encoder and torque ripple error they observed. Improvements in motors and encoders in the last decade have reduced the effect of torque ripple and encoder error so that random bearing errors may no longer be negligible in comparison. Their results, however, provided an upper bound of about 4 μrad to the amount of random error expected from ball bearings.

Using the 10 μrad figure from above and the finding of Siegmund et al. (1995) that approximately 25% of the total was random error, each of the three bearings in a telescope introduces about 2.5 μrad of random error. The total repeatable and random errors are 17.3 and 4.3 μrad respectively when the effects are added in quadrature. Because bearing errors result from a combination of several independent effects, they will be approximately normally distributed according to the central limit theorem (CLT).

2.4.1.4 Encoders

The encoders sense the mount position during calibration and operation. Mancini et al. (1997b) discussed the sources of error in packaged optical encoders typical of those used on telescopes and described strategies for minimizing the effect of those errors on performance. Low frequency errors result primarily from the mount of the encoder and can be reduced using multiple sensor heads and careful mounting design. These errors are typically eliminated during assembly or set up. Two low frequency, static encoder errors are typically compensated for in mount models: scale errors and offset errors (Lewis et al., 1994). A scale error is an error that is proportional to position while an offset error is a constant error regardless of encoder position. Both can be removed in the mount model or in a separate encoder model.

Medium frequency errors arise from imperfect manufacturing of the encoder scale (Mancini et al., 1997b). High quality manufacturing, inspection, and calibration make medium frequency errors negligible (Ravensbergen, 1994). High frequency errors are caused by electronic noise and are typically of order 0.1 μrad (Mancini et al. 1997b). Techniques for calibrating high precision encoders were described by Kimbrell et al. (1991), Ulich (1981) and Hall (1976).

Most encoders used on modern telescopes are digital and produce small decimation errors related to the fact that a small range of axis position is read identically by a digital encoder. The magnitude of the decimation error is the same as the resolution of the encoder and will be uniformly distributed because, within the range of identically-read positions, any true position is equally likely. Newer telescopes typically use encoders with 27 bit resolution corresponding to a decimation error of 0.047 μrad (Mancini et al., 1997b).

When an encoder is not mounted directly on the telescope axis, relatively large errors can occur in the mounting system or in the mechanism that couples the encoder to the telescope axis. Some telescopes use friction-driven encoders that transfer the motion through a friction roller. An analysis of the additional errors introduced by this type of mounting was provided by Siegmund (1992) and the W. M. Keck Observatory uses a separate kinematic model to remove harmonic errors resulting from the encoder mounting (Lewis et al., 1994).

Rue and Fisk (1964) presented a model for the error in induction resolvers, a type of position sensor sometimes used on telescopes but which utilizes magnetic rather than optical techniques to sense position. The same principles used for considering the errors in optical encoders can be applied to resolvers without significant changes to the mount model. The telescope analyzed by Keitzer et al. (1991) and discussed above incorporates induction resolvers.

2.4.1.5 Other Manufacturing Errors

This analysis assumed that the there were no pointing errors introduced by the optical design, manufacturing, or alignment. In practice, there are optical errors present in a telescope but they are generally too small to significantly affect pointing. Errors related to the design or manufacturing of the optics usually do not depend on position and are constant. Optical errors related to structural deformation of a telescope may be position-dependent.

2.4.2 Installation Errors

Even a perfectly manufactured telescope is subject to errors being introduced during installation at an observing site. Installation involves preparing the site with a rigid foundation and usually a protective enclosure for the telescope. The telescope is then attached to the foundation, leveled, and oriented with respect to north. The geographic location and current time are also set to ensure that true star positions are calculated correctly.

2.4.2.1 Leveling and Compass Orientation

When a telescope is installed on a foundation, it will seldom be perfectly leveled. Any tilt changes the pointing direction and must be compensated for in the mount model.

Tilt in an arbitrary direction can be decomposed into tilt in two separate, orthogonal directions. For this work, the tilt was decomposed into a northward component and an eastward component. The effects of these tilts on the telescope axes are illustrated in Figs. 2.9 and 2.10.

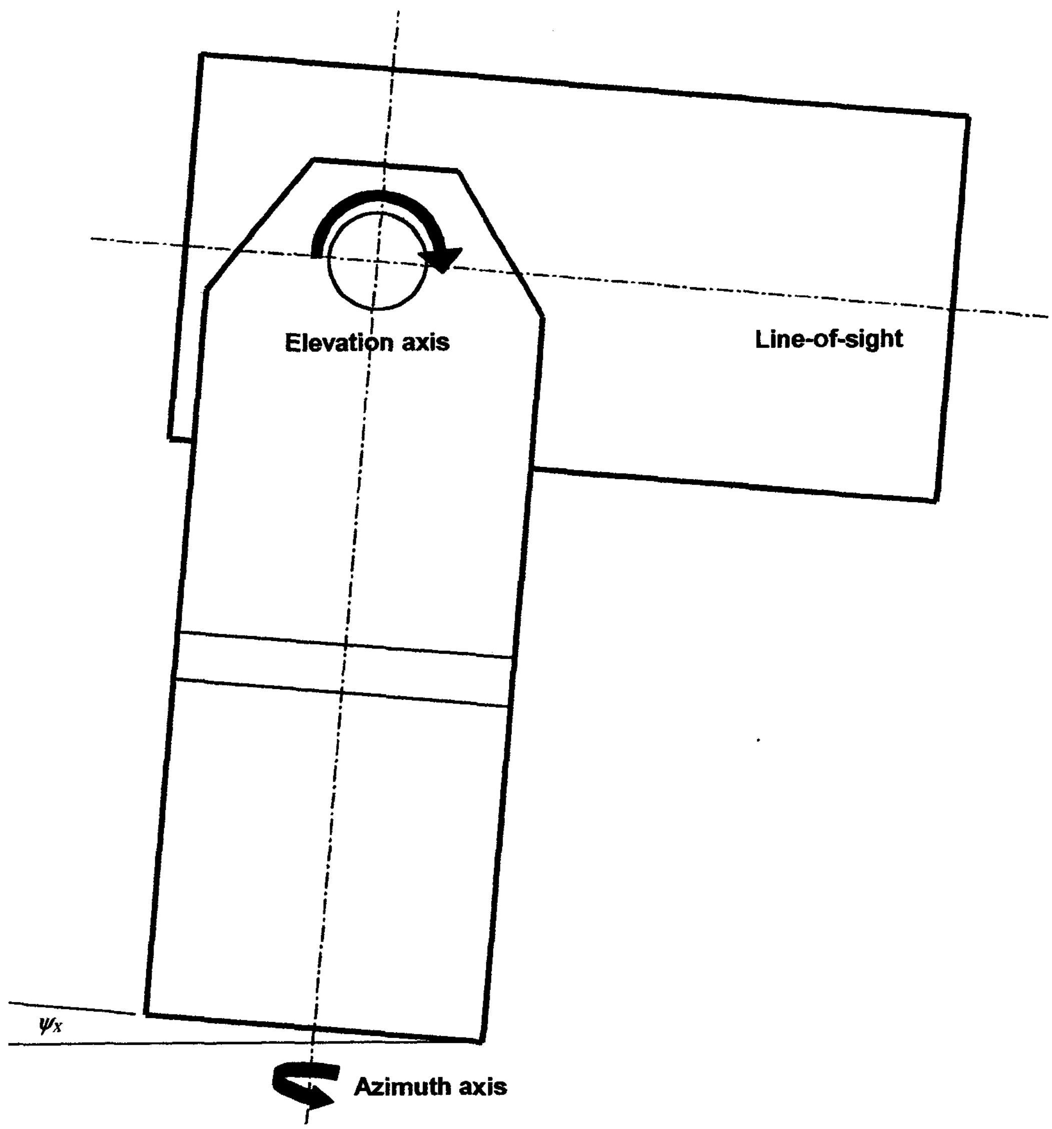

Figure 2.9 A telescope tilted toward the north (from east, looking west)

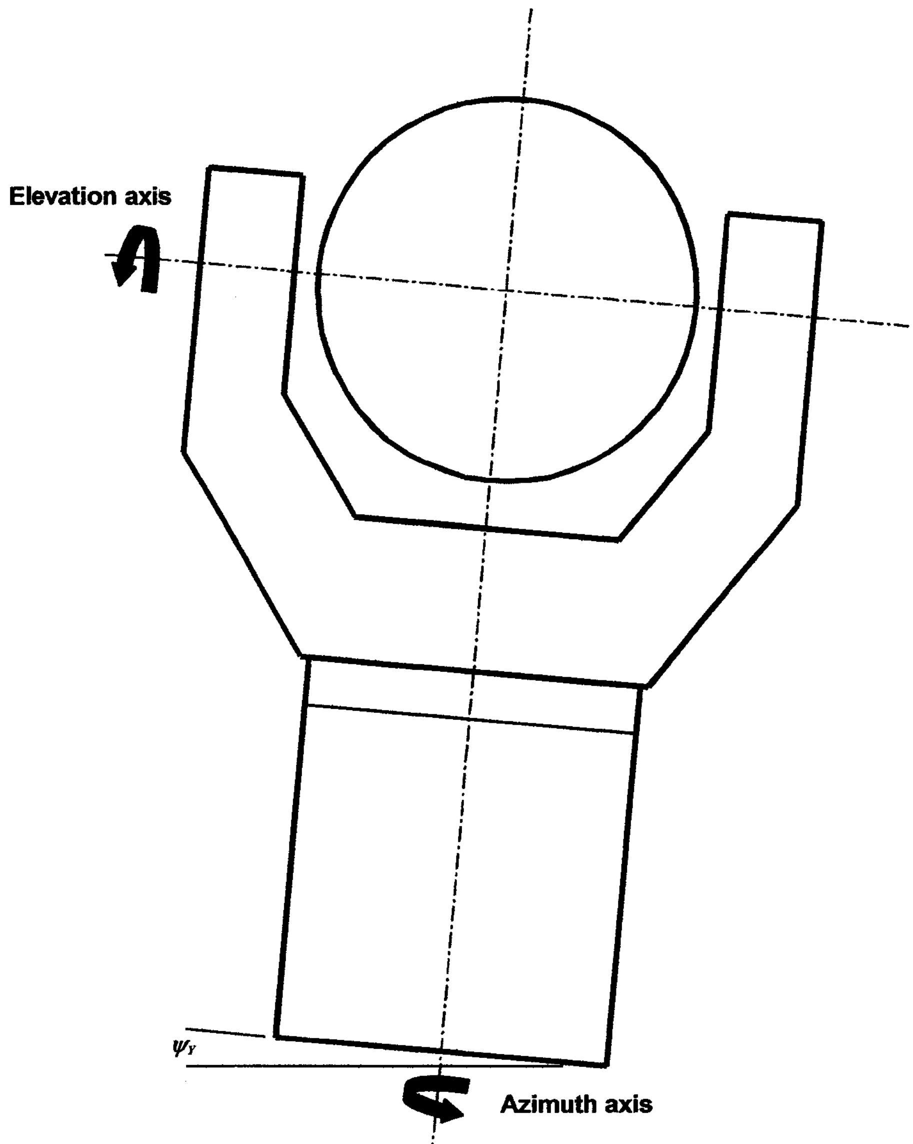

Figure 2.10 A telescope tilted toward the east (from south, looking north)

During installation, leveling is usually carried out using precision bubble levels or survey techniques to sense the local direction of gravity. Precision levels can be used to orient a telescope with respect to gravity to within about 300 μrad. However, a telescope should be aligned parallel to the earth's axis of rotation which, because of the equatorial bulge of the earth, differs from the direction of gravity by about 300 μrad in the north-south direction at middle latitudes (National Almanac Office, 2000). A 300 μrad bias results even when there are no other installation errors. The error in detecting level adds in quadrature so a value of 425 μrad was used to estimate the maximum expected tilt error in the north-south direction. East-west tilt is not subject to this bias so a maximum error of about 300 μrad was assumed. Once the telescope is level, it is usually permanently attached to the foundation using grout to establish a rigid connection. This "locks in" the tilt errors and they would not be expected to exhibit significant variability over a short period. Over a longer period of time settling and other effects could change the tilt angles.

Even when a telescope is rigidly attached to the foundation, movement of the foundation in response to external disturbances or reaction torque from the telescope drives will cause random variations in the tilt of the telescope. Sobek and Kimbrell (1999) discussed the effect of the telescope foundation on the control system and showed that, for several hypothetical examples, foundation motion contributes less than 1 μrad to the overall jitter. They noted, however, that the actual magnitude depends on the particular design of the foundation and telescope in combination. This error will be normally distributed by the CLT.

Aligning the zero-point of the telescope encoders with true north requires rotating the entire telescope on the foundation. Since installation is often carried out under adverse conditions on a mountaintop, a relatively large allowance of up to a few degrees is often made for this. The effect of compass orientation errors is similar to that of encoder offset errors and is compensated using the same term.

2.4.2.2 Initialization

The calculations for the true locations of the calibration stars require accurate knowledge of the geographic location of the telescope and of time. Small errors in geographic position have negligible impact on pointing but errors in the measurement of time can be important.

Geographic (geodetic) position is established through surveys, GPS signals, or other techniques and can be determined with high accuracy. There may be a small difference between the astronomical coordinates of an observatory and the geodetic coordinates and the difference may vary with time (National Almanac Office, 2000). This difference may affect calculations of the true position of celestial objects but was ignored here. Similarly, at modern observatories time is measured using clocks with negligible error. Historically, time errors were inseparable from longitude errors but this is no longer the case.

2.4.3 Operating Errors

Telescopes are usually exposed to the environment during operation and are subjected to a variety of disturbances, chiefly gravity, temperature, and wind. Gravity causes the truss to deflect as the elevation angle changes but may also have other effects. Temperature changes modify the shape of the structure through thermal expansion and can alter the physical properties as well. Wind introduces vibration into the telescope and creates forces on the structure that must be counteracted by the drives. In addition, kinetic effects caused by a telescope's own motion, geophysical and seismic movement, and factors relating to telescope maintenance and operating procedures may have an impact. Most operating errors are random and unpredictable and were considered only as sources of variation. Flexure and atmospheric refraction are exceptions and have significant deterministic components.

2.4.3.1 Flexure

The optics and instruments on a large telescope are often massive and can produce significant structural loads on the telescope that must be supported by the gimbal structure and tube. One advantage of the altazimuth configuration is that the fork itself maintains the same orientation with respect to gravity regardless of where the telescope is pointed and only tube flexure is significant. Other configurations do not have this characteristic and one or more mount deflections must be considered.

There are four sources of loads in a telescope: the weight of the optical components and instruments, inertial forces from the motion of the telescope, forces from wind and other environmental disturbances, and the weight of the structure itself. If a telescope is small enough or rigid enough, structural deformations will be negligible but, as size increases, material limitations make it increasingly difficult to maintain high rigidity. Maintaining a low thermal mass is also important in telescopes and this requirement restricts the structural design choices available. Sacrifices in rigidity lead to significant structural deformations in large telescopes.

Loads on the telescope structure change due to inertial forces from the motion, wind, and the changing direction of gravity as the telescope is pointed to different parts of the sky. The only major component of an altazimuth telescope that experiences significant changes in the direction of gravity loading is the tube. Because such a wide range of truss designs are used and because the flexure depends on the size of the telescope, it was difficult to estimate the flexure for this work based on structural calculations. Figure 2.11 illustrates how flexure affects the line-of-sight.

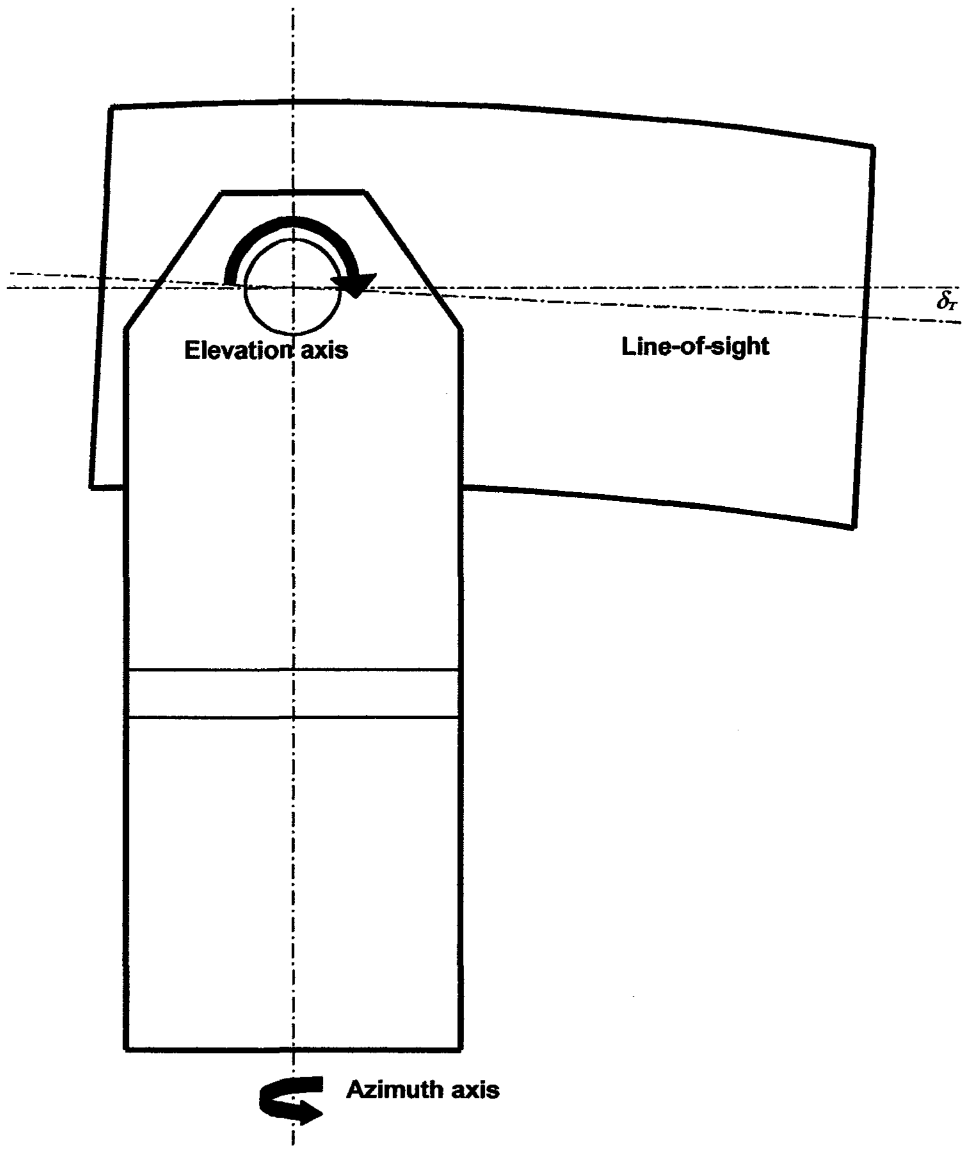

Fig 2.11 The effect of flexure on telescope pointing

Tube flexure may not always be completely repeatable, especially when the temperature changes because the elastic properties of a material depend on temperature. Boyer and Gall (1985) said that, for a metal, Young's modulus is inversely proportional to the fourth power of the unit cell dimension. They provided a graph of the variation for iron showing the Young's modulus decreasing about 22 GPa for a 100° C temperature rise, a change of about 0.1% per degree Celsius. For a telescope operated at a temperature that is 10° C different from that at which it was calibrated, the change in elastic modulus decreases the flexure by 1% and this was assumed for this work. This suggests the flexure term of a mount model may exhibit a small temperature dependence that will contribute to the random error if not modeled.

Elastic hysteresis refers to failure of a structure to deform exactly the same amount during successive applications of the same load and is typically insignificant unless a structure is loaded close to its yield strength (Young, 1989). Because telescope structures are designed for rigidity, their internal stresses are usually very low but, in some instances, especially when composite materials are used, hysteresis could be a factor. Siegmund (1997) allocated about 5 μrad to mechanical hysteresis in a large telescope. Combining this allocation with the effect of uniform temperature change yielded a flexure nonrepeatability error of 5.4 μrad. Since hysteresis is a manifestation of a large number of microscopic effects, the errors will be approximately normally distributed by the CLT.

2.4.3.2 *Thermal Expansion*

Good optical performance of a telescope often requires it to be operated at the same temperature as the surrounding air. This not only means that the telescope is usually operated at a different temperature from which it was calibrated, but also that its operating temperature is continuously changed to match the environment. These temperature changes may affect pointing by causing the structure to change shape.

Thermal expansion causes a structure to increase in volume as temperature increases. Over the distances spanned by large telescope structures, dimensional changes are significant. Mechanical symmetry and the properties of common optical designs mitigate the impact of uniform temperature changes but nonuniform temperature changes may have a significant and complex impact on pointing. Low thermal expansion materials are available and are commonly used for telescope components but they are relatively expensive and cost prohibits their widespread use for telescope structures. Instead, steel or cast iron is usually used and special devices are implemented to mitigate the effects of thermal expansion. For this work, it was assumed that there were no pointing errors due to thermal expansion. Several authors have described techniques for mitigating the effects of thermal distortion in large structures.

Lugten (1998) proposed the use of a thermally stable reference structure to improve pointing of an array of radio telescope antennas. The reference structure would be constructed from low thermal expansion material and would be used to detect changes in the shape of the mount that could then be compensated for using active pointing corrections.

Soons (1997) instrumented the struts of a hexapod milling machine with thermocouples and used the measurements in a thermal model to correct positioning errors caused by temperature changes. The W. M. Keck Observatory has experimented with using measured temperatures and a thermal model of the structure to correct for the effects of thermal expansion on pointing with generally good results (Sirota, 1998).

Related expansion phenomena are also exhibited by materials occasionally used for telescopes. For instance, some composite materials expand in response to changes in humidity when not properly sealed. Because these materials are sometimes used for telescope tubes, this effect should be recognized as a potential source of random error. Similarly, dimensional instability of any material may produce changes over time but would not be expected to be significant in a telescope when the mount model is periodically updated.

2.4.3.3 Optical Alignment

Optical errors produced during operation also degrade pointing. For the most part these errors are caused by the flexure and thermal expansion of the truss which cause the optical elements to move relative to each other and produce misalignment and optical aberrations. Schroeder (1987) provided expressions for the aberrations produced in the classical Cassegrain optical design considered here. Huang (1993) derived expressions for the influence of various errors on the line-of-sight of the Gemini telescopes, a pair of 8-meter altazimuth telescopes recently constructed. Schroeder's and Huang's formulas can be used to estimate the line-of-sight errors produced by structural deflections.

It is common practice to relax the required optical quality when a telescope is pointed away from zenith, partly to account for flexure and partly to recognize the fact that the optics mounts will not perform as well under changing gravity loading. One approach is to relax the system optical specification at the same rate that atmospheric distortion degrades the optical performance away from zenith. Levi (1968b) gave an equation that showed this degradation is proportional to the cosine of the zenith angle to the three-fifths power. Using Levi's formulas, the seeing at 45° elevation (a plausible mean elevation of calibration stars) when observing from a height of 2400 meters is approximately 1.25 times worse than at zenith. The error associated with detecting star positions during calibration was increased by the same factor. The atmosphere produces optical errors that are approximately normally distributed (Schroeder, 1987.)

2.4.3.4 Servo Error

The servo system requires a following error to function. A typical value for the following error is five encoder counts, about 0.5 μrad assuming an encoder resolution of 0.1 μrad. The distribution of the servo error on each axis was assumed to be normal with a standard deviation of 0.5 μrad. The resulting squared pointing error, defined by the quadrature sum of the two errors has a chi-squared distribution with two degrees-of-freedom. The distribution of the simple pointing error is the square root of this and is not a named distribution.

In addition, several disturbances cause dynamic errors in the control system that are generally not considered in mount models. They contribute to the pointing errors observed when the telescope is in operation and they produce variability in the calibration data. Three major contributors to this random error are friction, torque ripple, and kinetic coupling.

Friction affects the control system in two ways. Constant frictional drag increases the drive forces and produces additional deformation in drive components. Stick-slip friction at low velocity creates nonlinearities in the telescope response that are difficult to handle. Because tracking stars involves moving very slowly, the effects of low velocity friction on the control system is important. Haessig and Friedland (1991) described several models for predicting stick-slip friction at low velocity. Armstrong and Canudas (1996) also described modeling approaches and noted that friction generally increases at higher velocity but is not position dependent. This suggests that the effect of friction appears as random error in the mount model and in terms related to velocity.

The motors typically used on modern large telescopes exhibit an error known as *torque ripple*. Torque ripple refers to variations in torque that depend on the rotation angle of the motor. Improvements in drive and control system technology have reduced the magnitude of this effect on newer telescopes but it could be significant on older designs. Ravensbergen (1994) stated that analysis showed that torque ripple contributes negligible angular error to the performance of the Very Large Telescope (VLT), a group of 8.2 meter telescopes currently being commissioned.

Kinetic coupling refers to the quasistatic errors introduced by the fact that the telescope axes are moving. Variations in acceleration of the axes change the forces acting on the telescope structure and on the power demands from the drives. Velocity changes effect the axis friction and therefore the following error (Mancini et al., 1994a). Except near zenith, these effects are small and are generally ignored. The term *kinetic* is used to distinguish this effect from what are normally called *dynamic* effects: vibration, gusting wind, and similar rapidly varying disturbances.

2.4.3.5 Geophysical Factors

The geographical position and orientation of the telescope change constantly due to a variety of geophysical factors. These effects are very small and have historically been ignored. In a precise analysis of pointing errors, however, they may not be negligible. For example, satellite laser ranging (SLR) measurements have detected a 70 mm per year drift of an SLR station in Hawaii (Noll, 1999). Over a few years this motion can contribute to pointing error by effectively changing the geographic position of the telescope.

Earth tides are changes in the shape of the earth resulting from the pull of the moon and sun. They cause elevation and tilt changes in the earth's surface which affect the orientation of a telescope with respect to the earth. These changes have the same effect as the installation error produced by tilting the telescope on its foundation but are periodic and predictable, much like ocean tides. Earth tides introduce a bias error of approximately 0.2 μrad in calibration measurements if not accounted for. Short period, random changes in the surface of the earth resulting from seismic activity also occur but the effect is usually negligible.

2.4.3.6 Observatory Operations Factors

Several factors related to the operation and management of an observatory may also affect the reliability, accuracy, and usefulness of mount model results. If calibration is not carried out on a regular basis, observations made between runs may be less accurate. Similarly, if substantial maintenance or instrument changes are made to a telescope many of the physical errors corrected by the mount model may be changed. Finally, systematic errors in the catalog or procedures used to calculate the true calibration star position may affect results.

Local practice regarding the frequency of recalibration, the procedure for doing so, the time of day observations are made, the stars used in relation to local facilities, and many other factors may effect the quality of model produced. For example, if observations for a mount model are routinely performed on nights with marginal seeing, the resultant variability in the observations might unduly degrade the model.

For some telescopes, it is common to change instrumentation daily or even several times during an observing session. After a change, the telescope might be rebalanced but a new calibration may not be performed. On an astronomical telescope the dark observing time might be too valuable to use for mount modeling and, on a ranging or tracking system, instrument changes might be made during the day when no stars are available. These unmodeled changes would need to be considered as additional sources of error in pointing, not in the estimates of the physical errors.

Routine preventive maintenance of a telescope can also introduce changes. If part of the telescope is disassembled, loosened, or similarly adjusted, geometric changes might result that affect the kinematics. Undetected component failures would have a similar effect. A mount model performed immediately after a bearing is greased might not work as well when the grease breaks down and friction affects the servo system differently. This is not a concern when estimating physical errors but should be considered when making pointing error predictions.

Errors in the calculation of the true star positions must also be considered. While expected to be rare, at least one major observatory uses a separate calculation of star position during calibration as a check on the calculations made in the telescope control system (Lewis, 2000). Calculation errors in telescope control software would be expected to be systematic and might be detected through an analysis of the mount model similar to that used to detect physical errors in the telescope. Errors in the star catalogs used as the starting point for calculations also occur. In early 2001, a suspected fault in a navigational star tracker used for navigating NASA's Galileo spacecraft turned out, upon investigation, to result from a variation in the brightness of a reference star. Variation of star brightness is not unusual but in this case had not been recorded in the catalog (NASA, 2001). The star in question is one of the 50 brightest stars in the sky and would be a candidate for use when calibrating a telescope.

2.4.4 Measurement Errors

When calibration measurements are made, the measured star positions are affected by noise and unmodeled deterministic effects in the data. Observed star positions would be affected by errors in the atmosphere and the calibration detector, even if the telescope were perfect and had no physical errors. Understanding how these measurement errors affect the calibration results was useful for validating the results and for creating appropriate simulated data sets to use to validate the solution methods described in Chapter 5.

2.4.4.1 Atmosphere

The atmosphere blurs star images by spreading the light energy out. A statistical model of this behavior were developed by Fried (1966) and Racine (1996) derived simple expressions for the atmospheric blurring seen by a telescope. The atmosphere also causes star images to move around in the sky. The image motion can be separated into a constant term called *refraction* and a random term called *seeing* (Stock and Keller, 1960).

Refraction tends to raise objects above the horizon by an amount that depends on their elevation as well as the local temperature, humidity, and atmospheric pressure (Smart, 1977). Refraction corrections are relatively large and must be made for all observations, including those for calibration. The measured temperature and barometric pressure or the air near the telescope used for refraction calculations will typically not be exactly the same as for the air the telescope is looking through and an error will result.

Wallace (1996) gave a typical value of 0.7 μrad for this error when iterative corrections are not made. This error produces a random error in the calibration measurements as well as a random error in observed position after the correction applied by the mount model.

Correcting for seeing effects is a very active area of telescope research. Much of the seeing error can be removed by slightly tilting the secondary mirror or another small optic, effectively repointing the telescope enough to eliminate the error. This must typically be done at rates between 0.1 Hz and 10 Hz (Cullum et al., 1994). Because active corrections are seldom made during telescope calibration, they were not considered here. This means, however, that seeing errors must be considered as a source of variability in the mount model. Typical seeing at the zenith at good astronomical sites is about 2.5 μrad (Olivier and Gavel, 1994), defined as the root-mean-square (rms) motion of the image center.

2.4.4.2 Detector Errors

Calibration measurements for a mount model are made by pointing the telescope to a reference star and visually centering the star by moving the telescope axes. The position error on each axis is the angle through which that axis of the telescope had to be moved to center the star. Alternatively, the position errors can be measured directly using an electronic detector and sensing the position of the star in the field-of-view (Keitzer et al., 1991).

Cullum et al. (1994) listed the sources of measurement errors when using electronic cameras to detect the observed position of a star. Olivier and Gavel (1994) provided a detailed study of these errors and said that detection of star positions using a CCD and simple centroiding algorithms results in an error of approximately 0.2 μrad.

Gardiol et al. (1999) pointed out that resolution for a detector is limited by the pixel size and the scale of the telescope image on the camera. They gave a resolution limit of about 1.7 μrad for the Telescopio Nazionale Galileo although they noted that subpixel interpolation is possible. A 2 μrad random error was attributed to the position detection system for this work. Since, within a small region, the image of a star has an equal probability of falling anywhere with respect to the pixel grid, this error will have a uniform distribution.

2.4.5 Summary of Errors

Table 2.1 summarizes the maximum geometric error expected from each of the effects described in this section. Encoder offsets have been omitted because no realistic estimate of their magnitude can be made. Table 2.2 lists the estimated random error contribution from each component. Each table is a summary of the information presented in this section.

Table 2.1 Summary of geometric errors

Geometric Errors	Maximum Error (μrad)
Azimuth encoder offset	-
Elevation encoder offset	-
Optical axis misalignment	125
Axis nonperpendicularity	25
Tilt toward north	425
Tilt, toward east	300
Tube flexure	200
Bearings, low frequency	17.3

Table 2.2 Summary of random error sources in calibration data

Source	Error (μrad rms)	Estimated distribution
Bearings	4.3	Normal
Encoders	0.1	Uniform
Foundation motion	1.0	Normal
Flexure nonrepeatability	5.4	Normal
Optical errors (away from zenith)	0.6	Normal
Servo error	0.5	-see text-
Atmosphere (seeing)	0.5	Normal
Detection system	2.0	Uniform

2.5 Typical Results

Several astronomical observatories make their mount modeling results available and these can be used to quantify the expected magnitude of individual parameters and the amount of error typically present in models. The results presented below describe actual mount models used on large research telescopes obtained from several sources. Because telescopes are usually recalibrated periodically these results should be taken as representative, not the most recent or the best. In each table, the first column describes the source of the physical error being modeled, the second gives the mean value of the parameter, and the third its standard error. The units for all figures have been converted to microradians (μrad). In many cases the standard error of a parameter is relatively large and would seem to indicate the parameter is not statistically significant. It is common practice, however, to retain such terms in a mount model if they produce better pointing than a model lacking the term.

2.5.1 Approaches and Errors Modeled

Each of the telescopes for which results are described below uses TPOINT to analyze pointing data. The TPOINT program has its own nomenclature to refer to the various error terms and using that terminology here facilitated comparison. The names for the most common geometric terms are listed in Table 2.3 below along with the TPOINT expression for the error produced on each axis. Axis corrections are obtained by multiplying the expression in the table by a constant parameter determined during calibration. For example, northward tilt of the telescope is compensated by multiplying a parameter by $\cos A$ to calculate the elevation error and $\sin A \tan E$ to determine the azimuth error. In each case, A indicates azimuth angle, E indicates elevation angle, z indicates zenith angle ($90° - E$).

Table 2.3 TPOINT nomenclature for common telescope geometric errors

Source of Geometric Error	TPOINT Name	Azimuth Effect	Elevation Effect
Azimuth encoder offset	IA	1	0
Elevation encoder offset	IE	0	1
Optical axis misalignment	CA	$-\sec E$	0
Axis nonperpendicularity	NPAE	$\tan E$	0
Tilt toward north	AN	$\sin A \tan E$	$\cos A$
Tilt toward east	AW	$\cos A \tan E$	$\sin A$
Tube flexure (2 alternative models)	TX	0	$-\cot E$
	TF	0	$-\cos E$

In many cases the common terms are supplemented with empirical corrections to improve the results. When this is the case it is noted in each table and the equation for the correction is provided where available. Also, because there are two common representations for tube flexure, TX or TF is noted to indicate which is used.

2.5.2 Results for Working Telescopes

The Sloan Digital Sky Survey (SDSS) 2.5-meter telescope in New Mexico was dedicated in 2000. It is part of a project to systematically map one-quarter of the sky to determine the position and absolute brightness of more than 100 million celestial objects. Table 2.4 lists the parameters from a mount model provided by Owen (2001).

Table 2.4 Mount model results for the SDSS telescope

Source	Mean (μrad)	Standard Error (μrad)
Azimuth encoder offset	-1017.6	11.8
Elevation encoder offset	-894.3	10.7
Elevation encoder scale	+667.7	29.7
Tilt toward north	-21.9	3.8
Tilt toward east	-308.1	3.7
Optical axis misalignment	-1.79	9.1
Empirical: $\Delta A = \cos A \;\; \cos 2A \;\; \tan E$ $\Delta E = \sin A \;\; \cos 2A$	-2.81	5.1
Empirical: $\Delta A = \cos A \;\; \sin 2A \;\; \tan E$ $\Delta E = \sin A \;\; \sin 2A$	-5.04	4.7
Empirical: $\Delta A = \sin A \;\; \cos A \;\; \tan E$ $\Delta E = \cos A \;\; \cos A$	+0.73	5.6
Empirical: $\Delta A = \sin A \;\; \sin A \;\; \tan E$ $\Delta E = \cos A \;\; \sin A$	+8.78	5.6
Empirical: $\Delta A = \cos A$	-16.5	6.47
Empirical: $\Delta A = \sin A$	-4.95	6.24
Tube flexure (TX)	-6.06	12.6

The Astronomical Research Consortium (ARC) 3.5-meter telescope is located near the SDSS telescope and is operated by the same organization. Parameters from an early pointing model are listed in Table 2.5. The special empirical term is a third order harmonic term to compensate for runout in the elevation bearing (Owen et al., 1990).

Table 2.5 Mount model results for the ARC telescope

Source	Mean (μrad)	Standard Error (μrad)
Azimuth encoder offset	+439.2	36.8
Elevation encoder offset	-642.4	14.06
Tilt toward north	-1.9	2.9
Tilt toward east	+8.2	2.9
Axis nonperpendicularity	+103.7	52.4
Optical axis misalignment	-256.5	41.2
Empirical: special	+60.6	7.3
Empirical: $\Delta A = \cos A$	+15.0	5.3
Empirical: $\Delta A = \sin A$	+57.7	5.3

The Telescopio Nazionale Galileo (TNG) is a 3.6-meter altazimuth telescope located on the Canary Islands which became operational in 1997. Information for an early pointing model is listed in Table 2.6 (Gardiol et al., 1999).

Table 2.6 Mount model results for the TNG

Source	Mean (μrad)	Standard Error (μrad)
Azimuth encoder offset	+176.0	9.2
Elevation encoder offset	+249.2	5.3
Tilt toward north	+65.4	2.4
Tilt toward east	+145.0	2.4
Axis nonperpendicularity	set to 0	-
Optical axis misalignment	+63.5	5.3
Flexure (TF)	+210.9	9.2

The W. M. Keck Observatory operates a pair of 10-meter, segmented mirror telescopes on Mauna Kea on the island of Hawaii. Information for an early pointing model for Keck I was described by Lewis et al. (1994) and is repeated in Table 2.7. The standard errors of the parameters were not provided so that column has been excluded from the table.

Table 2.7 Mount model results for Keck I telescope

Source	Mean (μrad)
Tilt toward north	+2.9
Tilt toward east	+48.5
Axis nonperpendicularity	set to 0
Tube flexure (TF)	+198.8
Empirical: $\Delta E = \cos 2A$	+16.5
Empirical: $\Delta E = \sin 2A$	+15.5
Empirical: $\Delta A = \cos 2A$	-2.3
Empirical: $\Delta A = \sin 2A$	-26.7
Empirical: $\Delta E = \cos 2z$	+67.4

2.5.3 Modeling Problems

Because terms are introduced into a mount model to compensate for specific mechanical errors, it is generally believed that the mount model coefficients relate directly to the physical errors present in a telescope. The value of the coefficient on a particular term is interpreted as the magnitude of the physical error in the telescope. Because the physical errors are usually small and because the interest in mount modeling is usually focused on improving pointing performance, little attention has been paid to the accuracy of the individual parameter estimates. Comparing the standard error of each coefficient with the value of the coefficient in Tables 2.4 through 2.6 shows that some of the individual coefficients are not statistically significantly different from zero. This means that there may not be any true underlying error and would ordinarily suggest that the term related to that coefficient should be dropped from the model. Doing so, however, often produces a model that does not correct pointing as well as the model that includes that term.

Imprecision of the coefficients was a major focus of this research and arises partly because of random error in the data and partly because of the nature of the regression model used for pointing correction. When the effects of mechanical errors are put together in a kinematic model of a telescope, some individual effects are mathematically related causing the predictor terms in the statistical model to be correlated and degrading the estimates of the individual model coefficients. While this is a well-known problem in regression, no research was found which specifically addresses it in the telescope mount modeling application. Several authors, however, mentioned predictor correlation, generally only anecdotally.

Keitzer et al. (1991) explained that the correlation between two particular physical error terms, axis nonperpendicularity and optical axis misalignment, depends on elevation angle. They said that using terms that correspond to physical errors was better even though it results in a non-orthogonal set of predictors.

Ulich (1981) said that many of the model terms are not orthogonal and recommended using a large number of stars evenly distributed across the sky to ensure accurate estimates of individual coefficients. While increasing the number of stars improves the precision of the individual coefficient estimates, the improvement is gradual and it is impractical to use enough stars to reduce the error to a level that makes the individual estimates useful.

Wallace (2000) noted that predictor correlation causes the variance on individual terms in an analysis to become very large and commented that it is not unusual for the standard error in a single term to be larger than the standard error of the model as a whole.

No other literature was found which related specifically to the problem of precisely estimating the physical errors in a telescope or which analyzed the statistical relationship between the mount model parameters and the physical errors. Some relevant literature discussing statistical techniques for improving coefficient estimates in regression is discussed in section 3.3 but this work is unique in applying those methods to telescope pointing and to estimating physical errors.

3 REVIEW OF RELATED LITERATURE

3.1 Introduction

The process of constructing a telescope mount model is similar to the process used to calibrate industrial machines. To recognize that similarity and take advantage of progress in the machine calibration field, techniques developed there were reviewed. The literature on robot calibration was found to be especially useful because the procedures utilized closely match those used for constructing a telescope mount model.

Solution techniques were also reviewed to identify those most appropriate to the task of estimating physical errors. Three solution techniques discussed in the statistical literature, ridge regression, bootstrapping, and Bayesian regression were considered to have the greatest potential for improving error parameter estimates and were researched further. This chapter presents some of the key findings of the review of that literature.

3.2 Modeling and Calibration of Machines and Robots

3.2.1 Overview

Some of the literature related to machine and mechanism modeling is directly applicable to telescopes. More researchers are working to improve machine modeling than to develop better telescope mount models. A wide range of techniques are discussed in the machine modeling literature for representation, solution and application. In this section, several relevant and representative works related to machine modeling will be discussed. Particular effort was made to identify references that described methods or solution techniques that could be applied to telescope modeling.

Selig (1996) presented an historical overview of the development of mathematical approaches and representations for modeling machines and robots. He traced the subject back to the invention of the piston engine and early interest in converting reciprocating motion into rotary motion. Selig also suggested that there are still many unsolved problems in robotics that could benefit from development of modern mathematical tools.

Selig differentiated between mechanisms and robots based on their degrees-of-freedom. Robots typically have a large number of degrees-of-freedom while mechanisms have only a few. Any of the common telescope configurations can be modeled as a robot with all rotary joints. The basic motion requires two joints: the azimuth axis and the elevation axis. Geometric errors can be represented with additional joints, increasing the number of degrees-of-freedom.

Zhuang and Roth (1996) presented a brief historical review of robot calibration. They described the early programming of robots as a "teaching by doing" approach where the robot simply retraced routes it was moved through in advance. This was suitable for applications with a limited number of points to which the robot had to move. The primary requirement on the robot mechanism was repeatability, not accuracy.

Zhuang and Roth described Paul's book (1981) as a major influence on all robotics researchers. They explained how the systematic use of the Denavit-Hartenberg formulation, discussed later, combined with the development of advanced sensors and computing technology moved robotics into a new era where accuracy and the ability to move to previously unvisited positions were important. This fueled research into the effects of geometric errors on positioning performance.

3.2.2 The Robot Calibration Process

Robot calibration is an important subset of the machine modeling field because it has a very large body of literature associated with it. The approach used in robot calibration is similar to that used for telescope mount modeling and follows the telescope mount modeling steps previously described by Keitzer et al (1991).

Everett (1993) classified robot calibration into two types: forward and inverse. In the forward calibration approach an error equation is formulated based on physical errors while inverse calibration uses empirical corrections. These two approaches roughly correspond to the two approaches to telescope mount calibration discussed above. This work was restricted to forward calibration.

The four steps in forward robot calibration, modeling, measurement, identification, and implementation, were discussed by numerous authors including Everett (1993) and Zhuang and Roth (1996):

- determination of a mathematical model that represents the robot geometry and its motions (kinematic modeling);
- measurement of the position and orientation of the robot end-effector in world coordinates (pose measurement);
- identification of the relationship between joint angles and end-point positions (kinematic identification); and

- modification of the control commands to allow a successful completion of a programmed task (kinematic compensation).

Kinematic modeling is discussed below and kinematic identification is discussed in the next section. Data collection techniques for calibrating robots differ significantly from those used for telescope modeling and will not be discussed. Implementation of a model in hardware to correct positioning errors is beyond the scope of this work.

3.2.3 Kinematic Representation

3.2.3.1 Overview

The choice among several available methods for representing the kinematic behavior can have significant implications. All representations, if applied correctly, should yield the same results but a particular representation could provide unique insight into the problem or suggest a more efficient approach to the solution. The representation selected for this work had to be compatible with the available data, had to have a form that could be directly related to telescope performance, and had to facilitate efficient solution to the parameter estimation problem.

When developing a kinematic model, two questions arise: which errors should be included and which representation should be used. Chen and Chao (1986) stressed the importance of including all error sources to avoid inaccuracies and to preserve the relationship between the model parameters and real physical effects.

Veitschegger and Wu (1987) described a method for selecting a set of independent kinematic errors to include in a model, a procedure that might be useful when there are interdependencies among the physical errors. Shamma and Whitney

(1987) described a method for inverse calibration of a robot and noted that accuracy is not limited by the ability to identify all sources of error.

Several kinematic representations have been used for modeling robots. A general kinematic model requires representing 6 degrees-of-freedom, three translations and three rotations. In a robot these correspond to position and orientation of the end-effector. In a telescope, only two degrees-of-freedom are required to represent the basic pointing performance. It may be useful, however, to include additional degrees-of-freedom in the representation to model field rotation (rotation about the line-of-sight) and translation errors which might affect optical performance. Several possible representations are discussed below.

3.2.3.2 The Finite Element Method Approach

In the finite element approach to structural analysis, the position and orientation of a point in a structure are represented by a vector with six components. This representation is widely used and understood and would facilitate combining a mount model with control system models already in use. The stiffness matrix obtained from finite element modeling has already been used for modeling telescope pointing behavior.

Masten et al. (1986) described a technique for incorporating structural disturbances into a line-of-sight stabilization system. The stabilization problem is a dynamic version of the pointing problem and techniques developed for that application can often be simplified and used to improve pointing. Masten et al. used structural matrices developed from a finite element model as transfer matrices in the dynamic stabilization model. Ravensbergen (1994) showed how the structural matrices can be used to model the response of a telescope subjected to wind, friction, torque ripple, and other disturbances.

3.2.3.3 The Denavit-Hartenberg Approach

Paul (1981) presented a systematic method for using homogeneous transformations to model robots. He used the Denavit-Hartenberg (D-H) formulation introduced by Denavit and Hartenberg (1955) for modeling the kinematic joints in a robot. Sciavicco and Siciliano (1996) also described this convention and provided examples for simple robot configurations including the spherical wrist, which is kinematically equivalent to a perfect telescope.

The D-H convention has become the standard representation used in modeling robots. Donmez et al. (1986) also used it to develop a generalized, six degree-of-freedom model for machine tool errors and Wang and Masory (1993) analyzed static errors in hexapod machines using a model based on the D-H convention.

A simplification of the D-H convention providing only for rotational joints is also used. This representation has a significant mathematical advantage in that the resulting transformation matrices are orthogonal and can be inverted by simple transposition. Since telescope motions usually consist only of rotation, this representation may be useful if it significantly simplifies the kinematic representation without introducing serious limitations. It would not, however, allow for the extension to translation errors.

3.2.3.4 The Screw Representation

Screw theory uses the idea that any motion can be represented by a rotation about an axis in space and a translation along the axis. By associating a pitch with a vector, any movement can be completely specified using the vector components, the pitch, and a rotation angle about the vector.

A *screw* is a type of *quaternion,* a mathematical construct consisting of a real number and a vector. An algebra has been developed by mathematicians to manipulate screws and describe complex motion problems in a compact form. Levi (1968a) provided an overview of quaternion algebra and used screws to model optical systems. Selig (1996) surveyed similar mathematical representations (Lie groups) that could be used for kinematic representation.

Several authors have used screw theory to model robot kinematics. While this appears to be a good technique for certain problems, it is more difficult to apply to the inverse problem faced for a telescope. Zeigert et al. (1990) gave an overview of screw theory and used it to model machine tool errors. Payandeh and Goldenberg (1987) used screw operators to model a general six degree-of-freedom manipulator.

3.2.3.5 Optical System Modeling Representations

The kinematic analysis of optical systems, especially those with plane mirrors has been discussed by several authors. Beggs (1960; 1975) presented matrix methods for analyzing image kinematics in plane mirror optical systems. Polasek (1967) and Royalty (1990) extended the work to the analysis of systems with gimbaled mirrors. Levi (1968a) showed that the transformation matrix for a plane mirror is a screw operator.

In a series of papers, Debruin (1991) and Debruin and Johnson (1992, 1994) developed a technique for analyzing pointing in plane mirror optical systems using line-of-sight reference frames and a matrix transform approach. The approach was developed for analyzing the pointing of airborne cameras but is generalized to any optical system consisting of plane mirrors. The papers focused on the optical effects once the mirror positions are determined using a kinematic model. The work of Beggs, Polasek, and Debruin and Johnson was addressed at modeling perfect systems, not at finding the errors in imperfect systems. The representations they developed and basic approach to the problem, however, may be useful because they allow the complete orientation of the image to be modeled, not just the position in the sky.

Fisk and Rue (1966) favored a graphical representation of the kinematic model. They used a *Piogram* of the system coordinate transformations to produce the effect of each geometric error. Piograms are a method for compactly representing coordinate transformations first described by Pio (1966). They were common in the literature at the time but are not often seen anymore.

The direct use of analytical functions is the prevailing approach used for telescope mount models. The effect of each geometric error is calculated separately using trigonometric expressions and the results are added to obtain the total error (Wallace, 1993). The manipulation of the analytical functions is straightforward when only a few errors are considered but becomes cumbersome with a large number of degrees-of-freedom.

3.2.4 Research Topics in Robot Calibration

Zhuang and Roth (1996) listed four open research issues in robot calibration, all of which relate to the research questions in Chapter 1. First, "what is the relative importance of robot geometric errors compared to nongeometric errors?" The magnitude and uncertainty of the individual model term coefficients determine the relative importance of each factor. The model used for telescopes includes both geometric and nongeometric errors. A related question that might be more interesting for telescopes concerns the relative importance of geometric errors compared to random errors. Ultimately, if precisely known, geometric errors can be removed through adjustment or through better manufacturing. Much of the random error is likely to arise from environmental influences (Keitzer et al., 1991) and must be removed using other means.

The second open research issue Zhuang and Roth listed related to how calibration quality is affected by the resolution and accuracy of the calibration method and instrumentation. This issue is not specifically addressed by any of the research questions but concerns the effect of measurement errors during calibration. It is also related to the selection of stars for calibration, a topic that is discussed in Chapter 6.

The third open research issue concerned the choice of robot calibration configurations and relates to the criteria for selecting calibration stars. The coordinates of the reference stars define the calibration configurations for the telescope. Star selection is an important issue in mount modeling but is not addressed in the literature except anecdotally. In an analogous problem in robot calibration, Mooring and Pack (1986) proposed standardized methods for selecting calibration positions and expressing robot repeatability. They suggested calibrating at the midpoint and extremes of the range of each joint.

The final research issue related to how observability of robot kinematic error parameters relates to calibration procedures. *Observability* essentially refers to whether the input to the system can be deduced by observing the output over a finite period of time (Ogawa, 1997). This is an important question here because the entire telescope mount modeling problem rests on the ability to deduce the inputs (geometric errors) through analysis of the output (pointing errors).

Hollerbach (1989) identified the issue of coordinate system selection as a key question to be addressed in robot modeling. The question involved choosing among several available representations. He questioned when a representation with more parameters would be appropriate given the redundancy introduced. For this work, two similar questions arise: which of several kinematic representations should be used for modeling telescope pointing and how general should the model be. The basic pointing problem involves only rotations but a more general telescope kinematic problem also requires consideration of translations.

Everett (1993) also discussed a variety of research areas in robot calibration. Several research topics concerning the parameter identification problem relate closely to this work. Many of these are discussed in the next section.

A number of authors have also investigated problems related to uncertainty in robot motion. Donald (1989) listed three sources of uncertainty in robot tasks: errors in the sensor, errors in control, and uncertainty in the environment. In the early 1990s, much of the research in robotics uncertainty focused on sensor and control error, essentially studying ways to appropriate accomplish a task when the characteristics of the environment are known. Lozano-Perez et al. (1984) described strategies for planning robot motions using a worst-case analysis of the possible geometric errors. Knowledge of the robot construction and environment were used to bound each error and those bounds were used to determine the total impact on behavior. Brost and Christiansen (1993) described a probabilistic approach to determining whether a task (inserting a peg in a hole) could be completed in the presence of uncertain geometric errors. This technique might be useful for determining whether a telescope with uncertain errors could accomplish a similar task such as establishing or maintaining a communication link.

More recent work has addressed how robot motion should be carried out in an uncertain and dynamically changing environment. Since most of the characteristics of the environment in which a telescope operates are known (geographic position, locations of reference and target stars, and so forth), the telescope modeling problem is simpler than the robot problem and the recent uncertainty research is not directly relevant.

3.3 Solution Techniques

3.3.1 Overview

A kinematic model relates pointing error to axis position when certain geometric errors are assumed to be present in a telescope. The model can be used in two ways: to correct pointing or to estimate the magnitude of the geometric errors. The first use describes current applications in telescope mount modeling while the second describes the goal of this work. Both require finding parameters for the kinematic model but the specific requirements for parameter determination may differ.

Determining the set of coefficients to use in the kinematic model is a type of parameter estimation problem. The solution to a parameter estimation problem is a set of values for the parameters that best achieves a stated objective. The choice of the objective will often influence the determination of the best parameter set.

For making corrections, the goal is to find a set of parameters that produces the best corrections. As long as the overall performance of the model is good, the accuracy of individual parameters is only a secondary concern. The quality of a particular set of parameters is judged by its ability to produce a good response demonstrated by accurate pointing of the telescope.

When the goal is to obtain accurate and precise estimates of each individual parameter in the kinematic model, a different approach may be required. It would be desirable to know the model parameters accurately even if they did not produce the best performance. Schröer (1993) pointed out that, in the case of robot modeling, the goals of improving performance and improving parameter estimation are somewhat contradictory and require different models.

3.3.2 Selecting the Objective Function

The objective function in an optimization problem defines the quantity to be minimized or maximized. When constructing a telescope mount model to correct pointing, the objective is to find the set of parameters that minimizes the pointing errors in future observations based on the assumption that errors in future observations will be affected in the same way as observations of calibration stars. A suitable objective is to minimize the squares of the errors in the observed positions of calibration stars. This is a common approach to many optimization problems and is referred to as the *least squares* or *ordinary least squares* (OLS) method. The TPOINT program uses the sum of the squared pointing errors of the reference stars for its objective (Wallace, 2000).

Everett (1993) described the choice of the proper objective function as a key research issue in robot calibration. He criticized the use of a least squares objective function because it fails to consider the relative spacing of the data points. For example, each member of a clustered group of data points has the same influence on the solution as an isolated, distant point. Everett suggested a weighted least squares approach and described an objective function that accounts for the amount of workspace each measurement represents. In a telescope mount model, weights might be applied based on the spatial distribution of the calibration stars used.

Everett (1993) also discussed a weighting scheme based on the type of measurement, translation or rotation. He noted that since translations and rotations are affected differently according to the location where the measurements are made they should be weighted differently in the objective function. A similar argument could be made for weighting elevation and azimuth pointing errors differently when one is expected to have higher error due to position dependent random effects. Neter et al. (1996) described several approaches to weighting in regression based on knowledge of the variance as a function of the predictors.

3.3.3 Model Classification and Estimation Methods

Several techniques are in wide use for solving a parameter estimation problem and deciding which is most appropriate often depends on the particular problem and characteristics of the data. Models can be classified as linear or nonlinear. Solution techniques for linear models are usually direct while nonlinear models often require iterative techniques. Nonlinear problems may also lack unique solutions and the solutions may be highly sensitive to noise in the data.

The telescope mount modeling problem involves trigonometric functions of the axis angles and is therefore nonlinear. However, since the error model only relates small pointing errors to the angles, it is nearly linear and can be linearized using simple transformations involving trigonometric functions of the axis angles. Several common techniques for solving the parameter estimation problem are discussed below.

3.3.3.1 Regression

Regression refers to a class of statistical techniques that utilize the relation between two or more quantitative variables to predict one (the response) from the others (the predictors). Simple regression involves a single predictor variable while multiple regression may involve many. Techniques exist for performing regression on linear and nonlinear functions (Neter et al., 1996).

The OLS method is commonly used to define the objective function. Transformations can often be used to linearize a model that uses nonlinear predictors (Box and Tidwell, 1962). Formulas are widely available for fitting linear models using an OLS objective function when the errors are unbiased, independent, and have constant variance. Several sources also provide closed form equations to estimate the response, confidence limits on the model parameters, and related phenomena (Robinson, 1981; Neter et al., 1996).

When there is substantial correlation and interdependency among the predictor variables OLS regression often produces good estimates of the response. This makes it a good choice for corrective telescope mount models and is used by both TPOINT (Wallace, 2000) and FIT9, a program formerly used for the James Clerk Maxwell Telescope (JCMT) (Kenderdine and Fairclough, 1988).

Unfortunately, the estimates of individual model term coefficients are poor when using OLS for data with correlation or interdependency. The theoretical sampling distributions of the response and the individual coefficient estimates are developed using the assumption that the errors are independent and identically normally distributed (Robinson, 1981). When this assumption is violated or, more seriously, when the terms in the model are correlated, the variance in the parameter estimates is exaggerated (Neter et al., 1996). Confidence levels constructed for the geometrical errors based on these estimates are wide and imprecise.

Ridge regression is a variation of basic regression developed to address correlation among the predictors. The STARCAL program uses ridge regression (Keitzer et al., 1991) and it was formerly used for model checking by the JCMT (Kenderdine and Fairclough, 1988). It introduces a small amount of bias into the regression model to control the variance in the individual coefficient estimates (Neter et al., 1996). According to Ross (1990), ridge regression is equivalent to adding extra hypothetical observations symmetrical to the centroid of the data.

Several methods have been developed for addressing problems in regression analysis when multicollinearity and interdependence are present in the model or data. One of these techniques is called *bootstrapping* and involves taking subsamples of size *n* from the *n* data points with replacement and fitting a model to each subsample (Neter et al., 1996). The result is a set of estimates for each coefficient that provides information on the sampling distribution of the coefficient, not just the mean and variance. This provides useful knowledge but is computationally intensive and might not be feasible for routine operations at an observatory.

Efron (1982) and Efron and LePage (1992) explained the basis and theoretical background for the bootstrap technique. Efron (1985) described the construction of confidence intervals for a function of a random vector using bootstrapping and showed it eliminates much of the uncertainty associated with other estimation techniques. Barbe and Bertail (1995) reviewed several approaches to using a weighted bootstrap but concluded that there was no good general method for selecting appropriate weights. Agrawal, Lawless, and Mackay (1999) described the use of bootstrapping to estimate confidence intervals on the parameters of a model of error in a manufacturing process.

Other techniques are also available for improving the parameter estimates. Variance inflation factors measure how much the variances of the estimated regression coefficients are inflated compared to what they would be if the predictors were not linearly related. They are calculated by fitting a new model that does not include one of the predictors and studying the effect on the parameters.

Similarly, *orthogonal polygon transformations* can be used to produce new predictor variables that are uncorrelated (Neter et al., 1996). Fisk and Rue (1966) used this approach to improve the precision of confidence intervals on sensor gimbals. A drawback of this approach is that the predictor functions lose their direct physical interpretation.

3.3.3.2 Maximum Likelihood Estimation

In maximum likelihood estimation (MLE), information about the distribution of the error in the model is used to find the set of model parameters that is most consistent with the observed data (Neter et al., 1996). The technique is widely used and methods are available for constructing confidence intervals using MLE (Ross, 1990). For linear regression the estimated parameters found using MLE are the same as those obtained using OLS and thus have the same properties (Neter et al., 1996).

3.3.3.3 Other Methods

Ross (1990) classified alternative (as opposed to MLE) methods of estimation into three categories: simplified methods providing unique estimates without iteration, methods that employ additional information, and methods robust to gross errors in the data. Linear regression is a simplified method; Bayesian estimation is a technique employing additional information about the distribution of the errors and is similar to MLE; robust estimation techniques are resistant to outliers and other gross errors in the data and often use rank statistics.

In describing an application to telescope mount modeling, Ulich (1981) said that an iterative simultaneous linear estimation technique is used but did not provide any details. Various search or iterative techniques are also used in robot calibration to find kinematic parameters. The nominal joint parameters are known from the robot design and can be used as a starting point in an iterative solution (Zhuang and Roth, 1996). These techniques are more general than the linear approach and are necessary when the errors are large.

Fisk and Rue (1966) calculated confidence limits for the pointing error in a altazimuth gimbal by direct calculation of the probability density function for pointing error phase and magnitude. Their analysis was based on an algebraic expression of the pointing error as a function of 9 geometric errors and assumed small geometric errors. They did not address the estimation of the geometric errors using the observed pointing errors, nor did they describe how their results could be used to correct pointing errors.

3.3.4 Data Considerations

The trigonometric functions of the axis angles used as predictors in the mount model are not orthogonal (Keitzer et al., 1991). They are correlated with each other and the degree of correlation depends on the range of angle spanned by the data. As noted above, this causes the variance of the individual terms to be exaggerated.

Telescope calibration data also exhibit dependence between the azimuth and elevation errors. Ulich (1981) claimed that these errors were independent but they will not be when they are both influenced by the same random effect such as servo error or the atmosphere. Similarly, the error associated with each measurement does not have constant variance. Measurements taken near the horizon will have greater error from the atmosphere. These effects complicate the analysis but may also provide opportunities for improving the analysis. Neter et al. (1996) described techniques for transforming the data to eliminate problems of nonconstant variance.

Finally, errors in the measurement of the true telescope axis positions produce bias in the parameter estimates. These measurements are expected to be small but they might need to be considered. Agrawal et al. (1999) discussed a similar situation in modeling a manufacturing process. When the distribution of the measurement error is known, as would usually be the case for a telescope model, the influence of measurement errors can be determined analytically (Fuller, 1987). When the distribution of measurement errors is not known, *interval probability theory* can be used to estimate the effect of measurement errors.

The techniques developed in this work provide several tools that may be useful for improving the precision of parameter estimates in mount modeling. Determining which procedures produce the best results, applying those procedures, and quantifying the underlying physical errors based on the results is the subject of this work. The methods used are described in the next chapter.

4 RESEARCH METHODOLOGY

4.1 Overview

A procedure was developed to allow data collected during mount modeling to be used to make precise interval estimates of the physical errors. In addition, expressions were developed for confidence and prediction limits on pointing performance and on the actual position of an observed object. This process involved the following steps:

1. A kinematic model of a typical telescope was developed to relate true optical line-of-sight to encoder reading when specific geometric errors are present.

2. Telescope pointing data obtained from four large research telescopes, as well as simulated data sets with known errors, were used to quantify the variability and correlation present in real data.

3. A statistical model was used to estimate the parameters of the kinematic model most consistent with the observed data.

4. Expressions were derived for prediction and confidence limits on the pointing error and the parameter estimates. Characteristics of the data required the use of special estimation techniques

5. An analysis of the mathematical model was used to develop guidelines for producing better mount models to achieve various objectives.

This chapter develops the kinematic and statistical models employed, explains how the data is collected and used in the models, describes each of the solution techniques, and discusses how mount model results can be used to assess pointing and position determination accuracy.

4.2 Kinematic Model

4.2.1 Representation

The kinematic model incorporates the geometric error and axis angle setting information for the telescope and relates it to true optical line-of-sight. The relationships in the kinematic model are determined by the geometry of the telescope and the parameters that quantify the relationships are estimated during the calibration process.

Several possible ways to represent the kinematic model were discussed in Chapter 3. The rotation-only Denavit-Hartenberg (D-H) representation was selected because it is compatible with available data, has a form that can be directly related to telescope performance, and facilitates an efficient solution to the problem of estimating the coefficients.

The D-H convention is widely used in the robot calibration literature and accommodates translations as well as rotations. In the D-H convention, the coordinates of a point are represented by a vector with four entries, x, y, z and a coordinate that is always 1. This system is referred to as a *homogeneous coordinate system.* Translation and rotation of the point is produced by multiplication with a 4 by 4 transformation matrix. For example, multiplying a point vector by the transformation matrix

$$\mathbf{T} = \begin{bmatrix} \cos\theta & 0 & \sin\theta & 0 \\ 0 & 1 & 0 & 0 \\ -\sin\theta & 0 & \cos\theta & 0 \\ 3 & 4 & 5 & 1 \end{bmatrix} \tag{4.1}$$

rotates the point by an angle θ about the y-axis and translates it 3 units along the x-axis, 4 units along the y-axis, and 5 units along the z-axis. The point vector may be a column vector or a row vector provided that the matrix algebra is developed accordingly.

For telescope pointing, generally only rotation of the pointing vector is important. Translations are usually small with negligible effect on pointing. The rotation-only D-H formulation was utilized for this work because it allowed significant simplifications to be made. Because rotation matrices are orthogonal, their inverse is equal to their transpose.

Unfortunately, the full D-H transformation matrices do not have this property. The rotation matrix, **R**, corresponding to a D-H transformation matrix, **T**, is obtained by omitting the fourth row and fourth column. For example, the rotation matrix, **R**, corresponding to the transformation matrix, **T**, in eqn. (4.1) is

$$\mathbf{R} = \begin{bmatrix} \cos\theta & 0 & \sin\theta \\ 0 & 1 & 0 \\ -\sin\theta & 0 & \cos\theta \end{bmatrix} \tag{4.2}$$

and produces the same rotation of the point but no translation. When rotation matrices are used, point vectors have three components, x, y, and z.

The rotation errors in a telescope are typically very small and a further simplification can be made. For a small angle, θ, the following approximate relationships hold:

$$\sin\theta \approx \theta \tag{4.3a}$$

$$\cos\theta \approx 1 \tag{4.3b}$$

These relationships can be used to simplify the rotation matrix in eqn. (4.2) to

$$\mathbf{R} = \begin{bmatrix} 1 & 0 & \theta \\ 0 & 1 & 0 \\ -\theta & 0 & 1 \end{bmatrix} \tag{4.4}$$

A rotation restricted to be less than 0.5° will have an error from this approximation of less than 0.15 μrad. Referring to the results from actual telescope mount models listed in Chapter 2 confirms that the geometric errors are typically much less than 0.5°. This simplification only applies for rotations caused by the geometric errors such as flexure, not for the larger rotations of the telescope about the azimuth or elevation axes.

Manipulation of the telescope line-of-sight is produced by premultiplying a pointing vector by a rotation matrix. Rotations are produced by each of the physical errors as well as by the axis settings. The combined effect of all rotations is the actual pointing direction of the telescope. The desired pointing direction is the line-of-sight direction produced by simply rotating about the azimuth and elevation axes. The difference between the actual pointing direction and the desired pointing direction is the pointing error. Before developing the rotation matrices for the geometric errors and axis settings, several important telescope references were defined.

4.2.2 Telescope References

For an ideal altazimuth telescope in "zero" position, i. e. pointed to the northern horizon, the coordinate vectors for several important axes and reference lines are given below. These definitions are not necessarily standard but were used here. Several of these references are rotated by the geometric errors and axis settings described below so the vectors listed apply only to the initial orientation of the reference. Figure 4.1 illustrates these references.

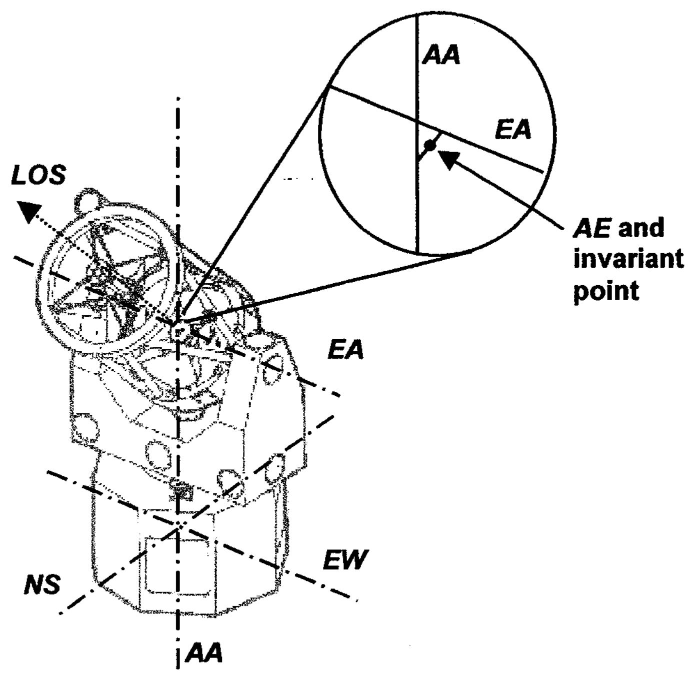

Figure 4.1 Telescope references

The *azimuth axis*, initially defined by the vector, $AA = [0 \quad 0 \quad 1]^{\mathrm{T}}$, is the vertical rotation axis of the telescope. Rotation about this axis changes the angle along the horizon that the telescope would point to if its elevation axis were set to zero. The *elevation axis*, initially defined by the vector, $EA = [1 \quad 0 \quad 0]^{\mathrm{T}}$, is the second rotation axis of the telescope. Motion about this axis changes the distance above the horizon to which the telescope points.

The *AZ-EL line*, initially defined by the vector, $AE = [0 \quad 1 \quad 0]^T$, is the line connecting the elevation axis and the azimuth axis and is normal to each. In an ideal telescope the AZ-EL line has length zero and is represented only by its direction vector. The *invariant point* is the midpoint of the AZ-EL line. If the azimuth and elevation axes intersect, the invariant point is the intersection point. The invariant point is also called the *pivot point* and is important because it is, at least in principal, the only point on the gimbal that does not move when the axes are rotated. It is the theoretical origin of the telescope when used for interferometry or laser ranging.

The *pointing direction*, also sometimes called the *line-of-sight* (*LOS*), is the direction to which the telescope points. For convenience, before application of any geometric errors or axis settings, the initial pointing direction of the telescope was defined to be zero degrees azimuth and zero degrees elevation, i. e., pointed at the northern horizon and represented by the initial pointing vector, $LOS = \mathbf{P}_0 = [0 \quad 1 \quad 0]^T$.

The *north-south line*, $NS = [0 \quad 1 \quad 0]^T$, is a vector pointing toward true north. The azimuth angle of the telescope is measured from this line, positive toward east. The *east-west line*, $EW = [1 \quad 0 \quad 0]^T$, is a vector pointing toward east.

4.2.3 Ideal Axis Settings

Setting the telescope to the desired position in the sky involves a rotation about the azimuth axis and a separate rotation about the elevation axis. When there are no physical errors in the telescope the rotations are about the axes, *AA* and *EA*, defined above. If a global coordinate system is placed at the telescope invariant point, all rotations can be defined about principal axes of that global coordinate system. Sciavicco and Siciliano (1993) provided the matrix, $\mathbf{R}_x$, for elementary rotation about the x-axis (see Fig. 4.2a) by an angle x,

$$\mathbf{R}_x = \begin{bmatrix} 1 & 0 & 0 \\ 0 & \cos x & -\sin x \\ 0 & \sin x & \cos x \end{bmatrix} \approx \begin{bmatrix} 1 & 0 & 0 \\ 0 & 1 & -x \\ 0 & x & 1 \end{bmatrix} \tag{4.5a}$$

and similarly, the matrices for rotation about the y-axis (Fig. 4.2b) and z-axis (Fig. 4.2c) by angles y and z respectively were given by

$$\mathbf{R}_y = \begin{bmatrix} \cos y & 0 & \sin y \\ 0 & 1 & 0 \\ -\sin y & 0 & \cos y \end{bmatrix} \approx \begin{bmatrix} 1 & 0 & y \\ 0 & 1 & 0 \\ -y & 0 & 1 \end{bmatrix} \tag{4.5b}$$

$$\mathbf{R}_z = \begin{bmatrix} \cos z & -\sin z & 0 \\ \sin z & \cos z & 0 \\ 0 & 0 & 1 \end{bmatrix} \approx \begin{bmatrix} 1 & -z & 0 \\ z & 1 & 0 \\ 0 & 0 & 1 \end{bmatrix} \tag{4.5c}$$

In eqns. (4.5a) through (4.5c), the approximate matrix can be used when the rotation angle is small.

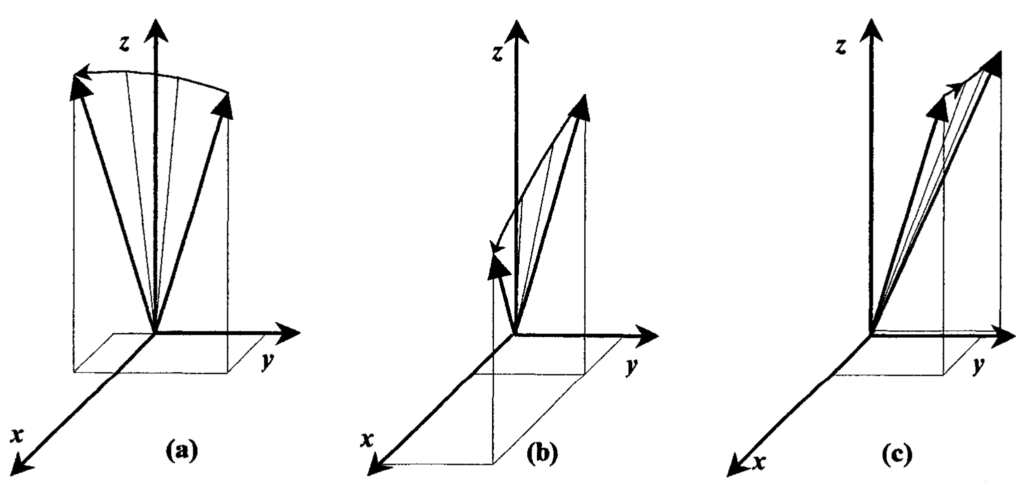

Figure 4.2 Principal axis rotations

Setting the azimuth angle of the telescope involves rotating about the azimuth axis, which is initially parallel to the *z*-axis. Rotation of the telescope about the azimuth axis by angle A is produced by substituting the rotation angle, A, in the elementary matrix, $\mathbf{R}_z$, for rotation about the *z*-axis, resulting in the matrix

$$\mathbf{R}_\mathbf{A} = \begin{bmatrix} \cos A & \sin A & 0 \\ -\sin A & \cos A & 0 \\ 0 & 0 & 1 \end{bmatrix} \tag{4.6}$$

Rotation about the elevation axis is produced by the matrix

$$\mathbf{R}_\mathbf{E} = \begin{bmatrix} 1 & 0 & 0 \\ 0 & \cos E & -\sin E \\ 0 & \sin E & \cos E \end{bmatrix} \tag{4.7}$$

Because rotation about the azimuth axis changes the orientation of the elevation axis, the elevation rotation must be performed first. The combined transformation matrix for sequential rotations is obtained by successively premultiplying the initial pointing vector by each rotation matrix in the order the rotation is performed. Setting the desired pointing direction of the telescope is given by

$$\mathbf{R}_\mathbf{S} = \mathbf{R}_\mathbf{A}\mathbf{R}_\mathbf{E} = \begin{bmatrix} \cos A & \sin A & 0 \\ -\sin A & \cos A & 0 \\ 0 & 0 & 1 \end{bmatrix} \begin{bmatrix} 1 & 0 & 0 \\ 0 & \cos E & -\sin E \\ 0 & \sin E & \cos E \end{bmatrix} \tag{4.8}$$

$$\mathbf{R}_\mathbf{S} = \begin{bmatrix} \cos A & \sin A \cos E & -\sin A \sin E \\ -\sin A & \cos A \cos E & -\cos A \sin E \\ 0 & \sin E & \cos E \end{bmatrix} \tag{4.9}$$

and produces the ideal line-of-sight vector, $\mathbf{P}$, when premultiplied by the initial pointing vector, $\mathbf{P_0}$, defined above

$$\mathbf{P}_S = \begin{bmatrix} \cos A & \sin A \cos E & -\sin A \sin E \\ -\sin A & \cos A \cos E & -\cos A \sin E \\ 0 & \sin E & \cos E \end{bmatrix} \begin{bmatrix} 0 \\ 1 \\ 0 \end{bmatrix} \tag{4.10}$$

$$\mathbf{P}_S = \begin{bmatrix} \sin A \cos E \\ \cos A \cos E \\ \sin E \end{bmatrix} \tag{4.11}$$

The azimuth and elevation angles, A and E respectively, can be extracted from a pointing vector in this form using the relations

$$A = \tan^{-1}\left(\frac{P_1}{P_2}\right) \tag{4.12a}$$

$$E = \sin^{-1}(P_3) \tag{4.12b}$$

where P_1, P_2, and P_3 are the components of the pointing vector **P**. Because only rotations are performed to produce a new pointing vector, the length is unchanged from its initial unit length and the elevation angle can be obtained from eqn. (4.12b). In the more general case when translation is included, the change in length of the pointing vector must be considered and eqn. (4.12b) becomes

$$E = \sin^{-1}\left(\frac{P_3}{\sqrt{P_1^2 + P_2^2 + P_3^2}}\right) \tag{4.12c}$$

4.2.4 Geometric Error Effects

Each of the geometric errors discussed in Chapters 1 and 2 produces a small rotation of the telescope line-of-sight. Table 4.1 summarizes these errors. For each error, the geometric cause is shown, the symbols used to denote the angle of rotation and the rotation matrix are listed, the axis each causes the line-of-sight to rotate about is stated, and the references that are changed by the rotation are noted. This table is useful as a summary and also as a tool for establishing the order of rotation as discussed below.

The rotation axis is given in terms of the telescope reference the rotation occurs about, which may have been changed by a previous rotation, and the global coordinate axis the rotation axis is parallel to, e. g., *AE* (y) is a rotation about the AZ-EL line, which is initially parallel to the global y-axis. The axis settings are included here because they must be included in the total effect and performed in the proper order as indicated in the following table and discussed below.

Table 4.1 Summary of all axis rotations and geometric error effects

Effect	Symbol	Matrix	Rotation axis	Changes
Optical axis misalignment	γ	$\mathbf{R_M}$	*AA* (z)	*LOS*
Flexure	$\delta_T \cot E$	$\mathbf{R_F}$	*EA* (x)	*LOS*
Elevation setting	E	$\mathbf{R_E}$	*EA* (x)	*LOS*
Nonperpendicularity	η	$\mathbf{R_N}$	*AE* (y)	*EA, LOS*
Azimuth setting	A	$\mathbf{R_A}$	*AA* (z)	*EA, LOS*
Elevation bearing	$\xi_{B1} \sin E$	$\mathbf{R_{B1}}$	*AA* (z)	*EA, LOS*
Elevation bearing	$\xi_{B2} \cos E$	$\mathbf{R_{B2}}$	*AA* (z)	*EA, LOS*
Azimuth bearing (NS term)	$\xi_{B3} \cos A$	$\mathbf{R_{B3}}$	*NS* (y)	*AA, EA, LOS*
Azimuth bearing (EW term)	$\xi_{B4} \cos A$	$\mathbf{R_{B4}}$	*EW* (x)	*AA, EA LOS*
Tilt toward east	ψ_Y	$\mathbf{R_Y}$	*NS* (y)	*AA, EA, LOS*
Tilt toward north	ψ_X	$\mathbf{R_X}$	*EW* (x)	*AA, EA, LOS*

Table 4.1 can be used to find any of the rotation matrices for the constant geometric errors using the appropriate parameter and elementary rotation matrix defined in eqns. (4.5a) through (4.5c). For example, to produce the rotation matrix, $\mathbf{R_N}$, for

nonperpendicularity of the axes the parameter η is used in the elementary matrix for rotation about the y-axis provided in eqn. (4.5b) to obtain

$$\mathbf{R}_{\mathrm{N}} = \begin{bmatrix} 1 & 0 & \eta \\ 0 & 1 & 0 \\ -\eta & 0 & 1 \end{bmatrix} \tag{4.13}$$

The rotation matrices for each of the other fixed errors can be found similarly.

The effects from bearing wobble and flexure are not fixed. They can be obtained from the elementary rotations but the magnitude of the rotation depends on one of the axis positions. A simple rotation about the elevation axis, initially the x-axis, produces the effect of flexure but the magnitude of the rotation depends on the elevation angle. Thus, the rotation matrix for flexure, $\mathbf{R}_{\mathrm{F}}$, is given by

$$\mathbf{R}_{\mathrm{F}} = \begin{bmatrix} 1 & 0 & 0 \\ 0 & 1 & -\delta_T \cot E \\ 0 & \delta_T \cot E & 1 \end{bmatrix} \tag{4.14}$$

As shown in Chapter 2, most of the repeatable error from a bearing occurs in low frequency harmonic terms. Modeling bearing wobble requires two parameters to account for the magnitude and phase of the error but these can be converted to a sine term and a cosine term. Table 4.1 lists terms for bearing errors with a cyclic frequency of once per revolution of each bearing. Errors with higher cyclic frequencies can be included in a similar fashion. Table 4.2 lists the resulting algebraic representation for each error in Table 4.1.

Table 4.2 Algebraic representation of telescope geometric errors

Source	Azimuth Effect	Elevation Effect
Azimuth encoder offset	1	0
Elevation encoder offset	0	1
Azimuth encoder scale	A	0
Elevation encoder scale	0	E
Optical axis misalignment	$-\sec E$	0
Axis nonperpendicularity	$\tan E$	0
Tilt toward north	$\sin A \tan E$	$\cos A$
Tilt toward east	$\cos A \tan E$	$-\sin A$
Azimuth bearing, NS term	$\sin A \tan E \cos A$	$\cos A \cos A$
Azimuth bearing, EW term	$\cos A \tan E \cos A$	$-\sin A \cos A$
Elevation bearing, sin term	$\sin E$	0
Elevation bearing, cosine term	$\cos E$	0
Tube flexure	0	$-\cot E$

The final pointing direction of the telescope is found by applying each of the rotations in Table 4.1 in the order the rotations occur. Because matrix multiplication is not commutative, a problem occurs if, for example, the azimuth rotation is applied before the elevation rotation. In this situation, the azimuth motion moves the elevation axis and the elevation rotation must be about the new elevation axis. If each rotation is about an axis that has not yet been rotated from its initial position, all rotations are about the initial principal axes. The sequence listed in Table 4.1 accomplishes this.

The kinematic model for the telescope including all rotations is

$$\mathbf{P_T} = \mathbf{R_X R_Y R_{B4} R_{B3} R_{B2} R_{B1} R_A R_N R_E R_F R_M P_0} \tag{4.15}$$

which can be simplified by defining the total rotation matrix, $\mathbf{R_T}$, by

$$\mathbf{R_T} = \mathbf{R_X R_Y R_{B4} R_{B3} R_{B2} R_{B1} R_A R_N R_E R_F R_M} \tag{4.16}$$

and writing eqn. (4.15) as

$$\mathbf{P_T} = \mathbf{R_T P_0} \tag{4.17}$$

A pointing vector can be rotated back to the initial direction by solving eqn (4.17) for $\mathbf{P}_0$.

$$\mathbf{P}_0 = \mathbf{R_T}^{-1}\mathbf{P_T} \tag{4.18}$$

The matrix $\mathbf{R_T}$ in eqn (4.17) is a product of the several rotation matrices so its inverse is the product of the inverses of the individual matrices in reverse order of their occurrence in eqn (4.15). Since each matrix is orthogonal its inverse is equal to its transpose and eqn. (4.18) can be written as

$$\mathbf{P}_0 = \mathbf{R_T}^{\mathbf{T}}\mathbf{P_T} \tag{4.19}$$

so the initial pointing vector can be recovered simply by premultiplying by the transpose of the matrix that produced the rotation.

4.2.5 Pointing Error

The pointing vector resulting from applying all the rotations, the setting angles and the errors, defines the actual line-of-sight of the telescope. The actual azimuth angle is $A + \Delta A$ and the actual elevation direction is $E + \Delta E$. The pointing errors, ΔA and ΔE can be separated using eqns. (4.12a) and (4.12b) and trigonometric identities. Because the pointing errors are assumed to be small, the small angle approximation is applied and products of small angles are omitted. This yields the following expressions for the total pointing error

$$\begin{aligned}\Delta A = & -\gamma \sec E + \eta \tan E + \xi_{B1} \sin E + \xi_{B2} \cos E + \\ & \xi_{B3} \cos A \sin A \tan E + \xi_{B4} \cos A \cos A \tan E + \\ & \psi_X \sin A \tan E + \psi_Y \cos A \tan E\end{aligned} \tag{4.20a}$$

$$\begin{aligned}\Delta E = & \xi_{B3} \sin A \cos A + \xi_{B4} \cos A \cos A + \\ & \psi_X \cos A + \psi_Y \sin A - \delta_T \cot E\end{aligned} \tag{4.20b}$$

which include terms similar to those used by TPOINT and listed in Chapter 2. These expressions can be written in matrix form as

$$\Delta A = \begin{bmatrix} -\sec E & \cdots & \cos A \tan E & 0 \end{bmatrix} \begin{bmatrix} \gamma & \cdots & \psi_Y & \delta_T \end{bmatrix}^{\mathrm{T}} \tag{4.21a}$$

$$\Delta E = \begin{bmatrix} 0 & \cdots & \sin A & -\cot E \end{bmatrix} \begin{bmatrix} \gamma & \cdots & \psi_Y & \delta_T \end{bmatrix}^{\mathrm{T}} \tag{4.21b}$$

This was a convenient form of the kinematic model for use in fitting the statistical model and identifying the parameters related to the physical errors.

4.3 Data Sources and Collection

4.3.1 Sources of Data

The data for this work came from two sources: working telescopes and simulated data sets. Using data from working telescopes ensured that the results could be applied to the real-world problem while the simulated data were useful for evaluating the effectiveness of each solution method when known physical errors and known noise were present. This subsection describes the data used for this study and the following subsections discuss the general process used to obtain calibration data from a telescope.

4.3.1.1 Data from Telescopes

Calibration data were obtained from four large astronomical telescopes, the Sloan Digital Sky Survey (SDSS) 2.5-meter telescope, the Astronomical Research Consortium

(ARC) 3.5-meter telescope, and the two W. M. Keck Observatory (WMKO) 10-meter telescopes (Keck I and Keck II). Each of the organizations that operate these telescopes provided data that is routinely collected for mount modeling as part of their ongoing operations. The following paragraphs provide additional information on the telescope data sets and each data set is listed in Appendix A.

Sloan Digital Sky Survey 2.5-meter telescope. The SDSS 2.5-meter telescope is located at the Apache Point Observatory in southern New Mexico. Observed and actual star position coordinates and the corresponding pointing errors for 47 stars measured on February 12, 2001 were obtained from Russell Owen of the University of Washington. The coordinates and errors in the SDSS data follow the TPOINT internal coordinate system with azimuth angles measured from south toward east. This required that a transformation be applied for this work. The results of a TPOINT fit performed for this data were also supplied and the results for this model were presented in Table 4.2.

Astronomical Research Consortium 3.5-meter telescope. The Astronomical Research Consortium (ARC) 3.5-meter telescope is located on the same mountain in southern New Mexico as the SDSS telescope and is operated by the same organization. Owen (2002) also provided star position and pointing error data for 82 stars measured with this telescope on November 8, 2001 as well as two TPOINT solutions. One of the solutions included all the terms used in the current telescope mount model and the other excluded a special empirical term used to model a known problem with the elevation bearing (drive ring). The current model differs from the preliminary model presented in Table 2.5 but the mechanical errors are of similar magnitude. The ARC data also required a coordinate system transformation.

W. M. Keck Observatory 10-meter telescopes. The W. M. Keck Observatory (WMKO) operates two identical 10-meter telescopes located in close proximity to one another on Mauna Kea in Hawaii. Pointing error data for several calibration runs during 2001 for both telescopes were provided by Dahl (2002). One set for each telescope was arbitrarily selected for comparing the precision of the mechanical error estimates for each method considered in this work. The coordinate system used for the WMKO data agreed with that used for this work, so no transformation was required.

4.3.1.2 Simulated Data Sets

In addition to the data from working telescopes, six simulated data sets were used. These sets were similar to those collected on real telescopes but had known effects present and known random error. This allowed the accuracy and precision of each solution method to be compared without the uncertainty of not knowing what the true errors were or how much random noise was present in the data. Using several sets with identical mechanical effects but different random error allowed the effect of random error to be evaluated.

The simulated data sets were created by generating random hypothetical calibration star positions uniformly distributed over the region of the sky above 20° elevation. The positions were then perturbed by introducing the effect of mechanical errors and normally distributed random noise with mean zero. Each set had identical mechanical errors but the standard deviation of the noise varied. The characteristics of these simulated data sets are summarized in Tables 4.3 and 4.4 and each data set is listed in Appendix A.

Table 4.3 Geometric errors introduced into simulated data sets

Source	Physical Error (μrad)
Azimuth encoder offset	150.0
Elevation encoder offset	100.0
Azimuth encoder scale	-20.0
Elevation encoder scale	30.0
Axis nonperpendicularity	12.5
Optical axis misalignment	-62.5
Tilt toward north	212.5
Tilt toward east	-150.0
Tube flexure (TX)	100.0
Azimuth bearing, NS term	12.0
Azimuth bearing, EW term	7.5
Elevation bearing, cosine term	8.0
Elevation bearing, sine term	6.0

Table 4.4 Random error present into simulated data sets

Simulated data set	Random error (standard deviation) (μrad)
Set 0	0
Set 1	1
Set 2	5
Set 3	10
Set 4	20
Set 5	50

The magnitude of the setup errors (axis nonperpendicularity, optical axis misalignment, and level errors) introduced in each set were selected to be approximately half the maximum values listed in Table 2.1. The encoder errors were arbitrarily chosen to be reasonable but not excessive because large encoder errors would ordinarily be pre-corrected before use in a mount model. The bearing errors were selected to produce approximately 10 μrad of error for the elevation bearing and 14.1 μrad for the azimuth bearings when added in quadrature, consistent with the estimates in Chapter 2. The magnitude in each direction was arbitrarily selected to avoid aligning the phase of the bearing error with a cardinal point of either axis. Because the effect of bearing errors is correlated with some of the other errors, if a bearing error is in phase with another error it would complicate the analysis. In practice, bearing errors have random orientation and it would be unlikely to encounter a situation where it was perfectly aligned with a cardinal direction.

The amount of random error introduced into the simulated data sets was chosen to span the range of random error encountered in telescope pointing data. The random errors listed in Table 2.2 sum in quadrature to about 7.3 μrad while the SDSS and ARC telescopes each have about 15 μrad of residual pointing error. Using a range of random errors in the simulated data sets allowed its effect on model results to be studied. Sets 2, 3, and 4 would be typical of the random error encountered for astronomical telescopes while sets 0, 1, and 5 represent extreme cases of very small or very large errors.

4.3.2 Selecting Calibration Stars

The quantity and location of reference stars used in calibration effects the precision of the mount model. A large number of stars distributed throughout the observing range would seem to be ideal for producing precise corrections but, because the errors in individual observations depend on the position of the telescope, restricting the region of sky from which calibration stars are selected may reduce the total error in the data and produce a better model. Similarly, because observing more calibration stars takes more time, it may be desirable to limit the number of calibration stars used if doing so does not significantly reduce the precision of the model.

The telescope pointing error data used in this research primarily came from archived data so the selection method was restricted to using the stars originally observed. Application of the results of this work, however, might benefit from more deliberate star selection.

4.3.3 Determination of True Coordinates

Because stars are used as references for telescope pointing, it is important to accurately know the absolute positions of the calibration stars. Stars maintain nearly fixed positions relative to each other but move with respect to the earth on a daily basis. Variations in the relative positions also occur slowly over centuries and must be considered in calculating the location of a star at a particular time. The process of calculating the location of a particular star relative to an earthbound observer involves obtaining star coordinates from a star catalog, reducing the coordinates to the current date and time, and transforming the coordinates to telescope axis positions. Each step is briefly discussed below.

It is becoming standard convention to use a Cartesian coordinate system for precise astronomical calculations and rotation matrices to perform coordinate transformations. The rotation matrix approach used in this work enables it to be utilized directly with that convention. However, the available data were not in Cartesian form and producing the astronomical coordinate transformations was beyond the scope of this work so that method of coordinate reduction was not developed for this work.

4.3.3.1 Star Catalog Coordinates

Star catalogs list the *mean positions* of stars in the sky and have been published for centuries. Many specialize in certain types of stars, those in specific sections of the sky, and so forth. For telescope calibration, bright stars are required, and are usually those found in the *Fundamental Katalog* (FK), a standard position reference for bright stars.

Because stars move over time, the positions for stars in any catalog are stated for a particular instant, referred to as the *epoch* of the catalog. It is generally not important which epoch the catalog uses as long as it is known and the appropriate corrections are applied to adjust the catalog positions for the current date and time. Procedures for making these conversions are detailed in the *Astronomical Almanac* (2000).

4.3.3.2 Reduction of Coordinates

Once the mean position of a reference star is obtained from a star catalog, its *apparent position* at the time of observation is calculated. The apparent position is the position at which an object would be observed from the center of the earth. Converting from mean position to apparent position involves applying corrections for the long term motion of the star (*proper motion*); parallax caused by the revolution of the earth around the sun (*annual parallax*); the gravitational effect of the sun's mass on the starlight (*light deflection*); the effect of the wobble of the earth's rotation axis (*precession*); and other small effects. These are straightforward corrections that can be computed with an accuracy that introduces negligible error in star coordinates.

After the catalog positions are reduced to apparent position, the *true position* is found by applying the effects of the geographic position of the observer and refraction of the atmosphere. *True position* is an incorrect term but was used to distinguish it from the correct term, *observed position*. Here, *observed position* means the position at which a star is observed during the calibration process as measured by the telescope's encoders. Although this is not standard usage in astronomy it was considered less confusing for the engineering problem considered here and is consistent with the statistical terminology used for the measured values.

The fact that the observer's geographic position is not at the center of the earth requires two additional adjustments to the apparent position of a star, corrections for daily parallax and other small diurnal effects and transformations from the astronomical coordinate system (right ascension and declination) to a suitable telescope coordinate system, in this case azimuth and elevation.

A correction for refraction of starlight by the earth's atmosphere must also be applied. This requires a relatively large correction that depends on the elevation angle obtained from the coordinate transformation. Coordinate transformation and refraction correction is discussed in the next section.

4.3.3.3 Coordinate Transformations

Astronomers describe the position of celestial objects using a coordinate system based on the projection of the earth's equator into the sky, an imaginary circle called the *celestial equator*. An object's position is indicated by two coordinates, an angle along the celestial equator from a fixed reference point and another angle perpendicular to the celestial equator. The first angle is called the *right ascension (RA)*, α, and is measured from the *vernal equinox*, the point on the celestial equator where the sun crosses it in the spring. The vernal equinox is a (nearly) fixed point in the sky. The second angle is referred to as the *declination (DEC)*, δ. Star coordinates are fixed in the *RA-DEC* system and adopting it greatly simplifies many astronomical calculations.

Another invention of astronomers also simplifies calculations. Because most of the apparent motion of stars results from the rotation of the earth and its revolution about the sun, stars appear to move around the earth with a period of slightly less than one day. Astronomers developed a system of timekeeping called *sidereal time* to exploit this periodicity and simplify coordinate transformations. One sidereal day is the time between successive appearances of a particular star at a particular location in the sky and is approximately 23 hours and 56 minutes.

In astronomical calculations, local sidereal time is usually used to determine the precise location of stars and is found from

$$LST = GST + \lambda \tag{4.22}$$

where GST is the Greenwich sidereal time and λ is the east longitude of the telescope. A special type of astronomical calendar called an ephemeris is used to calculate GST from the civil time.

The star coordinates and local sidereal time lead directly to the axis settings for an equatorial telescope. The angle that the polar axis should be set to, known as the *hour angle,* is found from

$$H = LST - \alpha \tag{4.23}$$

and the angle for the declination axis is fixed at the star's declination coordinate.

For an altazimuth telescope, these angles must be transformed to azimuth and elevation angles. These can be found using

$$\sin E = \sin\phi \sin\delta + \cos\phi \cos\delta \cos H \tag{4.24a}$$

$$\sin A = -\cos\delta \sin H \sec E \tag{4.24b}$$

where H is as defined above, ϕ is the latitude, positive for the northern hemisphere and negative for the southern hemisphere (Smart, 1977; National Almanac Office, 2000).

Atmospheric refraction increases the elevation of any object but there is no effect on the azimuth angle. Wallace (1996) provided an expression for the angle through which refraction appears to raise an object. His expression can be rewritten as

$$\Delta E = B \cot E_r + C \cot^3 E_r \tag{4.25}$$

where B and C are functions of temperature, pressure, humidity, and wavelength. Equation (4.25) gives the apparent elevation change, ΔE of an object in terms of the position where it is observed, the *refracted position*, E_r. For a typical observing site B is about 200 μrad and C is about –0.2 μrad. Finding the correction to apply to an apparent position of a star to find the true position requires that eqn. (4.25) be rewritten in terms of the apparent (unrefracted) position, E_a. No exact solution exists but Wallace (1996) gave an approximation which is accurate to better than 0.005 μrad:

$$\Delta E = \frac{B \cot E_a + C \cot^3 E_a}{1 + (B + 3C \cot^2 E_a) \csc^2 E_a} \tag{4.26}$$

Additional error will result from uncertainty in measuring the temperature, pressure, and humidity of the atmosphere as well as unmeasured variation in these properties along the light path through the atmosphere. The error will be a function of elevation angle as well as the sensitivity of B and C to the measured properties of the air. Refraction corrections made using air properties measured near the telescope are typically accurate to within about 30 μrad for stars above 15° elevation (National Almanac Office, 2000).

4.3.4 Making Observations

Calibration observations are made by pointing the telescope to the predicted position of a reference star and measuring the difference between the observed position, indicated by the telescope's encoders, and the true position, established by calculation. The measurement may be made visually or with an electronic sensor. Initially, several crude iterations may be required before the differences are small enough so that the star always appears within the field-of-view of the telescope. Such iteration is generally only required during installation and initialization and is not usually a part of calibration.

The measurements of the position deviations are influenced by three major sources of error: the atmosphere, the detector, and the observing process. The atmosphere and detector introduce random error into each observation as discussed in Chapter 2. The error caused by the atmosphere varies with elevation angle while the detector errors are constant everywhere in the sky. This means the individual pointing errors are not exactly identically distributed and do not have constant variance. Similarly, tracking a star to make calibration observations requires the telescope axes to move at different rates depending on the elevation angle. If there are servo errors that depend on velocity, they will produce position-dependent variation in the model. These effects, however, were found to be negligible and were ignored for this work.

4.3.5 Resulting Data

Position error measurements are recorded in a file for later processing by the mount model software. Part of a file obtained from the ARC 3.5-meter telescope is shown in Fig. 4.3 below and is typical of the data files used by many observatories. The file contained 57 star observations but all except the first two and the last two have been eliminated to save space.

```
! Pointing data for TPOINT; read using the GETDAT command

! TAI date = 14-MAR-2000 07:11:00.69

 32.780361  ! latitude north (deg)

! User Pos       Actual Physical       Des Mt - Act Phys      Des Mt - Act Mt

! 1       2       Az          Alt        Az         Alt        Az         Alt

!(deg)  (deg)   (deg)       (deg)      (deg)      (deg)      (deg)      (deg)

146.47  18.68 291.964098  61.321391  0.026667   0.089960   0.004779   0.003480

145.93  14.02 298.371526  57.881591  0.020711   0.077757   0.000816  -0.001825

.

.

.

155.86  -4.07 306.652739  37.625731 -0.003257   0.019627   0.000141   0.000606

165.65  -3.51 315.872587  44.056342  0.003988   0.036395   0.000519   0.000368
```

Figure 4.3 Partial data file containing reference star observations

The terms in the headings of the file shown in Fig. 4.3 have the following meaning:

User Pos is the user-supplied position for the object. In this case, right ascension and declination of the star in the J2000.0 FK5 catalog.

Actual Physical (Act Phys) is the true location of the star.

Actual Mount (*Act Mt*) is the mount position the telescope actually went to according to the telescope encoders.

Desired Mount (*Des Mt*) is what the encoder readings should have been to center the reference star, determined by combining the measured pointing error of the reference star with the current mount position.

Des Mt - Act Phys is the correction that should have been calculated from the pointing model. This is the pointing error.

Des Mt - Act Mt is the error in the correction being calculated with the current mount model.

A ninth column, containing the mean Julian date to a resolution of 10 milliseconds is also included in the data file but has been removed in the sample above because it is not routinely used in the mount model calculations, but provides a record of the precise time of each observation.

4.4 Statistical Model

4.4.1 Overview

A statistical model allows the deterministic and stochastic influences to be separated and provides the means for estimating the underlying static physical errors. Regression is commonly used for fitting a mount model and was used here for consistency. However, since the goal here was to make precise estimates of the coefficients of the model instead of producing a good overall fit, a modification to the standard approach was required.

4.4.2 Regression Model

A regression model of the form

$$\Delta\mathbf{P}_i = \mathbf{F}(A_i, E_i) + \boldsymbol{\varepsilon}_i \tag{4.27}$$

was used where $\Delta\mathbf{P}_i$ is the pointing error vector, A_i and E_i are the desired azimuth and elevation angles of the i^{th} calibration star respectively, $\mathbf{F}$ is a functional representation of the kinematic model, and ε_i is the error vector associated with the measurement. Each of the vectors $\Delta\mathbf{P}_i$ and ε_i have an azimuth component and an elevation component. Using eqns. (4.19a) and (4.19b), the model can be written as

$$\Delta\mathbf{P}_i = \begin{bmatrix} \Delta\mathbf{P}_\mathrm{A} \\ \Delta\mathbf{P}_\mathrm{E} \end{bmatrix}_i = \begin{bmatrix} \mathbf{X}_\mathrm{A} \\ \mathbf{X}_\mathrm{E} \end{bmatrix}_i [\boldsymbol{\beta}] + \varepsilon_i \tag{4.28}$$

Various methods are described in the literature for estimating the vector $\boldsymbol{\beta}$ and the components of $\boldsymbol{\beta}$ can then be related to the underlying physical errors in the telescope. The methods for estimating the $\boldsymbol{\beta}$ vector used in this work are discussed in the following section.

4.5 Parameter Identification

4.5.1 Modified Ordinary Least Squares Regression

4.5.1.1 Parameter Estimates

As discussed in Chapters 2 and 3, modified ordinary least squares (MOLS) regression is commonly used to estimate the model parameters. In MOLS regression, the objective is to minimize the sum of the squared differences between the pointing error predicted by the statistical model and the observed pointing error. The observed pointing errors are contained in the response vectors

$$\Delta\mathbf{P}_\mathrm{A} = [\Delta A_1 \quad \Delta A_2 \quad \cdots \quad \Delta A_n]^\mathrm{T} \tag{4.29a}$$

$$\Delta\mathbf{P}_\mathrm{E} = [\Delta E_1 \quad \Delta E_2 \quad \cdots \quad \Delta E_n]^\mathrm{T} \tag{4.29b}$$

and the estimated pointing errors are found from

$$\Delta\hat{\mathbf{P}}_\mathrm{A} = \mathbf{X}_\mathrm{A}\boldsymbol{\beta} \tag{4.30a}$$

$$\Delta\hat{\mathbf{P}}_\mathrm{E} = \mathbf{X}_\mathrm{E}\boldsymbol{\beta} \tag{4.30b}$$

where the model matrices $\mathbf{X_A}$ and $\mathbf{X_E}$ are given by

$$\mathbf{X}_\mathbf{A} = \begin{bmatrix} \cdots & \cdots & -\sec E_1 & \cdots & \cos A_1 \tan E_1 & 0 \\ \cdots & \cdots & -\sec E_2 & \cdots & \cos A_2 \tan E_2 & 0 \\ \vdots & \vdots & \vdots & \vdots & \vdots & \vdots \\ \cdots & \cdots & -\sec E_n & \cdots & \cos A_n \tan E_n & 0 \end{bmatrix} \tag{4.31a}$$

and

$$\mathbf{X}_\mathbf{E} = \begin{bmatrix} \cdots & \cdots & 0 & \cdots & \sin A_1 & -\cot E_1 \\ \cdots & \cdots & 0 & \cdots & \sin A_2 & -\cot E_2 \\ \vdots & \vdots & \vdots & \vdots & \vdots & \vdots \\ \cdots & \cdots & 0 & \cdots & \sin A_n & -\cot E_n \end{bmatrix} \tag{4.31b}$$

The parameter vector

$$\boldsymbol{\beta} = \begin{bmatrix} \cdots & \gamma & \cdots & \psi_Y & \delta_T \end{bmatrix}^\mathbf{T} \tag{4.32}$$

is the independent variable to be determined. The first four columns of the model matrices and parameter vector allow for encoder scale and offset to be included for each axis.

The difference between the predicted error and the observed error for each component is

$$\Delta\mathbf{P} - \Delta\hat{\mathbf{P}} = \Delta\mathbf{P} - \mathbf{X}\boldsymbol{\beta} \tag{4.33}$$

and the sum of the squares of the differences for all the observations is given by

$$Q = (\Delta\mathbf{P}_\mathbf{A} - \mathbf{X}_\mathbf{A}\boldsymbol{\beta})^\mathbf{T}(\Delta\mathbf{P}_\mathbf{A} - \mathbf{X}_\mathbf{A}\boldsymbol{\beta}) + (\Delta\mathbf{P}_\mathbf{E} - \mathbf{X}_\mathbf{E}\boldsymbol{\beta})^\mathbf{T}(\Delta\mathbf{P}_\mathbf{E} - \mathbf{X}_\mathbf{E}\boldsymbol{\beta}) \tag{4.34}$$

or

$$Q = \left(\Delta\mathbf{P_A}^{\mathrm{T}}\Delta\mathbf{P_A} + \Delta\mathbf{P_E}^{\mathrm{T}}\Delta\mathbf{P_E}\right) - 2\boldsymbol{\beta}^{\mathrm{T}}(\mathbf{X_A}^{\mathrm{T}}\Delta\mathbf{P_A} + \mathbf{X_E}^{\mathrm{T}}\Delta\mathbf{P_E}) \\ + \boldsymbol{\beta}^{\mathrm{T}}(\mathbf{X_A}^{\mathrm{T}}\mathbf{X_A} + \mathbf{X_E}^{\mathrm{T}}\mathbf{X_E})\boldsymbol{\beta} \tag{4.35}$$

Minimization was performed by differentiating Q with respect to the vector $\boldsymbol{\beta}$ and equating the result to $\mathbf{0}$. The derivative of the scalar Q with respect to the vector $\boldsymbol{\beta}$ is given by

$$\frac{\partial Q}{\partial \boldsymbol{\beta}} = \begin{bmatrix} \frac{\partial Q}{\partial \beta_1} & \frac{\partial Q}{\partial \beta_2} & \cdots & \frac{\partial Q}{\partial \beta_p} \end{bmatrix}^{\mathrm{T}} \tag{4.36}$$

which can be written as

$$\frac{\partial Q}{\partial \boldsymbol{\beta}} = -2\left(\mathbf{X_A}^{\mathrm{T}}\Delta\mathbf{P_A} + \mathbf{X_E}^{\mathrm{T}}\Delta\mathbf{P_E}\right) + 2\left(\mathbf{X_A}^{\mathrm{T}}\mathbf{X_A} + \mathbf{X_E}^{\mathrm{T}}\mathbf{X_E}\right)\boldsymbol{\beta} = \mathbf{0} \tag{4.37}$$

and the estimated $\boldsymbol{\beta}$, given by $\hat{\boldsymbol{\beta}}$ was found from

$$\hat{\boldsymbol{\beta}} = \left(\mathbf{X_A}^{\mathrm{T}}\mathbf{X_A} + \mathbf{X_E}^{\mathrm{T}}\mathbf{X_E}\right)^{-1}\left(\mathbf{X_A}^{\mathrm{T}}\Delta\mathbf{P_A} + \mathbf{X_E}^{\mathrm{T}}\Delta\mathbf{P_E}\right) \tag{4.38}$$

In practice, the first matrix in eqn. (4.38) is often ill-conditioned so eqn. (4.37) is solved using singular value decomposition (SVD) instead (Wallace, 2000). The source of the ill-conditioning is the correlation among the predictor functions. In principal, calibration stars could be selected in positions that reduced or eliminated the correlation. This would usually not be feasible in practice, however, because there generally are not enough bright stars visible to select from. Too many would have to be rejected because they failed to meet the "correlation criterion" and the remaining set of calibration stars would be too small to produce good results.

Selecting calibration stars in positions that mitigate the correlation is the approach taken in designed experiments. An attempt was made to use this approach for this research but it was found that, of the large number of possible combinations of calibration stars, few had significantly lower internal correlation. The search procedure required to identify these "good" set of stars was considered impractical.

The SVD procedure has the potential for introducing bias into a solution because it calls for modifying some values of the matrix to reduce the degree of ill-conditioning. The SVD process involves decomposing the matrix into three square matrices, two orthogonal matrices that can be inverted by transposing and a diagonal matrix which can be inverted by forming another diagonal matrix with elements equal to the reciprocals of the elements of the original diagonal matrix. When these reciprocals are taken, if an element of the original matrix is very close to zero, its reciprocal is set to zero (Press et al., 1989). This has the effect of introducing bias into the result. The solutions preformed for this work, however, did not require this adjustment.

4.5.1.2 Parameter Precision

The purpose of the statistical model is to partition the variation in the observed data into a portion that can be explained by the kinematic model and a portion that cannot. In general, one model is considered better than another if it is able to explain more of the variation in the data. Neter et al. (1996) provided an analysis of the variance in a standard regression model and the following pages develop analogous expressions for the model proposed here.

The total variability in the pointing errors about their means is given by

$$SSTO = \sum_{i=1} \left\{ \left(\Delta P_{A,i} - \Delta \overline{P}_A \right)^2 + \left(\Delta P_{E,i} - \Delta \overline{P}_E \right)^2 \right\} \tag{4.39}$$

where $\Delta P_{A,i}$ and $\Delta P_{E,i}$ are the azimuth and elevation pointing errors for the i^{th} reference star respectively and $\Delta \overline{P}_A$ and $\Delta \overline{P}_E$ are the mean azimuth and elevation pointing errors. This can be written in matrix form as

$$SSTO = \mathbf{\Delta P_A}^{\mathbf{T}} \mathbf{\Delta P_A} + \mathbf{\Delta P_E}^{\mathbf{T}} \mathbf{\Delta P_E} - \frac{1}{n} \left(\mathbf{\Delta P_A}^{\mathbf{T}} \mathbf{J} \mathbf{\Delta P_A} + \mathbf{\Delta P_E}^{\mathbf{T}} \mathbf{J} \mathbf{\Delta P_E} \right) \tag{4.40}$$

where $\mathbf{J}$ is an n by n matrix of 1s. The amount of variability not explained by the data, the sum of the squares of the residuals, was the quantity minimized in the regression. From eqn. (4.34) it is

$$SSE = \left(\mathbf{\Delta P_A} - \mathbf{X_A} \hat{\boldsymbol{\beta}} \right)^{\mathbf{T}} \left(\mathbf{\Delta P_A} - \mathbf{X_A} \hat{\boldsymbol{\beta}} \right) + \left(\mathbf{\Delta P_E} - \mathbf{X_E} \hat{\boldsymbol{\beta}} \right)^{\mathbf{T}} \left(\mathbf{\Delta P_E} - \mathbf{X_E} \hat{\boldsymbol{\beta}} \right) \tag{4.41}$$

which can be simplified to

$$SSE = \left(\mathbf{\Delta P_A}^{\mathbf{T}} \mathbf{\Delta P_A} + \mathbf{\Delta P_E}^{\mathbf{T}} \mathbf{\Delta P_E} \right) - \hat{\boldsymbol{\beta}}^{\mathbf{T}} \left(\mathbf{X_A}^{\mathbf{T}} \mathbf{\Delta P_A} + \mathbf{X_E}^{\mathbf{T}} \mathbf{\Delta P_E} \right) \tag{4.42}$$

The remaining variation, the portion explained by the model is

$$SSR = SSTO - SSE \tag{4.43}$$

or

$$SSR = \hat{\boldsymbol{\beta}}^{\mathbf{T}} \left(\mathbf{X_A}^{\mathbf{T}} \mathbf{\Delta P_A} + \mathbf{X_E}^{\mathbf{T}} \mathbf{\Delta P_E} \right) - \frac{1}{n} \left(\mathbf{\Delta P_A}^{\mathbf{T}} \mathbf{J} \mathbf{\Delta P_A} + \mathbf{\Delta P_E}^{\mathbf{T}} \mathbf{J} \mathbf{\Delta P_E} \right) \tag{4.44}$$

These sums of squares can be used to assess the overall model. One widely used measure is the coefficient of multiple determination

$$R^2 = \frac{SSR}{SSTO} \tag{4.45}$$

which ranges from 0 to 1. The value of R^2 is the fraction of variability in the data that is explained by the model. A model with a higher value of R^2 explains more of the variability in the data and is sometimes considered a better model. Such a model might produce better pointing corrections but would not necessarily provide more precise estimates of the parameters. All the models used in this work had R^2 values in excess of 99% so the coefficient of multiple determination was not a good measure for discriminating among models and is not reported a part of the results.

The first part of research question 1 concerned finding the precision of the geometric errors. The precision can be computed directly from the standard error associated with each regression parameter. When the differences between the observed pointing errors and the fitted pointing errors follow a normal distribution, the estimated difference between the actual value of parameter β_j and the estimated value of the parameter is a random variable given by

$$\frac{\hat{\beta}_j - \beta_j}{s_j} \tag{4.46}$$

which has a t-distribution with $2n - p$ degrees-of-freedom where n is the number calibration stars, p is the number of parameters fitted, and s_j is the standard error associated with the parameter, which can be found using eqn. (4.49). The $1 - \alpha$ confidence interval for the parameter is then given by

$$\hat{\beta}_j \pm t(1 - \frac{\alpha}{2}, 2n - p) s_j \tag{4.47}$$

Determining the precision of individual parameter estimates required more detailed knowledge of the variation within the model. The variance-covariance matrix provided that information and was found using

$$\boldsymbol{\sigma}^2\left[\hat{\boldsymbol{\beta}}\right] = \sigma^2\left(\mathbf{X_A}^\mathbf{T}\mathbf{X_A} + \mathbf{X_E}^\mathbf{T}\mathbf{X_E}\right)^{-1} \tag{4.48}$$

where σ^2 was the constant variance of the residual pointing errors. Ordinarily σ^2 is unknown but can be estimated to give the estimated coefficient variance-covariance matrix

$$\mathbf{s}^2\left[\hat{\boldsymbol{\beta}}\right] = MSE\left(\mathbf{X_A}^\mathbf{T}\mathbf{X_A} + \mathbf{X_E}^\mathbf{T}\mathbf{X_E}\right)^{-1} \tag{4.49}$$

where *MSE* is the mean square error given by

$$MSE = \frac{SSE}{2n - p} \tag{4.50}$$

The expression in eqn. (4.49) contains the variance of each estimated parameter of the kinematic model based on the overall error, *MSE*. It also contains the same ill-conditioned matrix as eqn. (4.38) that often must be evaluated using SVD.

The second part of research question 1 concerned improving the precision of the parameter estimates. The ill-conditioning inflates the estimate of the variance obtained using eqn. (4.49) and makes the error estimates less precise than those that might be obtained from a model without correlated predictors.

Identifying an alternative method for estimating this variance was key to answering the second part of research question number one. Several methods that can be used to reduce the standard errors in the coefficients were discussed briefly in Chapter 2.

Three of these, bootstrapping, ridge regression, and Bayesian regression were applied to the data and compared to determine which, if any, produced the best improvement in the precision of the individual parameter estimates over MOLS. In this case, improvement was defined as producing a narrower parameter estimate without introducing an unknown bias. Because the precision of the estimated parameter depends only on its standard error, not on the method used to obtain it, eqn (4.47) could be used any method.

Answering research questions 2 and 3 required knowledge about the pointing error in a telescope when corrections (the response) were calculated using the coefficients estimated above. Because the coefficients are not known precisely, the resulting corrections are uncertain and a pointing error results. Several ways of describing the overall pointing error are discussed in section 4.6 and several of those require the estimated variance of the response. This can be found directly from the regression model given in eqn. (4.28). It is

$$\mathbf{s}^2\left[\Delta\hat{\mathbf{P}}\right] = \mathbf{s}^2\left[\begin{bmatrix}\mathbf{X}_{\mathbf{A}h}\\ \mathbf{X}_{\mathbf{E}h}\end{bmatrix}\hat{\boldsymbol{\beta}}\right] \tag{4.51}$$

and after expansion is

$$\mathbf{s}^2\left[\Delta\hat{\mathbf{P}}\right] = \begin{bmatrix}\mathbf{X}_{\mathbf{A}h}\mathbf{s}^2\left\{\hat{\boldsymbol{\beta}}\right\}\mathbf{X}_{\mathbf{A}h}^{\mathbf{T}}\\ \mathbf{X}_{\mathbf{E}h}\mathbf{s}^2\left\{\hat{\boldsymbol{\beta}}\right\}\mathbf{X}_{\mathbf{E}h}^{\mathbf{T}}\end{bmatrix} \tag{4.52}$$

In eqns (4.51) and (4.52), $\mathbf{X}_{\mathbf{A}h}$ and $\mathbf{X}_{\mathbf{E}h}$ are row vectors containing the predictor functions for the new desired azimuth and elevation angles respectively. The columns are similar to those of $\mathbf{X}_{\mathbf{A}}$ and $\mathbf{X}_{\mathbf{E}}$ defined in eqns. (4.31a) and (4.31b).

4.5.2 Bootstrapping

Bootstrapping refers to various statistical methods that have been developed to deal with correlation or heteroscedasticity problems in models or with situations where the distribution of errors is nonnormal or unknown. Bootstrapping methods generally involve resampling from the original data to create new data sets based on the original set. A model is fit to each new data set and the parameter estimates form samples from which inferences about the true values of the parameters are made.

For this work, resamples of size n were taken with replacement from the n original observations. This produced data sets that contained the same number of observations as the original set but some observations were randomly excluded and others were randomly duplicated. A MOLS model was fit for each resample resulting in a set of estimates for each component of β. These estimates represented a sample drawn from the population of values for that coefficient and were used to estimate the expected value of each physical error as well as its variability and distribution.

4.5.2.1 Parameter Estimates and Precision

In a bootstrapping analysis, the median value of the set of estimates for each β_j is used to estimate the expected value of the population parameter and the $\alpha/2$ and $1 - \alpha/2$ percentiles estimate the confidence limits for each parameter. For this work, the confidence limits obtained from bootstrapping were converted to an approximate standard error for each term to facilitate comparisons with other methods. The conversion was accomplished by assuming the confidence limits were symmetric about the median and solving eqn. (4.47) for s_j. The result yielded the following approximation for the standard error:

$$s_j \approx \frac{q_{1-\alpha/2} - q_{\alpha/2}}{2t(1-\frac{\alpha}{2}, 2n-p)} \tag{4.53}$$

where $q_{\alpha/2}$ and $q_{1-\alpha/2}$ are the $\alpha/2$ and 1 - $\alpha/2$ percentiles of the bootstrapped estimates respectively. This method for computing the standard error relies on the assumption that each coefficient sample follows a *t*-distribution. An evaluation of the bootstrapping results for this work showed that the sampling distributions of all the coefficients were mound-shaped but formal goodness-of-fit tests were not performed. Because the bootstrapping method was found to be relatively ineffective at improving the precision of the estimates, there would have been little benefit to formally verifying the parameter distributions to justify eqn. (4.53).

4.5.2.2 Determining the Required Number of Resamples

The number of resamples required to achieve a specified precision for a bootstrap estimate varies among applications. In general, the necessary number of resamples must be experimentally determined for each application. The required number depends on the degree of correlation present in the model, the relative amount of random error present, and whether the random component of the errors is constant.

For this work, the required number of resamples was determined by plotting the standard error of all coefficients against the number of samples for simulated data set 3 to observe when the standard error stabilized and asymptotically approached a limiting value. Simulated set 3 was used because it had similar error to that in the data from working telescopes.

4.5.3 Ridge Regression

4.5.3.1 Estimated Parameters

Ridge regression is a type of biased estimation which mitigates the effect of the ill-conditioning of the matrix in eqn. (4.38) by introducing bias into the model (Seber, 1977). In general, biased estimation involves adding a small amount to the ill-conditioned matrix to reduce the variance of the parameter estimates. Using ridge regression involves two steps, selecting the amount of bias to introduce into the model and choosing which of the many similar formulations described in the literature to use to apply the bias.

For this work, a vector-response modification of a formulation described by Seber (1977) was used. A small constant term, k, was added to each diagonal element of the first matrix of eqn. (4.38) and the *ridge estimator* of the model coefficients was obtained from

$$\hat{\boldsymbol{\beta}}_{(k)} = \left(\mathbf{X_A}^{\mathbf{T}}\mathbf{X_A} + \mathbf{X_E}^{\mathbf{T}}\mathbf{X_E} + k\mathbf{I}\right)^{-1}\left(\mathbf{X_A}^{\mathbf{T}}\Delta\mathbf{P_A} + \mathbf{X_E}^{\mathbf{T}}\Delta\mathbf{P_E}\right) \tag{4.54}$$

A different set of coefficient estimates is obtained for each value of k. Other formulations involve replacing the $k\mathbf{I}$ matrix with a more general biasing matrix, $\mathbf{C}$, to handle special problems with the model or applying the bias to the standardized regression model to improve results. Neither of these was found to be necessary here.

Writing the estimated coefficient vector as a product of a biasing matrix, $\mathbf{K}$, and the MOLS estimate of the parameters allows the solution to be expressed in terms of the MOLS solution. When the biasing matrix is written as

$$\mathbf{K} = \left[\mathbf{I} + k\left(\mathbf{X_A}^{\mathbf{T}}\mathbf{X_A} + \mathbf{X_E}^{\mathbf{T}}\mathbf{X_E}\right)^{-1}\right]^{-1} \tag{4.55}$$

The ridge estimate for the model parameters becomes

$$\hat{\boldsymbol{\beta}}_{(k)} = \mathbf{K}\hat{\boldsymbol{\beta}} \tag{4.56}$$

and the variance-covariance matrix can be found to be

$$\boldsymbol{\sigma}^2\left[\hat{\boldsymbol{\beta}}_{(k)}\right] = \mathbf{K}\,\boldsymbol{\sigma}^2\left[\hat{\boldsymbol{\beta}}\right]\mathbf{K}^{\mathrm{T}} \tag{4.57}$$

Once the ridge estimates of the parameter vector and variance-covariance matrix are found, they can be used in place of the MOLS estimates in the eqns. (4.39) through (4.52) above to calculate the corresponding values for the ridge regression solution.

4.5.3.2 Selecting the Biasing Parameter

An appropriate value for k must be selected to reduce the coefficient variances without introducing too much additional error into the model. One widely used technique for selecting the bias parameter utilizes the *ridge trace*, a plot of all the estimated coefficients versus the parameter k. The appropriate value is selected by noting where the estimated parameters begin to stabilize without substantially increasing the total error in the model. Some judgment is involved and, in general, a different ridge parameter must be used for each application.

For each data set considered in this work, a simultaneous plot of all the estimated model parameters and a separate plot of the estimated standard deviation of the residual pointing errors, $\hat{\sigma}$, were made for values of k ranging from 0 to 1. As the value of k was increased from 0, the estimated parameters initially remained stable at their MOLS values but then began to approach other stable values. At the same time, $\hat{\sigma}$ remained close to its MOLS value at first but increased rapidly as k became large. A value of k was selected where the parameters had stabilized at new values but $\hat{\sigma}$ had not increased dramatically above its MOLS value.

4.5.4 Bayesian Regression

Bayesian regression uses previously known information about one or more of the regression parameters to refine the solution. In the special case where one of the physical errors is known exactly, it can be removed from the parameter estimation problem directly by preprocessing the data to eliminate the effect of the known error and then fitting a reduced model. This is commonly done for telescope mount modeling. Bayesian regression, by contrast, is used when the true value of an error is known only with uncertainty. Knowledge of the distribution of the parameters is used to determine which values are most consistent with the observed data and other assessments of the physical errors.

4.5.4.1 Parameter Estimates

In ordinary least squares regression, the coefficients obtained are those most consistent with the observed data only. Each observed sample point (telescope pointing error in this case) is a random variable and the regression procedure yields the conditional expected value of the model coefficient vector given the observed data, that is:

$$\hat{\boldsymbol{\beta}} = \mathrm{E}(\boldsymbol{\beta} \mid \Delta\mathbf{P}_{\mathrm{A}}, \Delta\mathbf{P}_{\mathrm{E}}) \tag{4.58}$$

This expected value is obtained from the conditional distribution $f(\boldsymbol{\beta} \mid \Delta\mathbf{P}_{\mathrm{A}}, \Delta\mathbf{P}_{\mathrm{E}})$ which, using Bayes' Rule, can be written as

$$f(\boldsymbol{\beta} \mid \Delta\mathbf{P}_{\mathrm{A}}, \Delta\mathbf{P}_{\mathrm{E}}) = \frac{f(\Delta\mathbf{P}_{\mathrm{A}}, \Delta\mathbf{P}_{\mathrm{E}}, \boldsymbol{\beta})}{f(\Delta\mathbf{P}_{\mathrm{A}}, \Delta\mathbf{P}_{\mathrm{E}})} \tag{4.59}$$

The numerator of eqn. (4.59) can be found using the data and prior knowledge of the distribution of the parameters. The joint probability distribution of the observed residual pointing errors occurring when a certain correction is applied is represented by $f(\mathbf{\Delta P_A}, \mathbf{\Delta P_E} \mid \boldsymbol{\beta})$ and, using Bayes' Rule again, can be expressed as

$$f(\mathbf{\Delta P_A}, \mathbf{\Delta P_E} \mid \boldsymbol{\beta}) = \frac{f(\mathbf{\Delta P_A}, \mathbf{\Delta P_E}, \boldsymbol{\beta})}{f(\boldsymbol{\beta})} \tag{4.60}$$

which can be rearranged to give

$$f(\mathbf{\Delta P_A}, \mathbf{\Delta P_E}, \boldsymbol{\beta}) = f(\mathbf{\Delta P_A}, \mathbf{\Delta P_E} \mid \boldsymbol{\beta}) f(\boldsymbol{\beta}) \tag{4.61}$$

which is the numerator of eqn. (4.59). This can be integrated to obtain the denominator of eqn. (4.59).

Under the assumptions of the normally distributed error regression model employed for this research, the individual pointing errors remaining after fitting the MOLS solution are independently and identically distributed following a normal distribution with mean zero and standard deviation σ. Their joint distribution is:

$$f(\mathbf{\Delta P_A}, \mathbf{\Delta P_E} \mid \boldsymbol{\beta}) = \frac{1}{(2\pi)^n \sigma^{2n}} e^{-\frac{1}{2\sigma^2}\left((\mathbf{\Delta P_A} - \mathbf{X_A}\boldsymbol{\beta})^T(\mathbf{\Delta P_A} - \mathbf{X_A}\boldsymbol{\beta}) + (\mathbf{\Delta P_E} - \mathbf{X_E}\boldsymbol{\beta})^T(\mathbf{\Delta P_E} - \mathbf{X_E}\boldsymbol{\beta})\right)} \tag{4.62}$$

The prior joint distribution of the parameter estimates was also required in eqn. (4.61). For this research, it was assumed that all the individual physical errors were independent, normally distributed random variables with known mean and standard deviation. The joint distribution of these parameters follows a multivariate normal distribution described by (Vinod, 1981):

$$f(\boldsymbol{\beta}) = \frac{1}{(2\pi)^{p/2}\left|\sigma^2\mathbf{V}\right|^{1/2}} e^{-\frac{1}{2\sigma^2}(\boldsymbol{\beta}-\boldsymbol{\beta}_0)^T\mathbf{V}^{-1}(\boldsymbol{\beta}-\boldsymbol{\beta}_0)} \tag{4.63}$$

where $\sigma^2\mathbf{V}$ is the variance-covariance matrix for the prior distribution of the parameters and σ is the MOLS estimate of the random error in the model. Although it was assumed that the physical errors were independent and normally distributed, similar expressions can be written when the physical errors are correlated or follow other distributions.

Substitution of eqn. (4.62) and eqn. (4.63) into eqn. (4.61) and the result into eqn. (4.59) yields an expression for the joint distribution of the model parameters given the observed data and the prior distribution. When the residual pointing errors follow a normal distribution and the prior distribution of the parameters is multivariate normal, all the joint distributions are also multivariate normal and, following Vinod (1981), the Bayesian estimate of the parameters given in eqn. (4.59) has normal distribution with parameters

$$\boldsymbol{\beta}^* = \left(\mathbf{X_A}^T\mathbf{X_A} + \mathbf{X_E}^T\mathbf{X_E} + \mathbf{V}^{-1}\right)^{-1}\left[\left(\mathbf{X_A}^T\mathbf{X_A} + \mathbf{X_E}^T\mathbf{X_E}\right)\hat{\boldsymbol{\beta}} + \mathbf{V}^{-1}\boldsymbol{\beta}_0\right] \tag{4.64a}$$

and

$$\left(\boldsymbol{\sigma}^*\right)^2 = \sigma^2\left(\mathbf{X_A}^T\mathbf{X_A} + \mathbf{X_E}^T\mathbf{X_E} + \mathbf{V}^{-1}\right)^{-1} \tag{4.64b}$$

Inspection of eqn. (4.64a) and comparison with eqn. (4.38) reveals that a Bayesian regression solution may be thought of as a variance-weighted mean of the MOLS solution and the mean prior value of each parameter. Bayesian regression can also be related to ridge regression. The Bayesian estimate for a particular parameter is produced by ridge regression when the biasing constant is set to $k = \frac{\sigma^2}{\sigma_0{}^2}$ where σ^2 is the model variance and $\sigma_0^{\,2}$ is the variance of the prior distribution of the particular parameter (Seber, 1977).

4.5.4.2 Prior Distribution Information

Applying Bayesian regression requires knowledge of both the form and the parameters of the prior distribution. When the prior distribution of the parameters is normal, the mean and standard deviation are needed and might be obtained from previous mount models, measurements, or design calculations.

Previous mount model results may provide some useful information but should be used with caution because the coefficient estimates may be correlated and imprecise. Measurements taken on the telescope itself may also be useful. When the prior distribution is obtained from a measurement, the measured value is used as the mean of the prior distribution and the precision of the measurement is used for the prior standard deviation.

Finally, calculations performed during the telescope design phase may be precise enough to improve the model. For example, flexure of the tube is usually predicted with a finite element model. Similarly, specifications on bearings or other components may allow certain errors to be bounded and therefore provide some improvements. In each of these cases the mean and standard deviation must be found based on an analysis of the calculation used to arrive at the result.

Alternatively, when better information is not available, the prior mean for a coefficient may be assumed to be zero (or any other number) provided an appropriately large standard deviation is applied to represent the lack of certainty. When infinite standard deviation is assigned to every prior coefficient estimate, the coefficient estimates obtained using Bayesian regression are identical to those obtained using ordinary least squares regression, regardless of the values used for the prior means. When the form of the prior distribution of the parameters is unknown, Bayesian regression can still be used following the procedure described by Vinod (1981) and others.

For the data obtained from the working telescopes in this study, three sources of prior information are often available: design calculations and specifications, measurements, and basic observations about the maximum errors that could be present without causing obvious problems with telescope function. Design calculations and specifications were useful for estimating tube flexure effects, encoder scaling errors, and encoder offset errors. Measurements published in technical reports provided useful prior information for bearing errors and some installation errors. Considerations of operating performance allowed errors such as telescope tilt, axis nonperpendicularity and optical axis misalignment to be bounded and those bounds were used to infer prior information.

Comprehensive and reliable prior information was not available for any of the telescopes considered in this study. Information from several telescopes was used to construct a set of prior information that constituted typical values and was used for all the telescopes. Specific bases for the assumed prior mean and standard deviation for each physical error are discussed below and summarized in Tables 4.5 and 4.6.

Encoder offset. It is usually impossible to install an encoder so that the absolute zero point is perfectly aligned with respect to the sky. The encoder offset term in the mount model compensates for any discrepancy. In practice, incremental encoders are often used on telescopes instead of absolute encoders and high precision fiducials are mounted so that the true absolute position is periodically updated. Even if the encoder is installed perfectly, other physical errors produce effects that are indistinguishable from encoder offsets. To allow for the uncertainty in installing encoders or separating other effects from encoder offsets, both encoder offset terms were assumed to have zero mean with 1000 μrad standard deviation reflecting high uncertainty in their value.

Encoder scale. The coefficient of the encoder scale term in the mount model is the angular error that develops as a telescope axis is rotated through 90°. For a packaged encoder mounted directly on a telescope axis, scale errors are negligible. When the encoder is coupled to the telescope axis through a friction roller, errors in the size of the rollers contributes to scale error. A similar situation occurs with tape encoders if the mounting surface has a small error in diameter. Scale effects were assumed to have zero mean and contribute an error of 0.01% of any rotation angle. For a 90° rotation the error would be 157 μrad and this was taken as the 3σ value to yield a standard deviation of 52 μrad.

Axis nonperpendicularity. The exact angle between the mechanical axes of an altazimuth telescope is difficult to measure precisely but must be kept close to 90° to avoid introducing optical errors. Morgan (1997) estimated that the angle must be within 872.7 μrad (3 arcminutes) for the ARC telescope to avoid seriously impacting telescope optical performance. Although the optical effect of axis nonperpendicularity depends on the optical design of the telescope, this value was taken as a typical 3σ value for "good practice" in telescope assembly. This resulted in an estimated standard deviation in axis nonperpendicularity of 290.9 μrad. Because there is no reason to assume the angle deviates in any particular direction, the prior mean was assumed to be zero.

Optical axis misalignment. Alignment of the mechanical axes to the optical axis is also difficult to measure and, for reasons similar to those discussed above for axis nonperpendicularity, the prior distribution was assumed to have a mean of zero and standard deviation of 358.8 μrad (Morgan, 1997).

Leveling. The northward and eastward tilt of a telescope are easily estimated from any mount model because they are not highly correlated with other terms. The precision obtained from even a crude mount model is usually much better than any independent measurement that can be made. In Chapter 2 it was explained that it would be possible to level a telescope within 300 μrad using a precision level. If this is taken as the 3σ value, the standard deviation would then be 100 μrad. There is no reason to expect that the telescope would be more likely to be tilted east or west so the east-west term was assumed to have a prior distribution of zero. There is a bias in north-south leveling as explained in Chapter 2 so the prior distribution of the coefficient corresponding to northward tilt was assigned a mean of 300 μrad, roughly the bias expected for a telescope located in northern mid-latitudes.

Tube flexure. In addition to causing a pointing error, flexure of the telescope tube has a major impact on optical performance and must be predicted accurately during the design phase. For the simulated data, it was assumed that the flexure has been predicted by a finite element analysis to 95% of the actual value and the standard deviation of the prediction is believed to be 5% of the predicted value. For the simulated data the actual value is known to be 100 μrad, so the prediction would have been 95 μrad with standard deviation 4.8 μrad. A preliminary finite element analysis of the ARC telescope tube predicted that the flexure along the 4800 millimeter tube would be approximately 250 microns producing an angular deflection of 52.1 μrad. Assuming the predicted value is within 5% of the actual value, the standard deviation was 2.6 μrad. This was used as a typical value for large telescopes.

Bearings. As explained in Chapter 3, the azimuth bearings are modeled as tilting the azimuth axis along the north-south and east-west directions by independent terms which both depend on $\cos A$. If the components of these effects were measured with the accuracy assumed in Chapter 2, the precision of each term would be about 20% of the total magnitude or about 2.8 μrad for the known errors in the simulated data. The measurement technique would not be expected to introduce significant bias so the actual values of the errors were used for the means of the prior distributions. Similar measurements would be possible on most telescopes. However, measurements were not available for the four telescopes from which data was obtained for this work so a different estimate of the prior distribution had to be used. For the real telescopes, the prior mean for each bearing component was assumed to be zero with standard deviation of 5 μrad. This is consistent with the measurements of bearing errors reported by Siegmund (1995) and others.

Table 4.5 Prior distribution information for the working telescopes

Parameter	Mean (μrad)	Standard Error (μrad)
Azimuth encoder offset	0.0	1000.0
Elevation encoder offset	0.0	1000.0
Azimuth encoder scale	0.0	52.0
Elevation encoder scale	0.0	52.0
Axis nonperpendicularity	0.0	290.9
Optical axis misalignment	0.0	358.8
Tilt toward north	300.0	100.0
Tilt toward east	0.0	100.0
Tube flexure	52.1	2.6
Azimuth bearing, NS term	0	5.0
Azimuth bearing, EW term	0	5.0
Elevation bearing, cosine term	0	5.0
Elevation bearing, sine term	0	5.0

For the simulated data, since the true errors were known, using the known values as prior information and assuming small variances would have produced excellent, but trivial, results. To produce more realistic results, the prior distribution of all errors except bearing and flexure errors were assumed to be normal with mean zero and standard deviations similar to those found for the working telescopes.

Table 4.6 Prior distribution information for the simulated data sets

Parameter	Mean (μrad)	Standard Error (μrad)
Azimuth encoder offset	0.0	1000.0
Elevation encoder offset	0.0	1000.0
Azimuth encoder scale	0.0	52.0
Elevation encoder scale	0.0	52.0
Axis nonperpendicularity	0.0	290.9
Optical axis misalignment	0.0	358.8
Tilt toward north	300.0	100.0
Tilt toward east	0.0	100.0
Tube flexure	95.0	4.8
Azimuth bearing, NS term	12.0	2.8
Azimuth bearing, EW term	7.5	2.8
Elevation bearing, cosine term	8.0	1.8
Elevation bearing, sine term	6.0	0.9

In many cases multiple prior estimates of some mechanical errors may be available and choosing among them would present a challenge. In most cases, the prior estimate with the lowest standard error, the most precise prior estimate, should be used. When the choice between two or more prior estimates is unclear, Dempster-Shafer Theory (the Dempster Rule) can provide a framework for combining prior estimates into a composite value for use in subsequent analysis, in this case Bayesian regression.

Dempster-Shafer Theory was originally described by Shafer (1976) but several authors have built upon that work and Liu (2001) provided a good, recent overview. Dempster-Shafer Theory is a flexible, convenient method for combining different pieces of evidence but must be used with caution. It produces counterintuitive results in some cases and can only be used when certain conditions are met. Barnett (1981) showed that the Dempster Rule reduces to Bayes' Rule when the distribution of the individual prior estimates is known but is more flexible in cases of greater ignorance. Zhang (1994) and Voorbraek (1991) separately discussed criteria for the application of the theory and concluded that the individual estimates to be combined must be "independent" is a way different from the ordinary concept of statistical independence.

4.6 Assessing Pointing Accuracy

The regression model provides a method for calculating the appropriate corrections to apply to the azimuth and elevation axes. After these corrections are applied, the telescope still will not point perfectly because of variation not explained by the model and because the estimates of the model parameters will not be exactly correct.

4.6.1 Observed Performance

In general, methods for assessing pointing performance fall into two categories, those based on observations and those based on predictions. The simplest measure of pointing accuracy using observed data uses the pointing error measurements made for the calibration. The position the telescope would have pointed to had the corrections been applied during the calibration measurements is calculated and the root mean square (rms) error is determined from

$$\Delta P_{rms} = \sqrt{\frac{\mathbf{\Delta P_A}^{\mathbf{T}}\mathbf{\Delta P_A} + \mathbf{\Delta P_E}^{\mathbf{T}}\mathbf{\Delta P_E}}{n}} \tag{4.65}$$

When a pointing model is fit to this data, the model results can be used to write eqn. (4.65) as

$$\Delta P_{rms} = \sqrt{\frac{\left(\Delta \mathbf{P}_A - \mathbf{X}_A \hat{\boldsymbol{\beta}}\right)^T \left(\Delta \mathbf{P}_A - \mathbf{X}_A \hat{\boldsymbol{\beta}}\right) + \left(\Delta \mathbf{P}_E - \mathbf{X}_E \hat{\boldsymbol{\beta}}\right)^T \left(\Delta \mathbf{P}_E - \mathbf{X}_E \hat{\boldsymbol{\beta}}\right)}{n}} \tag{4.66}$$

which can also be computed from the *MSE* using

$$\Delta P_{rms} = \sqrt{\frac{(2n-p)(MSE)}{n}} \tag{4.67}$$

where *MSE* is given in eqn. (4.50). Equation (4.65) defines a sample statistic for the calibration stars.

Sometimes pointing error is assessed by repointing to the calibration stars while applying the corrections from the first model, observing the resulting pointing errors, and finding the rms value using eqn. (4.65). A variation of this procedure involves repointing to different stars to assess accuracy. Each of these methods produces a sample statistic for the new set of observations.

Equation (4.65) yields the rms pointing accuracy for any set of stars. When the mean pointing error in each direction is zero, as it was here, rms values can be used to estimate the population standard deviation, a measure of the overall pointing accuracy of a telescope using

$$\hat{\sigma} = \Delta P_{rms} \tag{4.68}$$

4.6.2 Predicted Performance

In many cases, it is desirable to predict the pointing accuracy for future observations without making additional measurements. The population standard deviation determined from a mount model can be used for this.

A confidence interval for repointing to a single star in the original calibration set is given by

$$\Delta\hat{\mathbf{P}} \pm t(1-\frac{\alpha}{4}, 2n-p)\mathbf{s}\left[\Delta\hat{\mathbf{P}}\right] \tag{4.69}$$

where $\mathbf{s}\left[\Delta\hat{\mathbf{P}}\right]$ is formed from the square roots of the diagonal elements of the matrix defined in eqn. (4.52). Since two components of the pointing error are being estimated the confidence level of the t value has been adjusted to yield a Bonferroni confidence limit on the simultaneous estimates (Neter et al., 1996). A Bonferroni confidence interval for the two components simultaneously bounds both components of the pointing error at confidence level α.

Similarly, a confidence interval for the error in repointing to the n stars in the original set involves making $2n$ simultaneous inferences. The Bonferroni confidence interval for repointing to all n stars is given by

$$\Delta\hat{\mathbf{P}} \pm t(1-\frac{\alpha}{4n}, 2n-p)\mathbf{s}\left[\Delta\hat{\mathbf{P}}\right] \tag{4.70}$$

When a single new star is to be observed, all of the variability of the original calibration data must be accounted for plus the variability of the additional observations (azimuth and elevation). A Bonferroni confidence interval for the pointing error in pointing to a single new star is given by

$$\Delta\hat{\mathbf{P}} \pm t(1-\frac{\alpha}{4}, 2n-p)\mathbf{s}\left[\text{new}\right] \tag{4.71}$$

where

$$\mathbf{s}^2[\text{new}] = \begin{bmatrix} MSE + \mathbf{X}_{\mathbf{A}h}\mathbf{s}^2[\hat{\boldsymbol{\beta}}]\mathbf{X}_{\mathbf{A}h}^{\mathbf{T}} \\ MSE + \mathbf{X}_{\mathbf{E}h}\mathbf{s}^2[\hat{\boldsymbol{\beta}}]\mathbf{X}_{\mathbf{E}h}^{\mathbf{T}} \end{bmatrix} \tag{4.72}$$

and $\mathbf{X}_{\mathbf{A}h}$ and $\mathbf{X}_{\mathbf{E}h}$ are 1 by p matrices similar to those shown in eqn. (4.31a) and (4.31b) but computed using the coordinates of the new star.

Similarly, the mean error for m new observations at a position is given by

$$\Delta\hat{\mathbf{P}} \pm t(1-\frac{\alpha}{4m}, 2n-p)\mathbf{s}(m\text{ new}) \tag{4.73}$$

where

$$\mathbf{s}^2[m\text{ new}] = \begin{bmatrix} \dfrac{MSE}{m} + \mathbf{X}_{\mathbf{A}h}\mathbf{s}^2[\boldsymbol{\beta}]\mathbf{X}_{\mathbf{A}h}^{\mathbf{T}} \\ \dfrac{MSE}{m} + \mathbf{X}_{\mathbf{E}h}\mathbf{s}^2[\boldsymbol{\beta}]\mathbf{X}_{\mathbf{E}h}^{\mathbf{T}} \end{bmatrix} \tag{4.74}$$

and $\mathbf{X}_{\mathbf{A}h}$ and $\mathbf{X}_{\mathbf{E}h}$ are each 1 by p matrices filled using the coordinates of the new star.

4.6.3 Positions for Assessing Pointing

In order to compare the pointing results for the various solution methods used in this work, a consistent set of locations at which to calculate predicted performance was required. A grid of thirty positions distributed around the sky was used as shown schematically in Fig. 4.4.

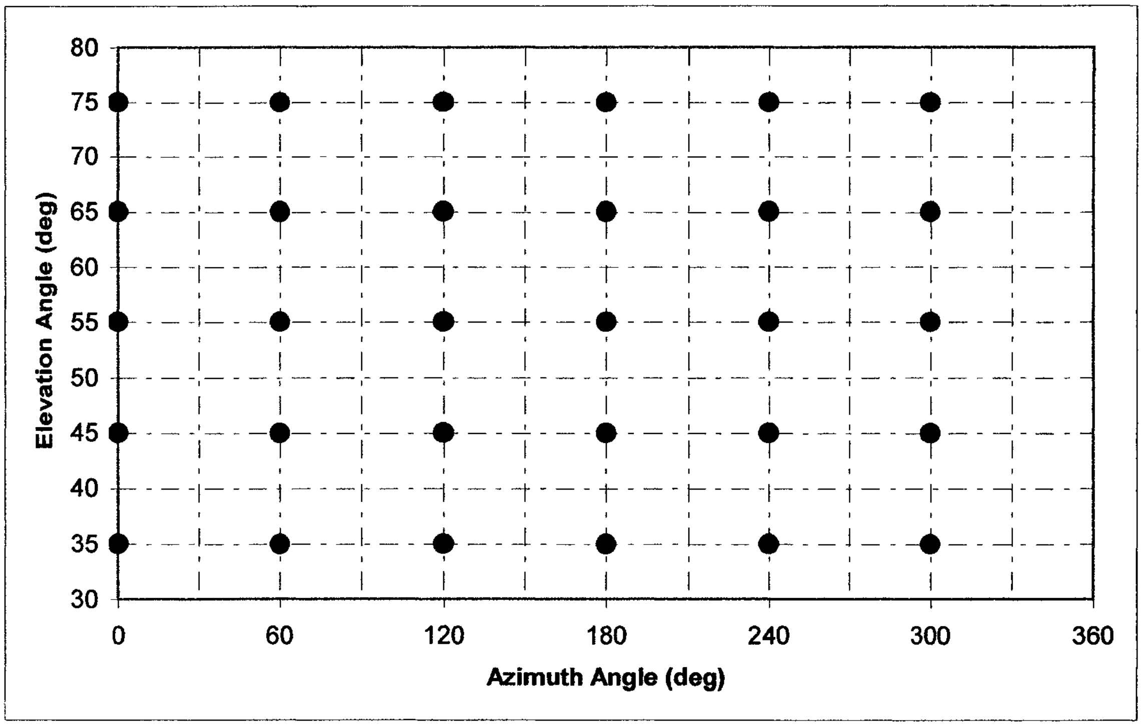

Figure 4.4 Location of reference positions for assessing pointing accuracy

4.7 Position Determination

When observations made through the telescope are used to determine the true position of an object, as would be the case in a tracking system, any error in telescope position affects the error in position determination. The uncertainty associated with the telescope position for a particular observation was given in eqn. (4.71). This uncertainty comes from imprecision in determining the physical errors in the telescope as well as unmodeled random and deterministic errors. The true position of an object is

$$\mathbf{P}_{\mathrm{T}} = \mathbf{P}_{\mathrm{e}} + \Delta\hat{\mathbf{P}} + \varepsilon \tag{4.76}$$

where $\mathbf{P}_{\mathrm{T}}$ is the true position of the object relative to the telescope, $\mathbf{P}_{\mathrm{e}}$ is the telescope position as measured by its encoders, $\Delta\hat{\mathbf{P}}$ is the correction applied by the mount model, and ε results from randomness and unmodeled telescope errors.

The uncertainty in the estimated true position is characterized by its variance and can be found by adding the variance of the components:

$$\mathbf{s}^2\left[\hat{\mathbf{P}}_{\mathbf{T}}\right]=\mathbf{s}^2\left[\mathbf{P}_{\mathbf{e}}\right]+\mathbf{s}^2\left[\Delta\hat{\mathbf{P}}\right]+\mathbf{s}^2\left[\varepsilon\right] \tag{4.77}$$

The first term on the right hand side is zero because it was assumed measurement errors were negligible. The second term was given by eqn. (4.52) and the final term is simply the variance of the residual pointing error, estimated by *MSE*. Combining these expressions gives an equation for the uncertainty in the position of an object observed at (A_{obs}, E_{obs})

$$\mathbf{s}^2\left[\hat{\mathbf{P}}_{\mathbf{T}}\right]=\begin{bmatrix}\mathbf{X}_{\mathbf{A}obs}\mathbf{s}^2\left[\hat{\boldsymbol{\beta}}\right]\mathbf{X}_{\mathbf{A}obs}{}^{\mathbf{T}}+MSE\\ \mathbf{X}_{\mathbf{E}obs}\mathbf{s}^2\left[\hat{\boldsymbol{\beta}}\right]\mathbf{X}_{\mathbf{E}obs}{}^{\mathbf{T}}+MSE\end{bmatrix} \tag{4.78}$$

which is identical to eqn. (4.72) when the observed coordinates are used for the new position.

A Bonferroni confidence interval for the true position can be found from

$$\Delta\hat{\mathbf{P}}_{\mathbf{T}}\pm t(1-\frac{\alpha}{4},2n-p)\mathbf{s}\left[\hat{\mathbf{P}}_{\mathbf{T}}\right] \tag{4.79}$$

Equation (4.79) provides a confidence interval for each component of the true position for an observed object.

The methods described in this chapter were applied to the simulated data and the data from the working telescopes. The results are summarized in the following chapter.

5 RESULTS

5.1 Overview

A kinematic model to relate the mechanical errors in a telescope to pointing performance was described in Chapter 4. The model contained effects from encoder offsets, encoder scale errors, telescope leveling errors, axis nonperpendicularity and optical axis misalignment assembly errors, first-order bearing errors, and tube flexure. The Denavit-Hartenberg rotation matrix approach was utilized to develop the model and then an algebraic representation was used in a statistical model based on parameters related to the physical errors.

Except for the reduced model discussed in section 5.3.6, the same kinematic model was used for each solution and included 13 terms resulting from encoder scale and offset errors, axis nonperpendicularity and misalignment, telescope mislevel, tube flexure and bearing errors. These are the fundamental physical errors that would be expected in any altazimuth telescope.

Four methods were described for estimating the model parameters. A baseline method developed from a modification of ordinary least squares was derived first because it is similar to the state-of-the-art approach. Three alternative methods, bootstrapping, ridge regression, and Bayesian regression were then developed as potential means for improving the precision of the baseline results. This chapter describes the validation of the methodology and presents the results.

The baseline statistical model was validated by comparing its solution with TPOINT results and by demonstrating that it successfully detected known features of simulated data. The alternative methods were validated by showing that they duplicated the baseline results under appropriate conditions.

After the validity of the model is demonstrated, results obtained by applying the baseline model to simulated and actual telescope data are listed and discussed and it is shown that many of the estimated parameters are highly imprecise, as expected. The application of each alternative method is then described including how any control parameters required for the methods were determined.

Finally, the impact of the solution method and the precision of the parameter estimates on pointing error and on position determination is considered. General expressions were presented in Chapter 4 while specific results obtained from each solution procedure and data set are listed in this chapter.

Each table in this chapter lists solutions obtained using one or more of the solution methods for one or more data sets. Each solution consists of a list of estimated physical error parameters and their respective standard errors in separate columns. The first column of each solution gives a point estimate of the parameter, either the mean or median as explained in the text. The second column, labeled "standard error" or "S. E." gives the estimated standard error for each parameter estimate. The last row of each table lists the estimated standard deviation for the overall model.

It was found that the baseline solution technique produced results that were very similar to state-of-the art methods. The results also demonstrate that each of the three alternative approached developed in this work improved the precision of the parameter estimates because they reduced the standard error associated with the estimate. Bayesian regression was found to produce the greatest overall improvement.

5.2 Model Validation

The kinematic model described in Chapter 4 is similar to that used by the TPOINT program. Although the kinematic model was derived using a matrix representation, identifying the parameters using a regression model is simplified if the effect of each term is expressed algebraically. The algebraic expression for each error is listed in Table 4.2 and derived in Appendix B. Each term agrees with the corresponding TPOINT term if the appropriate correction is made for the coordinate system used by TPOINT. Under the TPOINT convention, azimuth angles are measured from south with an eastward rotation being positive. For this work, azimuth angles are measured from north with a rotation toward east also being positive. This difference in convention introduces both a phase difference and a difference in sense for azimuth angles.

The statistical model was validated by demonstrating that it produced parameter estimates that were similar to those produced by TPOINT when the same terms were included. The terms used in the available TPOINT solutions varied from one telescope to another and those solutions often contained empirical and special terms that were not easily attributable to any specific mechanical error. For this reason, the statistical model was validated by comparison with parameter estimates made for telescope mount models fit using TPOINT, with the same terms included, not necessarily those used for the kinematic model developed for this work.

The TPOINT program uses a procedure similar to ordinary least squares regression but correction terms are introduced sequentially (by default). This causes each successive correction term to be calculated from an updated position (azimuth and elevation) coordinate. The changes introduce variation into the model and it would therefore be expected that TPOINT results would reflect the additional variation by estimating higher standard errors for the coefficients. The TPOINT program optionally allows the corrections to be applied in a way that coordinates are not incrementally updated but Wallace (1996) noted that there is usually little difference in the results obtained. The TPOINT program also uses a more direct, numerical approach to the solution which also might result in small differences in the solution.

Solutions obtained using TPOINT for the Sloan Digital Sky Survey (SDSS) 2.5-meter telescope and the Astronomical Research Consortium (ARC) 3.5-meter telescope data were compared with solutions obtained using the MOLS model. In each case, the TPOINT solution was provided by Owen (2001, 2002). Two values for the estimated error are given for the TPOINT solutions. During the course of this work it was found that TPOINT computes the estimated error using too many of degrees-of-freedom (Wallace, 1996). The first value is that reported by TPOINT and the second value, in parentheses, is the value calculated using the correct number of degrees-of-freedom.

Table 5.1 shows a comparison of the TPOINT results to the MOLS solution for the SDSS telescope. The TPOINT model included the terms currently used in the telescope mount model.

Table 5.2 compares a TPOINT solution to the MOLS solution for the ARC telescope. The actual telescope mount model includes a special polynomial term to model errors in the elevation drive disk. The TPOINT solution presented here is for a model that excluded that term. The differences between the actual model and the reduced model shown are negligible.

Table 5.1 Comparison of solutions for the SDSS telescope.

	TPOINT Solution		MOLS Solution	
Source	Mean (μrad)	S. E. (μrad)	Mean (μrad)	S. E. (μrad)
Azimuth encoder offset	1017.6	11.8	1014.3	6.1
Elevation encoder offset	-894.3	10.7	-899.5	10.0
Elevation encoder scale	-667.7	29.7	-683.4	27.4
Tilt toward north	21.9	3.8	23.2	2.3
Tilt toward east	308.1	3.7	311.3	2.4
Optical axis misalignment	1.8	9.1	2.1	4.4
Empirical: $\Delta A = \cos A \;\; \cos 2A \;\; \tan E$ $\Delta E = -\sin A \;\; \cos 2A$	2.8	5.1	5.2	3.3
Empirical: $\Delta A = \cos A \;\; \sin 2A \;\; \tan E$ $\Delta E = -\sin A \;\; \sin 2A$	-5.0	4.7	-3.2	2.9
Empirical: $\Delta A = \sin A \;\; \cos A \;\; \tan E$ $\Delta E = \cos A \;\; \cos A$	0.7	5.6	0.1	3.4
Empirical: $\Delta A = \sin A \;\; \sin A \;\; \tan E$ $\Delta E = \cos A \;\; \sin A$	-8.8	5.6	-3.7	3.7
Empirical: $\Delta A = \cos A$	-16.5	6.5	-19.2	4.5
Empirical: $\Delta A = \sin A$	4.9	6.2	4.4	4.3
Tube flexure (TX)	-6.1	12.6	-0.4	11.2
Estimated error (σ)		17.7 (19.3)		13.8

Table 5.2 Comparison of solutions for the ARC telescope.

	TPOINT Solution		MOLS Solution	
Parameter	Mean (μrad)	S. E. (μrad)	Mean (μrad)	S. E. (μrad)
Azimuth encoder offset	911.3	7.3	919.5	2.8
Elevation encoder offset	2715.1	4.5	2720.9	4.1
Optical axis misalignment	-651.1	5.2	-659.1	1.4
Tilt toward north	25.0	2.0	20.9	1.3
Tilt toward east	101.8	2.0	101.2	1.4
Elevation encoder scale	2459.8	5.4	2458.9	5.0
Empirical: $\Delta A = \cos A$	1.8	3.5	2.6	2.7
Empirical: $\Delta A = \sin A$	1.3	3.5	2.6	2.6
Empirical: $\Delta A = \cos 2A$	-14.9	3.0	-17.4	1.9
Empirical: $\Delta A = \sin 2A$	-5.3	3.1	-4.4	2.1
Empirical: $\Delta E = -\cos 2A$	2.1	2.1	2.1	1.9
Empirical: $\Delta E = -\sin 2A$	1.6	2.3	-1.8	2.1
Estimated error (σ)	14.6 (15.2)			12.9

For both telescopes, the solution for the mean coefficients obtained using the MOLS model agreed reasonably well with the TPOINT solution and the standard error was smaller for the MOLS solution. This was expected because of the variability added by incremental coordinate adjustments in TPOINT.

Because the MOLS model used for this work yielded smaller standard errors for the coefficients, it is more precise than the TPOINT model. However, it is impossible to say which model is more accurate because the true values of the physical errors are unknown. In most cases, the confidence interval calculated from the MOLS model fell completely within a similar confidence interval constructed from the TPOINT solution.

5.3 Baseline Solution

5.3.1 Summary

The MOLS regression model developed in Chapter 4 served as the baseline from which the effectiveness of each alternative analysis method was judged. The sections below discuss the results of the MOLS solution for each of the simulated data sets and the data obtained from actual telescopes.

5.3.2 Sloan Digital Sky Survey Telescope Data

Table 5.3 shows the MOLS results for the SDSS telescope. Note that several of the terms have very large standard errors even though the overall model error is relatively small. This effect is caused by correlation among the terms in the model.

Table 5.3 MOLS results for the SDSS telescope

Parameter	Mean (μrad)	Standard Error (μrad)
Azimuth encoder offset	-3023.5	1634.4
Elevation encoder offset	-894.2	10.0
Azimuth encoder scale	1.0	1.4
Elevation encoder scale	-671.0	27.7
Axis nonperpendicularity	-5205.4	1890.3
Optical axis misalignment	5295.4	1936.5
Tilt toward north	25.9	2.1
Tilt toward east	303.9	1.8
Tube flexure (TX)	-5.3	11.3
Azimuth bearing, NS term	-2.4	3.6
Azimuth bearing, EW term	3.7	3.7
Elevation bearing, cosine term	-865.8	241.4
Elevation bearing, sine term	3343.4	1301.5
Estimated error (σ)		14.1

5.3.3 Astronomical Research Consortium Telescope Data

Table 5.4 shows the MOLS results for the ARC telescope. The terms that had large standard errors in the SDSS model also had relatively large standard errors in this model. However, the standard errors were smaller for the ARC telescope even though the overall error in the model was similar.

Table 5.4 MOLS results for the ARC telescope

Parameter	Mean (μrad)	Standard Error (μrad)
Azimuth encoder offset	2821.6	741.9
Elevation encoder offset	2715.4	6.8
Azimuth encoder scale	-0.5	1.1
Elevation encoder scale	2431.3	21.3
Axis nonperpendicularity	2458.6	1012.6
Optical axis misalignment	-3144.2	1023.0
Tilt toward north	21.3	1.2
Tilt toward east	102.9	1.1
Tube flexure	12.8	9.6
Azimuth bearing, NS term	-2.1	2.7
Azimuth bearing, EW term	-13.4	2.0
Elevation bearing, cosine term	411.1	215.9
Elevation bearing, sine term	-1601.3	635.6
Estimated error (σ)		14.0

5.3.4 W. M. Keck Observatory Data

Tables 5.5 and 5.6 display the MOLS results for the two Keck telescopes which are of similar design and located close together on the same mountain. However, the Keck I telescope was constructed several years before the Keck II. Because they share the same structural design, the tube flexure for the two telescopes should be nearly identical but there is no reason to expect the other physical errors to be similar.

Table 5.5 MOLS results for the Keck I telescope

Parameter	Mean (μrad)	Standard Error (μrad)
Azimuth encoder offset	-291.1	849.5
Elevation encoder offset	456.8	9.6
Azimuth encoder scale	7.0	2.4
Elevation encoder scale	137.3	32.4
Axis nonperpendicularity	-354.5	1241.7
Optical axis misalignment	545.0	1246.7
Tilt toward north	100.5	1.4
Tilt toward east	-61.4	1.2
Tube flexure	-12.9	15.7
Azimuth bearing, NS term	14.0	2.5
Azimuth bearing, EW term	-9.3	2.4
Elevation bearing, cosine term	-39.0	316.2
Elevation bearing, sine term	247.4	761.1
Estimated error (σ)		38.3

Table 5.6 MOLS results for the Keck II telescope

Parameter	Mean (μrad)	Standard Error (μrad)
Azimuth encoder offset	3815.8	857.9
Elevation encoder offset	530.3	9.1
Azimuth encoder scale	2.6	2.2
Elevation encoder scale	-249.2	31.1
Axis nonperpendicularity	-1734.3	1271.8
Optical axis misalignment	1602.4	1276.9
Tilt toward north	146.0	1.4
Tilt toward east	-63.8	1.2
Tube flexure	199.9	15.5
Azimuth bearing, NS term	8.7	2.5
Azimuth bearing, EW term	0.8	2.4
Elevation bearing, cosine term	-644.0	329.0
Elevation bearing, sine term	834.9	771.0
Estimated error (σ)		35.1

Inspection of these tables revealed two noteworthy features of the results. First, the estimates of the magnitude of the flexure differed between the telescopes. Second, the standard errors on all the terms were remarkably similar, even where the mean estimates of a parameter were different. This was not expected and it is difficult to explain what might have caused this result.

5.3.5 Simulated Data

The simulated data sets provided a way to assess the effect of random error in the data and, because the physical error terms in the simulated data were known exactly, the accuracy (bias) of each solution method could also be evaluated. Tables 5.7a and 5.7b contain the baseline results for the simulated data sets. When no random error was present in the data (set 0), the MOLS model accurately and precisely estimated each mechanical error. A slight amount of random error (set 1) caused the estimates of some of the coefficients to differ substantially from the known, true values and caused the standard errors of the estimates to increase substantially. As the amount of random error increased, the effect became worse. However, even for the set with the largest random error (set 6), some of the terms remained relatively precise and unbiased.

Table 5.7a MOLS results for the simulated data

	Set 0		Set 1		Set 2	
	$\sigma = 0$ μrad		$\sigma = 1$ μrad		$\sigma = 5$ μrad	
Parameter	Mean (μrad)	S. E. (μrad)	Mean (μrad)	S. E. (μrad)	Mean (μrad)	S. E. (μrad)
Azimuth encoder offset	-150.0	0.0	-122.5	34.7	-405.6	163.8
Elevation encoder offset	100.0	0.0	100.2	0.4	101.3	2.1
Azimuth encoder scale	-20.0	0.0	-19.9	0.1	-19.6	0.5
Elevation encoder scale	30.0	0.0	30.4	1.6	43.5	7.7
Axis nonperpendicularity	12.5	0.0	74.7	53.9	-365.9	254.8
Optical axis misalignment	-62.5	0.0	-124.6	54.1	318.9	255.6
Tilt toward north	212.5	0.0	212.5	0.1	211.4	0.6
Tilt toward east	-150.0	0.0	-150.0	0.1	-150.2	0.4
Tube flexure (TX)	100.0	0.0	99.9	0.8	92.3	3.8
Azimuth bearing, NS term	12.0	0.0	12.0	0.2	11.9	0.9
Azimuth bearing, EW term	7.5	0.0	7.4	0.2	7.6	0.8
Elevation bearing, cosine term	8.0	0.0	33.7	15.3	-79.2	72.4
Elevation bearing, sine term	6.0	0.0	-21.4	31.4	228.4	148.2
Estimated error (σ)		0.0		1.0		4.8

Table 5.7b MOLS results for the simulated data (cont.)

	Set 3		Set 4		Set 5	
	$\sigma = 10\ \mu$rad		$\sigma = 20\ \mu$rad		$\sigma = 50\ \mu$rad	
Parameter	Mean (μrad)	S. E. (μrad)	Mean (μrad)	S. E. (μrad)	Mean (μrad)	S. E (μrad)
Azimuth encoder offset	60.5	339.1	976.7	837.2	-378.8	1662.4
Elevation encoder offset	94.1	4.3	89.9	10.7	137.5	21.3
Azimuth encoder scale	-19.4	1.0	-18.7	2.5	-11.4	5.0
Elevation encoder scale	5.0	16.0	-26.0	39.5	90.2	78.5
Axis nonperpendicularity	343.5	527.4	1791.6	1302.2	-344.4	2585.8
Optical axis misalignment	-391.9	529.1	-1845.7	1306.3	297.2	2593.9
Tilt toward north	210.7	1.3	212.53	3.1	209.2	6.1
Tilt toward east	-148.9	0.9	-147.6	2.1	-149.7	4.2
Tube flexure (TX)	109.5	7.8	124.7	19.2	80.6	38.1
Azimuth bearing, NS term	11.5	1.9	10.8	4.7	-2.2	9.4
Azimuth bearing, EW term	4.9	1.7	1.7	4.3	-1.3	8.5
Elevation bearing, cosine term	106.4	149.9	504.2	370.1	-105.1	734.8
Elevation bearing, sine term	-190.6	306.6	-1018.0	757.1	283.0	1503.3
Estimated error (σ)		9.9		24.4		48.4

5.3.6 Comparison with a Reduced Model

It is common practice to exclude terms for some of the mechanical errors in a telescope mount model to improve the fit and reduce the effect of correlation among the terms. For example, the actual mount models in use for both the SDSS and the ARC telescopes (see Tables 5.1 and 5.2) exclude the axis nonpependicularity term. This is not because this error is known to be absent. The term is excluded because it is very highly correlated with optical axis misalignment and its inclusion in the model would degrade the results. However, since the objective of this work was to estimate the mechanical errors, all terms that related to physical effects that would be expected to exist in an altazimuth telescope were included in the kinematic model and a statistical method was sought to make the estimate of each more precise.

To demonstrate how removing some terms may appear to improve the results, a reduced model was fit to simulated data set 3. Table 5.8 provides a side-by-side comparison of the two models.

Table 5.8 Comparison of full and reduced models for simulated data set 3

Parameter	True Value (μrad)	Full Model Mean (μrad)	Full Model S. E. (μrad)	Reduced Model Mean (μrad)	Reduced Model S. E. (μrad)
Azimuth encoder offset	-150.0	60.5	339.1	-143.5	3.0
Elevation encoder offset	100.0	94.1	4.3	93.0	2.6
Azimuth encoder scale	-20.0	-19.4	1.0	-19.5	0.9
Elevation encoder scale	30.0	5.0	16.0	-	-
Axis nonperpendicularity	12.5	343.5	527.4	-	-
Optical axis misalignment	-62.5	-391.9	529.1	-48.0	1.3
Tilt toward north	212.5	210.7	1.3	210.8	1.1
Tilt toward east	-150.0	-148.9	0.9	-148.8	0.8
Tube flexure (TX)	100.0	109.5	7.8	111.9	2.0
Azimuth bearing, NS term	12.0	11.5	1.9	11.6	1.9
Azimuth bearing, EW term	7.5	4.9	1.7	5.0	1.5
Elevation bearing, cosine term	8.0	106.4	149.9	-	-
Elevation bearing, sine term	6.0	-190.6	306.6	-	-
Estimated error (σ)			9.9		9.7

The estimated parameters for the reduced model had significantly lower standard errors and the overall error in the model was lower. The mean estimates from the reduced model were also closer to the true values. However, the mechanical errors omitted from the reduced model were not detected and 95% confidence intervals constructed for the coefficients in the reduced model did not always contain the true values while they did for the full model. The extent of the bias in a reduced model depends on which terms are omitted and their magnitude. In effect, the reduced model solution estimates the magnitude of each mechanical error *given that no other mechanical errors are present*. While this may often be a good assumption, a Bayesian approach might be better based on the results of the Bayesian regression solution presented later.

5.4 Bootstrapping

Estimating the mechanical errors using bootstrapping requires determining the number of resamples to make from the data, performing the solutions, constructing confidence intervals using percentiles from the sample of solutions, and then using those confidence intervals to determine the approximate standard error. Bootstrapping results also provided the opportunity to investigate the distribution of each parameter estimate.

5.4.1 Selecting the Number of Resamples

Selecting the number of resamples to use for bootstrapping required observing the effect of the number of resamples on the estimated standard error of the model parameters. Simulated data set 3 was used to study this effect because it contained a moderate amount of random error typical of that found in real data. Figure 5.1 displays the standard error of each coefficient for bootstrapping solutions as the number of resamples was increased. The data point for 1 resample represents the MOLS solution. The figure illustrates a substantial reduction in standard error for all the coefficients for bootstrapping over MOLS regression for as few as 10 resamples. Unfortunately, there was little improvement when more than about 20 resamples were used and the standard errors for several of the coefficients, those with the highest degree of correlation, were still relatively large.

The trough in the plot for 5 or 10 resamples is an artifact of the way the bootstrapped confidence intervals were determined. Bootstrapping confidence intervals are determined by percentiles and, when only a few resamples are used, averaging is performed in the calculation which smooths any extreme values. As the number of resamples is increased the tails of the distribution are sampled better and the confidence intervals stabilize. Based on the results summarized in Fig. 5.1, 100 resamples were used for all the bootstrapping solutions.

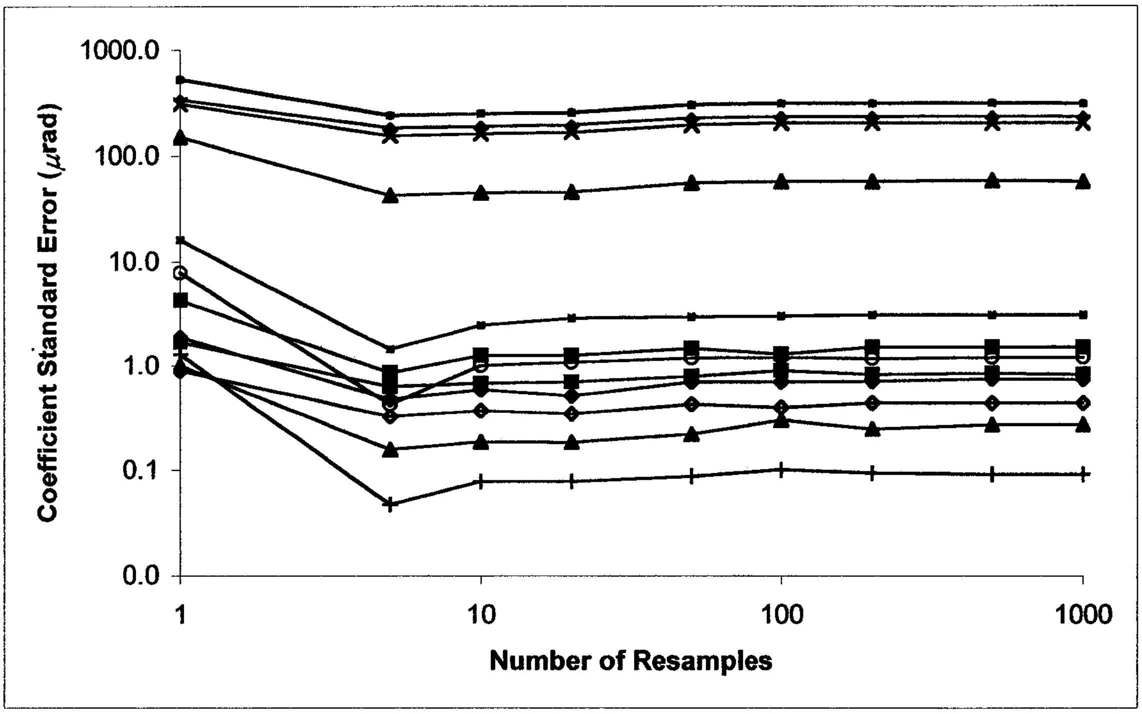

Figure 5.1 Effect of the number of resamples on coefficient precision

5.4.2 Sloan Digital Sky Survey Telescope Data

Bootstrapping results for the SDSS telescope data are summarized in Table 5.9. Comparison with Table 5.3 confirms that the precision of all the parameter estimates was reduced but many were still too imprecise for the improvement to have much practical use.

Table 5.9 Bootstrapping parameter estimates for the SDSS telescope

Parameter	Median (μrad)	Standard Error (μrad)
Azimuth encoder offset	2860.3	209.4
Elevation encoder offset	2715.2	0.9
Azimuth encoder scale	-0.4	0.4
Elevation encoder scale	2430.5	5.8
Axis nonperpendicularity	2510.7	313.5
Optical axis misalignment	-3196.5	315.7
Tilt toward north	21.3	0.2
Tilt toward east	102.8	0.1
Tube flexure	13.2	3.2
Azimuth bearing, NS term	-2.2	0.3
Azimuth bearing, EW term	-13.4	0.3
Elevation bearing, cosine term	416.1	82.0
Elevation bearing, sine term	-1633.5	184.6
Estimated error (σ)		14.2

5.4.3 Astronomical Research Consortium Telescope Data

Table 5.10 summarizes the results of a bootstrapping solution for the mechanical errors in the ARC telescope. Again, the parameter estimates were more precise than the baseline results presented in Table 5.4 but not enough for practical use.

Table 5.10 Bootstrapping parameter estimates for the ARC telescope

Parameter	Median (μrad)	Standard Error (μrad)
Azimuth encoder offset	2793.7	241.6
Elevation encoder offset	2715.6	0.9
Azimuth encoder scale	-0.5	0.4
Elevation encoder scale	2432.3	6.0
Axis nonperpendicularity	2421.6	353.0
Optical axis misalignment	-3106.8	355.9
Tilt toward north	21.3	0.2
Tilt toward east	102.9	0.1
Tube flexure	12.3	3.3
Azimuth bearing, NS term	-2.1	0.3
Azimuth bearing, EW term	-13.4	0.3
Elevation bearing, cosine term	406.7	84.2
Elevation bearing, sine term	-1577.5	211.2
Estimated error (σ)		14.1

5.4.4 W. M. Keck Observatory Data

Bootstrapping solutions for each of the Keck telescopes are shown in Tables 5.11 and 5.12. The point estimate (median) of each physical error was similar to the MOLS result but the standard errors were lower.

Table 5.11 Bootstrapping parameter estimates for the Keck I telescope

Parameter	Median (μrad)	Standard Error (μrad)
Azimuth encoder offset	-261.8	182.0
Elevation encoder offset	456.7	1.4
Azimuth encoder scale	7.0	0.1
Elevation encoder scale	137.3	2.5
Axis nonperpendicularity	-330.8	241.2
Optical axis misalignment	520.4	242.6
Tilt toward north	100.5	0.3
Tilt toward east	-61.4	0.4
Tube flexure	-12.9	0.8
Azimuth bearing, NS term	14.0	1.0
Azimuth bearing, EW term	-9.3	0.3
Elevation bearing, cosine term	-39.0	46.1
Elevation bearing, sine term	225.7	160.6
Estimated error (σ)		38.4

Table 5.12 Bootstrapping parameter estimates for the Keck II telescope

Parameter	Median (μrad)	Standard Error (μrad)
Azimuth encoder offset	3822.7	79.1
Elevation encoder offset	530.3	0.8
Azimuth encoder scale	2.6	0.1
Elevation encoder scale	-248.8	1.9
Axis nonperpendicularity	-1723.2	116.5
Optical axis misalignment	1591.4	117.0
Tilt toward north	146.0	0.2
Tilt toward east	-63.8	0.4
Tube flexure	199.7	0.8
Azimuth bearing, NS term	8.7	0.9
Azimuth bearing, EW term	0.8	0.4
Elevation bearing, cosine term	-640.3	28.9
Elevation bearing, sine term	827.2	70.9
Estimated error (σ)		35.1

5.4.5 Simulated Data

Bootstrapping solutions for 100 resamples for each of the simulated data sets are summarized in Table 5.13a and 5.13b. The bootstrapping solutions were significantly more precise than the MOLS solution for the most highly correlated parameters. The standard error in the parameter estimates was reduced by approximately a factor of 10 for these parameters and the bias in the median estimates was approximately one-third as much.

Table 5.13a Bootstrapping parameter estimates for the simulated data

Parameter	Set 0 $\sigma = 0\ \mu rad$ Median (μrad)	S. E. (μrad)	Set 1 $\sigma = 1\ \mu rad$ Median (μrad)	S. E. (μrad)	Set 2 $\sigma = 5\ \mu rad$ Median (μrad)	S. E. (μrad)
Azimuth encoder offset	-150.0	0.0	-117.2	8.6	-398.8	52.1
Elevation encoder offset	100.0	0.0	100.2	0.1	101.3	1.1
Azimuth encoder scale	-20.0	0.0	-19.9	0.0	-19.6	0.1
Elevation encoder scale	30.0	0.0	30.4	0.2	43.6	3.3
Axis nonperpendicularity	12.5	0.0	82.1	11.1	-357.0	66.4
Optical axis misalignment	-62.5	0.0	-132.0	11.2	310.0	67.6
Tilt toward north	212.5	0.0	212.5	0.0	211.4	0.1
Tilt toward east	-150.0	0.0	-150.0	0.0	-150.1	0.1
Tube flexure	100.0	0.0	99.9	0.1	92.2	1.4
Azimuth bearing, NS term	12.0	0.0	12.0	0.0	11.9	0.2
Azimuth bearing, EW term	7.5	0.0	7.4	0.0	7.6	0.3
Elevation bearing, cosine term	8.0	0.0	34.7	1.9	-76.5	10.7
Elevation bearing, sine term	6.0	0.0	-26.2	7.4	222.5	43.5
Estimated error (σ)		0		1.1		4.8

Table 5.13b Bootstrapping parameter estimates for the simulated data (cont.)

	Set 3		Set 4		Set 5	
	$\sigma = 10$ μrad		$\sigma = 20$ μrad		$\sigma = 50$ μrad	
Parameter	Median (μrad)	S. E. (μrad)	Median (μrad)	S. E. (μrad)	Median (μrad)	S. E. (μrad)
Azimuth encoder offset	146.0	234.8	1050.9	261.3	-212.3	173.3
Elevation encoder offset	94.0	1.4	89.7	1.5	137.5	9.0
Azimuth encoder scale	-19.3	0.3	-18.7	0.4	-11.4	1.0
Elevation encoder scale	4.9	3.1	-25.6	5.1	90.2	38.9
Axis nonperpendicularity	438.2	314.6	1895.7	313.6	-109.5	217.0
Optical axis misalignment	-490.4	318.2	-1950.5	319.3	63.9	220.7
Tilt toward north	210.6	0.1	212.4	0.1	209.1	0.8
Tilt toward east	-148.8	0.4	-147.5	0.4	-149.5	0.3
Tube flexure	109.4	1.2	123.9	2.6	80.4	21.0
Azimuth bearing, NS term	11.5	0.7	10.8	0.4	-3.2	1.8
Azimuth bearing, EW term	5.7	0.8	1.7	1.1	-1.3	1.6
Elevation bearing, cosine term	114.9	59.8	525.4	40.9	-59.0	72.6
Elevation bearing, sine term	-260.0	202.8	-1084.5	217.9	145.4	140.4
Estimated error (σ)		11.5		24.4		49.7

5.4.6 Coefficient Distributions

One advantage of bootstrapping is that it allowed the sampling distribution of each regression coefficient to be estimated. Figures 5.2 through 5.14 show histograms of each estimated parameter for the ARC telescope. The estimated distributions for the other telescopes and simulated data were similar. Each histogram is roughly mound-shaped but some exhibit noticeable skewness, especially those for axis nonperpendicularity, optical axis misalignment, and tube flexure. While it is apparent from the histograms that the distribution of most coefficients was not normal, the departure from normality was not enough to question the method used for estimating the parameters.

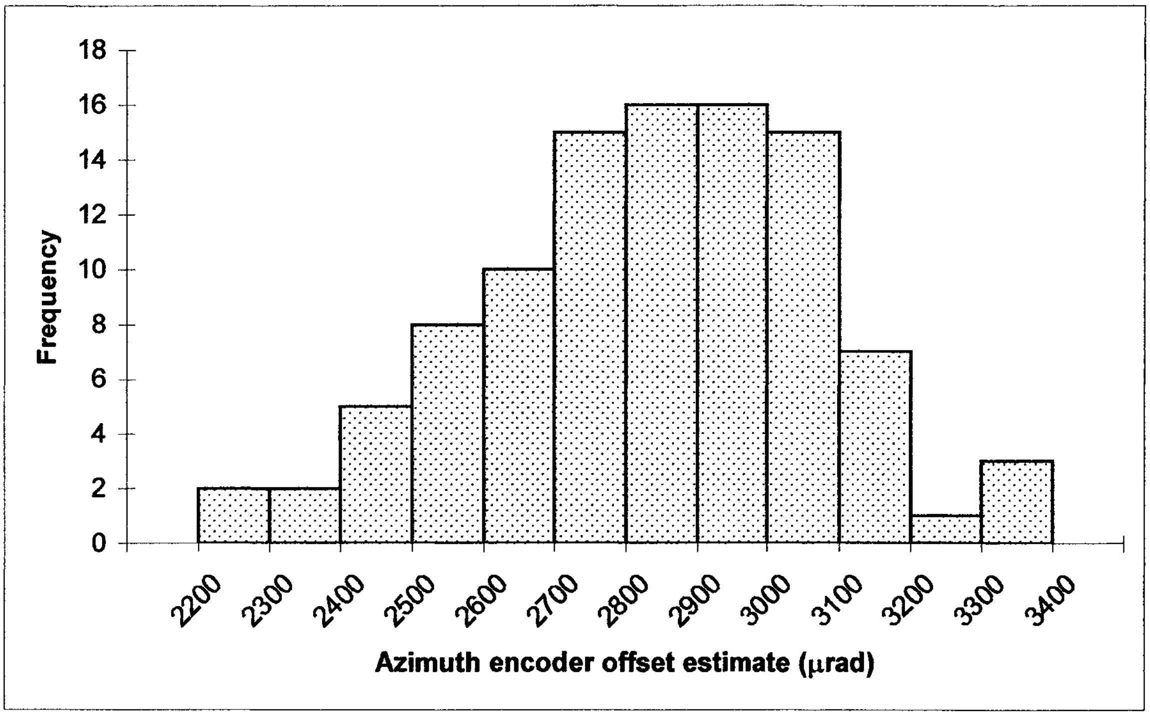

Figure 5.2 Bootstrap estimate histogram for azimuth encoder offset

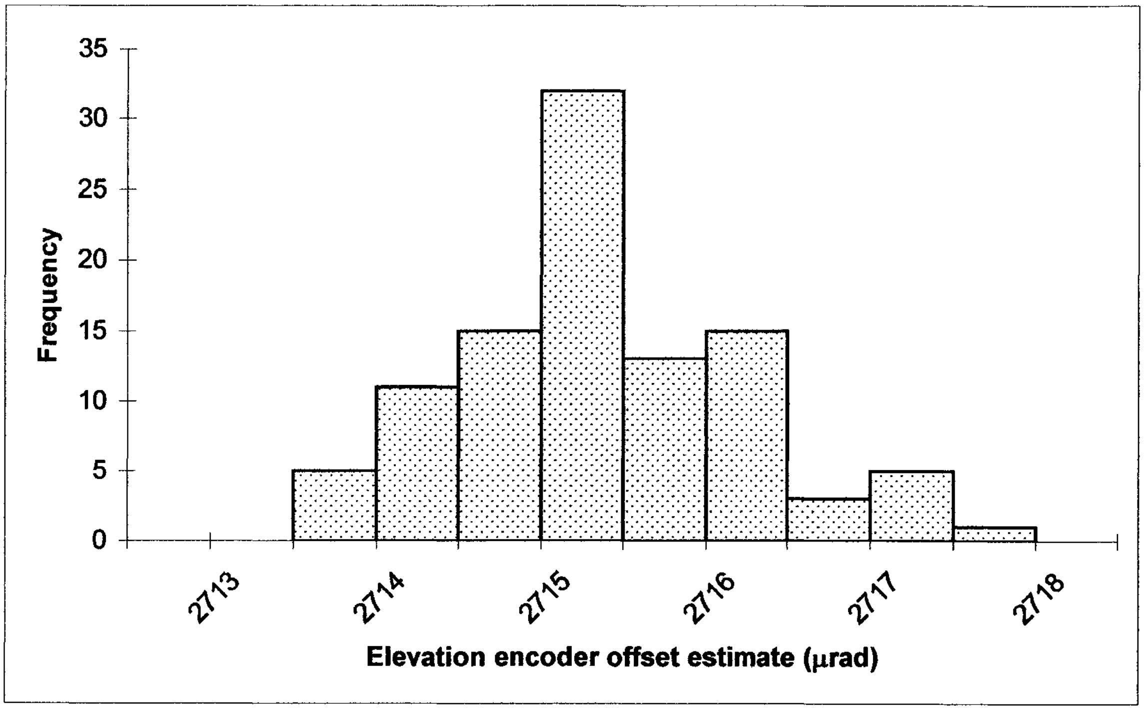

Figure 5.3 Bootstrap estimate histogram for elevation encoder offset

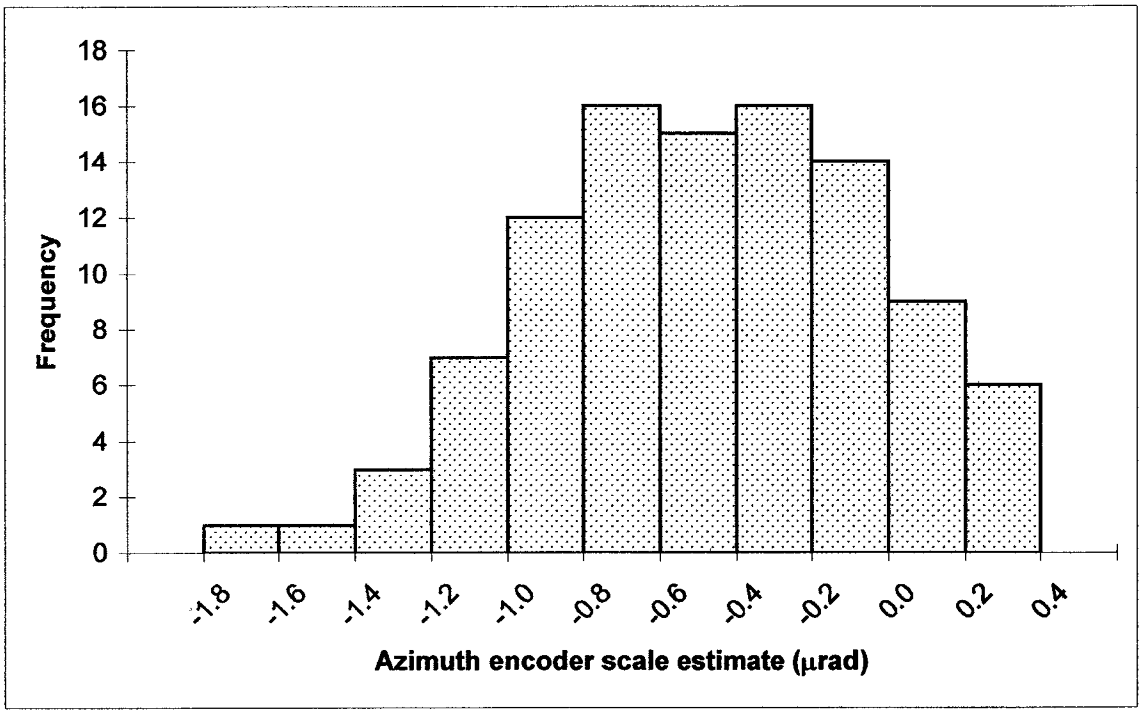

Figure 5.4 Bootstrap estimate histogram for azimuth encoder scale

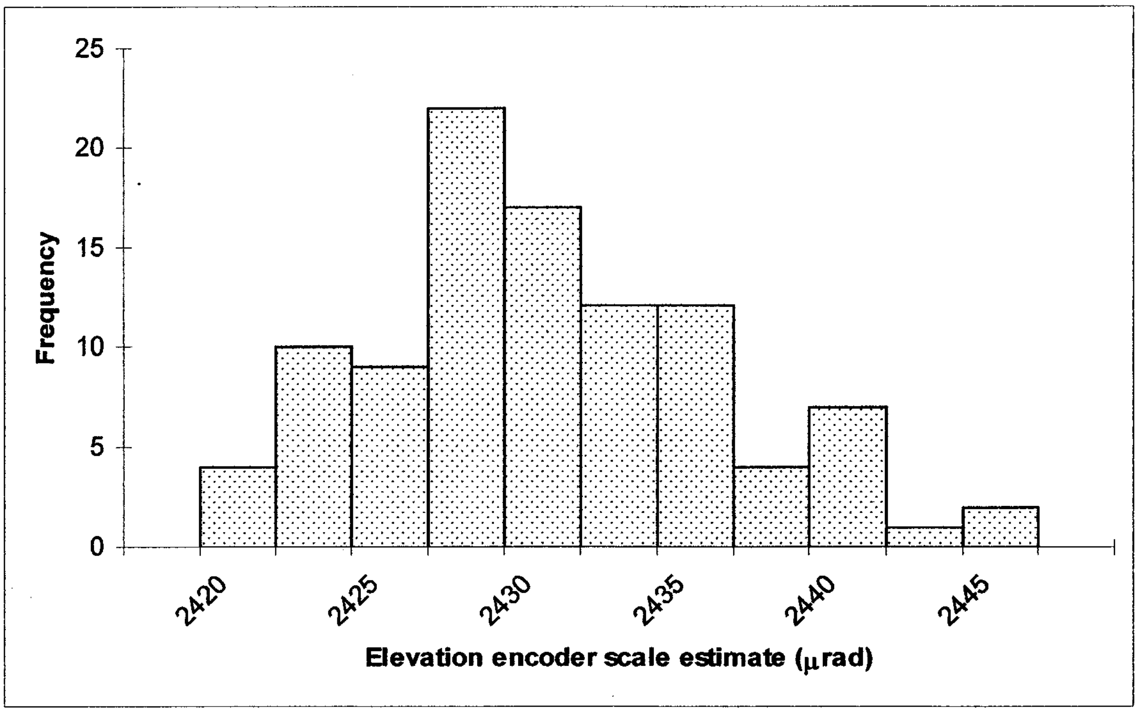

Figure 5.5 Bootstrap estimate histogram for elevation encoder scale

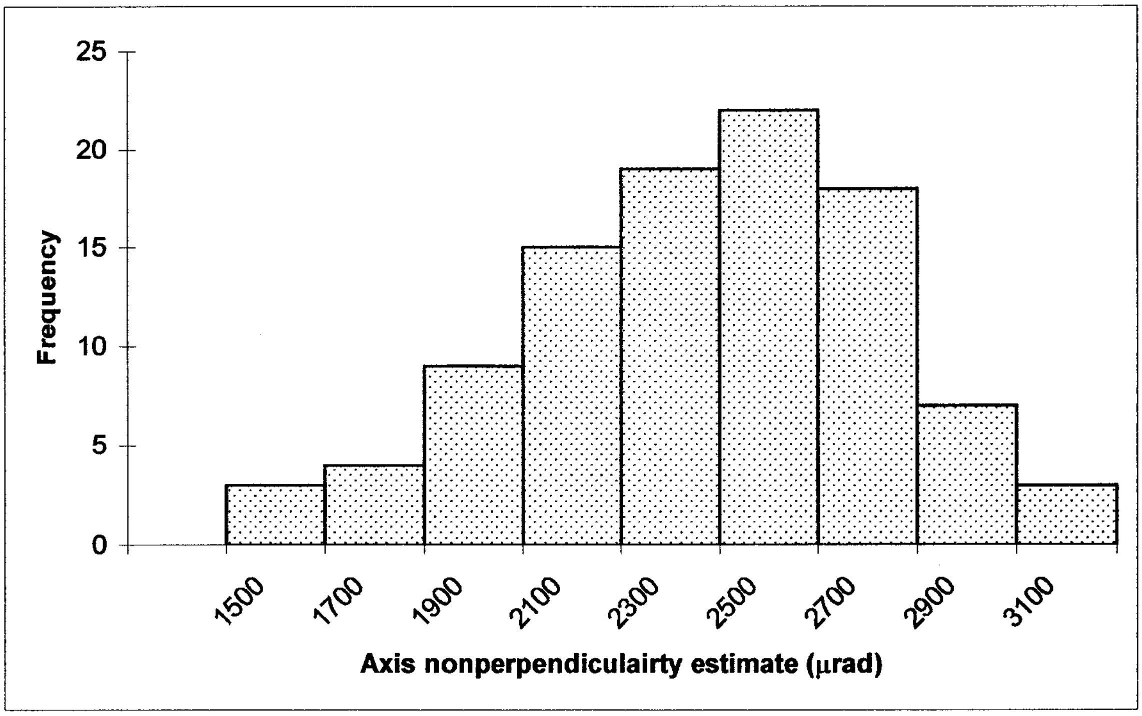

Figure 5.6 Bootstrap estimate histogram for axis nonperpendicularity

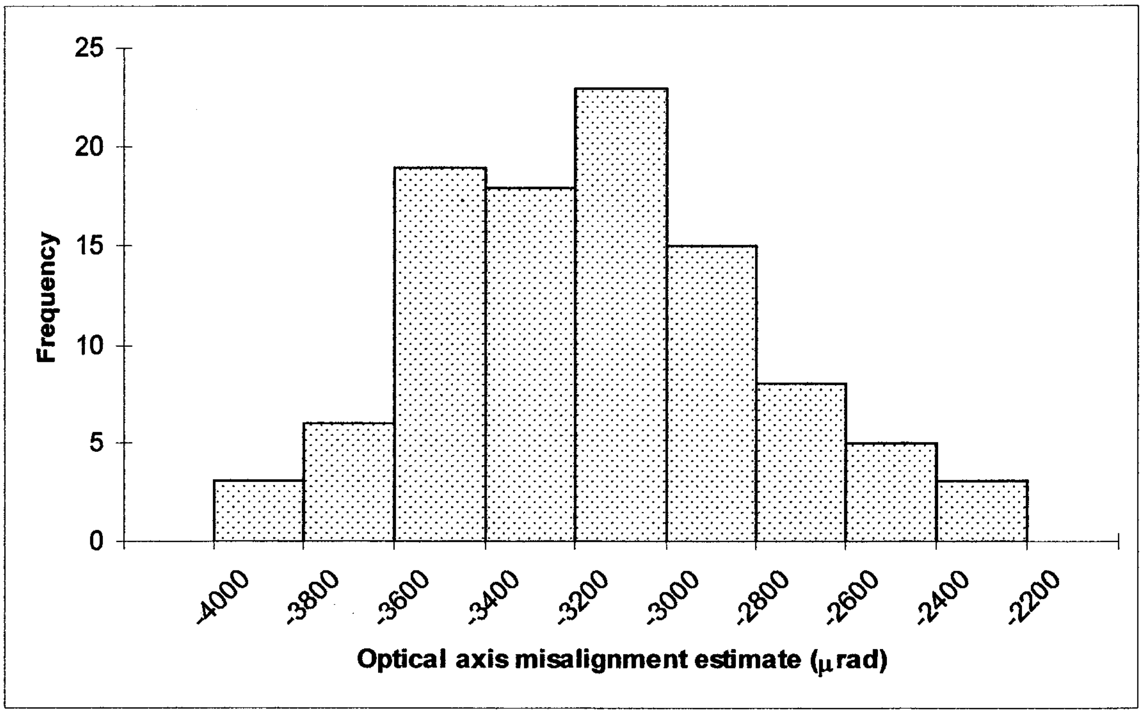

Figure 5.7 Bootstrap estimate histogram for optical axis misalignment

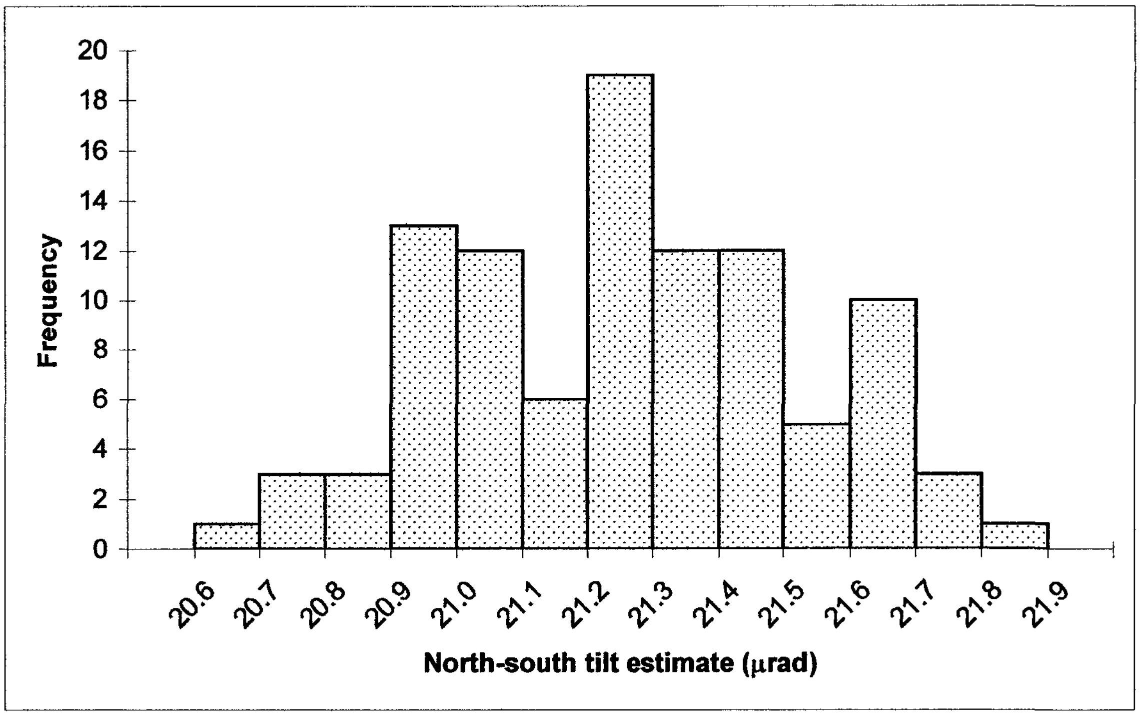

Figure 5.8 Bootstrap estimate histogram for north-south tilt

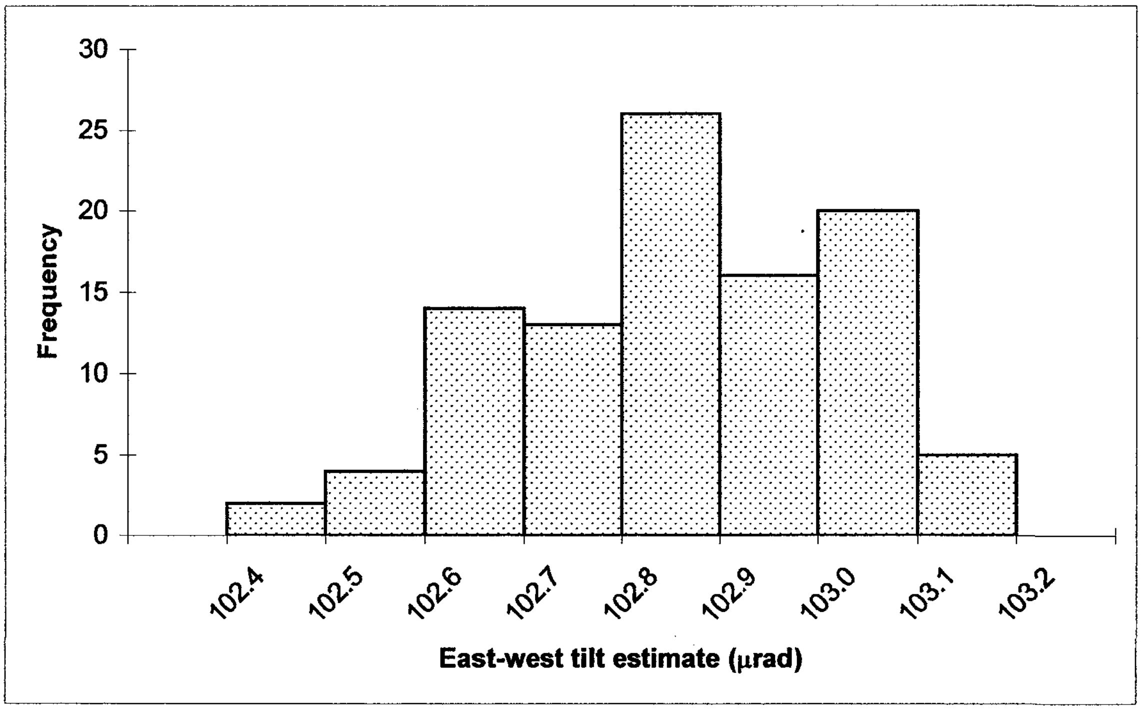

Figure 5.9 Bootstrap estimate histogram for east-west tilt

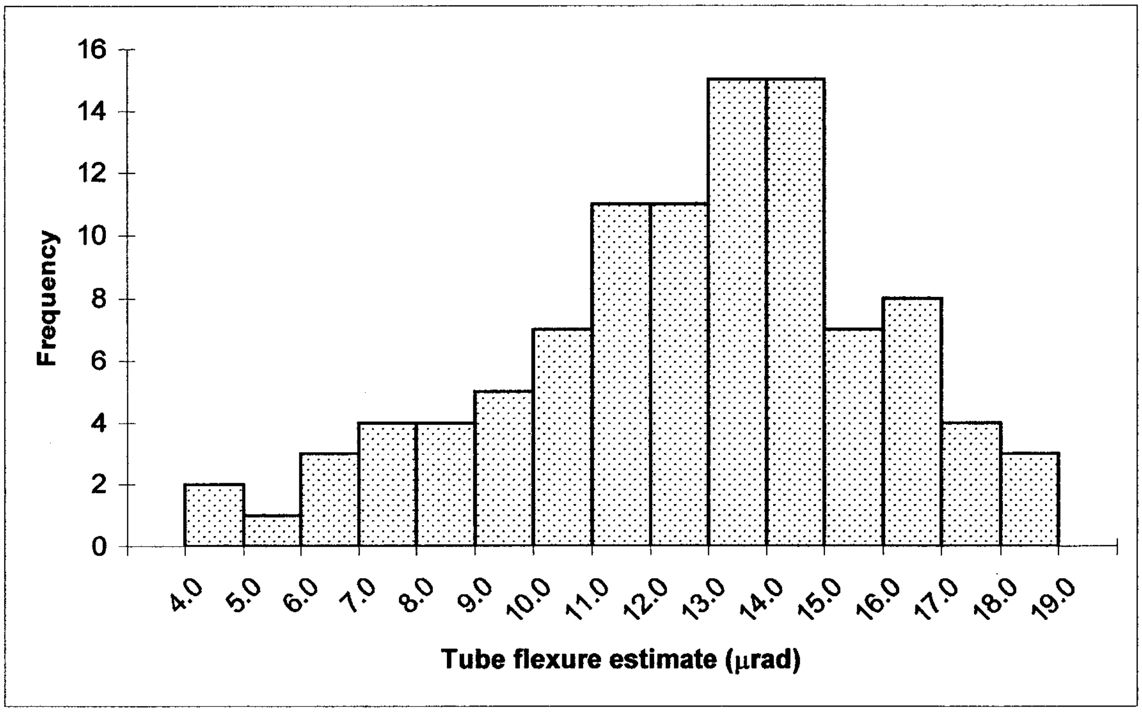

Figure 5.10 Bootstrap estimate histogram for tube flexure

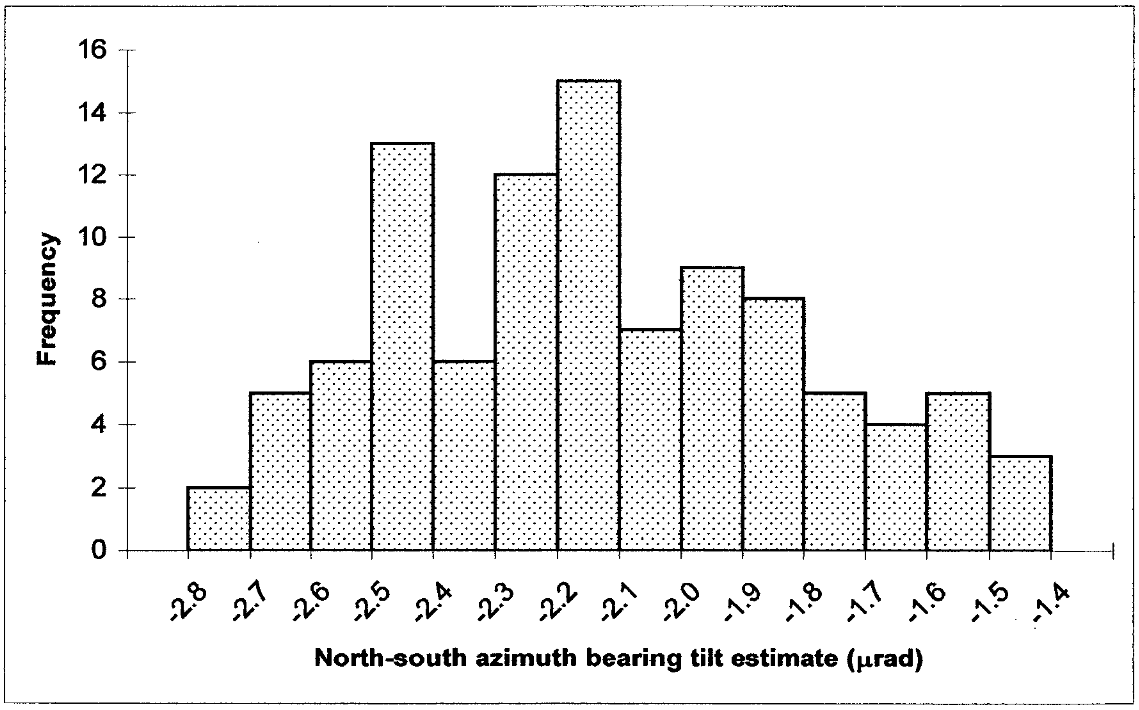

Figure 5.11 Bootstrap estimate histogram for north-south bearing wobble

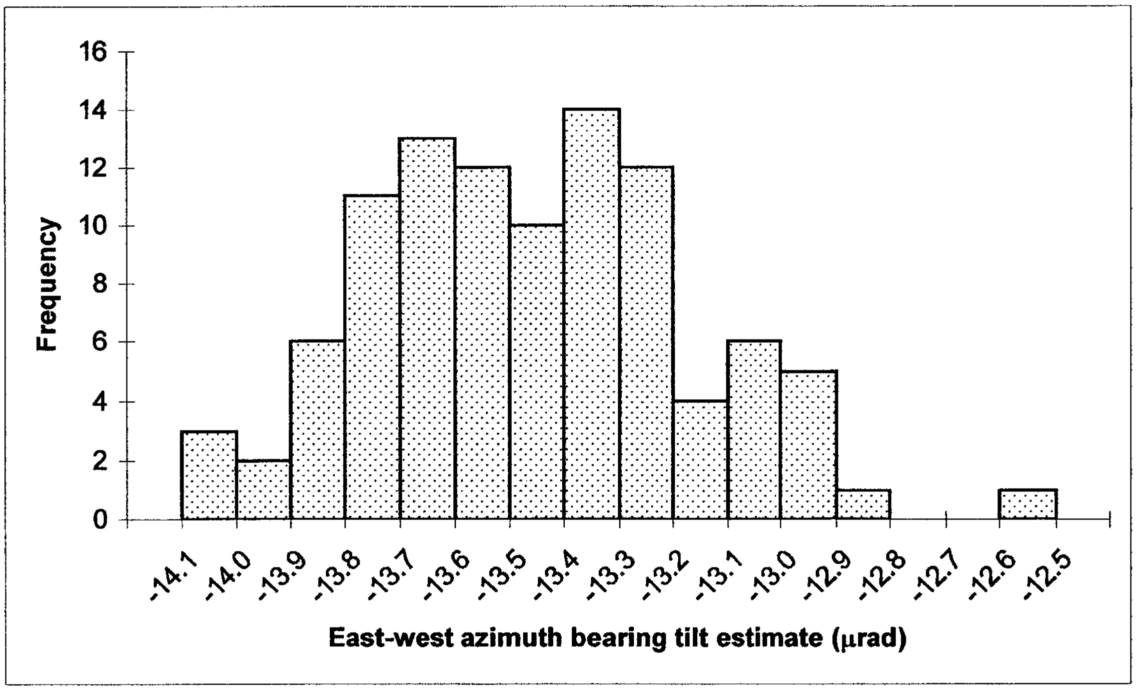

Figure 5.12 Bootstrap estimate histogram for east-west bearing wobble

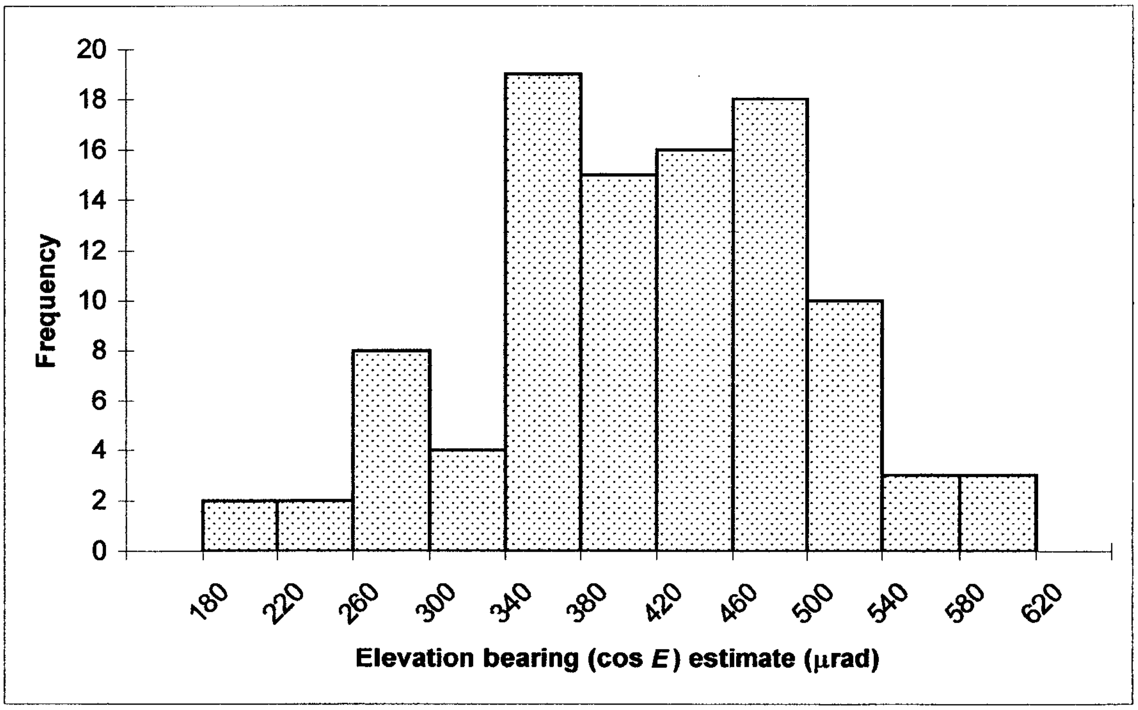

Figure 5.13 Bootstrap estimate histogram for elevation bearing wobble (cos *E*)

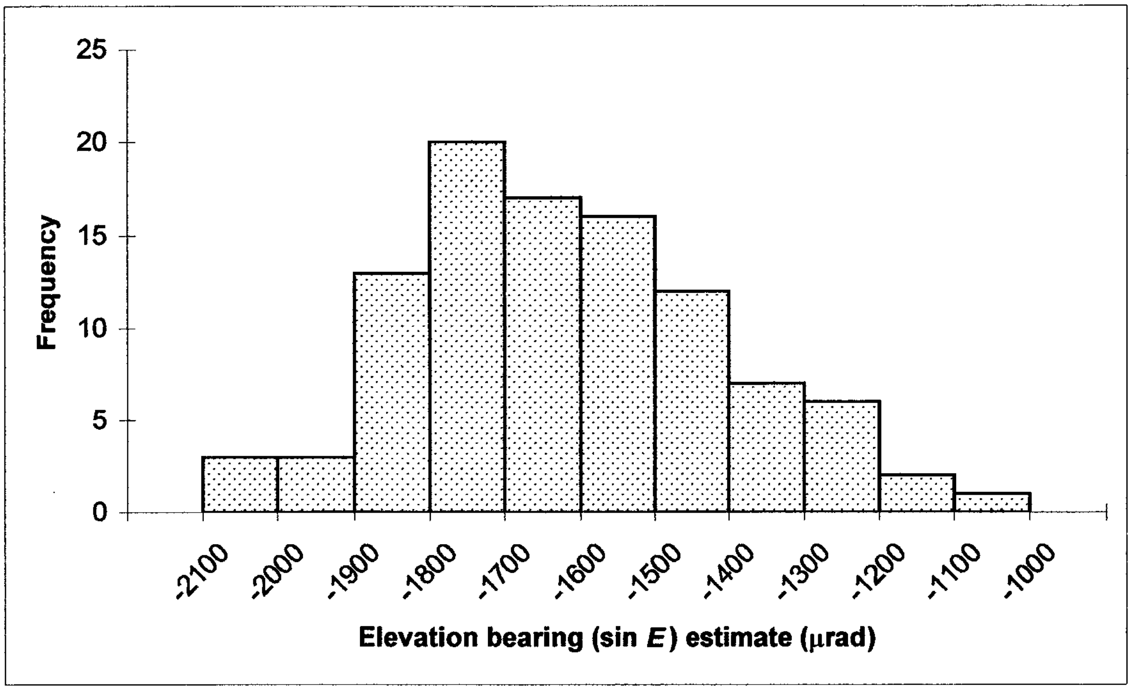

Figure 5.14 Bootstrap estimate histogram for elevation bearing wobble (sin *E*)

5.5 Ridge Regression

Using ridge regression required solving the model repeatedly with different bias parameters, selecting a parameter that represented an acceptable compromise between bias and precision, and then using that parameter in a new solution. Ridge traces and plots of the estimated model error were prepared for each data set as described in Chapter 4 and these were used to select an appropriate ridge parameter.

After reviewing the ridge traces and $\hat{\sigma}$ plots for all the data sets, the same value for the biasing constant, $k = 0.01$, was used for each. This value was judged to reasonably satisfy the criteria described in section 4.4 for every data set and using a consistent value was considered advantageous because it produces similar bias in all the solutions. Ultimately, if the same biasing constant can be used for a wide range of telescope mount modeling data, much of the judgment associated with ridge regression can be eliminated and more objective solutions obtained.

5.5.1 Sloan Digital Sky Survey Telescope Data

Figure 5.15 shows how the value of each model parameter changes as the ridge parameter is increased from near zero to one and Fig. 5.16 shows how the estimated error in the model, $\hat{\sigma}$, changes over the same range of ridge parameters. The parameters that exhibited the greatest change were those which were most correlated, the azimuth encoder offset, axis nonperpendicularity and misalignment, and one of the bearing errors. It is clear from the figure that most of the effect on the parameters occurred for ridge parameters of 0.0001 or less.

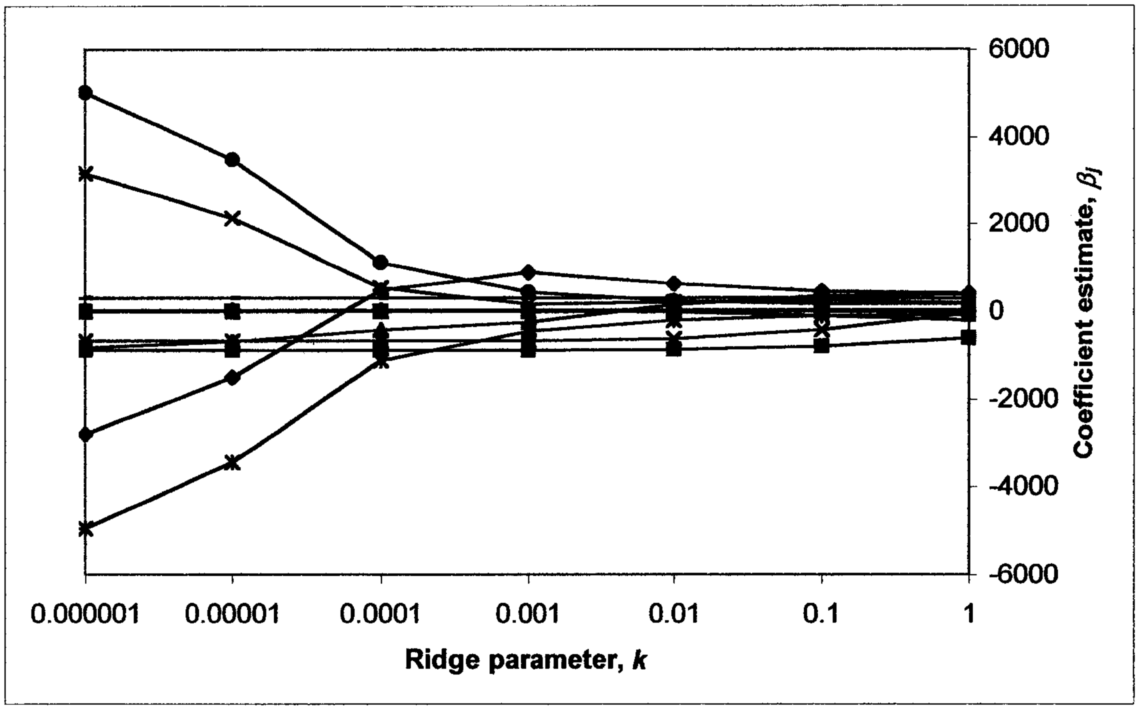

Figure 5.15 Effect of bias on estimated coefficients for the SDSS telescope

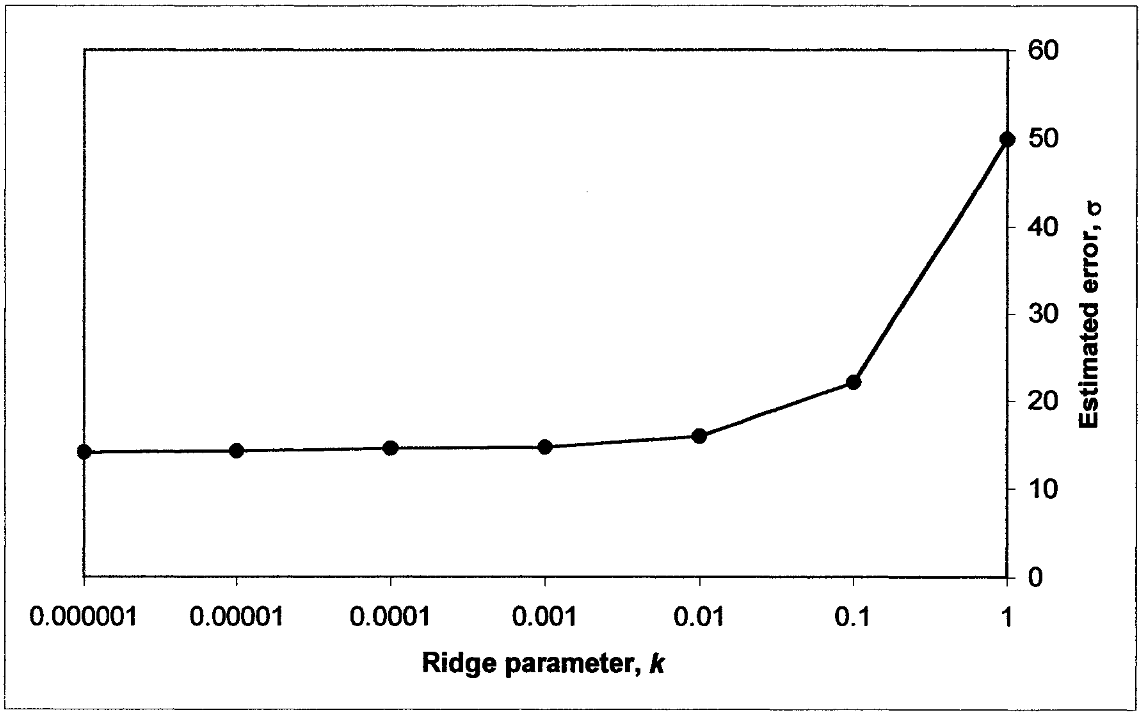

Figure 5.16 Effect of bias on estimated error for the SDSS telescope

The estimated error did not begin to increase substantially until the ridge parameter was increased above 0.01, justifying its use for the ridge parameter in the solution. In this case, a lower value for the ridge parameter could have been used but 0.01 was used for consistency with the solutions for the other telescopes. A lower value for the bias parameter would have improved the solution slightly.

The ridge regression results for the SDSS telescope are presented in Table 5.14 below. Most parameters were more precise than the corresponding MOLS estimate but the overall error in the model was slightly higher. Each parameter estimate also had an unknown bias introduced by the procedure. The improvement in precision was greatest for the most highly correlated errors and most of the error estimates were precise enough to be useful.

Table 5.14 Ridge estimates of parameters for the SDSS telescope

Parameter	Mean (μrad)	Standard Error (μrad)
Azimuth encoder offset	628.4	38.3
Elevation encoder offset	-881.9	9.7
Azimuth encoder scale	1.0	1.4
Elevation encoder scale	-636.2	26.4
Axis nonperpendicularity	-200.7	21.1
Optical axis misalignment	232.3	17.6
Tilt toward north	25.8	2.1
Tilt toward east	303.8	1.8
Tube flexure	-18.6	10.9
Azimuth bearing, NS term	-2.9	3.6
Azimuth bearing, EW term	4.4	3.7
Elevation bearing, cosine term	150.5	44.7
Elevation bearing, sine term	211.3	20.3
Estimated error (σ)		15.9

5.5.2 Astronomical Research Consortium Telescope Data

Figure 5.17 shows the effect of ridge parameter on the estimated model parameters for the ARC telescope and Fig. 5.18 shows how the estimated error was affected. As with the SDSS telescope, the parameters exhibiting the largest change were those which were most correlated. It is clear from Fig. 5.17 that most of the effect on the parameters occurred for ridge parameters of 0.001 or larger.

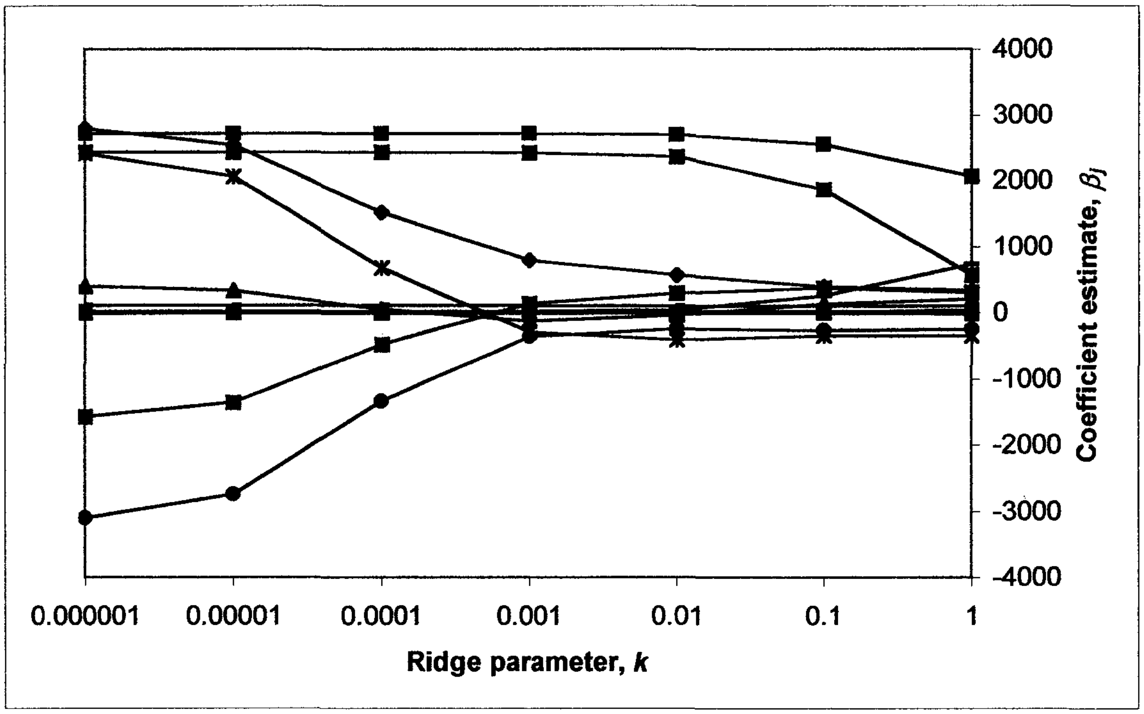

Figure 5.17 Effect of bias on estimated coefficients for the ARC telescope

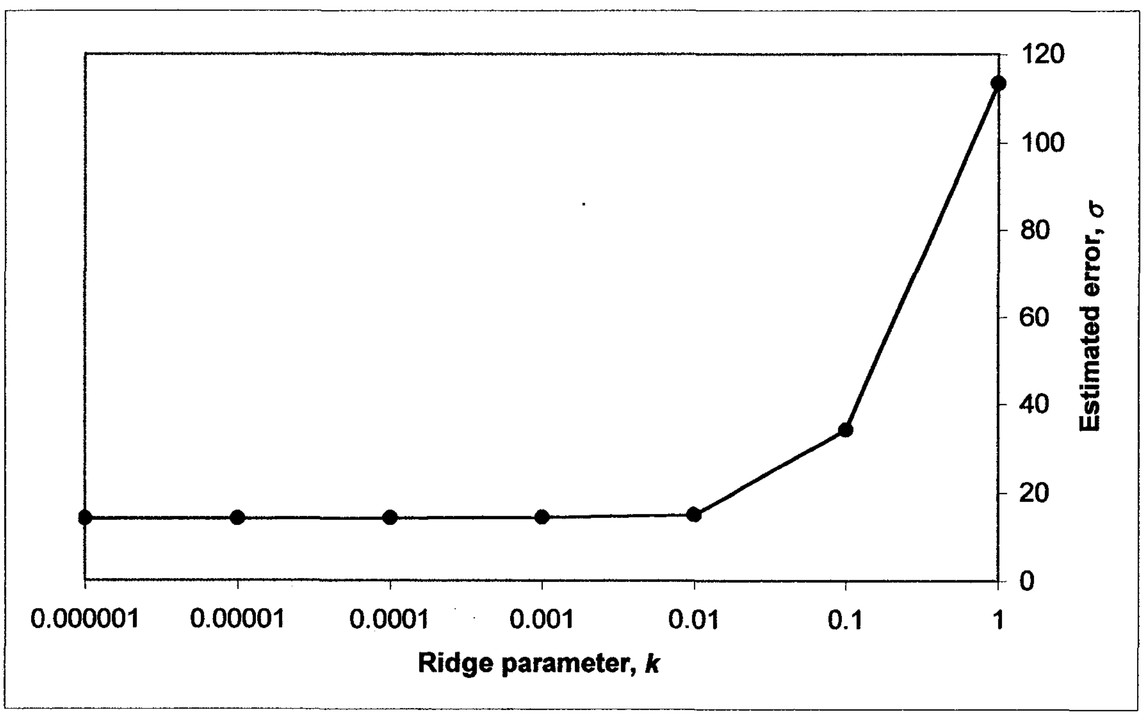

Figure 5.18 Effect of bias on estimated error for the ARC telescope.

The ridge regression results for the ARC telescope are presented in Table 5.15 below. A value of 0.01 was used for the ridge parameter because the estimated error only began to increase markedly when the ridge parameter was larger than this value. Once again, each parameter was more precise than the corresponding MOLS estimate but the overall error in the model was slightly higher. The best improvement occurred again for the most highly correlated terms.

Table 5.15 Ridge estimates of parameters for the ARC telescope

Parameter	Mean (μrad)	Standard Error (μrad)
Azimuth encoder offset	564.3	41.4
Elevation encoder offset	2694.4	6.6
Azimuth encoder scale	-0.5	1.0
Elevation encoder scale	2360.8	20.7
Axis nonperpendicularity	-406.8	19.5
Optical axis misalignment	-239.5	17.2
Tilt toward north	21.5	1.2
Tilt toward east	102.5	1.1
Tube flexure	42.7	9.4
Azimuth bearing, NS term	-1.4	2.7
Azimuth bearing, EW term	-12.0	2.0
Elevation bearing, cosine term	-42.3	44.3
Elevation bearing, sine term	291.1	22.5
Estimated error (σ)		15.0

5.5.3 W. M. Keck Observatory Data

Figures 5.19 through 5.22 show the effect of k on the parameter estimates for the Keck telescopes. Most of the effect occurred when k was 0.001 or larger and the most effected parameters were the same as for the SDSS and ARC telescopes.

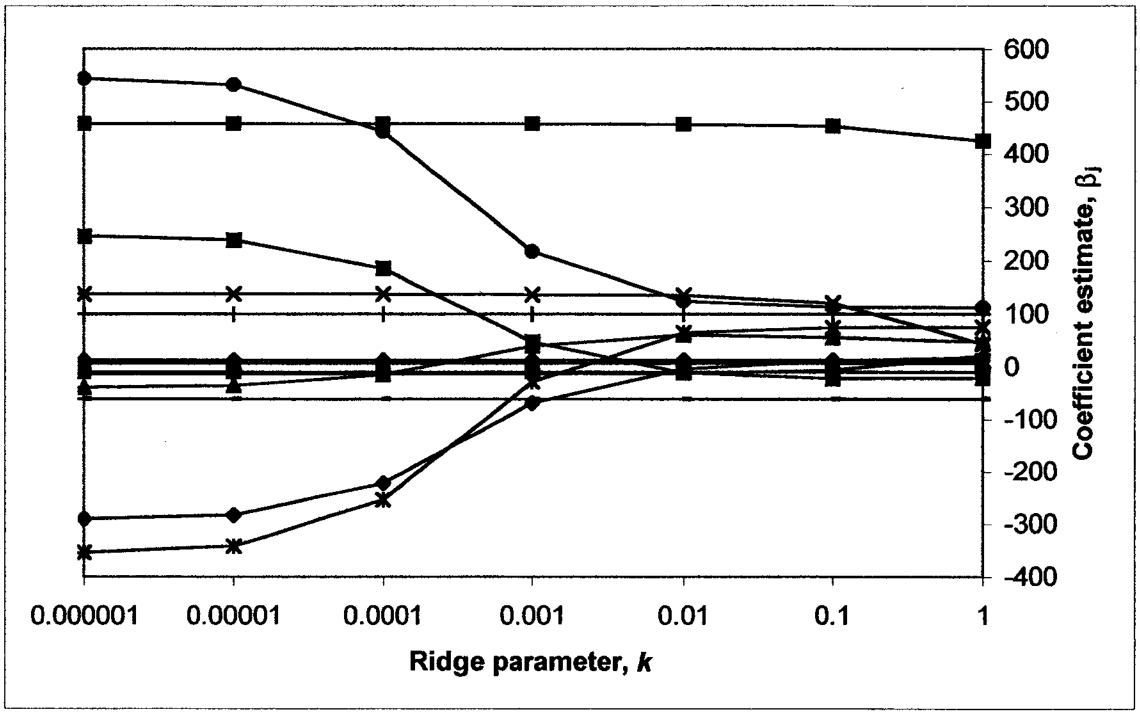

Figure 5.19 Effect of bias on estimated coefficients for the Keck I telescope

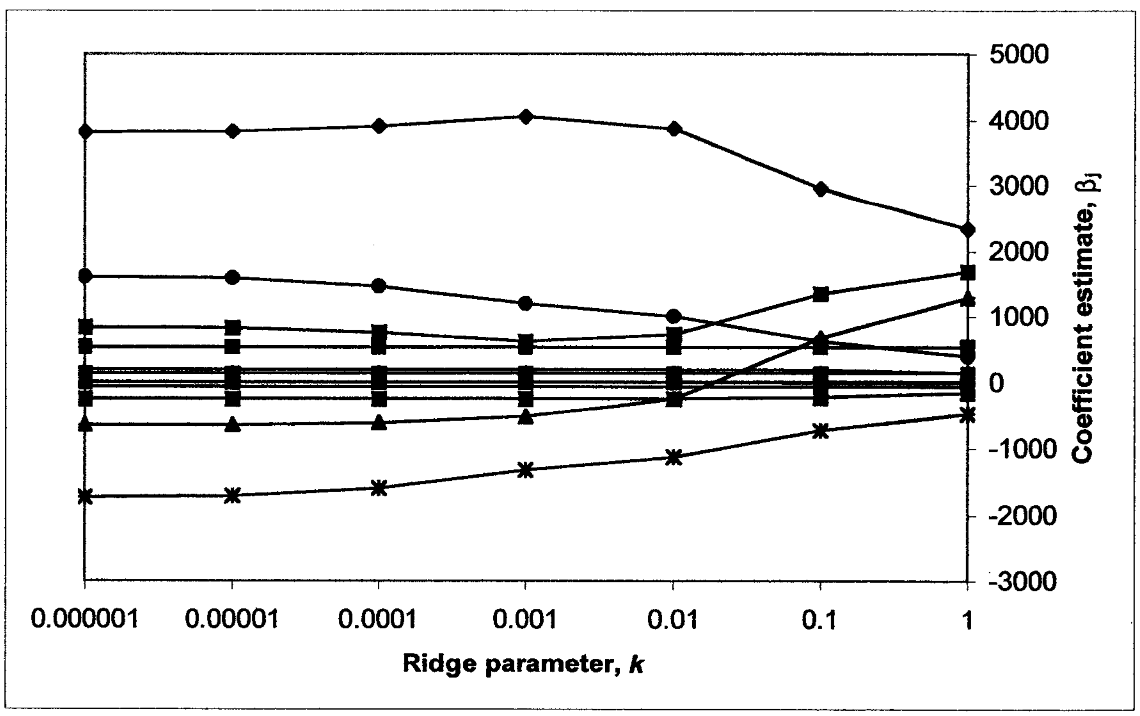

Figure 5.20 Effect of bias on estimated coefficients for the Keck II telescope

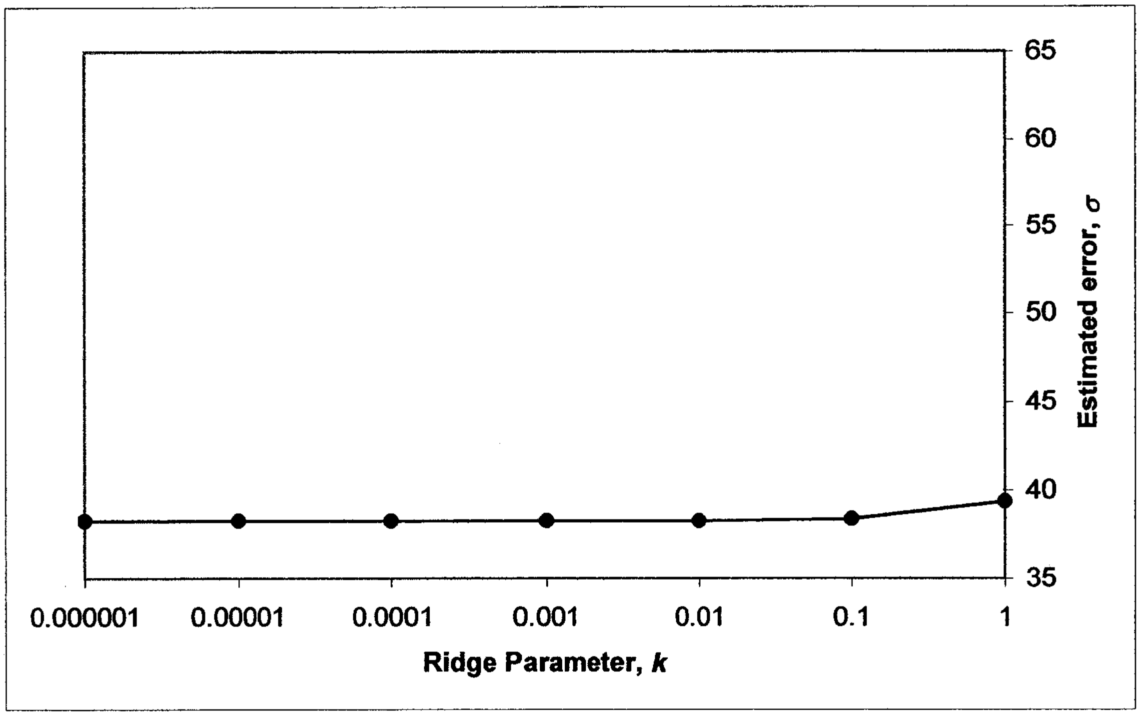

Figure 5.21 Effect of bias on estimated error for the Keck I telescope

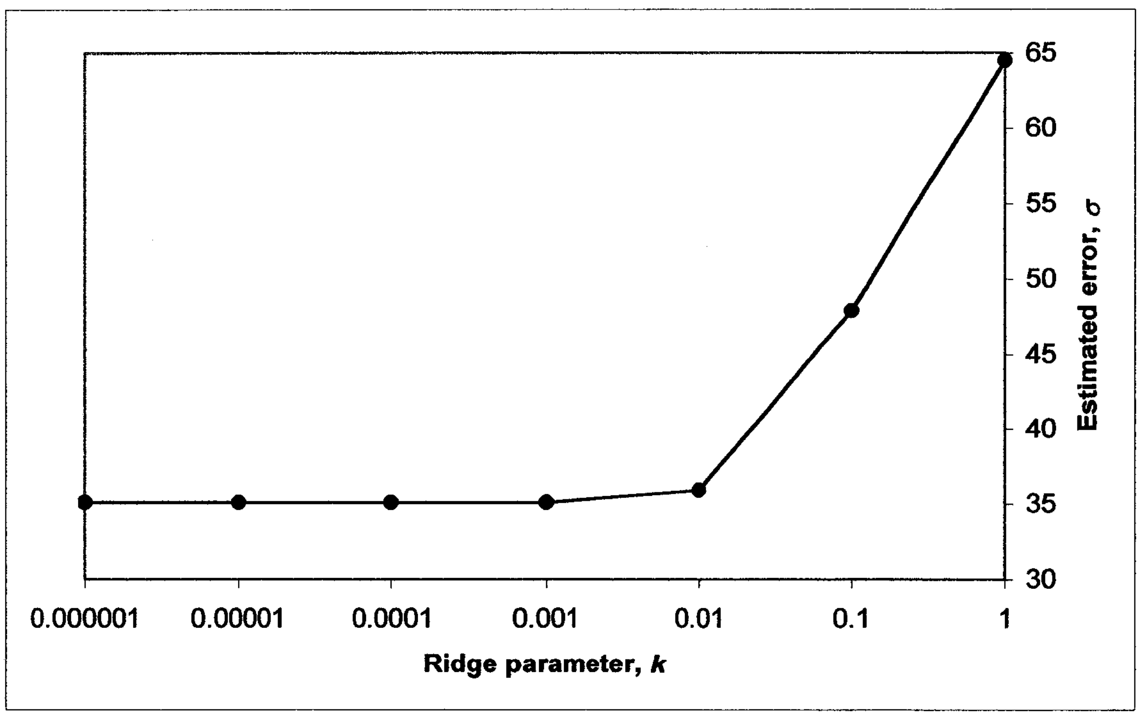

Figure 5.22 Effect of bias on estimated error for the Keck II telescope

The ridge regression results for the Keck telescopes are presented in Tables 5.16 and 5.17 below. A value of 0.01 was used again for the ridge parameter because the estimated error was relatively stable below that value. Each parameter was more precise than the corresponding MOLS estimate and the overall error in the model was slightly higher.

Table 5.16 Ridge estimates of parameters for the Keck I telescope

Parameter	Mean (μrad)	Standard Error (μrad)
Azimuth encoder offset	-3.1	84.6
Elevation encoder offset	456.4	9.5
Azimuth encoder scale	7.1	2.4
Elevation encoder scale	135.6	32.1
Axis nonperpendicularity	64.9	52.6
Optical axis misalignment	123.8	51.7
Tilt toward north	100.6	1.3
Tilt toward east	-61.4	1.2
Tube flexure	-12.2	15.6
Azimuth bearing, NS term	13.9	2.5
Azimuth bearing, EW term	-9.4	2.4
Elevation bearing, cosine term	60.9	82.1
Elevation bearing, sine term	-10.7	59.8
Estimated error (σ)		38.3

Table 5.17 Ridge estimates of parameters for the Keck II telescope

Parameter	Mean (μrad)	Standard Error (μrad)
Azimuth encoder offset	3866.9	77.4
Elevation encoder offset	530.5	9.0
Azimuth encoder scale	1.0	2.2
Elevation encoder scale	-247.3	30.8
Axis nonperpendicularity	-1127.6	45.8
Optical axis misalignment	1000.2	44.8
Tilt toward north	145.4	1.4
Tilt toward east	-63.9	1.2
Tube flexure	198.8	15.4
Azimuth bearing, NS term	8.8	2.4
Azimuth bearing, EW term	0.9	2.4
Elevation bearing, cosine term	-249.0	74.3
Elevation bearing, sine term	726.8	55.2
Estimated error (σ)		35.9

5.5.4 Simulated Data

Figures 5.23 through 5.33 show the effect of ridge parameter on the estimated model parameters and estimated error for the simulated data sets. Clearly the effect was greater when more noise was present in the data. No plot of the effect of bias on estimated error is shown for set 0 because the estimated error was zero for every value of the ridge parameter.

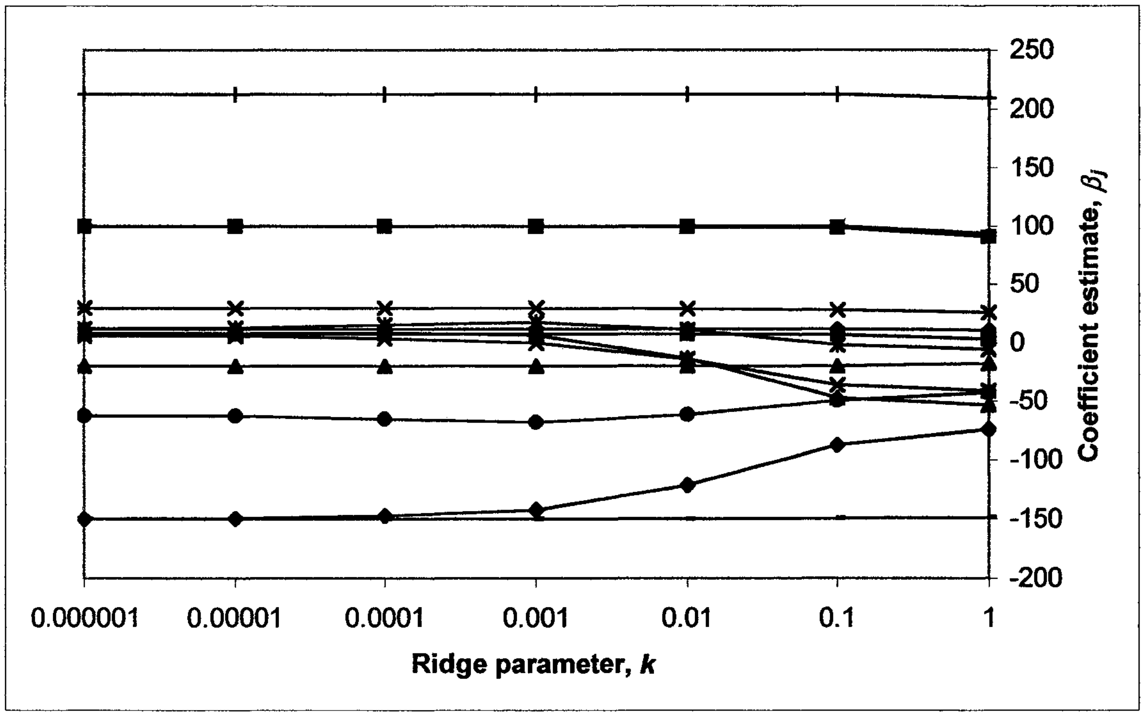

Figure 5.23 Effect of bias on estimated coefficients for simulated data set 0

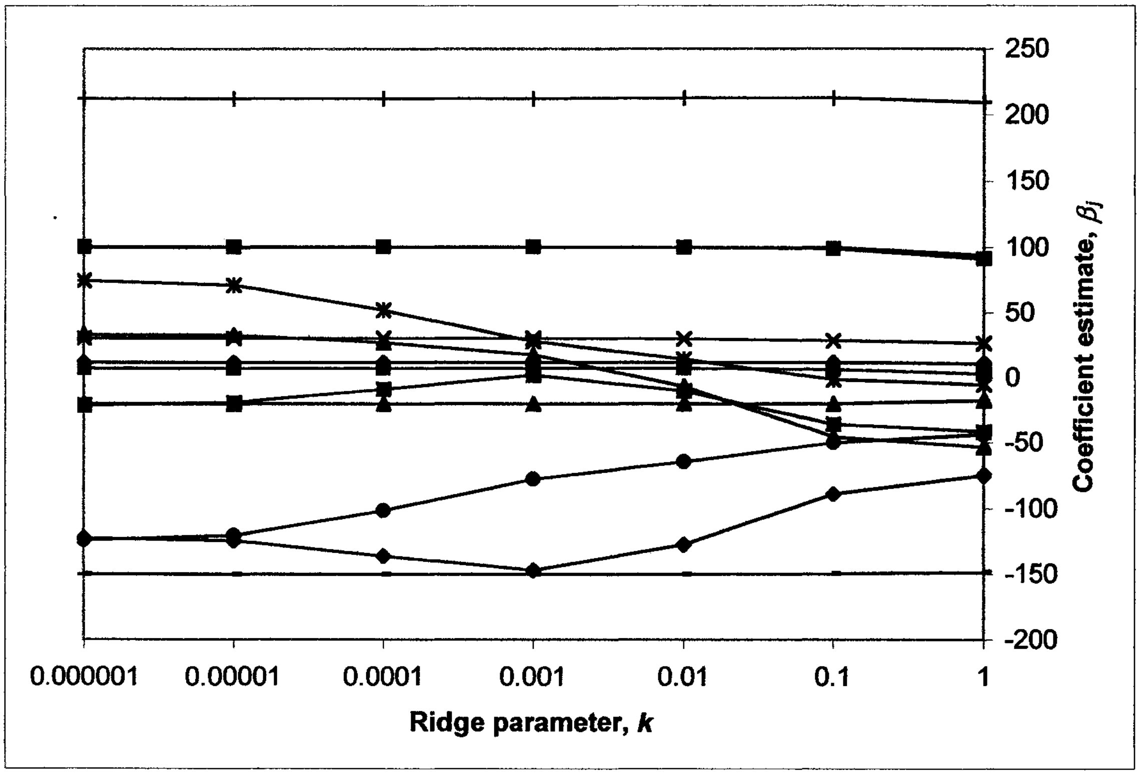

Figure 5.24 Effect of bias on estimated coefficients for simulated data set 1

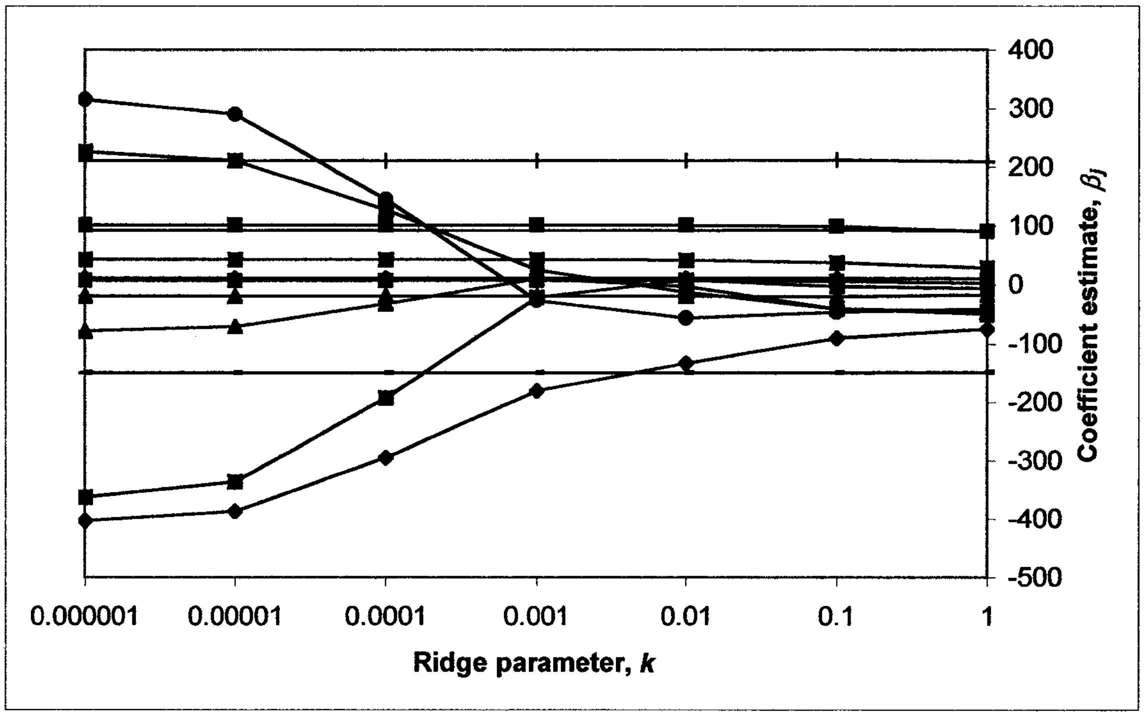

Figure 5.25 Effect of bias on estimated coefficients for simulated data set 2

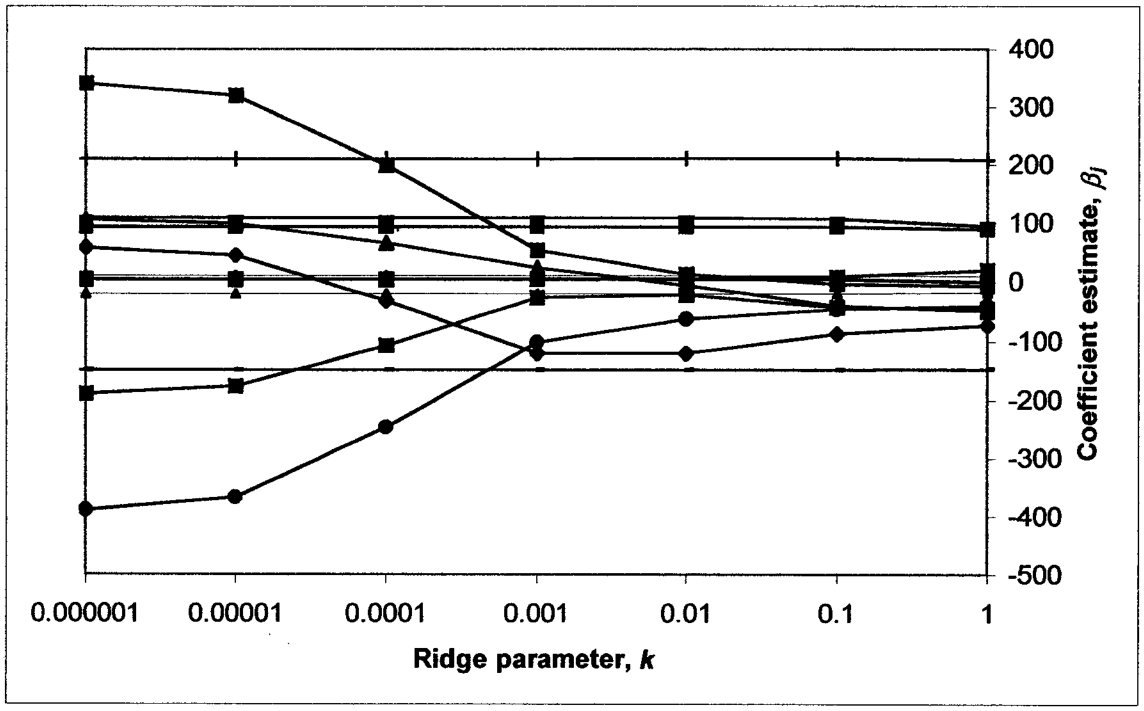

Figure 5.26 Effect of bias on estimated coefficients for simulated data set 3

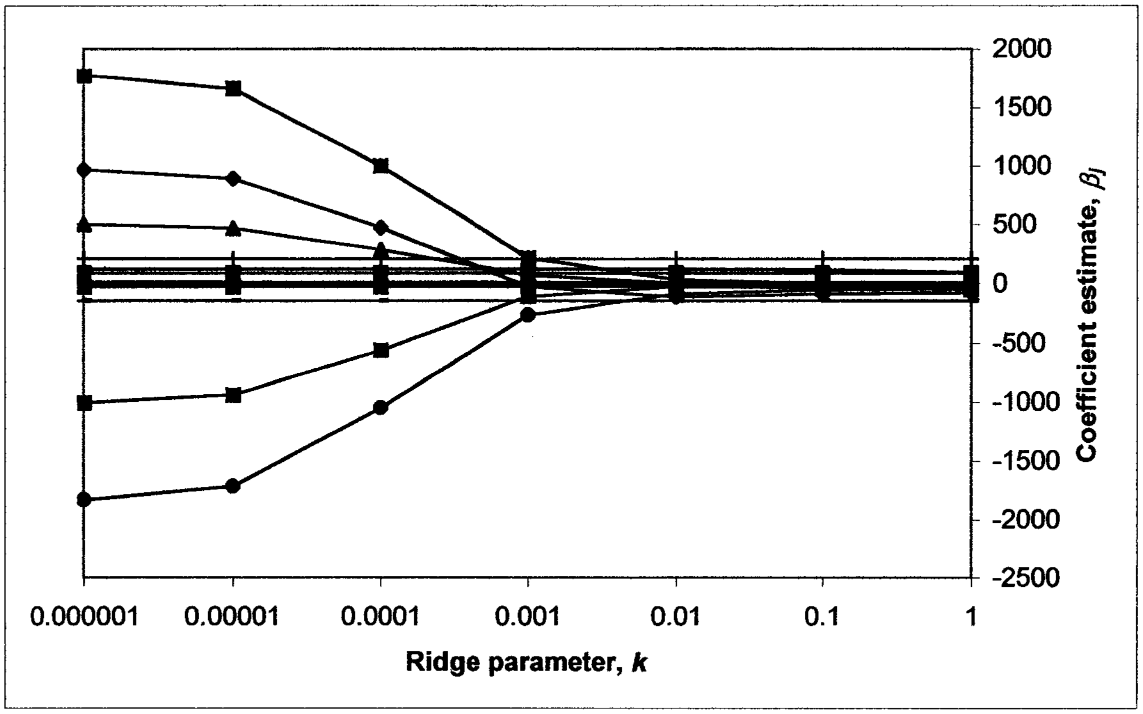

Figure 5.27 Effect of bias on estimated coefficients for simulated data set 4

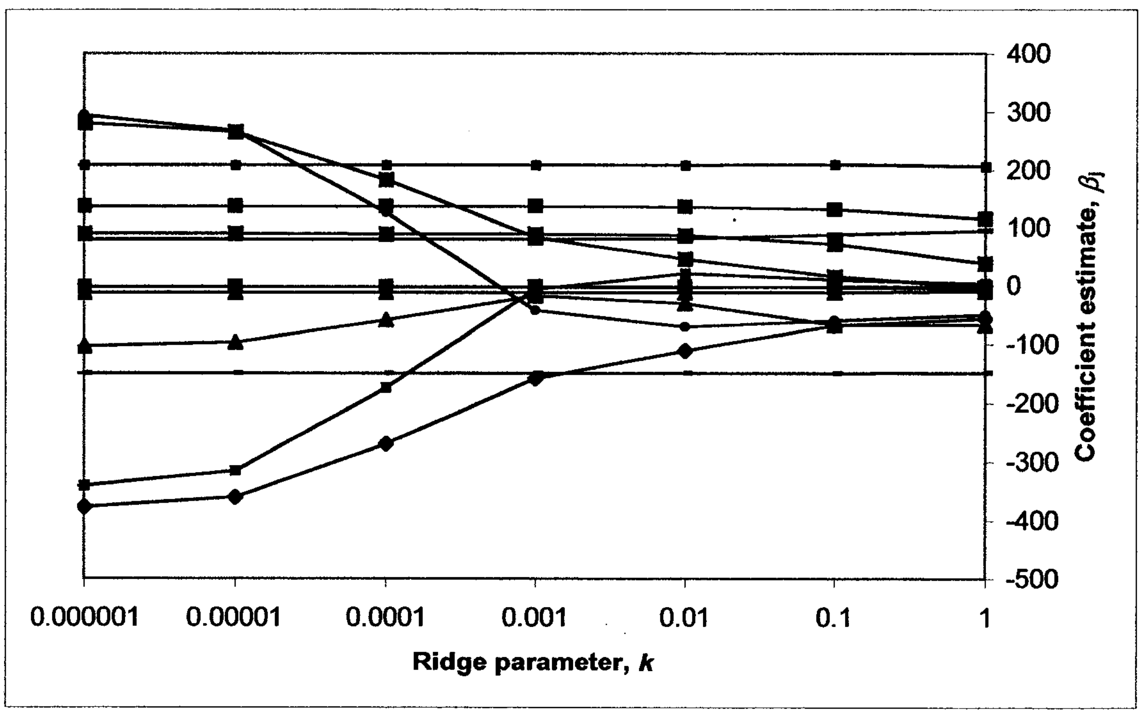

Figure 5.28 Effect of bias on estimated coefficients for simulated data set 5

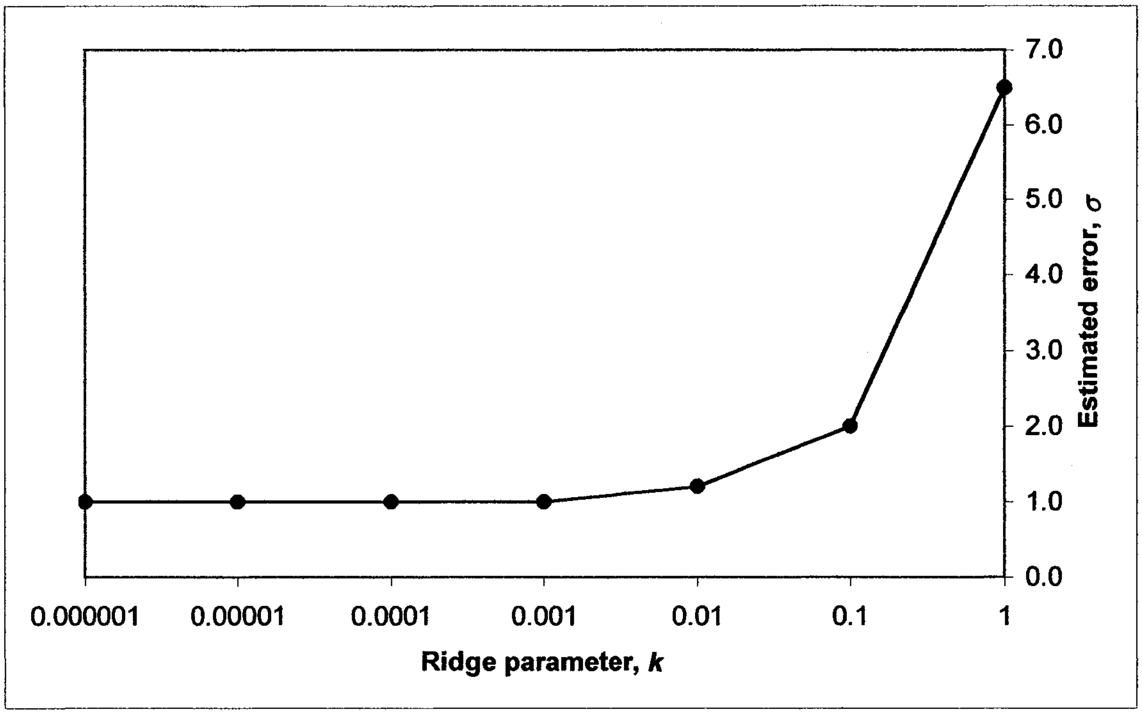

Figure 5.29 Effect of bias on estimated error for simulated data set 1

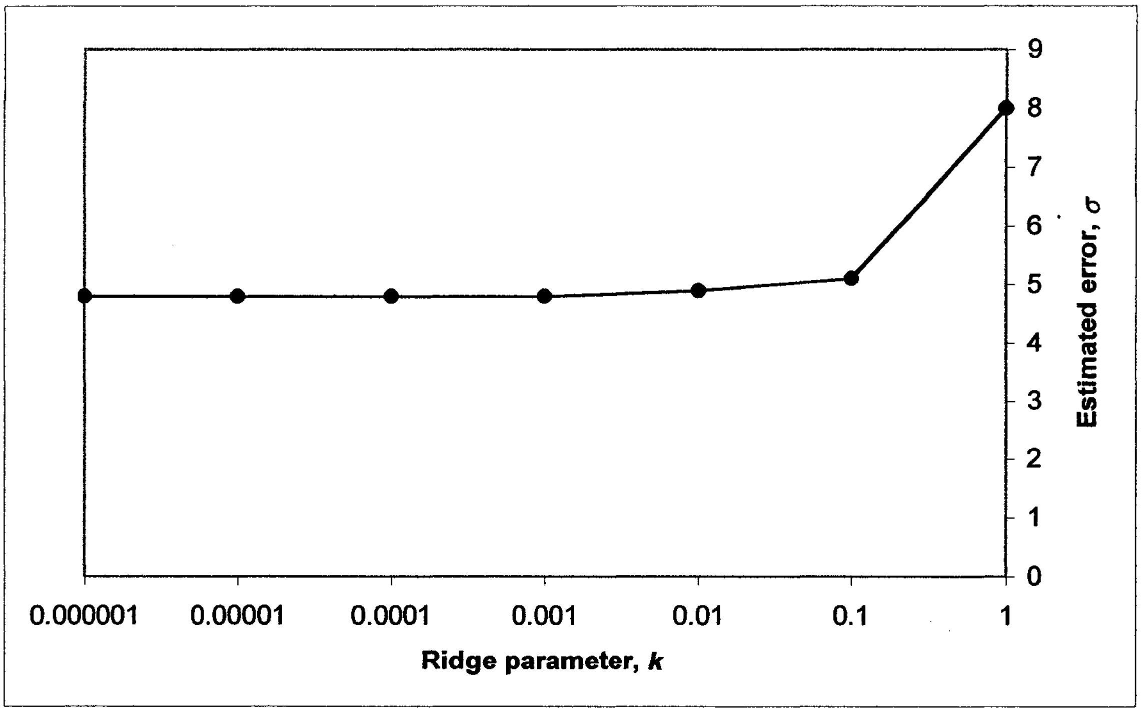

Figure 5.30 Effect of bias on estimated error for simulated data set 2

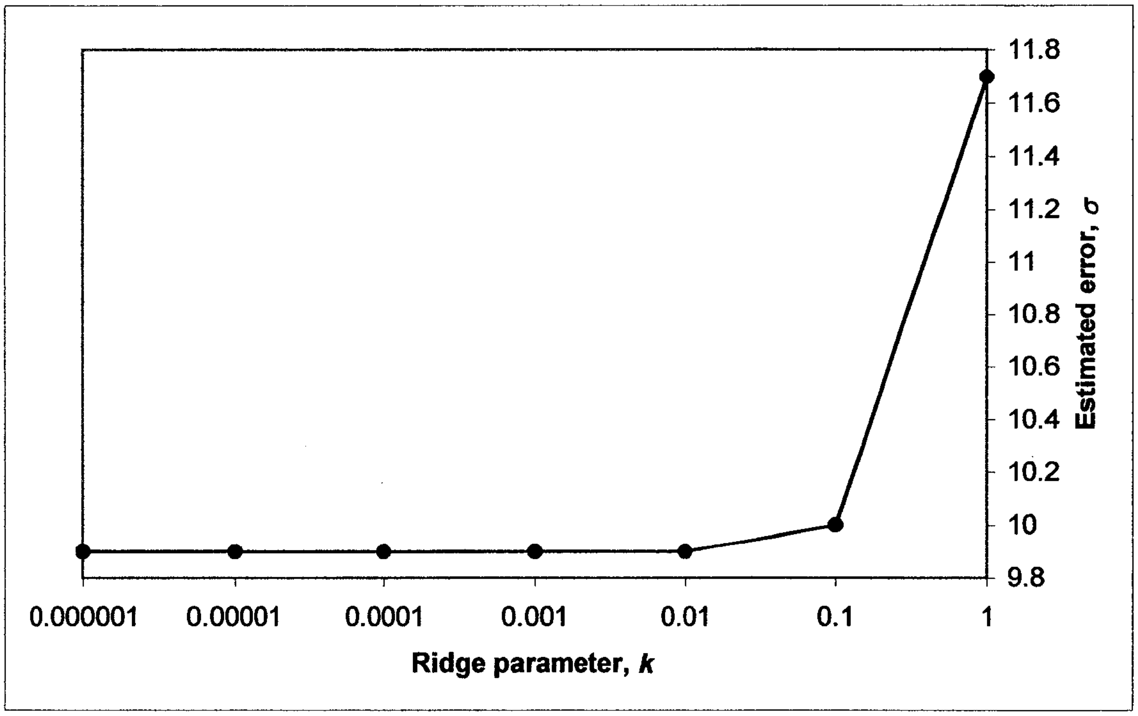

Figure 5.31 Effect of bias on estimated error for simulated data set 3

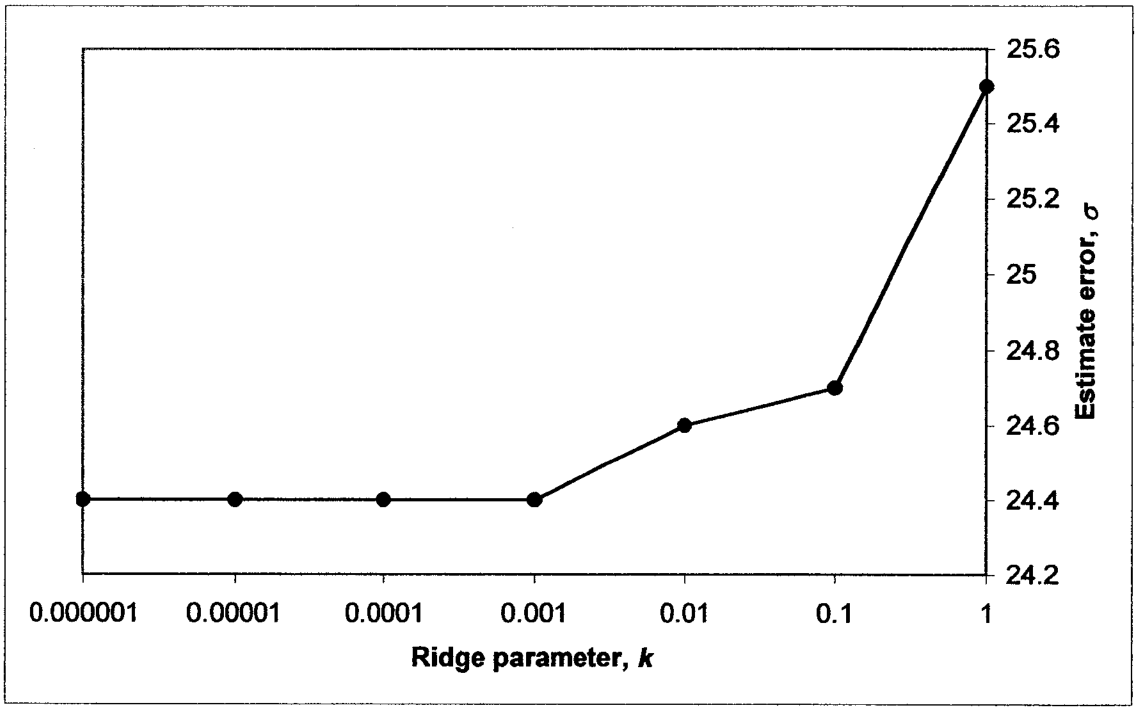

Figure 5.32 Effect of bias on estimated error for simulated data set 4

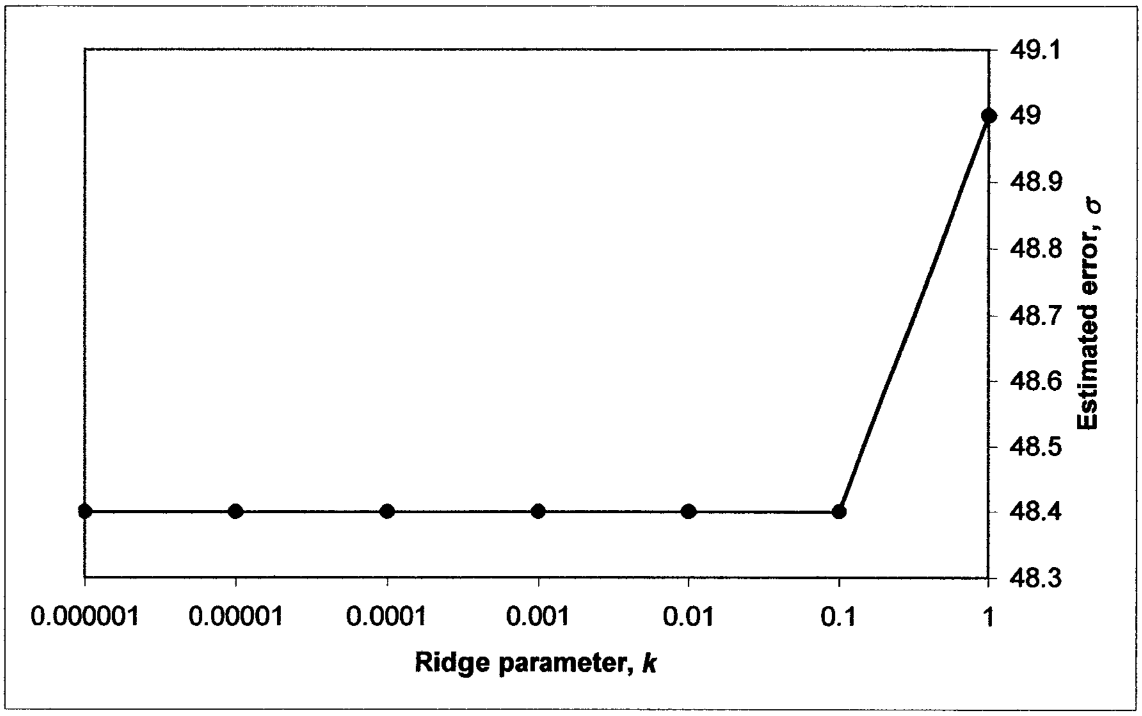

Figure 5.33 Effect of bias on estimated error for simulated data set 5

The ridge regression results for the simulated data sets are shown in Tables 5.18a and 5.18b below. A value of 0.01 was used for the ridge parameter for each data set. Each parameter estimate was more precise than the corresponding MOLS estimate and was more accurate because it was closer to the true value of the parameter. The overall error in the model, however, was slightly higher meaning that the ridge solution would produce somewhat poorer pointing performance.

Table 5.18a Ridge estimates of parameters for the simulated sets

	Set 0		Set 1		Set 2	
	$\sigma = 0\ \mu$rad		$\sigma = 1\ \mu$rad		$\sigma = 5\ \mu$rad	
Parameter	Mean (μrad)	S. E. (μrad)	Mean (μrad)	S. E. (μrad)	Mean (μrad)	S. E. (μrad)
Azimuth encoder offset	-121.8	0.0	-127.7	2.9	-133.1	13.8
Elevation encoder offset	99.8	0.0	100.0	0.4	101.0	2.1
Azimuth encoder scale	-20.2	0.0	-20.1	0.1	-19.8	0.5
Elevation encoder scale	29.4	0.0	29.8	1.6	41.9	7.5
Axis nonperpendicularity	11.0	0.0	14.2	1.3	7.9	6.2
Optical axis misalignment	-61.7	0.0	-64.8	1.2	-56.8	5.9
Tilt toward north	212.7	0.0	212.7	0.1	211.8	0.6
Tilt toward east	-150.0	0.0	-149.9	0.1	-150.1	0.4
Tube flexure	100.2	0.0	100.1	0.8	93.0	3.6
Azimuth bearing, NS term	12.0	0.0	12.0	0.2	11.8	0.9
Azimuth bearing, EW term	7.3	0.0	7.2	0.2	6.9	0.8
Elevation bearing, cosine term	-13.5	0.0	-6.9	3.0	-2.3	13.9
Elevation bearing, sine term	-13.9	0.0	-10.1	2.0	-12.3	9.6
Estimated error (σ)		0.6		1.2		4.9

Table 5.18b Ridge estimates of parameters for the simulated data (cont.)

	Set 3		Set 4		Set 5	
	$\sigma = 10\ \mu$rad		$\sigma = 20\ \mu$rad		$\sigma = 50\ \mu$rad	
	Mean	S. E.	Mean	S. E.	Mean	S. E
Parameter	(μrad)	(μrad)	(μrad)	(μrad)	(μrad)	(μrad)
Azimuth encoder offset	-119.8	28.6	-111.8	70.6	-111.1	140.2
Elevation encoder offset	94.1	4.3	90.3	10.5	136.8	20.9
Azimuth encoder scale	-19.6	1.0	-19.1	2.4	-11.6	4.7
Elevation encoder scale	5.7	15.5	-22.0	38.2	87.1	75.8
Axis nonperpendicularity	14.2	12.8	34.2	31.7	21.6	62.9
Optical axis misalignment	-62.3	12.2	-83.5	30.1	-70.9	59.7
Tilt toward north	210.8	1.2	212.4	3.0	209.5	5.9
Tilt toward east	-148.8	0.8	-147.5	2.1	-149.6	4.2
Tube flexure	109.1	7.5	122.7	18.5	82.1	36.8
Azimuth bearing, NS term	11.6	1.9	11.3	4.7	-2.3	9.4
Azimuth bearing, EW term	5.1	1.6	3.4	4.0	-1.9	7.9
Elevation bearing, cosine term	-4.8	28.8	2.5	71.2	-30.2	141.4
Elevation bearing, sine term	-21.1	19.8	-23.7	48.8	46.4	97.0
Estimated error (σ)		9.9		24.6		48.4

5.6 Bayesian Regression

Bayesian regression uses prior estimates of the distribution of each regression coefficient to influence the solution. If the prior estimates are precise enough, i. e. if they are known with sufficient certainty, a significantly better solution can be obtained compared to that produced by the MOLS method. Prior estimates for the mean and standard deviation of each parameter were listed in Chapter 4. This information was used in a Bayesian regression estimate of the model parameters.

5.6.1 Sloan Digital Sky Survey Telescope

Table 5.19 lists the Bayesian estimates of the parameters for the SDSS telescope. The precision of every parameter was improved over the MOLS estimate and most were more precise than the ridge regression estimate. The parameters that showed the most improvement were those that were most highly correlated. In spite of the fact that each parameter estimate was more precise, the overall estimated error in the model was somewhat higher.

Table 5.19 Bayesian parameter estimates for the SDSS telescope

Parameter	Mean (μrad)	Standard Error (μrad)
Azimuth encoder offset	985.3	23.2
Elevation encoder offset	-914.4	6.7
Azimuth encoder scale	0.7	1.4
Elevation encoder scale	-773.0	9.4
Axis nonperpendicularity	-42.4	28.1
Optical axis misalignment	48.7	33.8
Tilt toward north	25.0	2.0
Tilt toward east	304.3	1.8
Tube flexure	44.9	2.5
Azimuth bearing, NS term	-1.5	2.9
Azimuth bearing, EW term	2.3	3.0
Elevation bearing, cosine term	-0.4	5.0
Elevation bearing, sine term	-0.0	5.0
Estimated error (σ)		17.1

5.6.2 Astronomical Research Consortium Telescope Data

Bayesian estimates of the model parameters for the ARC telescope are presented in Table 5.20. Every parameter estimate was more precise than the MOLS estimate and most were better than the ridge regression estimate. The most improvement occurred in the highly correlated parameters and the overall error in the model was estimated to be somewhat higher than it was in the MOLS solution.

Table 5.20 Bayesian parameter estimates for the ARC telescope

Parameter	Mean (μrad)	Standard Error (μrad)
Azimuth encoder offset	920.8	12.5
Elevation encoder offset	2671.4	4.8
Azimuth encoder scale	-0.5	1.0
Elevation encoder scale	2303.5	7.5
Axis nonperpendicularity	4.9	17.7
Optical axis misalignment	-659.4	19.5
Tilt toward north	21.4	1.2
Tilt toward east	102.4	1.1
Tube flexure	60.9	2.5
Azimuth bearing, NS term	-1.9	2.4
Azimuth bearing, EW term	-10.7	1.8
Elevation bearing, cosine term	-0.4	5.0
Elevation bearing, sine term	0.0	5.0
Estimated error (σ)		16.3

5.6.3 W. M. Keck Observatory Data

Tables 5.21 and 5.22 list the Bayesian parameter estimates for the Keck telescopes. The parameter precision in both solutions is better than the ridge regression solutions but the overall estimated error is higher. An important feature of the Bayesian regression solutions for these telescopes was the fact that the estimates for the tube flexure were similar while they differed substantially in the solutions obtained using other methods. This was an important result because, as noted in section 5.3.4, the fact that the telescopes have a nearly identical design suggests that the elastic behavior of the tube trusses should be similar.

Table 5.21 Bayesian parameter estimates for the Keck I telescope

Parameter	Mean (μrad)	Standard Error (μrad)
Azimuth encoder offset	-2.5	15.1
Elevation encoder offset	436.9	7.9
Azimuth encoder scale	7.5	2.3
Elevation encoder scale	13.8	11.9
Axis nonperpendicularity	-18.4	29.2
Optical axis misalignment	205.4	30.3
Tilt toward north	100.7	1.3
Tilt toward east	-61.1	1.2
Tube flexure	50.4	2.6
Azimuth bearing, NS term	11.3	2.2
Azimuth bearing, EW term	-7.8	2.1
Elevation bearing, cosine term	0.2	5.0
Elevation bearing, sine term	0.0	5.0
Estimated error (σ)		40.0

Table 5.22 Bayesian parameter estimates for the Keck II telescope

Parameter	Mean (μrad)	Standard Error (μrad)
Azimuth encoder offset	4681.7	14.2
Elevation encoder offset	576.9	7.5
Azimuth encoder scale	1.5	2.2
Elevation encoder scale	20.0	11.6
Axis nonperpendicularity	4.7	28.4
Optical axis misalignment	-137.6	29.5
Tilt toward north	145.6	1.4
Tilt toward east	-63.2	1.1
Tube flexure	56.2	2.6
Azimuth bearing, NS term	7.0	2.2
Azimuth bearing, EW term	0.6	2.2
Elevation bearing, cosine term	-0.6	5.0
Elevation bearing, sine term	-0.0	5.0
Estimated error (σ)		42.0

5.6.4 Simulated Data

Tables 5.23a and 5.23b provide the Bayesian parameter estimates for the simulated data sets. Not only was the precision of each parameter better than for any other solution method, the mean estimate of each parameter remained close to the known value until the error became very large (sets 4 and 5).

Table 5.23a Bayesian parameter estimates for the simulated data

	Set 0		Set 1		Set 2	
	$\sigma = 0\ \mu$rad		$\sigma = 1\ \mu$rad		$\sigma = 5\ \mu$rad	
Parameter	Mean (μrad)	S. E. (μrad)	Mean (μrad)	S. E. (μrad)	Mean (μrad)	S. E. (μrad)
Azimuth encoder offset	-150.0	0.0	-150.4	1.3	-157.2	3.3
Elevation encoder offset	100.0	0.0	100.2	0.4	100.7	1.9
Azimuth encoder scale	-20.0	0.0	-20.0	0.1	-19.7	0.4
Elevation encoder scale	30.0	0.0	30.5	1.6	40.4	6.2
Axis nonperpendicularity	12.5	0.0	13.8	2.5	-1.8	5.7
Optical axis misalignment	-62.5	0.0	-63.8	2.5	-46.8	6.0
Tilt toward north	212.5	0.0	212.6	0.1	211.7	0.6
Tilt toward east	-150.0	0.0	-150.0	0.1	-150.2	0.4
Tube flexure	100.0	0.0	99.8	0.8	93.8	2.9
Azimuth bearing, NS term	12.0	0.0	12.0	0.2	11.9	0.9
Azimuth bearing, EW term	7.5	0.0	7.4	0.2	7.1	0.7
Elevation bearing, cosine term	8.0	0.0	9.2	1.7	8.1	1.8
Elevation bearing, sine term	6.0	0.0	6.1	0.9	6.0	0.9
Estimated error (σ)		0.0		1.0		4.8

Table 5.23b Bayesian parameter estimates for the simulated data (cont.)

Parameter	Set 3 $\sigma = 10$ μrad Mean (μrad)	S. E. (μrad)	Set 4 $\sigma = 20$ μrad Mean (μrad)	S. E. (μrad)	Set 5 $\sigma = 50$ μrad Mean (μrad)	S. E (μrad)
Azimuth encoder offset	-155.5	6.4	-151.3	15.3	-88.8	29.5
Elevation encoder offset	97.5	3.5	98.2	7.8	119.0	14.6
Azimuth encoder scale	-19.5	0.9	-19.4	2.1	-15.4	4.0
Elevation encoder scale	25.2	9.0	27.8	13.4	52.3	20.8
Axis nonperpendicularity	-4.1	11.0	1.0	26.2	91.6	50.4
Optical axis misalignment	-43.6	11.7	-51.0	28.0	-145.1	54.2
Tilt toward north	210.8	1.1	213.3	2.4	214.9	4.5
Tilt toward east	-149.0	0.8	-148.2	1.9	-151.9	3.6
Tube flexure	99.3	4.0	97.1	4.6	95.7	4.7
Azimuth bearing, NS term	11.5	1.6	11.6	2.4	10.8	2.7
Azimuth bearing, EW term	5.9	1.4	6.2	2.3	6.4	2.6
Elevation bearing, cosine term	8.0	1.8	8.0	1.8	8.0	1.8
Elevation bearing, sine term	6.0	0.9	6.0	0.9	6.0	0.9
Estimated error (σ)		10.0		24.9		49.3

5.7 Pointing and Position Determination Accuracy

Expressions for describing the pointing accuracy of a telescope when a particular mount model is applied were given in Chapter 4. Those expressions were used to calculate the predicted pointing accuracy for each of the models above using the reference positions displayed in Chapter 4. Two values are reported to assess the pointing accuracy of each model: the maximum predicted pointing error when pointed to each reference position in the set of reference positions and the predicted rms pointing error for the same set of positions. These values are presented in Table 5.24.

Table 5.24 Predicted pointing and position determination accuracy

	MOLS Regression		Ridge Regression		Bayesian Regression	
Telescope	Maximum Error (μrad)	rms Error (μrad)	Maximum Error (μrad)	rms Error (μrad)	Maximum Error (μrad)	rms Error (μrad)
SDSS	41.7	22.1	38.5	20.1	35.7	18.8
ARC	24.7	13.6	23.0	12.6	21.4	11.9
Keck I	36.6	24.4	34.8	22.7	32.3	21.3
Keck II	34.8	23.1	32.4	21.5	31.2	20.2
Set 0	0.0	0.0	0.0	0.0	0.0	0.0
Set 1	1.5	1.0	1.4	0.9	1.4	0.9
Set 2	7.1	4.5	6.8	4.2	6.6	3.9
Set 3	14.7	9.4	14.2	8.6	12.8	7.8
Set 4	36.3	23.2	35.0	21.2	28.3	17.4
Set 5	72.0	46.1	69.5	42.2	52.8	32.7

The values in Table 5.24 are the upper 95% confidence limits on each measure of pointing error. The estimated pointing accuracy for the bootstrapping solution was not computed because the procedure used did not estimate the entire variance-covariance matrix as required for the accuracy calculations. However, because the precision of the bootstrap estimates of the parameters were between the MOLS solution and the ridge regression solution, bootstrapping would be expected to produce pointing accuracy somewhere between those methods.

5.8 Summary of Results

The results presented in this chapter clearly demonstrate that both ridge regression and Bayesian regression are superior to modified ordinary least squares for identifying telescope physical errors using mount model data. The ridge regression and Bayesian regression solutions for the actual telescopes were similar but the parameter estimates made with Bayesian regression were slightly narrower and therefore more precise. Analysis of the simulated data sets, however, revealed that Bayesian regression was superior because the parameter estimates made with that method were both precise and accurate because they were close to the known values of the parameters. Bootstrapping produced some improvement over MOLS but was inferior to ridge regression and Bayesian regression.

The predicted pointing accuracy was also better for the Bayesian regression solution. Although the Bayesian solution estimated a higher overall error in the model, it still produced better predicted pointing. This illustrates the danger of focusing only on a single value to judge a mount model. One common way to assess pointing accuracy uses the overall estimated error either calculated from the rms pointing error in the calibration stars or estimated from regression statistics, usually *MSE*. Either of these approaches would have predicted the best performance from the MOLS solution because it had the lowest estimated error.

6 DISCUSSION

6.1 Conclusions

In this work, four methods were explored for using telescope mount modeling data to make precise estimates of the physical errors that affect telescope pointing. A modified ordinary least squares (MOLS) process was used as a baseline because it is similar to the approach currently used on many large astronomical telescopes. Bootstrapping, ridge regression, and Bayesian regression were each used as alternatives to try to improve the precision of the physical error estimates. Each of the alternative methods produced some improvement over the baseline solution but Bayesian regression was found to be most effective.

Chapter 4 described the procedure used for each method and Chapter 5 presented the results obtained. This chapter discusses some of the advantages and disadvantages of each method, outlines some applications for the results, and suggests areas where further research would be beneficial.

6.1.1 Baseline Results

Based on the estimated error in the residuals, the baseline results obtained using modified ordinary least squares (MOLS) regression were marginally better than results obtained from the widely used program TPOINT. This is believed to result from the way TPOINT incrementally adjusts the axis angles during the solution and from the fact that

TPOINT uses a completely numerical approach. Each of these add variability to the solution but may actually produce more accurate results.

The baseline MOLS solution developed here, however, suffered from the same coefficient imprecision that characterizes conventional methods. While good pointing corrections can be made to compensate for physical errors, only limited information can be extracted from the model to quantify those errors.

6.1.2 Other Techniques

6.1.2.1 Bootstrapping

Bootstrapping produced some improvement in the precision of the estimated parameters. The greatest improvements occurred in the estimates of the uncorrelated errors and were better using bootstrapping than any other technique. The precision of the estimates of the correlated errors improved somewhat using bootstrapping but other techniques produced better results.

It was found that a relatively small number of resamples was adequate for producing most of the improvement in parameter precision. The fact that using a larger number of bootstrap samples did not improve results probably relates to the fact that most of the bootstrapping samples had the same correlation problems as the full set of calibration stars. As discussed previously, since there are such a large number of possible subsets of the calibration stars and since most of those have similar correlation problems, the chance of randomly selecting a "good" set in a bootstrapping solution is very small. The bootstrapping results might improve if a large fraction of the $n!$ subsets of the n calibration stars were included in the bootstrap sample but this would be infeasible in practice.

One advantage of the bootstrapping solution was that it produced useful information about the distribution of the parameter estimates. This information might be useful in special applications employing a sophisticated mount model.

6.1.2.2 Ridge Regression

The ridge regression results were significantly more precise than the MOLS results and estimated the physical error with similar precision to that of Bayesian regression. However, because ridge regression involved introducing bias to the model, the physical error estimates were biased.

Another drawback of ridge regression is that selection of the ridge parameter requires judgment and different selections produce different results. For the data sets considered here, both the actual data and the simulated data, the same value for the biasing constant was used and produced good results. This indicates that, for similar models and for noise typical of that found in telescope pointing data, much of the judgment can be eliminated and a fixed value always used.

6.1.2.3 Bayesian Regression

The Bayesian regression solution improved the precision of all the physical error estimates for each of the actual and simulated data sets. For some errors, such as those related to mislevel, the improvement was modest and would not lead to significant improvements in telescope modeling. However, for the highly correlated errors, especially nonperpendicularity of the axes and optical axis misalignment, use of Bayesian regression allowed the correlation among the predictors to be overcome and produced substantially more precise estimates of the physical errors.

The main drawback of Bayesian regression is that it requires prior estimates of the physical errors, usually from measurements or design calculations. In many cases these measurements would be difficult to obtain. However, the prior information assumed for this work was relatively crude and could reasonably be measured on most telescopes without special equipment.

It would also be easy to "fool" a Bayesian regression procedure by assuming highly precise prior information near a desired set of parameters. The result would be (apparently) precise estimates of every parameter but a poor overall model. This suggests that it is easy to introduce subjective bias into a Bayesian model while the bias in a ridge regression model is objective in the sense that it is more difficult to drive the solution to a desired result. This could be an important consideration in some applications.

6.1.3 Pointing and Positioning

The improvements in model parameter precision also lead to better over mount models that result in better pointing. This was an unanticipated result but could have significant implications. Using the modeling techniques developed in this work will substantially improve pointing on existing telescopes, in most cases without major changes to existing equipment, software, or procedures. Similar improvements would also result in position measurements made through a telescope.

6.2 Applications

6.2.1 Telescope Operations and Maintenance

An immediate application of the results of this work would be to identify and correct some of the physical errors present in existing telescopes. Although current mount models are used to compensate for the effects of these errors, physically adjusting a telescope to remove the source of the problem would be expected to improve pointing. Eliminating or mitigating some of the errors may also improve the estimates of the remaining physical errors and further improve pointing. Ultimately, use of the techniques developed here could result in better mount models because each term in the model would more closely relate to the true physical error it compensates for. While current mount models make good corrections to telescope pointing, models that more closely predict the physical errors would be expected to do better.

The ability to precisely estimate physical errors could also be used for identifying the need for corrective maintenance. Even if the methods described here are not used for correcting observations, they could be useful in analyzing calibration data to monitor the physical state of the telescope and quantify the need for maintenance. For example, it is not unusual for a newly installed telescope to settle over time and slowly become misleveled. This is usually corrected in the mount model or through periodic realignment of the telescope when the problem becomes severe. If, however, the movement could be tracked precisely, adjustment could be carried out when necessary. Extrapolated corrections could also be made between models.

Similarly, bearings wear over time and eventually require replacement. Monitoring the mount model terms related to the bearings may provide useful information on their condition and allow the need for replacement to be predicted well in advance, before becoming critical.

Understanding the expected pointing error at different axis positions is also useful. The predicted pointing error is not the same everywhere and pointing will be better at some axis positions than it will at others. This feature could be used to schedule observing so that critical observations are made at the better telescope positions. The predicted error could also be used, to improve position determination calculations by providing some estimate of the uncertainty in the measurement. Specialized models could also be constructed as discussed below.

This work has also demonstrated how correlation among the terms in the model severely degrades modeling results unless special techniques are used. Mathematically, the correlation affects the solution through the first matrix in eqn. (4.38). The elements of this matrix are affected only by the positions of the calibration stars, not the observed pointing errors. This implies that much of the uncertainty in the model can be controlled by careful selection of calibration stars.

Current practice involves randomly selecting a large number of bright stars distributed throughout the visible region of the sky. No effort is made to choose positions that control the variance in the model. A better approach would be to identify all possible calibration stars visible when observations are to be made and then searching for a combination of stars that will produce a well-conditioned matrix. This would be a computationally intensive process due to the high number of combinations to search but computations could be carried out well in advance.

6.2.2 Telescope Design and Manufacturing

Understanding the limitations of the mount modeling process and knowing the precision with which each physical error can be estimated and compensated is also useful during the design process. In the early stages of telescope design, scientific requirements are translated into engineering specifications that define the overall performance requirements for the telescope. These requirements are then allocated to specific sources through an error budgeting process. Often, the allocation is based on subjective estimates regarding how well the mount model will correct each physical error. Better information regarding how well each physical error can be estimated and corrected could be used to allocate tolerances more appropriately and focus design efforts where they would be most effective.

The ability to precisely measure certain assembly errors may also lead to lower manufacturing costs for telescopes. Presently, telescope components must be machined to high precision and substantial effort is needed during assembly to ensure that the system is precisely aligned. Much of the need for this precision arises from the fact that conventional mount modeling cannot completely correct for the effects of these misalignments. By producing more precise estimates for these parameters, more accurate corrections would be possible and the accuracy required during assembly relaxed.

A mathematically robust analysis of the precision of each parameter estimate will also facilitate use of mount model data for telescope acceptance testing. Large telescopes are usually built and tested individually. Acceptance testing is performed prior to final delivery to verify each critical specification requirement. Often these requirements are extremely difficult to verify because there is no reliable way to measure some of the physical misalignments. For example, the error in axis nonperpendicularity is often specified to be smaller than can be measured using available instruments and must be demonstrated indirectly. A precise estimate made using the methods described in this work might be a useful improvement over current practice.

6.2.3 Observatory Systems Engineering

Mount modeling at large observatories is usually restricted to correcting pointing errors in individual telescopes. The same techniques, however, could be applied to mechanical errors throughout a large system. The methods used in this work are general and need not be restricted to the two degrees-of-freedom required for telescope pointing. A complete system model could be implemented to correct for similar geometric effects in instruments, relay optics, and so forth. Correcting errors in the delay line and beam combining mechanisms required for interferometry are one such application.

6.2.4 Robot Calibration

The robot calibration literature provided background information for this work and the results developed here may be especially applicable to that field. One question that arises in robot calibration involves how much of the calibration should be done by the user and how much by the factory. A compromise solution could involve the factory providing prior distribution information for expected errors and the user carrying out calibration measurements and applying a Bayesian regression model supplied by the manufacturer.

6.3 Recommendations for Future Research

6.3.1 Model Improvements

The methods used for this work could be improved by developing the model without linearizing the effects of each error and without making the small angle assumption. For the telescope applications studied here, these improvements would be unlikely to significantly improve results. Recent versions of the TPOINT program and similar custom pointing analysis software do not linearize the error effects and do not require the small angle assumptions but produce similar results (Wallace, 1996). For other applications, however, a more general model might be superior.

Since Bayesian regression produced much better error estimates than are currently obtained with conventional mount modeling techniques, significant improvements to telescope pointing might be possible using more sophisticated models based on Bayesian statistics. These models could incorporate prior information about the telescope physical state, previous performance, current meteorological information, and details of the planned observing run to produce a high fidelity model. As noted in Chapter 2, a similar approach is used to produce a custom model for the Air Force Maui Optical Station tracking telescope for observing a satellite during a single pass. Incorporating known prior information could similarly improve performance of many existing telescopes and Bayesian regression provides a useful framework for this.

Mount model results may also be improved by diligently collecting useful information throughout the design and manufacturing process. Information for constructing the prior distribution for the geometric errors estimates may be produced during each phase of telescope development and operation and should be recorded and maintained for use in the mount model. Results of structural analyses during the design phase, inspection measurements during assembly and installation, and ongoing metrology during operation are routinely performed but are seldom used for mount modeling.

6.3.2 Extensions

This work has focused only on estimating the physical errors which affect pointing. Some telescope physical errors, however, do not produce pointing errors but affect performance in other ways. For example, in a satellite laser ranging (SLR) telescope, if the azimuth and elevation axes do not intersect, a position-dependent path length difference will be introduced and this can degrade ranging performance. A similar effect occurs for telescopes used in interferometers. The kinematic modeling techniques used in this work to model pointing error could be used to model more complex behavior and similar approaches could be used to estimate the parameters of such a model.

A current trend in astronomy involves building arrays of telescopes located close to one another. The proximity of these telescopes can be exploited to improve the mount models for all of them. Much of the random error in a mount model comes from effects in the atmosphere. Simultaneous observations of the same object made through separate telescopes located very close together will have similar random errors. In principal, these errors can be canceled statistically during the mount modeling process. The approach would involve fitting a separate model to each telescope conditioned on the error components from the atmosphere being identical for each observation. While such a model would be complex, the atmosphere is by far the largest source of random error affecting observations through modern large telescopes and any technique that can significantly mitigate atmospheric effects is potentially very useful.

A field of stars observed through an altazimuth will appear to rotate as it is tracked across the sky. For some applications this is undesirable so a device is used to counteract this field rotation. This device is subject to errors similar to those in the telescope and the mount model sometimes includes terms to correct these errors. However, since some of the physical errors considered in the mount model also produce field rotation errors, these field rotation errors could be recorded during calibration to improve the model fidelity.

REFERENCES

Agrawal, R., Lawless, J. F., and Mackay, R. J.,1999, "Analysis of Variation Transmission in Manufacturing Processes – Part II," *Journal of Quality Technology*, Vol. 31, No. 2, pp. 143-154.

Air Force Research Lab, 1999, *AMOS User's Manual*, Author.

Armstrong, B. and Canudas de Wit, C., 1996, "Friction Modeling and Compensation," *The Control Handbook*, W. S. Levine Ed., CRC Press.

Barbe, P. and Bertail, P., 1995, *The Weighted Bootstrap*, Springer-Verlag, NY

Barnett, J. A., 1981, "Computational Methods for a Mathematical Theory of Evidence," *Seventh International Joint Conference on Artificial Intelligence*, pp. 868-875.

Beggs, J. S., 1960, "Mirror-Image Kinematics," *Journal of the Optical Society of America*, Vol. 50, No. 1, pp. 388-393.

Bggs, J. S., 1975 "Mirror-Image Kinematics," *Journal of the Optical Society of America*, Vol. 65, No. 12, pp. 1517-1518.

Boyer, H. E. and Gall, T. L. Eds., 1985, *ASM Metals Handbook Desk Edition*, American Society for Metals, Metals Park Ohio.

Box, G. E. P., and Tidwell, P. W., 1962, "Transformation of the Independent Variables," *Technometrics*, Vol. 4, No. 4, pp. 531-550.

Brost, R. C. and Christiansen, A. D., 1993, "Probabilistic Analysis of Manipulation Tasks: A Research Agenda" *Proceedings of the IEEE International Conference of Robotics and Automation Vol. 3*, pp. 549-556.

Chen, J., and Chao, L. M., 1986, "Positioning Error Analysis for Robot Manipulators with all Rotary Joints," *Proceedings of the IEEE International Conference of Robotics and Automation*, pp. 1011-1016.

Chivens, D., R., and Chivens, D., E., 1999, "Impact of Hydrostatic Bearings on the Design and Performance of Telescopes," *Proceedings of the SPIE, Vol. 3692, Acquisition, Tracking, and Pointing XIII*, pp. 123-128

Cullum, M. J., Enard, D., and Ravensbergen, M., 1994, "Control of Image Position Errors with the VLT," *Proceedings of the SPIE, Vol. 2199*, pp. 959-968.

Dahl, W., 2002, Personal communication.

Debruin J. C., 1991, "Derivation of Line-of-Sight Stabilization Equations for Gimbaled-Mirror Optical Systems," *Proceedings of the SPIE, Vol. 1543, Active and Adaptive Optical Components*, pp. 236-247.

Debruin J. C. and Johnson, D. B., 1992, "Line-of-Sight Reference Frames: a Unified Approach to Plane-Mirror Optical Kinematics," *Proceedings of the SPIE, Vol. 1697, Acquisition, Tracking, and Pointing VI*, pp. 111-129.

Debruin,, J. C. and Johnson, D. B, 1995 "Derivation of Structural Influence Coefficients for Plane-Mirror Optical Systems," *Proceedings of the SPIE, Vol. 2221*, pp. 379-401.

Denavit, J. and Hartenberg, R. S., 1955, "A Kinematic Notation for Lower-Pair Mechanisms Based on Matrices." ASME *Journal of Applied Mechanics*, 22. pp. 215-221.

Donald, B. R., 1989, *Error Detection and Recovery in Robotics*, Springer-Verlag, NY.

Donmez, M. A., Liu, C. R., and Barash, M. M., 1986, "A Generalized Mathematical Model for Machine Tool Errors" in *Modeling, Sensing, and Control of Manufacturing Processes*, Srinivasan, Hardt, and Komanduri Eds., ASME.

Efron, B., 1982, *The Jackknife, the Bootstrap, and Other Resampling Plans*, John Wiley and Sons, NY.

Efron, B., 1985, "Bootstrap Confidence Intervals for a Class of Parametric Problems," *Biometrika,* Vol. 72, No. 1, pp. 45-58.

Efron, B. and LePage, R., 1992, "Introduction to Bootstrap," *Exploring the Limits of Bootstrap*, R. LePage and L. Billard Eds., John Wiley and Sons, NY.

Everett, L. J., 1993, "Research Topics in Robot Calibration," *Robot Calibration*, R. Bernhardt and S. L. Albright Eds., Chapman and Hall, NY.

Fisk, J. W. and Rue, A. K., 1966, "Confidence Limits for the Pointing Error of Gimbaled Sensors," *IEEE Transactions on Aerospace and Electronic Systems*, Vol. AES-2, No. 6, pp.648-654.

Freid, D. L., 1966, "Optical Resolution Through a Randomly Inhomogeneous Medium for Very Long and Very Short Exposures," *Journal of the Optical Society of America*, Vol. 56., No. 10, pp. 1372-1379.

Fuller W. A., 1987, *Measurement Error Models*, John Wiley & Sons, New York, NY.

Gardiol, D., Bonoli, C., and Corcione, L., 1999, "Pointing and Tracking Improvement at TNG," Author.

Haessig D. A., and Friedland, B., 1991, "On the Modeling and Simulation of Friction," *Proceedings of the SPIE Vol. 1482, Acquisition, Tracking and Pointing V*, pp. 383-396.

Hall, R. L., 1976, "Analysis Technique for Calibrating Angular Measuring Devices," *Proceedings of the AIAA Guidance and Control Conference 16-18 August 1976, San Diego CA.*

Hermann K. G., Finley, D., and Gienger, A., 2000, "High Performance Mount for the SOAR Telescope," *Proceedings of the SPIE. Vol. 4004, Telescope Structures, Enclosures, Controls, Assembly/Integration/Validation, and Commissioning*, T. A. Sebring and T. Andersen Eds., pp. 127-134.

Hodge, L., Gottesman, J., D., and Gullapalli, S. N., 1992. "Pointing Control of a Large Ground-Based Laser Tracking Telescope," *Proceedings of the SPIE, Vol. 1697 Acquisition, Tracking, and Pointing VI*, pp. 261-273.

Hollerbach, J. M., 1989. ``A Survey of Kinematic Calibration," in *The Robotics Review 1*, O. Khatib, J.J. Craig, and T. Lozano-Perez, Eds., MIT Press, Cambridge, Mass., pp. 207-242.

Huang, E., 1993, "Line of Sight Sensitivity Equations," Gemini Project Technical Note TN-O-G0017.

Kaydon Corporation, 1991, *Large Bearing Design Manual, Catalog 390,* Author., Muskegon, Michigan.

Keitzer, S., Kimbrell, J., and Greenwald, D., 1991, "Deterministic Errors in Pointing and Tracking Systems I: Identification and Correction of Static Errors," *Proceedings of the SPIE Vol. 3692, Acquisition, Tracking, and Pointing XIII*, pp. 129-138.

Kenderdine, S. and Fairclough, J., 1988, "Pointing Tests," *MT Project Note UN005.1,* Mullard Radio Astronomy Observatory, Cavendish Laboratory, Science and Engineering Research Council.

Kimbrell, J., Greenwald, D., Smith, R., and Kidd, K., 1991, "Deterministic Errors in Pointing and Tracking Systems II: Identification and Correction of Dynamic Errors," *Proceedings of the SPIE Vol. 1482 Acquisition, Tracking, and Pointing V*, pp. 415-424.

Levi, L., 1968a, *Applied Optics*, Vol I, John Wiley and Sons, New York

Levi, L., 1968b, *Applied Optics*, Vol II, John Wiley and Sons, New York

Lewis, H., Lupton, W., Sirota, M., Mast, T., and Nelson, J., 1994, "Pointing and Tracking performance of the W. M. Keck Telescope," *Proceedings of the SPIE Vol. 2199 Acquisition, Tracking, and Pointing V*, pp. 117-125.

Lewis, H., 2000, Personal Communication.

Liu, W., 2001, *Propositional, Probabilistic, and Evidential Reasoning:Integrating Numerical and Symbolic Approaches*, Physica-Verlag, NY.

Lozano-Perez, T., Mason, M. T., and Taylor, R. H., 1984, "Automatic Synthesis of Fine-Motion Strategies for Robots" *International Journal of Robotics Research Vol. 3, No. 1.*

Lugten J. B., 1998. *Millimeter Array Memo 232: A Simple Method to Improve Pointing on the MMA Antennas*, National Radio Astronomy Observatory, Tucson, AZ.

Mancini, D., Brescia, M., Cascone, E., and Schipani, P., 1997, "A Variable Structure Control Law for Telescopes Pointing and Tracking," *Proceedings of the SPIE, Vol. 3086*, pp. 72-84.

Mancini, D., Cascone, E., and Schipani, P., 1997, "Italian National Galileo Telescope System Description and Tracking Performance in the Workshop," *Proceedings of the SPIE, Vol. 3086*, pp. 85-95.

Masten, M. K., Heaton, M., and Chen, T., 1986, "Simulation of the Effects of Structural Deflection on LOS Stabilization Systems," *Proceedings of the Seventeenth Annual Conference of the Instrument Society of America,* pp. 1989-1997.

Martin, H. M., Davison, W. B., DeRigne, S. T., Hill, J. M., Hille, B. B., Meeks, R. L., and Trebisky, T. J., 1994, "Active Supports and Force Optimization for a 3.5-m Honeycomb Sandwich Mirror," in *Proceedings of the SPIE Vol. 2199, Advanced Technology Optical Telescopes V*, L. M. Stepp Ed., pp. 251-262.

McMath, R. R. and Mohler, O. C., 1960, "Telescope Driving Mechanisms," in *Telescopes*, G. P. Kuiper and B. M. Middlehurst Eds. University of Chicago Press

Meinel, A. B., 1965, "Introduction to the Design of Astronomical Telescopes,", *Technical Report 1*, Optical Sciences, The University of Arizona, Tucson, AZ.

Meinel, A. B. and Meinel, M., 1986, "Wind Deflection Compensated, Zero-Coma Telescope Truss Geometries," *Proceedings of the SPIE 628, Advanced Technology Optical Telescopes III*, 403-411

Morgan, J.,1997, "APO 3.5-m Collimation Report", Apache Point Observatory, New Mexico State University, Sunspot, NM.

Mooring, B. W. and Pack, T. J., 1986, "Determination and Specification of Robot Repeatability," *Proceedings of the IEEE International Conference of Robotics and Automation*, pp. 1017-1023.

National Aeronautics and Space Administration (NASA), 2001, "The Star, Not the Instrument, Was on the Blink," Press release 2001-065. Jet Propulsion Laboratory, Pasadena, CA.

National Almanac Office, United States Naval Observatory, 2000, *Astronomical Almanac for the Year 2001.* U. S. Government Printing Office: Washington.

Neter, J., Kutner, M. H., Nachtsheim, C. J., and Wasserman, W., 1996, *Applied Linear Statistical Models*, 4th ed., McGraw Hill:Boston.

Noll, C., 1999, *Satellite Laser Ranging and Earth Science*, NASA Space Geodesy Program.

Ogawa, K., 1997, *Modern Control Engineering*, 3rd ed., Prentice Hall, Upper Saddle River New Jersey.

Olivier, S. S. and Gavel, D. T., 1994, "Tip-tilt Compensation for Astronomical Imaging," in *Journal of the Optical Society of America*, Vol. 11, No. 1. pp. 368-378.

Owen, R., 2001, Personal communication.

Owen, R., 2002, Personal communication.

Owen, R., Hull, C., and Siegmund, W., 1990, *Performance of the Apache Point Observatory 3.5m Telescope II: Pointing and Tracking.*

Paul, R. P., 1981, *Robot Manipulators*, The MIT Press, Cambridge Massachusetts.

Payandeh, S. and Goldenberg, A. A., 1987, "Formulation of the Kinematic Model of a General (6 DOF) Robot Manipulator Using a Screw Operator," *Journal of Robotic Systems*, Vol. 4, No. 1. pp. 771-797.

Pio, R. L. 1966, "Euler Angle Transformations," *IEEE Transactions on Automatic Control*, Vol. AC-11, pp. 707-715.

Polasek, J. C., 1967, "Matrix Analysis of Gimbaled Mirror and Prism Systems," *Journal of the Optical Society of America*, Vol. 57, No. 10. pp. 1193-1201.

Press, W. H., Flannery, B. P., Teukolsky, S. A., and Vetterling, W. T., 1989, *Numerical Recipes in Pascal*, Cambridge University Press, Cambridge.

Prestage, R., Coulson, I., and Oliveira, F., 1998, *Treatment of Pointing in the New JCMT TCS, James Clerk Maxwell Telescope TCS Design Note 5.1.*

Ravensbergen, M., 1994, "Main Axes Servo Systems of the VLT," *Proceedings of the SPIE Vol. 2199 Acquisition, Tracking, and Pointing V*, pp. 997-1005.

Racine, R., 1996, "The Telescope Point Spread Function," *Publications of the Astronomical Society of the Pacific*, Vol. 108, pp. 699-705.

Robinson, E. A., 1981, *Least Squares Regression Analysis in Terms of Linear Algebra*, International Human Resources Development Corporation, Boston.

Robinson, G. M. and Spracklin, J. C., 1966, "Angular Contact Hydrostatic Bearing for Radar Pedestals," in *Deep Space and Missile Tracking Antennas*, ASME, pp. 1-14.

Rodkevich, G. V. and Robachevskaya, V. I., 1977, "Possibilities of Reducing the Mass of Large, Precision Mirrors," *Soviet Journal of Optical Technology*, Vol. 44, No. 9, pp. 515-519.

Ross,G., J., S., 1990, *Nonlinear Estimation,* Springer-Verlag, NY.

Rotek Incorporated, 1995, *Large Diameter Precision Bearings for Critical Tolerance Applications,* Author. Aurora, Ohio.

Royalty, J., 1990, "Development of Kinematics for Gimballed Mirror Systems," *Proceedings of the SPIE Vol. 1304, Acquisition, Tracking and Pointing IV*, pp. 262-274.

Rue, A. K. and Fisk, J. W., 1964, "Resolution Accuracy Confidence Limits for Cascaded Induction Resolvers," *IEEE Transactions on Aerospace and Navigational Electronics*, Vol. AES-X, No. X. pp. 271-277.

Rue, A. K. and Fisk, J. W., 1968, "Laser Ranging Capability as Affected by System Pointing Error," *IEEE Transactions on Aerospace and Electronic Systems*, Vol. AES-4, No. 3, pp. 360-368.

Sawyer, D. G., Corson, C., and Saha, A., 2000, "Optimizing the Delivered Image Quality at the WIYN 3.5-m Telescope," *Proceedings of the SPIE Vol. 4004, Telescope Structures, Enclosures, Controls, Assembly/Integration/Validation, and Commissioning*, T. A. Sebring and T. Andersen Eds., pp. 422-430.

Schroeder, D., 1987, *Astronomical Optics*, Academic Press, San Diego

Schröer, K., 1993, "Theory of Kinematic Modelling and Numerical Procedures for Robot Calibration," *Robot Calibration*, R. Bernhardt and S. L. Albright Eds, Chapman and Hall, NY.

Sciavicco, L. and Siciliano, B., *Modeling and Control of Robot Manipulators*, McGraw-Hill, NY, 1996.

Seber, G. A. F., 1977, *Linear Regression Analysis*, John Wiley and Sons, NY.

Selig, J. M., 1996, *Geometrical Methods in Robotics*. Springer-Verlag, NY.

Serrurier, M., 1938, Structural Features of the 200-Inch Telescope for Mt. Palomar Observatory, *Civil Engineering,* Vol. 8, No. 8, pp. 524-526.

Shafer, G., 1976, *A Mathematical Theory of Evidence*. Princeton University Press, Princeton, New Jersey.

Shamma, J. S. and Whitney, D. E., 1987, "A Method for Inverse Robot Calibration," *Transactions of the ASME, Journal of Dynamic Systems, Measurement and Control*, Vol. 109, pp. 36-43.

Siegmund, W. Hull, C., King, T., and Childs, D., 1995, *2.5-m Telescope Drive Measurements IV: Acceptance Testing. Sloan Digital Sky Survey Telescope Technical Note 19950608_01.*

Siegmund, W., 1992, *Telescope Tracking Smoothness. Sloan Digital Sky Survey Telescope Technical Note 19920608-03.*

Siegmund, W., 1997, *2.5-m Telescope Pointing Error Budget, Sloan Digital Sky Survey Telescope Technical Note 19970527.*

Sirota, M. J. and Thompson, P. M., 1994, "Azimuth/Elevation Servo Performance of the W. M. Keck Telescope," *Proceedings of the SPIE Vol. 2199 Acquisition, Tracking, and Pointing V*, pp. 126-141.

Sirota, M. J. and Thompson, P. M., 1988, "Azimuth/Elevation Servo Design of the W. M. Keck Telescope," *Proceedings of the SPIE Vol. 887 Acquisition, Tracking, and Pointing II*, pp. 168-175

Sirota, M. J., 1998, Personal communication.

Smart, W. M., 1977, *Spherical Astronomy*, 6th ed. Cambridge University Press: Cambridge.

Sobek, R. D. and Kimbrell, J., E., 1999, "Influence of Base Support on Large Gimbal Performance," *Proceedings of the SPIE Vol. 3692 Acquisition, Tracking, and Pointing XIII*, pp 129-138.

Soons, J. A., 1997, "Error Analysis of a Hexapod Machine Tool," *Laser Metrology and Machine Performance III*, D. G. Ford and S. R. Postlethwaite Eds., Computational Mechanics Publications, Southampton.

Stock, J. and Keller, G., 1960, "Astronomical Seeing," *Telescopes*, G. P. Kuiper and B. M. Middlehurst Eds., University of Chicago Press.

Ulich, B. L., 1981, "Millimeter Wave Radio Telescopes: Gain and Pointing Characteristics," *International Journal of Infrared and Millimeter Waves*, Vol. 2, No. 2, pp. 293-310.

Veitschegger, W. K., and Wu, C-H, 1987, "A Method for Calibrating and Compensating Robot Kinematic Errors," *Proceedings of the IEEE International Conference of Robotics and Automation*, pp. 39-44.

Vinod, P. 1981, *Recent Advances in Regression Methods.* Marcel Dekkar: New York.

Voorbraek, F., 1991, "On the Justification of Dempster's Rule of Combination," *Artificial Intelligence* 48, pp. 171-197.

Wallace, P. T., 1993, *TPOINT Telescope Pointing Analysis System.* Starlink User Note 100.9, Rutherford Appleton Laboratory.

Wallace, P. T., 1996, *Gemini Pointing Algorithms, Gemini Project Technical Note TN_PS_G0044.*

Wallace, P. T., 2000, Personal communication.

Wang, J. and Masory, O., 1993, "On the Accuracy of a Stewart Platform – Part I: The Effect of Manufacturing Tolerances," *Proceedings of the IEEE International Conference on Robotics and Automation*, pp. 114-120.

Yoder, P. 1993, *Opto-mechanical Systems Design.* Marcel Dekkar: New York.

Young, W. C., 1989, *Roark's Formulas for Stress and Strain, 6th ed.* McGraw-Hill: New York.

Zhang, L., 1994, "Representation, Independence, and Combination of Evidence in the Dempster-Shafer Theory" in *Advances in the Dempster-Shafer Theory of Evidence,* R. R. Yager, M. Fedrizzi, and J. Kacprzyk Eds., CRC John Wiley and Sons, NY.

Zhuang, Z. and Roth, S., 1996, *Camera-aided Robot Calibration*, CRC Press, Boca Raton.

Ziegert, J. C., Olson, D. G., and Datseris, P., 1990, "A Screw Coordinate Model of Machine Tool Errors," in *Modeling of Machine Tools: Accuracy, Dynamics, and Control.* P. M. Ferreira, S. G. Kapoor, and AC-Y Wang Eds., ASME, NY.

APPENDIX A: DATA LISTINGS

The tables in this Appendix list the raw data used to fit a mount model for the respective telescope or simulated data set. Two formats were used to minimize editing and preprocessing of the raw data files. For each table except those for the Keck telescopes, the first two columns list the azimuth and elevation angles of the calibration star and the last two columns list the measured pointing errors for that star. The tables for the Keck telescopes list the azimuth and elevation angles for the each star and the actual azimuth and elevation angles that the telescope pointed to.

Table A.1 ARC telescope data

A	E	ΔA	ΔE
321.299684	52.843231	0.017083	0.065813
333.385849	24.128849	-0.008437	-0.005400
325.263981	34.902009	-0.002326	0.022541
345.264750	33.399574	-0.003185	0.016800
293.580524	24.716956	-0.008113	-0.000417
302.504900	33.041123	-0.003276	0.020285
346.031252	77.825972	0.154145	0.126211
330.816128	61.276078	0.038024	0.087076
7.002727	61.994684	0.038540	0.085631
339.708690	70.882700	0.081290	0.110128
351.901489	25.560968	-0.007709	-0.003967
349.034126	53.010328	0.019513	0.063699
336.717949	43.469371	0.007267	0.042129
25.289744	43.838796	0.003672	0.038479
1.761385	42.865873	0.006037	0.038454
10.282968	24.812353	-0.008674	-0.006873
44.069624	52.561721	0.012653	0.058285
8.105682	34.859296	-0.000601	0.018493
17.153744	52.738653	0.018133	0.060692
47.523733	25.904055	-0.010492	-0.007470
49.908184	34.543004	-0.006318	0.014409
28.738000	34.309213	-0.002660	0.015313
73.024026	52.815648	0.008874	0.057815
42.325670	61.839025	0.034601	0.081182
31.401438	71.903163	0.082620	0.106942
29.242778	25.568790	-0.008411	-0.006992

67.399724	25.390235	-0.011450	-0.009130
72.940626	43.871835	-0.000882	0.036177
82.278155	69.712001	0.053831	0.099447
48.302155	42.898874	0.002386	0.034989
70.549329	34.670059	-0.007500	0.014110
95.891706	43.575656	-0.004295	0.036128
79.091091	62.548914	0.028699	0.081917
92.135232	34.154722	-0.009770	0.013177
80.680615	80.192987	0.167250	0.126112
112.945993	34.916320	-0.010138	0.016211
86.526281	25.180109	-0.011524	-0.009433
134.931254	70.379120	0.045694	0.104334
101.066664	52.149774	0.005978	0.058684
115.425459	61.863118	0.019838	0.081782
134.851287	34.073198	-0.011291	0.015976
105.691872	25.003538	-0.012336	-0.009116
120.788831	44.270700	-0.004718	0.039314
145.288312	43.529784	-0.005047	0.039507
124.575547	24.581316	-0.012920	-0.009135
129.238603	51.513505	0.002428	0.057443
152.442653	60.645166	0.014347	0.081954
155.469220	33.127696	-0.012411	0.015533
142.624626	26.327527	-0.013462	-0.003060
186.269858	71.160823	0.048623	0.111071
169.642998	43.285583	-0.005370	0.041383
193.203225	43.296598	-0.005513	0.043668
183.607344	52.359373	0.003069	0.065434
156.576273	53.352284	0.004645	0.065546
161.297327	25.781780	-0.012580	-0.002797
198.590373	34.566133	-0.010389	0.022915
200.476898	25.003909	-0.014511	-0.001005
187.141694	61.864486	0.017354	0.088285
169.574009	79.877621	0.130477	0.131985
218.589876	25.564726	-0.013430	0.001820
217.004174	43.109075	-0.004535	0.045028
176.272099	34.702877	-0.008852	0.021279
181.322040	25.486668	-0.012303	-0.001357
219.626467	34.024215	-0.010183	0.023431
223.396618	60.986733	0.018552	0.088981
237.330022	70.380562	0.052266	0.113023
241.035698	33.552899	-0.010468	0.023437
212.028446	52.851813	0.005416	0.068389
261.680060	33.518064	-0.007815	0.024017
265.095020	43.907619	-0.000708	0.049358
257.363259	25.922505	-0.010524	0.004152
267.078752	53.201921	0.009994	0.071189
282.541993	34.080216	-0.006886	0.024579
238.355507	24.953008	-0.011107	0.001308
238.743738	52.019135	0.007690	0.067887
276.704511	25.068625	-0.010724	0.001681
241.867141	43.001636	-0.001902	0.046389
258.551003	80.787257	0.182025	0.139588
258.133974	61.540545	0.024344	0.092899
288.376939	44.011144	0.001345	0.048058
287.186299	70.268958	0.065524	0.112266
295.192695	61.429310	0.032105	0.089699

293.860950	51.926866	0.012239	0.068082

Table A.2 SDSS telescope data

A	E	ΔA	ΔE
319.430625	20.071121	-0.058195	0.004356
334.752758	63.756119	-0.025325	-0.027311
328.488574	61.105856	-0.030270	-0.023707
0.955725	22.266556	-0.051879	-0.005447
342.616905	72.698593	-0.002212	-0.035276
356.379120	43.402993	-0.042056	-0.019606
306.589190	31.242239	-0.051978	0.001876
318.713392	44.488376	-0.044809	-0.010992
295.045167	27.554166	-0.054322	0.005826
12.716470	35.021034	-0.047008	-0.019011
19.704614	52.039445	-0.037925	-0.033084
44.244050	38.072957	-0.049248	-0.029591
336.085639	30.332221	-0.048918	-0.005136
24.085316	25.082793	-0.051237	-0.015414
69.350927	52.010624	-0.052240	-0.042526
38.428730	45.603730	-0.044424	-0.033035
58.693127	24.751333	-0.054554	-0.021816
50.027654	68.359660	-0.032983	-0.051270
126.156173	58.132969	-0.076707	-0.042775
109.676271	36.200192	-0.063599	-0.030441
77.510248	53.091905	-0.054988	-0.043550
112.177164	25.137780	-0.062305	-0.022326
119.525258	68.163109	-0.083211	-0.051442
108.192091	73.722166	-0.080499	-0.055825
117.429135	42.567922	-0.067163	-0.034390
75.541719	32.638563	-0.056041	-0.029311
143.768129	34.426010	-0.068769	-0.023232
85.016410	26.673133	-0.057831	-0.025650
146.152814	24.469374	-0.065450	-0.016128
173.834199	54.737102	-0.083026	-0.028536
154.768228	45.699762	-0.074116	-0.028022
193.178707	62.948694	-0.090637	-0.027819
193.817933	43.084432	-0.073269	-0.014247
210.602752	34.918686	-0.067170	-0.004285
235.100612	74.246453	-0.090416	-0.025571
244.516894	29.280803	-0.060660	0.007419
175.820826	27.014099	-0.065948	-0.008604
175.738430	35.463455	-0.069731	-0.014976
226.445504	60.141277	-0.077010	-0.017079
203.544981	25.079299	-0.064028	0.002166
276.499726	44.104715	-0.054839	-0.002697
230.671242	22.329414	-0.061412	0.009583
263.875074	23.488659	-0.057887	0.011945
238.783979	40.465142	-0.063882	-0.001844
246.416369	63.537592	-0.069126	-0.016820
274.487590	33.774506	-0.055261	0.005271
265.947663	52.059479	-0.057119	-0.007448

Table A.3 Keck I telescope data

Star *A*	Star *E*	Telescope *A*	Telescope *E*
-37.806432	85.083602	-37.759280	85.113041
-28.278082	71.671426	-28.266457	71.700228
-23.635685	58.666228	-23.628838	58.693338
-21.563904	46.137782	-21.555060	46.164195
-18.264028	33.123687	-18.252529	33.149169
-14.893216	20.018978	-14.884778	20.043935
-12.224457	32.897571	-12.217728	32.926253
-9.654940	46.176532	-9.647351	46.205543
-5.920502	59.430712	-5.907138	59.460657
-3.654429	72.401614	-3.632392	72.433254
-7.296265	85.141015	-7.228957	85.173196
1.408234	72.333665	1.430280	72.365001
5.260684	59.265986	5.278719	59.294377
9.430027	46.271691	9.438525	46.298963
12.204735	36.453912	12.214271	36.479134
15.408824	36.333743	15.419842	36.358742
18.408970	35.891319	18.421584	35.916270
20.242916	45.864987	20.256713	45.892895
23.916238	59.308330	23.933870	59.337406
24.490653	72.013338	24.523310	72.044663
20.927193	85.380087	21.040503	85.411832
33.609177	72.397241	33.644877	72.427285
35.091010	59.022272	35.114696	59.049809
39.028550	46.517754	39.044776	46.543817
41.616706	35.919654	41.629097	35.944574
44.831173	36.196743	44.848273	36.221408
48.144825	36.255304	48.162951	36.279779
50.532797	46.275948	50.550946	46.303057
53.688926	59.674389	53.724291	59.702650
56.208253	72.063147	56.253770	72.092595
58.437687	84.861910	58.592983	84.892361
62.348493	72.285878	62.396362	72.314645
65.020911	59.066139	65.047758	59.092814
72.460558	36.543922	72.478522	36.566879
75.223684	36.318239	75.244342	36.341486
77.855223	36.620221	77.880404	36.644005
80.600583	46.310672	80.622789	46.335578
84.697065	59.529424	84.726973	59.555029
86.769696	72.754407	86.824742	72.781719
87.359336	86.009967	87.595642	86.038431
94.507559	72.114001	94.560258	72.140724
99.206337	46.717021	99.227983	46.740085
101.772892	36.033321	101.796397	36.054947
105.393124	35.947986	105.409866	35.969163
108.214991	36.296530	108.232061	36.317764
111.881461	46.294901	111.901893	46.318439
113.947796	59.099508	113.977598	59.123606
118.338969	72.565669	118.392955	72.591092
126.227030	85.719282	126.449193	85.745331
126.638578	59.270293	126.667117	59.292572
128.738669	45.741272	128.757008	45.762110
131.883512	36.418267	131.898596	36.437088

135.480440	36.226939	135.495445	36.245148
141.856474	45.872923	141.880621	45.893577
144.215608	59.075562	144.244534	59.096975
147.408104	71.690487	147.457258	71.713959
153.222970	85.140522	153.413387	85.163941
154.460911	71.813643	154.507293	71.835633
155.774960	59.320126	155.801778	59.339817
159.038790	46.165647	159.055411	46.183788
162.379632	32.863394	162.393097	32.878971
165.231109	20.412647	165.242952	20.427222
167.733495	33.209403	167.745961	33.227002
171.145557	46.482249	171.163112	46.499301
174.523627	58.803425	174.548118	58.821253
178.058043	72.162304	178.101085	72.182104
-178.204634	84.841215	181.948095	84.862236
-175.333450	72.109595	184.706373	72.129309
-170.871939	45.679221	189.144421	45.695780
-168.166653	32.666353	191.847115	32.680380
-164.697352	19.694794	195.316610	19.707441
-161.873448	32.970817	198.146124	32.986478
-158.496382	45.820370	201.518005	45.835583
-155.100676	58.909440	204.922677	58.925298
-153.317082	71.824000	206.717699	71.841595
-145.812751	84.752813	214.301755	84.771702
-147.161179	71.660702	212.872953	71.678080
-144.396104	59.097964	215.624209	59.113508
-140.233705	46.225197	219.780377	46.238746
-137.458054	33.008421	222.555306	33.019513
-134.754885	19.847608	225.258466	19.857947
-131.968923	32.932939	228.044404	32.947421
-128.387205	45.788631	231.627631	45.803094
-126.026163	58.531765	233.991085	58.546636
-121.296073	71.966686	238.732165	71.982059
-119.530770	85.094051	240.560615	85.111698
-116.386436	71.431832	243.637118	71.449343
-114.603903	58.626928	245.419352	58.642271
-107.889207	32.382789	252.121704	32.395810
-104.587057	19.616102	255.426102	19.629131
-101.426706	32.691425	258.582447	32.708318
-98.166068	45.662858	261.851938	45.679897
-96.542025	58.479112	263.471622	58.497027
-94.050480	71.498483	265.968516	71.518142
-93.583497	84.792729	266.472318	84.814518
-84.091611	58.795740	-84.079531	58.813427
-75.137314	19.340239	-75.126823	19.357043
-72.238750	32.523671	-72.231208	32.543385
-68.747914	46.202151	-68.739458	46.222921
-66.328931	59.059273	-66.313449	59.081322
-63.090972	72.270593	-63.077311	72.294893
-62.030910	84.663454	-61.989548	84.689593
-55.965643	71.716601	-55.953219	71.741901
-53.584242	58.467636	-53.575906	58.490927
-50.907154	45.544006	-50.894425	45.566135
-47.728935	32.495499	-47.723203	32.516430
-45.157052	19.422921	-45.149844	19.444765
-42.374983	33.148671	-42.363628	33.174539

-39.649351	45.833624	-39.644261	45.859542
-37.001902	58.509738	-36.995555	58.536503
-35.464513	70.999552	-35.450227	71.030580

Table A.4 Keck II telescope data

Star A	Star E	Telescope A	Telescope E
-0.914984	50.368671	-0.662157	50.408309
-29.763708	85.004372	-29.666209	85.041053
-27.492369	72.376549	-27.273066	72.415585
-24.671593	58.638209	-24.426510	58.677728
-21.505151	45.635356	-21.254444	45.673903
-18.557458	32.723082	-18.303700	32.758309
-15.290744	20.104821	-15.029854	20.130551
-11.696896	33.367623	-11.442162	33.402474
-9.585847	46.292785	-9.336302	46.330236
-7.205312	58.926888	-6.958058	58.965336
-2.886122	72.319937	-2.650757	72.359321
1.775482	85.071117	1.906047	85.110484
2.704877	72.333791	2.935963	72.375250
5.459269	59.003875	5.705172	59.044920
8.108355	46.156724	8.365299	46.196829
11.359360	33.113956	11.615347	33.150285
15.257823	20.473399	15.516990	20.499779
17.840593	32.933482	18.099091	32.968376
20.833606	46.093810	21.095556	46.132461
23.198899	58.912552	23.453594	58.952141
25.664649	72.467774	25.909356	72.506937
27.642273	85.295134	27.830427	85.333573
31.795318	71.764328	32.048219	71.804365
34.893155	59.351046	35.149075	59.391526
39.122065	46.588534	39.384671	46.627254
41.381888	33.135322	41.641289	33.170095
45.442628	20.325181	45.708951	20.350173
50.938822	46.587811	51.200218	46.624982
54.075565	58.990551	54.337146	59.028742
55.643036	72.409487	55.902518	72.447777
59.691619	85.623830	59.933964	85.661258
61.263429	72.056879	61.526339	72.095553
66.103877	59.601987	66.370948	59.640504
68.830027	46.383696	69.094680	46.420020
72.505038	33.116169	72.769924	33.148486
75.580834	20.213892	75.843247	20.235289
78.456164	33.232237	78.718356	33.263908
81.394029	45.881090	81.657742	45.916522
83.877134	59.454019	84.142767	59.489688
86.963155	72.694204	87.235225	72.729340
93.262364	71.964626	93.536042	72.000197
95.575501	59.632580	95.847280	59.667859
99.412253	46.574194	99.677243	46.607683
101.874255	33.250099	102.137316	33.279362
104.769436	20.064084	105.034912	20.082887
107.779347	33.583080	108.041950	33.611350
110.788704	46.308432	111.052057	46.338829

114.141714	59.514309	114.411060	59.545438
118.074594	72.457557	118.340701	72.488363
122.558275	84.982770	122.836980	85.012105
123.300389	71.847365	123.563602	71.878027
126.207741	59.587380	126.469722	59.618171
129.468221	45.801062	129.732140	45.829661
137.833940	33.016094	138.097052	33.039088
141.477068	46.507887	141.743539	46.533768
144.996832	59.542459	145.263226	59.568654
149.154784	72.041134	149.421909	72.066827
156.827705	85.120215	157.084524	85.144363
154.581208	72.475614	154.843336	72.501604
156.250162	59.409130	156.514552	59.434821
159.694584	46.059524	159.956076	46.083245
161.792335	33.164017	162.054672	33.184733
165.319862	20.312721	165.583429	20.323037
167.809873	33.218246	168.072461	33.238067
171.900965	45.968328	172.163145	45.990044
174.543386	59.209931	174.803304	59.232921
176.261330	72.011819	176.517081	72.034738
-173.186816	84.815980	187.032947	84.837638
-176.101357	72.465218	184.146939	72.489156
-173.285933	58.735277	186.969688	58.758572
-170.466827	45.971652	189.792823	45.993444
-168.231473	42.006419	192.027839	42.027726
-164.245675	42.208362	196.013502	42.229060
-161.881271	41.636018	198.377670	41.656174
-158.327513	46.049499	201.930754	46.069639
-156.049646	59.128381	204.201811	59.149988
-151.684038	71.678231	208.561567	71.699755
-145.985045	71.875218	214.258252	71.899155
-143.149833	59.289950	217.103768	59.313701
-140.733740	45.643439	219.519891	45.665197
-138.179218	41.659507	222.074215	41.681120
-134.868438	42.315213	225.384190	42.336954
-131.188664	42.127485	229.064552	42.149275
-128.905571	45.747467	231.350811	45.769077
-126.196185	58.550679	234.047668	58.573919
-122.873197	71.504627	237.359286	71.527992
-120.903520	85.226518	239.207248	85.248729
-117.204457	71.595919	243.019876	71.620079
-113.945545	58.883138	246.297078	58.907844
-111.383381	45.506042	248.871381	45.529548
-107.447176	41.658584	252.803967	41.682143
-104.522059	42.311730	255.730889	42.335764
-101.648580	42.204189	258.599658	42.229220
-98.206514	45.647843	262.041672	45.672953
-94.992878	58.847634	265.244452	58.874376
-93.745717	71.357417	266.473307	71.384192
-90.415819	84.926318	269.676405	84.952194
-86.279233	72.196995	-86.062077	72.225342
-84.755734	58.539202	275.484455	58.568076
-80.597084	45.318065	-80.348881	45.346307
-77.830104	41.321765	-77.580958	41.350079
-74.790317	41.465562	-74.540946	41.494204
-72.011545	41.395695	-71.761625	41.424864

-68.446965	45.419076	-68.202795	45.448735
-66.642101	58.523750	-66.403874	58.555468
-62.547338	71.934925	-62.327743	71.967107
-62.621886	71.871799	-62.402135	71.903969
-61.956283	84.361318	-61.859466	84.392966
-58.683747	71.877974	-58.468480	71.911726
-54.443404	58.461209	-54.202096	58.495752
-51.161732	45.808308	-50.912704	45.841852
-47.725290	42.286318	-47.472088	42.319899
-45.452790	41.931104	-45.201781	41.965014
-42.154950	41.445534	-41.909279	41.479453
-38.978877	45.819680	-38.729458	45.853957
-36.742292	58.832652	-36.506473	58.869425
-36.635812	71.049967	-36.413523	71.088000

Table A.5 Simulated data set 0

A	E	ΔA	ΔE
129.982289	59.211591	0.013396	0.000650
9.767648	24.856123	-0.014174	0.005460
52.417964	51.044398	-0.005741	0.014213
95.106649	86.407758	0.152374	0.012782
356.559892	83.148061	-0.099376	0.017184
296.699630	29.190244	-0.014134	-0.008247
49.322593	59.037084	-0.005920	0.015897
161.760716	72.782870	0.024548	-0.004688
283.146722	40.280460	-0.018261	-0.007992
113.688821	46.247784	0.004875	0.002179
24.378027	20.978362	-0.011955	0.003762
200.659854	27.428240	-0.005422	-0.021152
164.963136	40.939333	0.001295	-0.011127
321.621573	56.465399	-0.028701	0.005767
79.822709	49.913516	0.001442	0.010262
132.330124	68.881079	0.024359	0.001563
222.887639	74.490944	-0.019595	-0.010941
338.031639	46.885059	-0.018982	0.007888
139.924645	40.512690	0.002920	-0.005630
107.173953	76.075913	0.038525	0.008689
62.930671	54.846056	-0.001630	0.013802
277.040065	26.729673	-0.012793	-0.014521
248.670054	32.296670	-0.011843	-0.017555
3.601264	80.370603	-0.068564	0.017818
91.501578	38.291098	-0.000416	0.005205
70.926794	69.340236	0.008811	0.014991
151.238624	37.014554	0.001186	-0.009288
153.627943	56.538993	0.009548	-0.005429
328.547470	70.821198	-0.049714	0.009755
288.234673	37.570380	-0.017313	-0.007449
57.902995	24.625028	-0.007655	0.005019
102.333794	66.357004	0.017738	0.008428
109.206875	23.142766	-0.003391	-0.005363
38.878843	23.458315	-0.010181	0.005609
57.175530	66.285259	-0.000539	0.016330
4.794369	81.194432	-0.072451	0.018076

300.916148	40.250701	-0.018831	-0.003278
212.798627	76.498082	-0.011064	-0.010651
286.505052	60.913009	-0.034068	-0.002939
339.175026	32.501886	-0.012811	0.004080
294.323697	30.365974	-0.014552	-0.008377
8.600653	27.987034	-0.014802	0.007020
335.774077	56.098352	-0.025640	0.009171
326.023721	48.318372	-0.021765	0.005343
5.828858	33.302104	-0.016199	0.008929
27.622836	78.180849	-0.028123	0.019312
196.772877	58.174183	-0.001224	-0.012407
81.045255	64.842711	0.009641	0.012619
290.860502	73.110456	-0.060407	0.000018
227.747513	62.852593	-0.015235	-0.012474

Table A.6 Simulated data set 1

A	E	ΔA	ΔE
129.982289	59.211591	0.013458	0.000679
9.767648	24.856123	-0.014176	0.005453
52.417964	51.044398	-0.005733	0.014243
95.106649	86.407758	0.152445	0.012776
356.559892	83.148061	-0.099422	0.017116
296.699630	29.190244	-0.014083	-0.008187
49.322593	59.037084	-0.005902	0.015854
161.760716	72.782870	0.024578	-0.004655
283.146722	40.280460	-0.018182	-0.008019
113.688821	46.247784	0.004894	0.002224
24.378027	20.978362	-0.011954	0.003814
200.659854	27.428240	-0.005505	-0.021027
164.963136	40.939333	0.001228	-0.011062
321.621573	56.465399	-0.028766	0.005808
79.822709	49.913516	0.001562	0.010277
132.330124	68.881079	0.024330	0.001755
222.887639	74.490944	-0.019638	-0.010882
338.031639	46.885059	-0.019001	0.007872
139.924645	40.512690	0.002933	-0.005694
107.173953	76.075913	0.038469	0.008673
62.930671	54.846056	-0.001620	0.013709
277.040065	26.729673	-0.012785	-0.014575
248.670054	32.296670	-0.011802	-0.017593
3.601264	80.370603	-0.068547	0.017846
91.501578	38.291098	-0.000463	0.005160
70.926794	69.340236	0.008830	0.015050
151.238624	37.014554	0.001234	-0.009325
153.627943	56.538993	0.009525	-0.005438
328.547470	70.821198	-0.049812	0.009779
288.234673	37.570380	-0.017338	-0.007433
57.902995	24.625028	-0.007696	0.004932
102.333794	66.357004	0.017687	0.008492
109.206875	23.142766	-0.003412	-0.005401
38.878843	23.458315	-0.010348	0.005684
57.175530	66.285259	-0.000546	0.016398
4.794369	81.194432	-0.072541	0.017996

300.916148	40.250701	-0.018821	-0.003314
212.798627	76.498082	-0.011144	-0.010680
286.505052	60.913009	-0.034139	-0.002909
339.175026	32.501886	-0.012765	0.003980
294.323697	30.365974	-0.014557	-0.008335
8.600653	27.987034	-0.014886	0.006977
335.774077	56.098352	-0.025626	0.009104
326.023721	48.318372	-0.021812	0.005382
5.828858	33.302104	-0.016102	0.008973
27.622836	78.180849	-0.028105	0.019260
196.772877	58.174183	-0.001253	-0.012452
81.045255	64.842711	0.009669	0.012546
290.860502	73.110456	-0.060411	0.000040
227.747513	62.852593	-0.015295	-0.012432

Table A.7 Simulated data set 2

A	E	ΔA	ΔE
129.982289	59.211591	0.013250	0.000552
9.767648	24.856123	-0.013838	0.005537
52.417964	51.044398	-0.005886	0.014157
95.106649	86.407758	0.152694	0.012390
356.559892	83.148061	-0.099679	0.017403
296.699630	29.190244	-0.013745	-0.008272
49.322593	59.037084	-0.005781	0.015884
161.760716	72.782870	0.024051	-0.004703
283.146722	40.280460	-0.018344	-0.007660
113.688821	46.247784	0.004726	0.002407
24.378027	20.978362	-0.011643	0.003836
200.659854	27.428240	-0.005156	-0.021030
164.963136	40.939333	0.001206	-0.011253
321.621573	56.465399	-0.028467	0.005560
79.822709	49.913516	0.000844	0.009253
132.330124	68.881079	0.024494	0.001666
222.887639	74.490944	-0.019465	-0.010714
338.031639	46.885059	-0.018471	0.007722
139.924645	40.512690	0.003208	-0.005825
107.173953	76.075913	0.038066	0.008527
62.930671	54.846056	-0.001421	0.014288
277.040065	26.729673	-0.012852	-0.014618
248.670054	32.296670	-0.012065	-0.017541
3.601264	80.370603	-0.068181	0.018157
91.501578	38.291098	-0.000429	0.005476
70.926794	69.340236	0.007970	0.014938
151.238624	37.014554	0.001023	-0.009295
153.627943	56.538993	0.009695	-0.005781
328.547470	70.821198	-0.049485	0.009798
288.234673	37.570380	-0.017396	-0.007491
57.902995	24.625028	-0.007367	0.005428
102.333794	66.357004	0.017813	0.008105
109.206875	23.142766	-0.003460	-0.004919
38.878843	23.458315	-0.009956	0.005862
57.175530	66.285259	-0.001059	0.016405
4.794369	81.194432	-0.072604	0.017867
300.916148	40.250701	-0.018828	-0.003258

212.798627	76.498082	-0.011051	-0.010460
286.505052	60.913009	-0.034219	-0.003069
339.175026	32.501886	-0.013022	0.004058
294.323697	30.365974	-0.014374	-0.008511
8.600653	27.987034	-0.014670	0.006987
335.774077	56.098352	-0.026062	0.009436
326.023721	48.318372	-0.021895	0.004997
5.828858	33.302104	-0.016190	0.008292
27.622836	78.180849	-0.028238	0.019443
196.772877	58.174183	-0.000929	-0.012475
81.045255	64.842711	0.009629	0.012630
290.860502	73.110456	-0.060536	-0.000565
227.747513	62.852593	-0.015150	-0.012372

Table A.8 Simulated data set 3

A	E	ΔA	ΔE
129.982289	59.211591	0.011549	0.000412
9.767648	24.856123	-0.013363	0.005344
52.417964	51.044398	-0.005597	0.013926
95.106649	86.407758	0.152731	0.013124
356.559892	83.148061	-0.099619	0.016923
296.699630	29.190244	-0.013894	-0.008457
49.322593	59.037084	-0.005653	0.016007
161.760716	72.782870	0.024328	-0.004839
283.146722	40.280460	-0.017607	-0.007555
113.688821	46.247784	0.005274	0.001637
24.378027	20.978362	-0.011654	0.003677
200.659854	27.428240	-0.005226	-0.020242
164.963136	40.939333	0.000951	-0.011638
321.621573	56.465399	-0.028583	0.005491
79.822709	49.913516	0.001882	0.009912
132.330124	68.881079	0.025002	0.002347
222.887639	74.490944	-0.020177	-0.011762
338.031639	46.885059	-0.018036	0.008837
139.924645	40.512690	0.002762	-0.004609
107.173953	76.075913	0.038503	0.008624
62.930671	54.846056	-0.001652	0.013781
277.040065	26.729673	-0.012409	-0.013766
248.670054	32.296670	-0.011576	-0.017087
3.601264	80.370603	-0.067285	0.018134
91.501578	38.291098	0.000384	0.005087
70.926794	69.340236	0.009398	0.014897
151.238624	37.014554	0.000609	-0.008382
153.627943	56.538993	0.008097	-0.005753
328.547470	70.821198	-0.049539	0.009332
288.234673	37.570380	-0.017070	-0.006898
57.902995	24.625028	-0.007014	0.005218
102.333794	66.357004	0.016906	0.009331
109.206875	23.142766	-0.003254	-0.006117
38.878843	23.458315	-0.010221	0.005092
57.175530	66.285259	-0.001233	0.016189
4.794369	81.194432	-0.072250	0.017703
300.916148	40.250701	-0.018557	-0.003186
212.798627	76.498082	-0.010651	-0.011246

286.505052	60.913009	-0.033383	-0.002682
339.175026	32.501886	-0.012415	0.004440
294.323697	30.365974	-0.014592	-0.007233
8.600653	27.987034	-0.014454	0.007150
335.774077	56.098352	-0.026041	0.009394
326.023721	48.318372	-0.021260	0.006321
5.828858	33.302104	-0.015434	0.008184
27.622836	78.180849	-0.028973	0.019410
196.772877	58.174183	-0.000885	-0.012605
81.045255	64.842711	0.010205	0.012570
290.860502	73.110456	-0.059528	-0.000721
227.747513	62.852593	-0.014617	-0.013124

Table A.9 Simulated data set 4

A	E	ΔA	ΔE
129.982289	59.211591	0.013769	0.001225
9.767648	24.856123	-0.012824	0.006501
52.417964	51.044398	-0.006874	0.013967
95.106649	86.407758	0.153134	0.013431
356.559892	83.148061	-0.100520	0.016827
296.699630	29.190244	-0.013527	-0.006861
49.322593	59.037084	-0.009979	0.016976
161.760716	72.782870	0.025000	-0.003931
283.146722	40.280460	-0.017601	-0.006936
113.688821	46.247784	0.005582	-0.000616
24.378027	20.978362	-0.012145	0.003272
200.659854	27.428240	-0.005364	-0.019056
164.963136	40.939333	0.000456	-0.010038
321.621573	56.465399	-0.027549	0.007554
79.822709	49.913516	0.002514	0.011114
132.330124	68.881079	0.023877	0.000431
222.887639	74.490944	-0.020757	-0.009452
338.031639	46.885059	-0.020517	0.005807
139.924645	40.512690	0.001120	-0.008705
107.173953	76.075913	0.039143	0.009679
62.930671	54.846056	-0.001931	0.015555
277.040065	26.729673	-0.013325	-0.014212
248.670054	32.296670	-0.008982	-0.017640
3.601264	80.370603	-0.068297	0.016243
91.501578	38.291098	0.001219	0.002854
70.926794	69.340236	0.010347	0.014261
151.238624	37.014554	0.002192	-0.008610
153.627943	56.538993	0.010305	-0.003426
328.547470	70.821198	-0.050711	0.009947
288.234673	37.570380	-0.016762	-0.008424
57.902995	24.625028	-0.007096	0.004815
102.333794	66.357004	0.016017	0.009907
109.206875	23.142766	-0.005684	-0.006254
38.878843	23.458315	-0.010278	0.004601
57.175530	66.285259	0.000633	0.014841
4.794369	81.194432	-0.072007	0.016045
300.916148	40.250701	-0.018825	-0.000379
212.798627	76.498082	-0.012954	-0.011984
286.505052	60.913009	-0.033334	-0.001675

339.175026	32.501886	-0.011541	0.007091
294.323697	30.365974	-0.014192	-0.006985
8.600653	27.987034	-0.014475	0.006219
335.774077	56.098352	-0.027378	0.011246
326.023721	48.318372	-0.022604	0.005212
5.828858	33.302104	-0.015823	0.008203
27.622836	78.180849	-0.027108	0.017747
196.772877	58.174183	0.000834	-0.011970
81.045255	64.842711	0.010503	0.012206
290.860502	73.110456	-0.060142	-0.001288
227.747513	62.852593	-0.015480	-0.010588

Table A.10 Simulated data set 5

A	E	ΔA	ΔE
129.982289	59.211591	0.016271	0.000332
9.767648	24.856123	-0.010565	0.012248
52.417964	51.044398	-0.000742	0.014774
95.106649	86.407758	0.155219	0.010320
356.559892	83.148061	-0.102511	0.017196
296.699630	29.190244	-0.015180	-0.011640
49.322593	59.037084	-0.000577	0.013908
161.760716	72.782870	0.024534	-0.006105
283.146722	40.280460	-0.017205	-0.006274
113.688821	46.247784	0.003037	0.001809
24.378027	20.978362	-0.011167	0.000988
200.659854	27.428240	-0.007650	-0.020812
164.963136	40.939333	0.001576	-0.010967
321.621573	56.465399	-0.029787	0.010536
79.822709	49.913516	0.001622	0.007092
132.330124	68.881079	0.026543	0.002207
222.887639	74.490944	-0.018273	-0.010937
338.031639	46.885059	-0.022770	0.010013
139.924645	40.512690	0.005251	-0.003384
107.173953	76.075913	0.042293	0.011418
62.930671	54.846056	-0.002026	0.012556
277.040065	26.729673	-0.015521	-0.010986
248.670054	32.296670	-0.011272	-0.021402
3.601264	80.370603	-0.068833	0.021036
91.501578	38.291098	0.000906	0.007622
70.926794	69.340236	0.009697	0.017693
151.238624	37.014554	0.001934	-0.008648
153.627943	56.538993	0.009747	-0.006752
328.547470	70.821198	-0.045088	0.010823
288.234673	37.570380	-0.020066	-0.002959
57.902995	24.625028	-0.011912	0.005591
102.333794	66.357004	0.022053	0.008660
109.206875	23.142766	-0.006523	-0.005765
38.878843	23.458315	-0.007254	0.009268
57.175530	66.285259	-0.001845	0.017619
4.794369	81.194432	-0.068873	0.017154
300.916148	40.250701	-0.022077	-0.003638
212.798627	76.498082	-0.009533	-0.009684
286.505052	60.913009	-0.030082	-0.004074
339.175026	32.501886	-0.005940	-0.002513

294.323697	30.365974	-0.018728	-0.012133
8.600653	27.987034	-0.011593	0.004643
335.774077	56.098352	-0.026599	0.008326
326.023721	48.318372	-0.019515	0.003173
5.828858	33.302104	-0.017881	0.009192
27.622836	78.180849	-0.032598	0.023040
196.772877	58.174183	-0.000449	-0.011244
81.045255	64.842711	0.013477	0.014891
290.860502	73.110456	-0.059725	0.006102
227.747513	62.852593	-0.018167	-0.008236

APPENDIX B: DERIVATIONS OF ERROR EFFECT TERMS

B.1 Introduction

In this Appendix, the terms used to model the effect of each physical error on each component of telescope pointing are derived. The terms used in this work are similar to those used by the commercial software package TPOINT except that a different coordinate system is used. In addition, while the terms used in TPOINT are widely accepted and used in many applications, no original source for their derivation was identified while researching this work. The derivations in this Appendix are presented both to verify the terms used for each error and to provide a reference for their derivation.

The coordinate system used for this work was described in Chapter 4. The pointing direction of the telescope is represented by a pointing vector with three components along three orthogonal axes of a right-handed coordinate system. The positive x-axis points toward east; the positive y-axis points toward north; and the positive z-axis points toward the zenith. The undisturbed azimuth axis is aligned with the z-axis and the initial elevation axis is parallel to the y-axis. When the azimuth and elevation rotation angles of the telescope are both set to zero the telescope points toward the northern horizon. A positive azimuth rotation of the telescope moves the telescope pointing direction from north toward east while a positive elevation motion moves the telescope pointing direction toward the zenith. This coordinate system differs from that commonly used for astronomical telescopes in that the sense of azimuth rotation is reversed.

The initial pointing direction of the telescope, pointing to the northern horizon, is represented by the initial pointing vector $\mathbf{P}_0 = [0 \quad 1 \quad 0]^{\mathrm{T}}$. Setting the azimuth and elevation axes changes this vector. Setting the azimuth angle involves a negative (y-axis toward x-axis) rotation about the z-axis. This is accomplished by premultiplying the initial pointing vector by the matrix

$$\mathbf{R}_{\mathrm{A}} = \begin{bmatrix} \cos(-A) & -\sin(-A) & 0 \\ \sin(-A) & \cos(-A) & 0 \\ 0 & 0 & 1 \end{bmatrix} = \begin{bmatrix} \cos A & \sin A & 0 \\ -\sin A & \cos A & 0 \\ 0 & 0 & 1 \end{bmatrix} \tag{B.1}$$

Similarly, elevation rotation is produced by premultiplying a pointing vector by

$$\mathbf{R}_{\mathrm{E}} = \begin{bmatrix} 1 & 0 & 0 \\ 0 & \cos E & -\sin E \\ 0 & \sin E & \cos E \end{bmatrix} \tag{B.2}$$

Because rotating the telescope about the azimuth axis changes the orientation of the elevation axis, elevation rotation must be performed first. The total rotation matrix for setting the telescope axes is given by

$$\mathbf{R}_{\mathrm{S}} = \mathbf{R}_{\mathrm{A}} \mathbf{R}_{\mathrm{E}} \tag{B.3}$$

$$\mathbf{R}_{\mathrm{S}} = \begin{bmatrix} \cos A & \sin A & 0 \\ -\sin A & \cos A & 0 \\ 0 & 0 & 1 \end{bmatrix} \begin{bmatrix} 1 & 0 & 0 \\ 0 & \cos E & -\sin E \\ 0 & \sin E & \cos E \end{bmatrix} \tag{B.4}$$

$$\mathbf{R}_S = \begin{bmatrix} \cos A & \sin A\cos E & -\sin A\sin E \\ -\sin A & \cos A\cos E & -\cos A\sin E \\ 0 & \sin E & \cos E \end{bmatrix} \tag{B.5}$$

Premultiplying the initial pointing vector by this matrix yields the pointing vector for the telescope when the azimuth and elevation axes have been set to A and E respectively.

$$\mathbf{P}_S = \begin{bmatrix} \cos A & \sin A\cos E & -\sin A\sin E \\ -\sin A & \cos A\cos E & -\cos A\sin E \\ 0 & \sin E & \cos E \end{bmatrix}\begin{bmatrix} 0 \\ 1 \\ 0 \end{bmatrix} \tag{B.6}$$

$$\mathbf{P}_S = \begin{bmatrix} \sin A\cos E \\ \cos A\cos E \\ \sin E \end{bmatrix} \tag{B.7}$$

Substituting the components of this vector into eqn. (4.12a) and (4.12b) confirms that the azimuth and elevation axes have been rotated by A and E respectively.

The effect of each physical error is found in a similar fashion except that three rotation matrices are used, the same azimuth and elevation matrices as above and an additional matrix to model the effect of the particular error. The azimuth matrix always precedes the elevation rotation in the matrix multiplication but the order of multiplication for the physical error effect differs among the effects with the order following that of eqn. (4.16).

The physical errors considered in this work were listed in Chapter 2 and are listed in Table 4.1. Because the mechanical errors are assumed to be small, their effects can be determined separately and added to find the combined effect. This involves applying a small angle approximation in the derivation of each term and neglecting products of small terms when deriving the effect of multiple simultaneous errors. The derivation of each term is shown below. The encoder offset and scale terms are not derived because they are trivial. Each encoder offset directly adds or subtracts from the angle of the respective axis and each scale factor multiplies the axis angle. Because the angles are assumed to be small, trigonometric functions of the adjusted angles are approximately equal to those of the unadjusted angles.

B.2 Optical Axis Misalignment

Misalignment of the optical axis occurs when the optical axis of the telescope does not point toward the zenith when the telescope axes are set to point to the zenith. One component of this error has the same effect as an elevation encoder offset and is indistinguishable from that term. The other component appears as a rotation of the line-of-sight about the initial azimuth axis. This *z*-axis rotation by the angle γ is produced by the matrix:

$$\mathbf{R}_\mathbf{M} = \begin{bmatrix} \cos\gamma & -\sin\gamma & 0 \\ \sin\gamma & \cos\gamma & 0 \\ 0 & 0 & 1 \end{bmatrix} \approx \begin{bmatrix} 1 & -\gamma & 0 \\ \gamma & 1 & 0 \\ 0 & 0 & 1 \end{bmatrix} \tag{B.8}$$

Since this error does not reorient either motion axis, its effect can be introduced before the azimuth or elevation rotations. The total effect when the telescope is pointed to a particular position is given by:

$$\mathbf{R}_\mathbf{T} = \mathbf{R}_\mathbf{A}\mathbf{R}_\mathbf{E}\mathbf{R}_\mathbf{M} \tag{B.9}$$

or

$$\mathbf{R}_\mathrm{T} = \begin{bmatrix} \cos A & \sin A & 0 \\ -\sin A & \cos A & 0 \\ 0 & 0 & 1 \end{bmatrix} \begin{bmatrix} 1 & 0 & 0 \\ 0 & \cos E & -\sin E \\ 0 & \sin E & \cos E \end{bmatrix} \begin{bmatrix} 1 & -\gamma & 0 \\ \gamma & 1 & 0 \\ 0 & 0 & 1 \end{bmatrix} \tag{B.10}$$

$$\mathbf{R}_\mathrm{T} = \begin{bmatrix} \cos A + \gamma \sin A \cos E & -\gamma \cos A + \sin A \cos E & -\sin A \sin E \\ -\sin A + \gamma \cos A \cos E & \gamma \sin A + \cos A \cos E & -\cos A \sin E \\ \gamma \sin E & \sin E & \cos E \end{bmatrix} \tag{B.11}$$

When this rotation matrix is applied to the initial pointing vector, $\mathbf{P}_0 = [0 \quad 1 \quad 0]^\mathrm{T}$

the resulting pointing vector is found.

$$\mathbf{P}_\mathrm{T} = \begin{bmatrix} \cos A + \gamma \sin A \cos E & -\gamma \cos A + \sin A \cos E & -\sin A \sin E \\ -\sin A + \gamma \cos A \cos E & \gamma \sin A + \cos A \cos E & -\cos A \sin E \\ \gamma \sin E & \sin E & \cos E \end{bmatrix} \begin{bmatrix} 0 \\ 1 \\ 0 \end{bmatrix} \tag{B.12}$$

$$\mathbf{P}_\mathrm{T} = \begin{bmatrix} -\gamma \cos A + \sin A \cos E \\ \gamma \sin A + \cos A \cos E \\ \sin E \end{bmatrix} \tag{B.13}$$

This vector represents the initial pointing vector $\mathbf{P}_0$ rotated about the undisturbed azimuth and elevation axes by the angles $A + \Delta A$ and $E + \Delta E$ respectively. The components of this vector can be used to find the rotation angles $A + \Delta A$ and $E + \Delta E$ using eqns. (4.12a) and (4.12b).

Substituting the components of $\mathbf{P}_\mathrm{T}$ and the total azimuth rotation, $A + \Delta A$, into (4.12a) yields:

$$\tan(A + \Delta A) = \frac{-\gamma \cos A + \sin A \cos E}{\gamma \sin A + \cos A \cos E} \tag{B.14}$$

or

$$\frac{\sin(A+\Delta A)}{\cos(A+\Delta A)} = \frac{-\gamma\cos A + \sin A\cos E}{\gamma\sin A + \cos A\cos E} \tag{B.15}$$

Using the sums-of-angles formulas, the left-hand-side can be expanded to produce

$$\frac{\sin A\cos\Delta A + \sin\Delta A\cos A}{\cos A\cos\Delta A - \sin\Delta A\sin A} = \frac{-\gamma\cos A + \sin A\cos E}{\gamma\sin A + \cos A\cos E} \tag{B.16}$$

Since ΔA is assumed to be small, the approximations given in eqns. (4.3a) and (4.3b) can be applied to obtain

$$\frac{\sin A + \Delta A\cos A}{\cos A - \Delta A\sin A} = \frac{-\gamma\cos A + \sin A\cos E}{\gamma\sin A + \cos A\cos E} \tag{B.17}$$

Equation (B.17) can be rearranged to

$$\Delta A\cos^2 A\cos E + \Delta A\sin^2 A\cos E = -\gamma(\sin^2 A + \cos^2 A) \tag{B.18}$$

which, after applying the trigonometric identity $\sin^2\theta + \cos^2\theta = 1$, simplifies to

$$\Delta A\cos E = -\gamma \tag{B.19}$$

or

$$\Delta A = -\gamma\sec E \tag{B.20}$$

Similarly, substituting the third component of $\mathbf{P_T}$ and the total elevation rotation angle $E + \Delta E$ into eqn. (4.12b) gives the relation

$$\sin(E + \Delta E) = \sin E \tag{B.21}$$

which can be solved for the effect of optical axis misalignment on the elevation angle:

$$\Delta E = 0 \tag{B.22}$$

B.3 Axis Nonperpendicularity

Failure of the azimuth and elevation axes of the telescope to be perpendicular can be modeled by a rotation of the elevation axis about the AZ-EL line. A y-axis rotation by angle η is given by

$$\mathbf{R}_\mathrm{N} = \begin{bmatrix} \cos\eta & 0 & \sin\eta \\ 0 & 1 & 0 \\ -\sin\eta & 0 & \cos\eta \end{bmatrix} \approx \begin{bmatrix} 1 & 0 & \eta \\ 0 & 1 & 0 \\ -\eta & 0 & 1 \end{bmatrix} \tag{B.23}$$

Axis nonperpendicularity reorients the elevation axis so its effect must be introduced after the effect of setting the elevation angle of the telescope. The total effect when the telescope is pointed to a particular position is given by:

$$\mathbf{R}_\mathrm{T} = \mathbf{R}_\mathrm{A}\mathbf{R}_\mathrm{N}\mathbf{R}_\mathrm{E} \tag{B.24}$$

or

$$\mathbf{R}_\mathrm{T} = \begin{bmatrix} \cos A & \sin A & 0 \\ -\sin A & \cos A & 0 \\ 0 & 0 & 1 \end{bmatrix} \begin{bmatrix} 1 & 0 & \eta \\ 0 & 1 & 0 \\ -\eta & 0 & 1 \end{bmatrix} \begin{bmatrix} 1 & 0 & 0 \\ 0 & \cos E & -\sin E \\ 0 & \sin E & \cos E \end{bmatrix} \tag{B.25}$$

$$\mathbf{R}_\mathrm{T} = \begin{bmatrix} \cos A & \sin A\cos E + \eta\cos A\sin E & -\sin A\sin E + \eta\cos A\cos E \\ -\sin A & \cos A\cos E - \eta\sin A\sin E & -\cos A\sin E - \eta\sin A\cos E \\ -\eta & \sin E & \cos E \end{bmatrix} \tag{B.26}$$

When this rotation matrix is applied to the initial pointing vector, $\mathbf{P}_0 = [0 \quad 1 \quad 0]^\mathrm{T}$ the resultant pointing vector is found.

$$\mathbf{P}_\mathrm{T} = \begin{bmatrix} \cos A & \sin A\cos E + \eta\cos A\sin E & -\sin A\sin E + \eta\cos A\cos E \\ -\sin A & \cos A\cos E - \eta\sin A\sin E & -\cos A\sin E - \eta\sin A\cos E \\ -\eta & \sin E & \cos E \end{bmatrix} \begin{bmatrix} 0 \\ 1 \\ 0 \end{bmatrix} \tag{B.27}$$

$$\mathbf{P}_\mathrm{T} = \begin{bmatrix} \sin A \cos E + \eta \cos A \sin E \\ \cos A \cos E - \eta \sin A \sin E \\ \sin E \end{bmatrix} \tag{B.28}$$

Substituting the components of $\mathbf{P}_\mathrm{T}$ and the total azimuth rotation, $A + \Delta A$, into eqn. (4.12a) yields:

$$\tan(A + \Delta A) = \frac{\sin A \cos E + \eta \cos A \sin E}{\cos A \cos E - \eta \sin A \sin E} \tag{B.29}$$

or

$$\frac{\sin(A + \Delta A)}{\cos(A + \Delta A)} = \frac{\sin A \cos E + \eta \cos A \sin E}{\cos A \cos E - \eta \sin A \sin E} \tag{B.30}$$

The left-hand-side can be expanded using the sum-of-angles formulas to produce

$$\frac{\sin A \cos \Delta A + \sin \Delta A \cos A}{\cos A \cos \Delta A - \sin \Delta A \sin A} = \frac{\sin A \cos E + \eta \cos A \sin E}{\cos A \cos E - \eta \sin A \sin E} \tag{B.31}$$

The small angle approximation given in eqns. (4.3a) and (4.3b) can be applied to obtain

$$\frac{\sin A + \Delta A \cos A}{\cos A - \Delta A \sin A} = \frac{\sin A \cos E + \eta \cos A \sin E}{\cos A \cos E - \eta \sin A \sin E} \tag{B.32}$$

which, after rearranging and simplifying becomes

$$\Delta A \cos E = \eta \sin E \tag{B.33}$$

or

$$\Delta A = \eta \tan E \tag{B.34}$$

Similarly, substituting the third component of $\mathbf{P}_\mathrm{T}$ and the total elevation rotation angle $E + \Delta E$ into eqn. (4.12b) gives the relation

$$\sin(E+\Delta E)=\sin E \tag{B.35}$$

which can be trivially solved for the effect of nonorthogonality on the elevation angle:

$$\Delta E = 0 \tag{B.36}$$

B.4 Tilt Toward North

Tilting the telescope toward the north by angle ψ_X rotates the entire telescope about the x-axis. Under the sign convention used in this work, the rotation is negative:

$$\mathbf{R_X}=\begin{bmatrix}1 & 0 & 0\\ 0 & \cos(-\psi_X) & -\sin(-\psi_X)\\ 0 & \sin(-\psi_X) & \cos(-\psi_X)\end{bmatrix}\approx\begin{bmatrix}1 & 0 & 0\\ 0 & 1 & \psi_X\\ 0 & -\psi_X & 1\end{bmatrix} \tag{B.37}$$

$$\mathbf{R_T}=\mathbf{R_X}\mathbf{R_A}\mathbf{R_E} \tag{B.38}$$

or

$$\mathbf{R_T}=\begin{bmatrix}1 & 0 & 0\\ 0 & 1 & \psi_X\\ 0 & -\psi_X & 1\end{bmatrix}\begin{bmatrix}\cos A & \sin A & 0\\ -\sin A & \cos A & 0\\ 0 & 0 & 1\end{bmatrix}\begin{bmatrix}1 & 0 & 0\\ 0 & \cos E & -\sin E\\ 0 & \sin E & \cos E\end{bmatrix} \tag{B.39}$$

$$\mathbf{R_T}=\begin{bmatrix}\cos A & \sin A\cos E & -\sin A\sin E\\ -\sin A & \cos A\cos E-\psi_X\sin E & -\cos A\sin E-\psi_X\cos E\\ -\psi_X\sin A & \psi_X\cos A\cos E+\sin E & \psi_X\cos A\sin E+\cos E\end{bmatrix} \tag{B.40}$$

Applying this rotation matrix to the initial pointing vector, $\mathbf{P_0}=[0 \quad 1 \quad 0]^T$ produces the pointing vector

$$\mathbf{P_T}=\begin{bmatrix}\cos A & \sin A\cos E & -\sin A\sin E\\ -\sin A & \cos A\cos E-\psi_X\sin E & -\cos A\sin E-\psi_X\cos E\\ -\psi_X\sin A & \psi_X\cos A\cos E+\sin E & \psi_X\cos A\sin E+\cos E\end{bmatrix}\begin{bmatrix}0\\ 1\\ 0\end{bmatrix} \tag{B.41}$$

$$\mathbf{P}_\mathrm{T} = \begin{bmatrix} \sin A \cos E \\ \cos A \cos E - \psi_X \sin E \\ \psi_X \cos A \cos E + \sin E \end{bmatrix} \tag{B.42}$$

This vector represents the initial pointing vector $\mathbf{P}_0$ rotated about the undisturbed azimuth and elevation axes by the angles $A + \Delta A$ and $E + \Delta E$ respectively. The components of this vector can be used to find the rotation angles $A + \Delta A$ and $E + \Delta E$ using eqns. (4.12a) and (4.12b).

Substituting the components of $\mathbf{P}_\mathrm{T}$ and the total azimuth rotation, $A + \Delta A$, into eqn. (4.12a) yields:

$$\tan(A + \Delta A) = \frac{\sin A \cos E}{\cos A \cos E - \psi_X \sin E} \tag{B.43}$$

or

$$\frac{\sin(A + \Delta A)}{\cos(A + \Delta A)} = \frac{\sin A \cos E}{\cos A \cos E - \psi_X \sin E} \tag{B.44}$$

Using the sums-of-angles formulas, the left-hand-side can be expanded to produce

$$\frac{\sin A \cos \Delta A + \sin \Delta A \cos A}{\cos A \cos \Delta A - \sin \Delta A \sin A} = \frac{\sin A \cos E}{\cos A \cos E - \psi_X \sin E} \tag{B.45}$$

Since ΔA is assumed to be small, the approximations given in eqn. (4.3a) and (4.3b) can be applied to obtain

$$\frac{\sin A + \Delta A \cos A}{\cos A - \Delta A \sin A} = \frac{\sin A \cos E}{\cos A \cos E - \psi_X \sin E} \tag{B.46}$$

This equation can be rearranged to

$$\Delta A \cos^2 A \cos E + \Delta A \sin^2 A \cos E = \psi_X \sin E \sin A + \psi_X \Delta A \cos A \sin E \tag{B.47}$$

and simplified to

$$\Delta A \cos E = \psi_X \sin E \sin A + \psi_X \Delta A \cos A \sin E \tag{B.48}$$

The second term on the right-hand side is the product of two small angles so it is much smaller than the other terms and can be neglected to yield

$$\Delta A \cos E = \psi_X \sin E \sin A \tag{B.49}$$

or

$$\Delta A = \psi_X \tan E \sin A \tag{B.50}$$

Eqn. (4.12b) can be used to write

$$\sin(E + \Delta E) = \psi_X \cos A \cos E + \sin E \tag{B.51}$$

which, after expanding the sum of angles, produces

$$\sin E \cos \Delta E + \sin \Delta E \cos E = \psi_X \cos A \cos E + \sin E \tag{B.52}$$

or, applying the small angle approximation

$$\sin E + \Delta E \cos E = \psi_X \cos A \cos E + \sin E \tag{B.53}$$

$$\Delta E \cos E = \psi_X \cos A \cos E \tag{B.54}$$

So, the elevation effect is given by

$$\Delta E = \psi_X \cos A \tag{B.55}$$

B.5 Tilt Toward East

Tilting the telescope toward the east rotates the entire telescope about the y-axis. The rotation is positive so:

$$\mathbf{R}_Y = \begin{bmatrix} \cos\psi_Y & 0 & \sin\psi_Y \\ 0 & 1 & 0 \\ -\sin\psi_Y & 0 & \cos\psi_Y \end{bmatrix} \approx \begin{bmatrix} 1 & 0 & \psi_Y \\ 0 & 1 & 0 \\ -\psi_Y & 0 & 1 \end{bmatrix} \tag{B.56}$$

and, following steps that are nearly identical to those used for the northward component of tilt, the azimuth and elevation effects of tilting the telescope to the east are

$$\Delta A = \psi_Y \tan E \cos A \tag{B.57}$$

$$\Delta E = -\psi_Y \sin A \tag{B.58}$$

B.6 Bearing Errors

Wobble of the elevation bearing disturbs the azimuth pointing direction of the telescope and produces a rotation about the line-of-sight. Two components are needed to model the pointing deviation:

$$\Delta A = \xi_{B1} \sin E \tag{B.59}$$

$$\Delta A = \xi_{B2} \cos E \tag{B.60}$$

There is no elevation effect.

Wobble of the azimuth bearing tilts the entire telescope as the telescope is rotated about the azimuth axis and is equivalent to misleveling the telescope by an amount that depends on azimuth axis position. The mean tilt in each direction is included with the northward and eastward tilt terms. Only the oscillation about the mean must be accounted for. Two components are required to model this, a north-south component and an east-west component, each using the same function of the azimuth angle.

The error terms derived above can be used to model the tilt introduced by azimuth bearing wobble by expressing the magnitude of the tilt as a function of azimuth axis position. Only the first harmonic of the azimuth bearing error was considered in this work but, in principal, a complex azimuth bearing behavior could be modeled using a large number of harmonic terms. The first order terms used for this work were

$$\Delta\psi_X = \xi_{B3}\cos A \tag{B.61}$$

$$\Delta\psi_Y = \xi_{B4}\cos A \tag{B.62}$$

These can be substituted into eqns. (B.50), (B.55), (B.57) and (B.58) to obtain the azimuth bearing wobble terms. The azimuth corrections are:

$$\Delta A = \xi_{B3}\cos A\tan E\sin A \tag{B.63}$$

$$\Delta A = \xi_{B4}\cos^2 A\tan E \tag{B.64}$$

and the elevation corrections are:

$$\Delta E = \xi_{B3}\cos^2 A \tag{B.65}$$

$$\Delta E = -\xi_{B4}\cos A\sin A \tag{B.66}$$

Radial or axial runout of the azimuth bearing translates the telescope vertically or horizontally by a small amount but the effect on pointing is negligible.

B.7 Flexure

Bending of the telescope tube under its own weight causes the telescope to point to a lower elevation. The magnitude of the deviation is greater when the telescope is pointed near the horizon. One of two terms is used to model this effect. One is

$$\Delta E = -\delta_T \cos E \tag{B.67}$$

where δ_T is the total elevation error at the horizon. Practical experience, however, has shown that a better model for the effect of flexure is often obtained using

$$\Delta E = -\delta_T \cot E \tag{B.68}$$

which was the relationship used throughout this work.

Near the zenith, the two relationships produce similar corrections but the difference becomes very large close to the horizon. It is unclear why the cotangent variation produces better models but the explanation may have relate to the fact that refraction corrections also involve the cotangent relationship. Errors in the refraction correction during calibration would produce relatively large residual errors that are absorbed into the flexure term when this relationship is used. This would appear to produce a better model because the residual random error would be lower.

GLOSSARY

Aberration, optical. Blurring or other distortions in an optical system

Altazimuth mount. A telescope configuration with a horizontal elevation axis and a vertical azimuth axis.

Annual parallax. The periodic change in star positions resulting from the motion of the earth about the sun.

Azimuth. The angular distance on the celestial sphere measured along the horizon.

Azimuth axis (*AA*). The vertical axis in an altazimuth telescope.

AZ-EL line (*AE*). The line connecting the azimuth and elevation axes of an altazimuth telescope and perpendicular to both axes.

Bonferroni confidence intervals. Confidence intervals that simultaneously bound two or more parameters at a specified confidence level.

Celestial equator. The projection of the earth's equator onto the celestial sphere.

Celestial pole. Either of the two points where the extension of the earth's axis of rotation intersects the celestial sphere.

Celestial sphere. An imaginary sphere of arbitrary radius upon which celestial bodies may be considered to be located.

Classical Cassegrain. A common optical design for telescopes. Several other common designs have the same general arrangement.

Decenter. The optical misalignment that results when a mirror or lens is displaced perpendicular to the optical axis.

Declination. The angular distance on the celestial sphere north or south of the celestial equator measured along the hour circle passing through the celestial object.

Despace. The optical misalignment that results when a mirror or lens is displaced along the optical axis.

East-west line (*EW*). A line perpendicular to the telescope azimuth axis and pointing to true east.

Elevation. The angular distance on the celestial sphere above the horizon measured along the hour circle of a celestial object.

Elevation axis (*EA*). The horizontal axis of rotation on an altazimuth telescope.

Encoder. A device for sensing position and converting it to an electronic signal. A device for measuring the rotational position of an axis.

Epoch. The exact date and time for which a position is stated.

Equatorial mount. A telescope configuration with a polar axis pointed toward the celestial pole and a declination axis perpendicular to it.

Fiducial. A trusted reference. Usually a position or distance known with high accuracy. Often an axis rotation position marked electronically by a precise sensor.

Flexure. Bending of the telescope tube or other component, usually due to gravity.

Focus mechanism. A device that translates the secondary mirror along the optical axis to focus the telescope by setting of maintaining the proper mirror separation.

Following error. In a servo system, the difference between the desired (commanded) position of an axis and the actual position.

Geodetic coordinates. Latitude and longitude determined by reference to a spherical earth.

Great circle. A circle on the surface of a sphere with its center coincident with the sphere's center.

Greenwich sidereal time. The sidereal time at 0° longitude in Greenwich, England.

Hour angle. The angular distance along the celestial equator from the meridian to the hour circle of a celestial object.

Hour circle. The great circle passing through the celestial poles and a celestial object.

Invariant point. The midpoint of the AZ-EL line. On a telescope without mechanical errors, this point stays fixed as the telescope axes are positioned.

Latitude. The angular distance on the earth measured north or south of the equator along the meridian of a geographic location.

Light deflection. The angle by which the apparent path of a light ray is altered from a straight line by the gravitational field of the Sun. The path is deflected radially away from the Sun by up to 9 μrad.

Line-of-sight (*LOS*). The direction to which the telescope points. The projection of the telescope optical axis out from the telescope's primary mirror.

Longitude. The angular distance from the Greenwich meridian to the meridian of a geographic location measured along the earth's equator.

Meridian. The great circle passing through the celestial poles and an observer's zenith.

Mirror, primary. The larger of the mirrors in a two-mirror telescope. Its diameter determines the aperture or size of the telescope.

Mirror, secondary. The smaller of the mirrors in a two-mirror telescope.

Mirror cell. The structure into which a mirror is mounted.

Mirror supports. Active or passive devices that support a mirror and distribute the weight forces in such a way that mechanical deformation of the mirror is controlled.

Mount model. The software and data components used to adjust signals sent to a telescope mount to minimize pointing errors.

Nadir. The point on the celestial sphere diametrically opposite to the zenith, directly beneath an observer.

North-south line (*NS*). A line perpendicular to the telescope azimuth axis and pointing to true north.

Nutation. The short period oscillations in the motion of the pole of rotation of the earth.

Optical axis. The centerline of the light path through the telescope

Optics support structure (OSS). See **tube**.

Pointing error. The difference between the sky position a telescope was directed to point to and the position it actually pointed to.

Position, apparent. The position at which a celestial object would be observed from the center of the earth.

Position, true. The actual position of a star relative to an observer after applying the effects of refraction and the geographic location of the observer. This usage in incorrect for astronomical calculations but conforms to statistical convention.

Position, observed. The position at which a star is observed during calibration. Observed position includes the effects of telescope errors and random noise.

Precession. The uniformly progressing motion of the pole the earth's rotation caused by gravity of the sun, moon, and planets acting on it.

Proper motion. The projection onto the celestial sphere of a star's true motion in space relative to earth's solar system.

Refraction. The bending of a light ray as it passes through the atmosphere. Refraction causes the elevation of an object to appear to be greater than it actually is.

Right ascension. The angular distance along the celestial equator of a star measured from a fixed reference point, the vernal equinox. Right ascension for a star is nearly fixed and only changes very slowly due to precession and proper motion.

Seeing. The nonconstant component of the motion of a star image. Seeing is caused by short period variations in refraction through the atmosphere.

Sidereal time. A measure of the rotation of the earth with respect to stars instead of the sun. One sidereal day is about 23 hours, 56 minutes.

Tube. In general, the structure that moves when the elevation angle is changed. Usually the mirrors of a telescope are mounted in the tube.

Tilt. In an optical system, rotation of an optical element about an axis perpendicular to the optical axis or the aberration caused by such a rotation. Also, the angle that a telescope is misleveled.

Vernal equinox. The point on the celestial equator where the sun crosses it in the spring.

Zenith. The point on the celestial sphere directly overhead.

Zenith distance. The angular distance from the zenith to a star or point in the sky.